THE UNIVERSITY
of EDINBURGH

Mitochondrial dynamics in demyelinated axons in a cerebellar slice culture system

Author:
Simon LICHT-MAYER

Supervisor:
Dr. Don MAHAD

A thesis submitted in fulfillment of the requirements for the degree of Doctor of Philosophy

UNIVERSITY OF EDINBURGH

August 21, 2018

Declaration of Authorship

I, Simon LICHT-MAYER, declare that this thesis titled, "Mitochondrial dynamics in demyelinated axons in a cerebellar slice culture system" and the work presented in it are my own. I confirm that:

- This work was done wholly while in candidature for a research degree at this University.
- Where any part of this thesis has previously been submitted for a degree or any other qualification at this University or any other institution, this has been clearly stated.
- Where I have consulted the published work of others, this is always clearly attributed.
- Where I have quoted from the work of others, the source is always given. With the exception of such quotations, this thesis is entirely my own work.
- Where the thesis is based on work done by myself jointly with others, I have made clear exactly what was done by others and what I have contributed myself.

Signed:

Date:

"Nobody ever figures out what life is all about, and it doesn't matter. Explore the world. Nearly everything is really interesting if you go into it deeply enough. "

— Richard Feynman

Abstract

Simon LICHT-MAYER

Mitochondrial dynamics in demyelinated axons in a cerebellar slice culture system

Axonal degeneration is the major cause of disability in progressive multiple sclerosis (MS). It has been shown that in MS and relevant disease models, demyelinated axons harbor an increased number of mitochondria, which is reflected in bigger stationary sites of mitochondria, increased mitochondrial activity and increased transport speed of mitochondria. This axonal response of mitochondria to demyelination (ARMD) is protective, as there is an increase in energy demand due to the redistribution of sodium channels along the axon following demyelination. However, it remains to be determined how this ARMD is mounted and how mitochondrial dynamics are involved. By using *in vivo* and *in vitro* systems we are determined to elucidate the transport and fusion dynamics of the ARMD and where these additional mitochondria come from. Using a cerebellar slice culture system with lysolecithin induced demyelination, we show that the increase in mitochondrial occupancy of the axon already occurs at 24 hours after demyelination and plateaus around 3 to 4 days after demyelination. At 24 hours, there was a steep increase in the mitochondrial numbers inside the axon, which is then followed by an increase in mitochondrial size over the following days. All parameters decrease again over the following days, but remain elevated compared to baseline even 12 days after demyelination. To determine the source of these additional mitochondria and to assess the fusion dynamics within the axon, we used a lentivirus expressing a mitochondrial targeted photoconvertible dye (mEOS2) to label mitochondria in Purkinje cells. The mitochondria that are labelled green in the Purkinje cell axons are then photoconverted to red by illuminating the

initial part of the axon with a 405-nm laser and imaged over the following 20 minutes to determine the transport and fusion dynamics. This showed an increased number of mitochondria moving from the cell body into the axon, as well as an increase in retrograde transport of mitochondria in the demyelinated compared to the myelinated axons. Furthermore the size of newly transported mitochondria and their speed was increased in the anterograde direction. Furthermore, the fusion rate of newly transported mitochondria with stationary converted mitochondria was increased in the demyelinated axons compared to myelinated control. These changes can also be observed in unmyelinated axons, as well as axons of cerebellar slices of the dysmyelinating *shiverer* mutant with or without lysolecithin treatment. The manipulation of mitochondrial dynamics after demyelination with the fission inhibitor mdivi-1 and the ATPase inhibitor oligomycin both showed an increasing or decreasing effect on the mitochondrial parameters after demyelination respectively. The effect on the axonal health after demyelination was detrimental with both of these treatments. Increasing mitochondrial biogenesis with pioglitazone increased axonal mitochondrial parameters, as well as ameliorated axonal damage after demyelination with lysolecithin. As the neuronal cell bodies in MS harbour mitochondrial DNA deletions, which affects their physiology, including energy production efficiency, another aim of this thesis was to model this deficiency *in vitro*. As it was not possible to model these mitochondrial defects *in vitro* within the experiments of this thesis, the characterization of a mitochondrial mutant *in vivo* model was done as a contribution to a greater set of experiments performed by other members of the Mahad lab.

Lay Summary

Multiple sclerosis (MS) is an incurable disease of the central nervous system affecting around 2.5 million people worldwide. MS usually presents first in young adults, disrupting their lives and future outlooks, with symptoms like numbness, weakness in the limb, vertigo or blurred vision. During the relapsing stage of the disease, these symptoms may improve and worsen again, but once the disease gets to the progressive stage, typically a continuous worsening of symptoms is observed. While there are therapies available that modify the relapsing-remitting stage of the disease, there are no therapies approved that stop the continuous degeneration of the nerve cells and their processes, which can be found from the beginning of diagnosis and goes into high gear during the progressive stage of the disease. It has been shown that the loss of axons, long processes of the nerve cells that send output signals to other nerve cells, is the best correlator of clinical disability in MS. These axons are surrounded by an insulating layer, which enhances signal transduction efficiency along the axon and supports the axon with nutrients, called myelin, that is lost during the process of demyelination which is widespread in MS, both in the white matter where the axons reside, as well as in the grey matter of the cell bodies. It was shown previously in MS autopsy tissue and relevant disease models that upon demyelination there is an increase of mitochondria, the powerhouses of the cell, inside the demyelinated axons. This response to the loss of myelin is protecting the axon from degeneration following demyelination, which is caused by the increase in energy demand and subsequent detrimental processes. Currently it is not known where these additional mitochondria, that are found in the demyelinated axon, are coming from and how the dynamics of this vital organelle develop in the axon after the loss of myelin. Here we show that the dynamics of these mitochondria change significantly after demyelination and that these mitochondria are transported from the cell body into the axon and are bigger and faster than mitochondria in the myelinated axons. We also show that this reaction of mitochondria reaches a peak a few days after demyelination and lessens again thereafter, without ever coming down to control levels. We also tried

to manipulate this mitochondrial response to test the effect on axonal health after demyelination and found that there was a significant amelioration when enhancing mitochondrial production. Lastly we tried to model mitochondrial deficiency, the reduced ability to generate energy, which is widespread in MS nerve cells and determined effect of mitochondrial deficiency on synapses, which have also been shown to be lost in MS.

In summary these experiments stress the importance of the nerve cell bodies, which are still mostly intact in the progressive stage of this disease, as they supply the much needed energy producing mitochondria into the vulnerable demyelinated axon. More importantly we show that manipulating mitochondrial dynamics, for example the production of new mitochondria, is a treatment target to tackle the widespread axonal loss seen in the progressive stage of MS and possibly could improve the clinical outcome of this devastating disease.

Acknowledgements

First I would like to thank my supervisor Don Mahad, who was supportive and encouraging every step of the way. He offered me the perfect balance of guidance and personal freedom in conducting the experiments for this thesis. My second supervisor David Lyons for his support and invaluable ideas, which influenced the course that the experiments took over time. As well as my thesis committee Catherina Becker and Richard Ribchester, who contributed important feedback during every thesis committee meeting, which helped to shape this thesis significantly.

I also want to thank Graham Campbell, post-doc in the Mahad lab during most of my PhD, for all the help and advice given and all the techniques he taught me; and Katie McGill for technical support and looking after the the lab and equipment. And all the people who joined the lab over the past years.

Most importantly I want to thank my wife Melina, for being the reason I could do this thesis at all. Without your constant support and love, I would not have made it half as far. Thank you being my home, support and reason, that's why I dedicated this work to you.

Contents

List of Figures

List of Abbreviations

AIS	**A**xon **i**nitial **s**egment
ARMD	**A**xonal **r**esponse of **m**itochondria to **d**emyelination
ATP	**A**denosine **t**ri**p**hosphate
BBB	**B**lood **b**rain **b**arrier
CD	**C**luster of **d**ifferentiation
CNS	**C**entral **n**ervous **s**ystem
COX	**C**ytochrome c **ox**idase
DAB	**Di**amino**b**enzidine
DNA	**D**esoxyribo**n**ucleic**a**cid
Drp1	**D**ynamin-1-like-**p**rotein 1
EBV	**E**pstein-**B**arr **v**irus
EDSS	**E**xpanded **d**isability **s**tatus **s**cale
ER	**E**ndoplasmic **R**eticulum
ETC	**E**lectron **t**ransport **c**hain
GM	**G**rey **m**atter
GTP	**G**uanosine **t**ri**p**hosphate
HHV	**H**uman **h**erpes **v**irus
HI HS	**H**eat-**I**nactivated **h**orse**s**erum
HLA	**H**uman **l**eukocyte **a**ntigen
IHC	**I**mmuno**h**isto**c**hemistry
IM	**I**nner mitochondrial **M**embrane
KO	**K**nock **o**ut
Lyso	**Lyso**lecithin
MAG	**M**yelin-**a**ssociated **g**lycoprotein
MAM	**M**itochondria **a**ssiociated **m**embranes
Mff	**M**itochondrial **f**ission **f**actor
Mfn	**M**ito**f**usi**n**
MRI	**M**agnetic **r**esonance **i**maging
MS	**M**ultiple **s**clerosis

mtDNA	**Mit**ochondrial **D**esoxyribo**n**ucleic**a**cid
NCX	**N**a-**C**a e**x**changer
NO	**N**itric **o**xide
OM	**O**uter mitochondrial **M**embrane
OPA1	**O**ptic **a**trophy 1
PC	**P**urkinje **c**ell
PCL	**P**urkinje **c**ell **l**ayer
PML	**P**rogressive **m**ultifocal **l**eukoencephalopathy
PMS	**P**rogressive **m**ultiple **s**clerosis
PNS	**P**eriphal **n**ervous **s**ystem
PPMS	**P**rimary **p**rogressive **m**ultiple **s**clerosis
RNA	**R**ibo**n**ucleic**a**cid
RNS	**R**eactive **n**itrogen **s**pecies
ROS	**R**eactive **o**xygen **s**pecies
RRMS	**R**elapsing **r**emitting **m**ultiple **s**clerosis
rRNA	**R**ibosomal **R**ibo**n**ucleic**a**cid
SDH	**S**uccinate **d**e**h**ydrogenase
SPMS	**S**econdary **p**rogressive **m**ultiple **s**clerosis
tRNA	**T**ransfer **R**ibo**n**ucleic**a**cid
WM	**W**hite **m**atter

Dedicated to my wife Melina

Chapter 1

Introduction

1.1 Multiple sclerosis

1.1.1 Disease course and etiology

Multiple sclerosis (MS), is an inflammatory disease of the central nervous system (CNS) of unknown etiology and is the second most frequent cause of disability in young adults (Noseworthy et al., 2000; Compston and Coles, 2002). The clinical manifestation of MS is very heterogenous, because it can affect many different part of the CNS (Ghasemi, 2017). This heterogeneity is also reflected in the pathological features of MS, as there are many different cell types involved in the disease process (Popescu, Pirko, and Lucchinetti, 2013). For the diagnosis of MS the most important tool, apart from neurological exams, is the magnetic-resonance-imaging (MRI) method, as it allows for non-invasive imaging of the brain, although some lesions, especially grey matter lesions, are not revealed by the MRI (McDonald et al., 2001; Polman et al., 2011; Miller, 1995; Miller et al., 1998). As for the disease course, officially there are still 3 different types of MS disease courses recognized at the onset of disease, however there is an ongoing debate as to whether classify the different subgroups of MS as one disease (Confavreux and Vukusic, 2006; Lublin et al., 2014; Barnett et al., 2009). The 3 different types mentioned are the relapsing-remitting (RRMS) type, which affects around 85% of newly diagnosed patients (Confavreux and Vukusic, 2006; Lublin et al., 2014; Dutta and Trapp, 2014). RRMS is characterized by relapses, with disease worsening, and subsequent remission, where the disease symptoms may improve again (Confavreux and Vukusic, 2006; Lublin et al., 2014; Dutta and Trapp, 2014). The second type of MS is the

primary-progressive MS (PPMS), which presents as a steady decline in neurological symptoms without relapses or remission (Confavreux and Vukusic, 2006; Lublin et al., 2014; Dutta and Trapp, 2014). The last type of MS that affect newly diagnosed patients, is the so-called relapsing-progressive MS (PRMS), which presents itself with relapses without phases of remission and steady worsening of clinical symptoms (Confavreux and Vukusic, 2006; Lublin et al., 2014). About 80% of the RRMS cases will develop the secondary-progressive MS (SPMS) disease course over 10-15 years, which judging from the clinical symptoms is similar to the PPMS disease course (Confavreux and Vukusic, 2006; Lublin et al., 2014). There are several therapies licensed for RRMS, that are mostly immune-regulatory or immune-suppressive and are categorized in first-line and escalation therapies (Polman et al., 2006; Wingerchuk and Carter, 2014; Gold et al., 2012; Fox et al., 2012; Comi et al., 2009). On the other hand, with the CD20 antibody Ocrelizumab there is only one therapy available for PPMS, which was only licensed recently (Montalban et al., 2017). Another compound possibly affecting disease progression in PMS is MD1003, which is high dose biotin and showed improvement in EDSS in a subgroup of patients during a Phase II trial (Tourbah et al., 2016).

In RRMS blood-brain-barrier (BBB) disruption is seen frequently, especially during disease relapses, while the inflammatory processes taking place in the progressive stage of the disease seem to be taking place behind a closed BBB (Minagar and Alexander, 2003; Mahad, Trapp, and Lassmann, 2015). The genetics of MS are also very heterogenous, as no gene was identified as being directly responsible for MS, but several genome-wide-association-studies (GWAS) have revealed over 100 genes, mostly immune-related genes like the HLA locus, associated with the disease (Compston and Sawcer, 2002; Akesson et al., 2002; Sawcer et al., 2002; Hafler et al., 2007; Allen et al., 1994). The fact that women are twice as much affected compared to men, suggests that hormones might play an important role in disease development, there are also therapies in development that involve hormone related drug targets (Goldenberg, 2012; Gold and Voskuhl, 2009). Also, environmental factors, such as sunlight and subsequent Vitamin D production seem to play a role in the etiology of MS, as people further away from the equator are more affected by the disease

(Hayes, 2000; Holick, 2007). There is also the hypothesis that a virus might be responsible for the development of multiple sclerosis, the main candidate is the Epstein-Barr-virus, which belongs the family of herpes-viruses (HHV-4) and also other members of the herpes viruses have been implicated in MS etiology (Lipton et al., 2007; Warner and Carp, 1988). Another disease triggering factor might be of bacterial origin, for example a bacterial toxin, as the case of a woman with MS with Clostridium perfringens type B infection demonstrated (Rumah et al., 2013). The mechanism for the autoimmune response seen in MS, could be molecular mimicry, or the tissue damage could be a result of the immune cells trying to destroy the infection and damaging the surrounding neuronal tissue in the process (Olson et al., 2001; Croxford, Olson, and Miller, 2002).

1.1.2 MS pathology

MS was considered a classical demyelinating disease, in which inflammation plays the main role of destruction of the myelin surrounding the axons (Love, 2006). While demyelination and inflammation are important factors in the pathology of MS, other factors, such as neuronal damage and astrogliosis are also considered pathological hallmarks of the disease (Ferguson et al., 1997; Fawcett and Asher, 1999; Bitsch et al., 2000a; Stichel and Muller, 1998; Popescu, Pirko, and Lucchinetti, 2013; Lassmann, 2013; Kutzelnigg and Lassmann, 2014). As mentioned above for many years the focus in MS research was the demyelination occurring in the white matter of the brain, because MS was long considered a disease affecting mainly the white matter of the brain, but during the last decades the grey matter (GM) damage, which plays a key role in MS progression, as there are several kinds of GM lesions occurring, sometimes very early in the disease course, came more into focus (Popescu and Lucchinetti, 2012a). These GM lesions are recognized as leukocortical lesion, which expand in the GM as well as in the WM, intracortical lesion, which like the name suggests are found inside the GM and subpial lesion, which are the only lesion type specific for MS (Popescu and Lucchinetti, 2012a; Bo et al., 2003). The heterogeneity of the disease mentioned in the previous section, also extends

to the pathology of MS lesions, as lesions are very heterogeneous between MS patients (Lassmann, Bruck, and Lucchinetti, 2001; Metz et al., 2014).

MS lesion can be categorized into four distinct lesion patterns, depending on the type of cells present within the lesion and the type of myelin protein degradation products within the cells (Lassmann, Bruck, and Lucchinetti, 2001). Furthermore the stage of the demyelinating lesion in MS can be subdivided according to their stage, classical active lesion are characterized by a substantial infiltration of macrophages that contain myelin degradation products and these lesions can be further described according to which myelin products are found within the macrophages, with the minor myelin products being found early and the major myelin products later during the lesion timecourse (Brück et al., 1995; Popescu and Lucchinetti, 2012b; Bitsch et al., 2000a). Chronic active plaques, which are mostly found in patients during the progressive phase of the disease, show sharp lesion edges with a rim of macrophages around the inactive lesion center (Brück et al., 1995; Popescu and Lucchinetti, 2012b; Bitsch et al., 2000a). Finally chronic inactive lesion, which are completely demyelinated and show a significant loss of axons and oligodendrocytes within the lesion, while they only display minor infiltration by macrophages or other immune cells (Brück et al., 1995; Popescu and Lucchinetti, 2012b; Bitsch et al., 2000a). In some cases remyelinated shadow plaques can be found, displaying thin myelin sheaths around the axon and only faint histochemical signal for myelin (Brück et al., 1995; Popescu and Lucchinetti, 2012b; Bitsch et al., 2000a).

Outside-in or inside-out

Although most of the lesions show lymphocyte infiltration either directly in the lesion or nearby, a study that showed 12 RRMS patients autopsy cases, who died shortly after the onset of a MS relapse suggested that the early MS lesion does not contain infiltrating lymphocytes (Barnett and Prineas, 2004). This finding fuelled the so-called inside-out hypothesis of MS, that the oligodendrocytes die because of some intrinsic factor and the immune cells infiltrate the brain as a reaction to the damage (Barnett and Prineas, 2004; Prineas and Parratt, 2012; Tsunoda and Fujinami, 2002). The more prominent theory to this date is the outside-in hypothesis of MS, which

suggests that the infiltrating immune cells from the periphery into the brain start the inflammatory reaction, possibly against an auto antigen resembling one of the myelin proteins, and damaging the oligodendrocytes and axons in the process (Lucchinetti et al., 2011; Guseo and Jellinger, 1975). Most of the current MS therapies are targeting the immune mediated part of the disease by either destroying, reducing, modifying immune cells or by preventing the lymphocytes to enter the brain (Polman et al., 2006; Wingerchuk and Carter, 2014; Gold et al., 2012; Fox et al., 2012; Comi et al., 2009).

Modes of tissue damage

The direct correlation of T-Cells (CD8+) within the lesion with the extent of axonal damage underlines the importance that the direct damage mediated by immune cells plays in the destruction of tissue in MS, also the number of macrophages within the lesion are correlated with tissue damage found (Kuhlmann et al., 2002; Trapp et al., 1998). Another important mechanism, also in great part mediated by the innate and adaptive immune system, is oxidative damage, which is now recognized as a major driving factor of tissue damage and mitochondrial injury (Kuhlmann et al., 2002; Haider et al., 2011; Horssen et al., 2011; Dutta et al., 2006; Horssen et al., 2006). Dysfunctional mitochondria are in turn a major source of reactive oxygen species (ROS) and enhance the oxidative damage done by immune mediated ROS and reactive nitrogen species (RNS) (Starkov, 2008; Orrenius, 2007). Since mitochondrial DNA is very vulnerable to oxidative damage, mitochondrial DNA deletions are also enhanced, which amplifies the number of dysfunctional mitochondria and leads to so-called virtual hypoxia (Lu et al., 2000; Campbell et al., 2011; Campbell and Mahad, 2012; Trapp and Stys, 2009). Although there are several animal models of MS, the extent of oxidative damage in MS cases is not found in any of these models, also mitochondrial DNA deletions were not observed (Trapp et al., 1998; unpublished data from Mahad lab).

Another factor contributing to the degeneration of axons in multiple sclerosis are changes in the demyelinated axon leading to an enhance calcium concentration inside the axon (Waxman, 1992; Craner et al., 2004b; Moll et al., 1991; Smith, 2007; Waxman, 2006). The axonal sodium channels

used for the saltatory conduction of action potentials are normally mainly concentrated around the node of Ranvier, these sodium channels have the NaV1.6 subtype and are characterized by a low threshold and persistent sodium current (Craner et al., 2004b). In the acutely demyelinated axon potassium channels, that were hidden under the myelin are unmasked by the process of demyelination and in addition the distribution of sodium channels is sparse, which leads to a failure in action potential propagation (Craner et al., 2004b; Waxman, 2006). To restore function of the axonal conductivity, the sodium channels redistribute along the demyelinated axon, which leads to an extensive expression of NaV1.6 and NaV1.2 sodium channels, in addition to the unmasked potassium channels, along the axon where the myelin was before (Craner et al., 2004b; Waxman, 2006). In contrast to the NaV1.6 sodium channels, the NaV1.2 sodium channels produce rapidly activating and inactivating sodium currents, which support action potential conduction along the axon. As mentinoned above, the NaV1.6 sodium channels produce a persistent sodium current, which leads to higher concentration of sodium inside the demyelinated axon compared to the myelinated axon (Craner et al., 2004b; Waxman, 2006). These NaV1.6 sodium channels are found to be co localized with $Na^+ - Ca^{2+}$-exchanger (NCX) along the demyelinated axon (Craner et al., 2004a). The accumulation of sodium inside the axon eventually leads to the reversal of the $Na^+ - Ca^{2+}$-exchanger, which in turn leads to an increase in intra-axonal accumulation of calcium (Stys et al., 1993; Stys, Waxman, and Ransom, 1992). The accumulation of calcium inside the axon then triggers several different signalling cascades leading to the activation of proteases and lipases, which in turn induce axonal injury (Waxman, 2006; Kornek et al., 2001). To pump the overload of sodium out of the axon, the Na^+/K^+ ATPase is used to get sodium out of the axon, while pumping potassium in, this requires ATP to work and that means that functional mitochondria are required to keep the ions balance favourable in order for the axon to survive (Mohd, 2010; Albers and Siegel, 1998; Lores Arnaiz and Ordieres, 2014).

As mentioned in the beginning of the section, reactive oxygen and nitrogen species, for example nitric oxide (NO), can trigger mitochondrial damage, leading to dysfunctional mitochondria inside the axon (Giovannoni et al., 1998; Smith and Lassmann, 2002). These dysfunctional

mitochondria are not able to produce enough energy to pump the excess sodium out of the axon, which leads to the above mentioned cascade leading to the accumulation of intra-axonal calcium and finally axonal injury (Coleman, 2005; Stys and Jiang, 2002; O'Hanlon et al., 2003; Xie and Barrett, 1991).

1.2 Mitochondria

Mitochondria, which are one of the key organelles of every eukaryotic cell and responsible for many life-maintaining functions, have once been a single cell organism which was engulfed by another organism billion years ago, a symbiosis between an aerobic bacterium and a primordial eukaryotic cell (Wallace, 2005; Chan, 2006a; Cavalier-Smith, 2006). This small organelle took over several functions from the host cell, giving it an evolutionary advantage over other cells that did not contain mitochondria (Wallace, 2005; Chan, 2006a; Cavalier-Smith, 2006). Besides being the power-house of most cells, especially neurons with their high energy demand are in need of massive amounts of adenosine triphosphate (ATP), mitochondria are involved in many essential function, like calcium buffering, fatty acid oxidation and apoptosis (Pinton et al., 2008; Friedman and Nunnari, 2014; Wanders et al., 2010). Every mitochondria has its own genome containing many copies of its 16kb sized circular mtDNA which encodes for just 37 genes, while most (900) of the genes that are needed for mitochondrial function are encoded inside the nuclear DNA (Wallace, 2005; Chan, 2006a; Cavalier-Smith, 2006; Iborra, Kimura, and Cook, 2004).

The proteins made from nuclear DNA have to be imported into the mitochondria from the cytoplasm, of the 37 genes encoded by the mitochondrial DNA, 13 are needed to make protein subunits of the respiratory complexes I, III, IV and V, while complex II is totally encoded in the nuclear DNA; see figure 1.1 (Wallace, 2005; Chan, 2006a; Cavalier-Smith, 2006; Iborra, Kimura, and Cook, 2004). Furthermore, there are 22 mitochondrial tRNAs and and 2 mitochondrial rRNAs, which are needed for the translation of mtDNA (Wallace, 2005; Chan, 2006a; Cavalier-Smith, 2006; Iborra, Kimura, and Cook, 2004). The most important part of

mitochondrial energy production is the mitochondrial respiratory chain, which is made up of 5 complexes; see figure 1.1 (Rich and Maréchal, 2010).

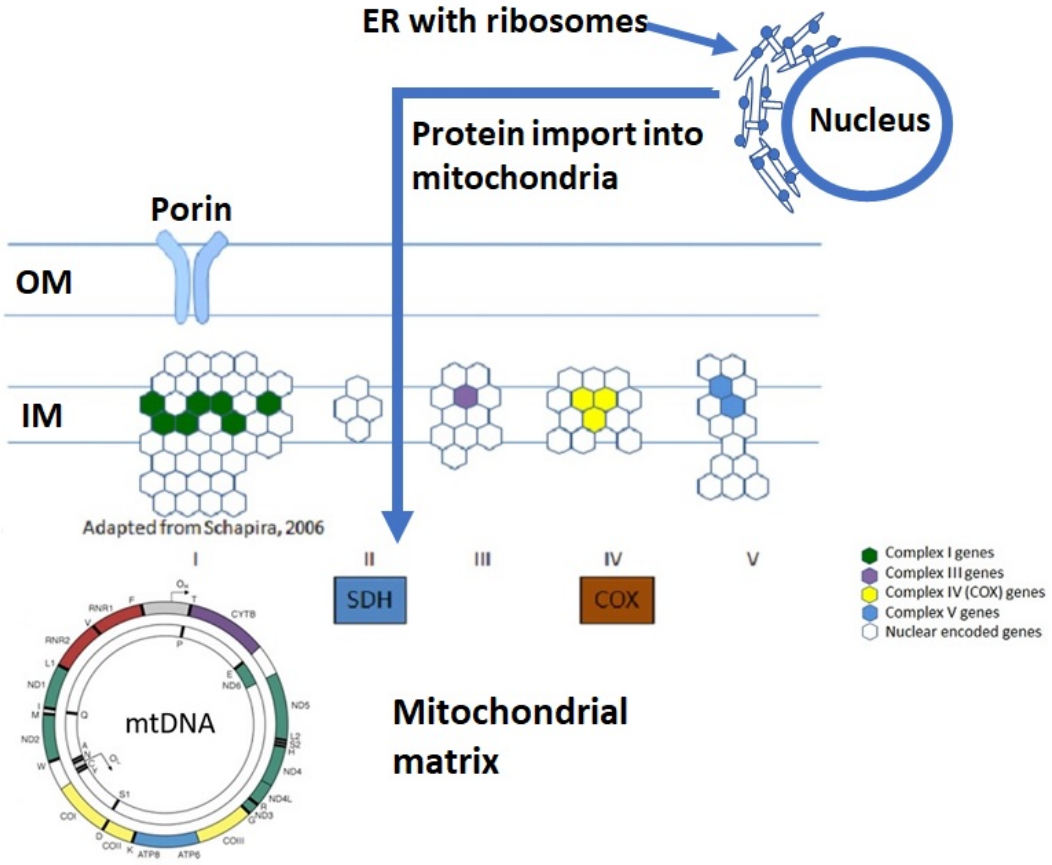

FIGURE 1.1: Mitochondrial respiratory chain complexes and their gene locations. All five complexes (I,II,III,IV,V) are located in the inner mitochondrial membrane. The colour code of the hexagons shows the location of the genes needed for the assembly of each complex. White represents genes encoded in the genomic DNA (Complex II is entirely nuclear encoded), which have to be translated and imported into the mitochondria. On the bottom is a schematic picture of the mitochondrial DNA and the coding locations of the complexes. Green=complex I; purple=complex III; yellow=complex IV; blue=complex V. On the outer membrane sits porin, a transmembrane protein on all mitochondria which can be used as a mitochondrial marker in immunohistochemistry. Complex II (SDH=succinate dehydrogenase) and complex IV (COX=cytochrome c oxidase) activity are used in the COX/SDH assay shown in the methods sections.

These complexes - through a series of electron transfers – create an electrochemical gradient between the matrix and the intermembrane space (Rich and Maréchal, 2010). This electrochemical gradient is then used by the ATP-Synthase (fifth complex of the respiratory chain) to generate ATP (Jonckheere, Smeitink, and Rodenburg, 2012). Each of these complexes, with the exception of complex II is at least partly encoded in the mitochondrial DNA; see figure 1.1 (Iborra, Kimura, and Cook, 2004).

1.2.1 Mitochondrial turnover and dynamics

Since the mitochondria are needed for efficient energy production, mitochondrial biogenesis and transport are important processes in coping with the local energy demand in cells, this is even more important in neurons with their polarized morphology and long axons (Schwarz, 2013; Britt et al., 2016; Sheng, 2014). Adjustments to mitochondrial biogenesis and transport allow the neuron to respond to changes in local energy demand (Schwarz, 2013; Britt et al., 2016; Sheng, 2014). Because mitochondrial proteins are encoded in both mitochondrial and nuclear genomes, proteins made in the cytoplasm have to be imported into the mitochondria and assemble with proteins synthesized in the mitochondria (Neupert, 1997; Chacinska et al., 2009). Once the components are made the mitochondrion may undergo fission and create a brand new mitochondrion, and the new mitochondrion may get transported to some other part of the cell and may fuse with other mitochondria (Chen and Chan, 2009b). The balance of fusion and fission is an important factor determining mitochondrial biogenesis, which makes mitochondrial biogenesis a very dynamic process and challenging one to study (Chan, 2006a; Chen and Chan, 2009b). The general assumption is that mitochondrial biogenesis occurs perinuclear, but there is also evidence for axonal biogenesis (Amiri and Hollenbeck, 2008). Severe defects in either mitochondrial fission or fusion results in embryonic lethality in mice, pointing towards an essential part mitochondrial dynamics of fusion and fission play in maintaining essential functions inside the cell (Chen et al., 2003; Elgass et al., 2013; Wakabayashi et al., 2009).

Mitochondrial fusion and fission

The fusion process allows for content mixing between the mitochondria in the cell and the fission to isolate defective mitochondria as well as create new functional mitochondria, that can be transported around the cell. This creation of a mitochondrial network allows for a healthy mixing of the mitochondrial population (Chan, 2012a; Chen et al., 2010). Apart from content mixing, mitochondrial fusion has several other important functions, among these respiratory chain complex activity and response to cellular stress environments (Chan, 2012a; Westermann, 2012; Muster et al., 2010; Cogliati et al., 2013; Youle and Bliek, 2012).

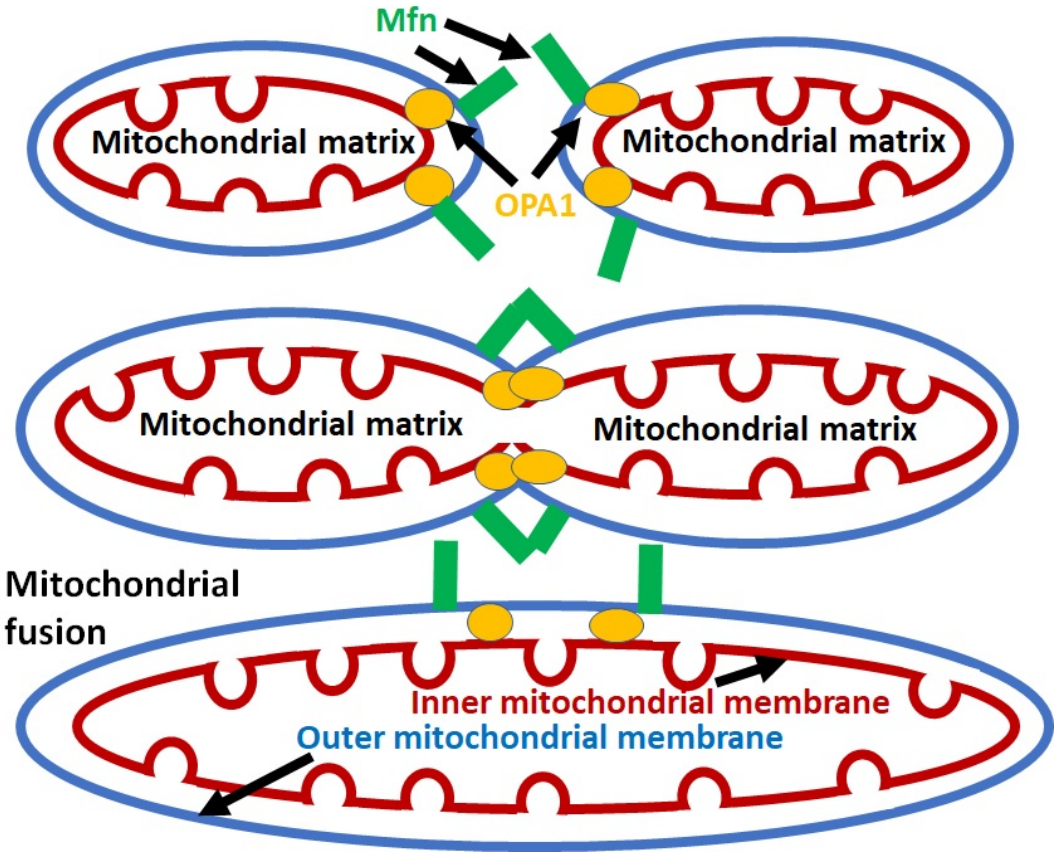

FIGURE 1.2: Mitochondrial fusion processes depicted in a simplified graphical image, showing the mitochondrial fusion proteins. The mitofusin (Mfn) shown in green are responsible for the fusion of the outer mitochondrial membrane, while the optic-atrophy-1 (OPA1) shown in orange mediates the fusion of the inner mitochondrial membrane.

This dynamic behaviour of mitochondria is associated with mtDNA stability, mitochondrial protein function including respiratory chain complex activity, apoptosis and mitophagy, as well as response to cellular stress including increase in energy demand (Chan, 2012a; Westermann, 2012; Muster et al., 2010; Cogliati et al., 2013; Youle and Bliek, 2012; Chen et al., 2010). The deletion of fusion mediators Mfn1, Mfn2 or OPA1 leads to the death of mouse embryos in midgestation, further highlighting the importance of mitochondrial fusion (Chen et al., 2003). Because mitochondria are double membrane organelles, mitochondrial fusion has to include fusion of the outer membrane as well as fusion of the inner membrane between two fusing mitochondria (Chan, 2012a; Scott and Youle, 2010). Fusion of outer and inner membrane takes place more or less at the same time after the mitochondria start to fuse (Chan, 2012a; Scott and Youle, 2010). The two GTPases Mitofusin 1 and 2 (Mfn1) and (Mfn2), which are proteins embedded within the outer membrane of mitochondria, are responsible for the fusion of the outer mitochondrial membrane in mammals; see figure 1.2 (Chen et al., 2003). For the fusion of the inner mitochondrial membrane another GTPase, named OPA1, is necessary; see figure 1.2 (Song et al., 2007; Chan, 2012a). There is also evidence that the mitofusins play a role in the contact between the mitochondria and the endoplasmatic reticulum (ER), called the mitochondria associated membranes (MAM), which have recently been implicated in multiple sclerosis (Marchi, Patergnani, and Pinton, 2014; Haile et al., 2017b). OPA1 deficiency, which got its name optic-atrophy-1, because its mutation leads to the most common form of optic atrophy, can lead to reduction in respiratory chain efficiency, loss of cristae complexity and increased apoptosis, while OPA1 conditional knockouts still retain the fusion of the inner mitochondrial membrane, which points towards mitochondrial fusion being a multistep process (Cogliati et al., 2013; Varanita et al., 2015; Song et al., 2009; Frezza et al., 2006; Chan, 2012a). In contrast to the mitofusin proteins, which are required on both mitochondria for the fusion of the outer mitochondrial membrane to take place, OPA1 deficient mitochondria are still able to fuse with OPA1 expressing mitochondria (Chan, 2012a). There are eight different isoforms of OPA1, some short and some long splice forms, a combination of short and long isoforms is required for

mitochondria inner membrane fusion under normal conditions, but it has been reported that under stress conditions the long isoforms are sufficient to mediate mitochondrial fusion (Chan, 2012a; Tondera et al., 2009; Song et al., 2007).

Opposing mitochondrial fusion, the process of mitochondrial fission is just as necessary to keep a healthy balance of form and function within the mitochondrial network (Chan, 2012a).

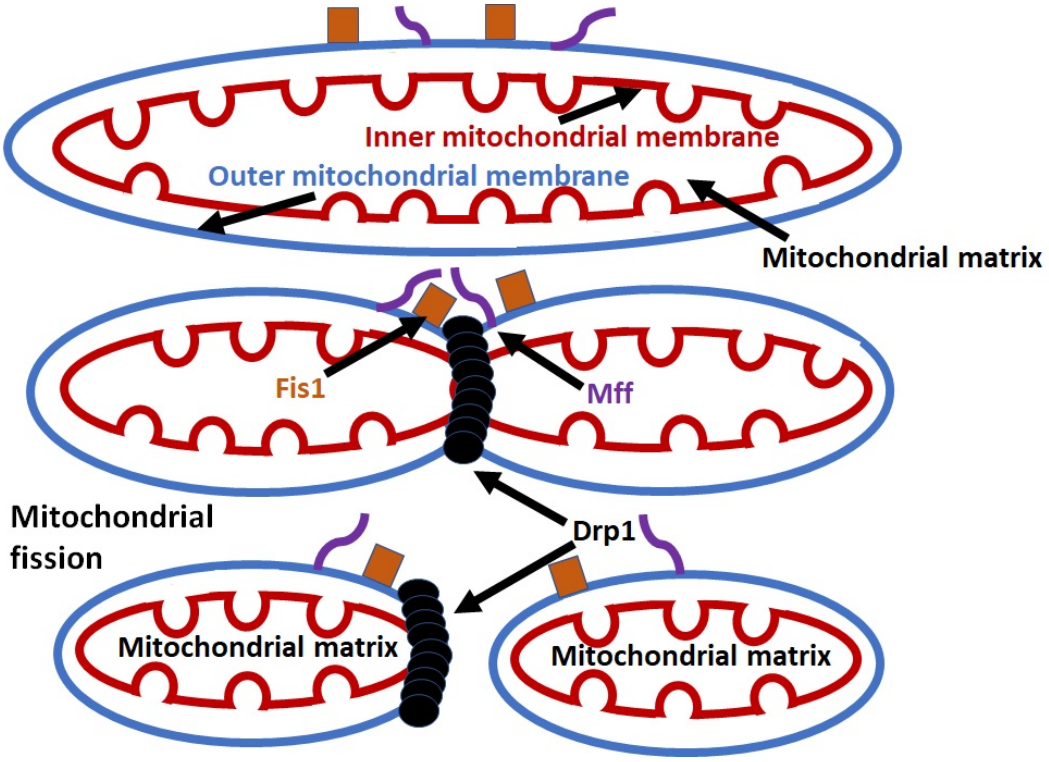

FIGURE 1.3: Mitochondrial fission processes depicted in a simplified graphical image, showing the proteins responsible for mitochondrial fission. The dynamin-related protein 1 (Drp1) shown in black is a GTPase mediating the constriction of the mitochondrial membrane and subsequently mitochondrial fission. Mitochondrial fission factor (Mff), shown in violet, and mitochondrial fission 1 protein (FIS1), shown in brown, are both potential candidates for interaction with Drp1.

Mitochondrial fission may also be involved in the mitochondrial segregation process between the daughter cells after cell division (Chan, 2012a; Taguchi et al., 2007). Another GTPase, namely dynamin-related protein 1 (DRP1), seems to be the key player mediating the fission process

via a dynamin like constriction along the mitochondrial membrane; see figure 1.3 (Chan, 2012a; Frank et al., 2001). Drp1 is located within the cytosol and upon interaction with another key player mediates mitochondrial fission, Fis1, Mff, MiD49 and MiD51 are all potential candidates for this interaction with Drp1, with recent evidence pointing towards mitochondrial fission factor (Mff) as being the interaction partner of Drp1, since its knockdown leads to a reduction of Drp1 recruitment; see figure 1.3 (Liu and Chan, 2015; Losón et al., 2013; Otera et al., 2010). Also, since Drp1 is assembled on the mitochondrial outer membrane, it is not known which proteins are responsible for the fission of the inner mitochondrial membrane or if the same process is responsible for both membranes (Chan, 2012a). Since Drp1 is needed for mitochondrial fission, deletion of Drp1 leads to elongated mitochondria that collapse (Chan, 2012a; Smirnova et al., 2001; Lee et al., 2004). Fission and fusion work opposing one another but also work together in maintaining the right balance of shape, size and number of mitochondria (Chan, 2012a). As mentioned above deletions of protein responsible for either of this processes are embryonic lethal (Chen et al., 2003; Elgass et al., 2013; Wakabayashi et al., 2009). That the deletion of OPA1 is as severe as the deletion of the mitofusins, points towards matrix mixing as being an important part of mitochondrial fusion, but it has also been reported that mitochondrial content mixing can occur when mitochondria touch each other briefly without fusing completely, this phenomenon has been named "kiss-and-run", which occurs frequently in a normal functioning mitochondrial network (Song et al., 2009; Chan, 2012a; Liu et al., 2009). This mixing of mitochondrial content is necessary because it constantly homogenizes the content of the mitochondrial population, which would otherwise become more and more heterogenized (Chan, 2012a; Chen, Chomyn, and Chan, 2005).

Fusion also allows for complementation of mtDNA mutations, because of this mitochondria can tolerate quite a high load of mutated mtDNA until the phenotype presents itself (DiMauro and Schon, 2003; Nakada, Inoue, and Hayashi, 2001). Loss of fusion diminishes mtDNA content, which shows its importance for mtDNA stability (Chen et al., 2010; Chan, 2012a; Chen, Chomyn, and Chan, 2005). Fusion is also depended on mitochondrial membrane potential and mitochondria with low membrane potential

cannot fuse and are subsequently degraded by mitophagy (Chan, 2012a; Song et al., 2007; Twig et al., 2008; Legros et al., 2002). These two mechanisms allow mitochondria that have some dysfunction to be rescued by fusing with other functional mitochondria, while severely dysfunctional mitochondria get singled out by fission and degraded by mitophagy (Chan, 2012a; Twig et al., 2008). Lack in fusion furthermore leads to defects in the mitochondrial respiratory chain and diminishes the ability for stress response (Chen et al., 2010; Chan, 2012a; Chen, Chomyn, and Chan, 2005; Chen, McCaffery, and Chan, 2007; Chen, Liu, and Dorn, 2011).

Mitochondrial transport

Due to their distinct morphology with an axon up to one meter long neurons in particular, but other cells as well, face the challenge to distribute their mitochondria to sites where energy demand is high, like synapses or nodes of ranvier, and where calcium buffering is needed (Schwarz, 2013; Britt et al., 2016; Sheng, 2014; Lin and Sheng, 2015; Cai and Sheng, 2009; Saxton and Hollenbeck, 2012; Sheng and Cai, 2012). To meet this challenge neuron have a specialized transport system for mitochondria, which allows mitochondria to be transported from the soma to the axon terminal via anterograde transport along the microtubule network and from the axon terminal to the soma retrogradely to the soma, mitochondria frequently make pauses and change direction of movement (Schwarz, 2013; Britt et al., 2016; Sheng, 2014; Lin and Sheng, 2015; Cai and Sheng, 2009; Saxton and Hollenbeck, 2012; Sheng and Cai, 2012). In most neurons, approximately 30% of mitochondria are motile, while the vast majority remain stationary throughout the cell, especially at places with high demand for energy or Ca^{2+} buffering (Sun et al., 2013; Yi, Weaver, and Hajnóczky, 2004).

Transport of mitochondria is important to adjust to changes in energy demand, to remove dysfunctional mitochondria and replace them with fresh mitochondria (Lin and Sheng, 2015; Cai and Sheng, 2009; Saxton and Hollenbeck, 2012; Sheng and Cai, 2012). Long distant transport relies on the microtubule network, while the plus end of the microtubule in the axon points towards the axon terminal and travel in this direction is mediated by the kinesin motor family, therefore kinesins drive anterograde transport of mitochondria; see figure 1.4 (Lin and Sheng, 2015; Cai and Sheng, 2009;

Saxton and Hollenbeck, 2012; Sheng and Cai, 2012; Morris and Hollenbeck, 1995). For mitochondria the most important kinesin subtype, is the kinesin-1 (KIF5), which has three isoforms: KIF5A, KIF5B and KIF5C (Schwarz, 2013; Sheng, 2014; Pilling et al., 2006; Glater et al., 2006). While KIF5B is expressed in every cell type, KIF5A and KIF5C is restricted to neurons (Schwarz, 2013; Sheng, 2014). The kinesin transport requires ATP hydrolysis for its function, this is mediated by the N-Terminus of the kinesin motor protein, while the C-Terminus is responsible for cargo binding; see figure 1.4 (Schwarz, 2013; Gilbert et al., 1995; Karcher, Deacon, and Gelfand, 2002; Marx, Hoenger, and Mandelkow, 2009). There are also two member of the kinesin-3 family which seem to be involved in mitochondrial transport, namely KIF1B-α and Kinesin-like-protein 6 (KLP6), but as opposed to the kinesin-1 family their role in mitochondrial transport needs to be further examined (Schwarz, 2013; Saxton and Hollenbeck, 2012).

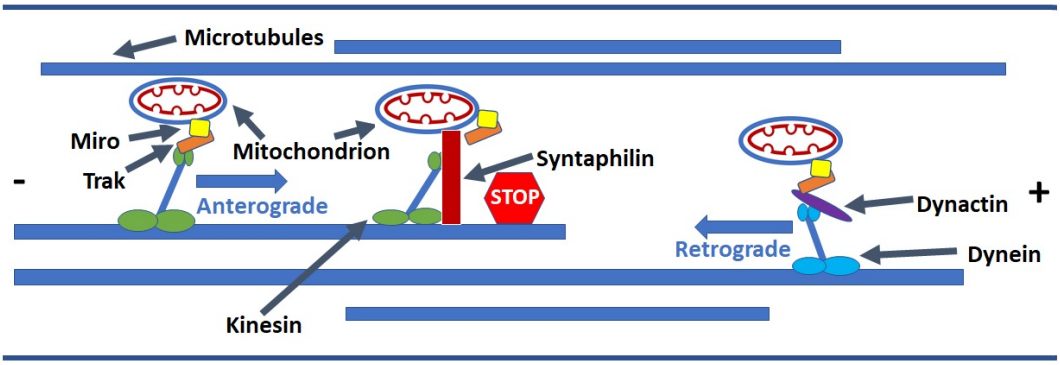

FIGURE 1.4: Mitochondrial transport in the axon depicted in a simplified graphical image, showing the proteins responsible for axonal mitochondrial transport. The kinesin motor proteins (green circles) are mediating anterograde transport along the microtubules (long blue lines), while dynein (light blue circles) mediates retrograde transport in the axon. There are several adaptor proteins binding the mitochondria to the motor proteins, with the TRAK (orange) proteins binding Miro1 (yellow), which is a calcium adapter protein and mediates mitochondrial transport to energy demanding spots in the axon. Dynactin (violet) is another adaptor protein connecting the TRAK proteins to the dynein motor proteins. Syntaphilin (red) acts as an anchor for mitochondria, which stops them in their tracks and helps keeping mitochondria and places with high energy demand.

Dynein drives mitochondrial transport in the direction of the minus end of the microtubule network, which in the axon is pointed toward the soma and thus dynein mediates retrograde transport of mitochondria; see figure 1.4 (Schwarz, 2013; Saxton and Hollenbeck, 2012; Pilling et al., 2006). Dynein contains multiple subunits, of which two heavy chains (DHC) are catalytic subunits, furthermore there are intermediate chains (DIC), light intermediate (DLIC) and light chains (DLC), which are responsible for ATP hydrolysis or cargo binding (Schwarz, 2013; Saxton and Hollenbeck, 2012; Roberts et al., 2013; Bhabha et al., 2016). Dynactin is also needed to bind to the microtubule network as well as dynein and mediate retrograde transport; see figure 1.4 (Schwarz, 2013; Saxton and Hollenbeck, 2012; Drerup et al., 2017). Since mitochondria can move anterograde as well as retrograde and dynein is attached to mitochondria moving in both direction, it is likely that kinesins and dynein coordinate the transport of mitochondria in concert (Schwarz, 2013; Saxton and Hollenbeck, 2012). Mitochondria attach to the motorproteins only indirectly via specialized adaptor proteins TRAK1 and TRAK2 in mammals, loss of either of these proteins disturbs mitochondrial transport; see figure 1.4 (Schwarz, 2013; Saxton and Hollenbeck, 2012; Brickley and Stephenson, 2011; Spronsen et al., 2013). TRAK1 is responsible for axonal transport of mitochondria by binding to both kinesins and dynein, while TRAK2 mainly mediates dendritic transport (Schwarz, 2013; Saxton and Hollenbeck, 2012; Brickley and Stephenson, 2011; Spronsen et al., 2013; Kimura and Murakami, 2014).

Another important protein for mitochondrial transport is the Rho GTPase Miro, which is located at the outer mitochondrial membrane and mediates binding of mitochondria to the TRAK1/2 proteins and therefore attachment to the kinesin or dynein motor proteins; see figure 1.4 (Schwarz, 2013; Lin and Sheng, 2015; Saxton and Hollenbeck, 2012; Ahmad et al., 2014; Las and Shirihai, 2014; Guo et al., 2005). Miro has four Ca^{2+} binding EF hands, which mediate dissociation of mitochondria from the motor proteins upon meeting increased calcium concentration, this directs mitochondrial movement to sites where they are needed for the buffering of calcium (eg synapses) (Lin and Sheng, 2015; Stephen et al., 2015b; Guo et al., 2005). Syntabulin is another kinesin mitochondria adaptor protein, which binds directly to the cargo binding site of the motor protein; see figure 1.4 (Cai,

Gerwin, and Sheng, 2005; Lin and Sheng, 2015). Another important protein that ensures mitochondria are present at sites with high energy demand, is the mitochondrial anchor protein syntaphilin, which is an axon targeted mitochondrial outer membrane protein; see figure 1.4 (Kang et al., 2008). Syntaphilin mediates binding of the microtubules to to mitochondria, thus bringing mitochondria to a stop (Kang et al., 2008). Deletion of syntaphilin leads to robust increase in mitochondrial movement, while overexpression abolishes mitochondrial transport in the axon (Kang et al., 2008; Sheng, 2014; Zhou et al., 2016). Syntaphilin is also required to halt mitochondrial transport via the Miro-Ca^{2+} pathway, as was shown by using synphilin knockout mice, in which activation of neurons, that normally activates dissociation of Miro from the TRAK proteins and thus stops mitochondrial transport, was not enough to stop mitochondria in neurons (Lin and Sheng, 2015; Chen and Sheng, 2013).

Mitochondrial changes in disease

Classical hereditary mitochondrial diseases result from mutations affecting mitochondrial genes and mostly lead to respiratory deficiency within the 5 complexes of the respiratory chain (Chan, 2006a; Wallace, 2005; Dimauro and Davidzon, 2005; DiMauro and Schon, 2003). There are now hundred of point mutations or changes within DNA encoding for mitochondrial proteins known, that lead to many different diseases, many of which affect the CNS (Chan, 2006a). All of these classical mitochondrial disease are maternally inherited, because the mitochondria are inherited from the zygote and the mitochondria in the sperm are marked with ubiquitin and targeted for degradation (Chan, 2006a; Wallace, 2005; Dimauro and Davidzon, 2005; DiMauro and Schon, 2003). As there are many copies of mitochondrial DNA within a single mitochondrion, the mutant DNA needs to pass a certain threshold for the phenotype to present itself, in many of individuals with mtDNA mutations there is still a mixture of wildtype mitochondrial DNA and mutant mitochondrial DNA within each mitochondrion, this state is called heteroplasmy (Chan, 2006a; Wallace, 2005; Dimauro and Davidzon, 2005; DiMauro and Schon, 2003; Hayashi et al., 1991; Nakada et al., 2001; Chen et al., 2010). This is the reason why most of the mitochondrial diseases progress with age, as there is an

accumulation of mutant DNA within the mitochondria over time (Chan, 2006a).

Because neurons are particularly dependant on mitochondrial function, they are one of the cells most easily affected by respiratory deficiency, but most cells do not lose respiratory function until there is a high load of mutated mtDNA, around 60%-90%, which is probably due to the dynamic state of mitochondria, which allows for the mixture of mtDNA and wild type via fusion with other healthy mitochondria, diluting mutated mtDNA (Chan, 2006a; Hayashi et al., 1991; Nakada et al., 2001; Youle and Bliek, 2012; Chen et al., 2010; Scott and Youle, 2010). Also constant mitophagy, the degradation of defective mitochondria via the PINK1 and parkin pathway, removes deficient mitochondria from the mitochondrial network (Bingo and Sheng, 2016; McWilliams and Muqit, 2017; Whitworth and Pallanck, 2017). In autopsy tissue of multiple sclerosis cases extensive neuronal damage can be found, and the main correlate of disability is axonal loss, which in turn is caused by inflammation, oxidative injury and demyelination of the axons (Mahad, Trapp, and Lassmann, 2015; Peterson et al., 2001; Trapp et al., 1998). Furthermore, it has been reported in several studies from independent institutes, that there is a neuronal mitochondrial dysfunction within the neurons, which in turn could lead to an energy deficiency in the neurons and their axons and contribute to the neurodegeneration taking place in multiple sclerosis (Dutta et al., 2006; Campbell et al., 2011; Broadwater et al., 2011; Witte et al., 2013; Kim et al., 2010; Hares et al., 2014; Fischer et al., 2013; Haile et al., 2017a). As reported in the section MS Pathology (1.1.2), demyelination leads to an intra-axonal accumulation of sodium, which needs to be pumped out of the axon by the Na^+/K^+ ATPase, which in turn requires ATP and is down regulated in multiple sclerosis lesions (Mahad, Trapp, and Lassmann, 2015; Mohd, 2010; Albers and Siegel, 1998; Lores Arnaiz and Ordieres, 2014; Young et al., 2008).

The combination of increased energy demand with dysfunctional mitochondria inside the axon leads to a state termed "virtual hypoxia" in the axon, which eventually leads to calcium overload and death of the axon (Trapp and Stys, 2009; Mahad, Trapp, and Lassmann, 2015). If the respiratory deficient mitochondria within the neuronal cell bodies of MS autopsy tissue reported previously, are transported to the axon to help with

the increase in energy demand after demyelination, an additional load of dysfunctional mitochondria would accumulate in the axon, leading to an even further increase of ROS and tissue damage, without the adequate energy production (Mahad, Trapp, and Lassmann, 2015). The accumulation of mitochondria inside the axon after demyelination was already reported previously, the question where these mitochondria come from is one of the aims of this thesis (Mahad et al., 2009; Witte et al., 2009; Zambonin et al., 2011; Ohno et al., 2011).

Mitochondrial changes in demyelinating diseases

Myelination of the axons not only allows for an increased speed in signal conduction, but also accounts for an energy efficient way of signal transmission (Mahad, Trapp, and Lassmann, 2015; Neishabouri and Faisal, 2011). As mentioned in section MS Pathology 1.1.2 in demyelinating diseases, like MS, demyelination of axons leads to a redistribution of NaV1.2 and NaV1.6 ion channels along the axon and increased sodium influx into the axon (Craner et al., 2004b; Witte et al., 2014). To pump the additional ions out of the cell, more ATP powered Na^+/K^+ exchangers are needed, which increases the energy demand of the demyelinated axon (Trapp and Stys, 2009; Mahad, Trapp, and Lassmann, 2015; Mohd, 2010; Albers and Siegel, 1998; Lores Arnaiz and Ordieres, 2014). To cope with this increased energy demand more mitochondria are needed at the demyelinated site, which leads to an accumulation of mitochondria in the demyelinated axon, as a compensatory mechanism (Mahad et al., 2009; Witte et al., 2009; Zambonin et al., 2011; Ohno et al., 2011).

How this mitochondrial axonal response to demyelination (ARMD) functions in detail, whether newly mitochondria are made on the site of demyelination or transport from other sites of the cell is increased, is currently unknown. ARMD means more mitochondria (biogenesis), more mitochondrial activity, different morphology (more elongated through fusion), faster mobile mitochondria (transport) (Mahad et al., 2009; Witte et al., 2009; Zambonin et al., 2011; Ohno et al., 2011). The ARMD protects the axons from degeneration following the increased energy demand and increased oxidative damage after demyelination (Kiryu-Seo et al., 2010; Ohno et al., 2014). It has also been reported that neurons in MS display a

decrease in nuclear encoded mitochondrial genes, mitochondrial DNA deletions and a reduction of complex IV activity (Campbell et al., 2011; Dutta et al., 2006; Broadwater et al., 2011; Witte et al., 2013; Kim et al., 2010; Hares et al., 2014; Fischer et al., 2013; Haile et al., 2017a). How the axonal response of mitochondria to demyelination is impacted in neurons harbouring mitochondrial respiratory chain defects has not been studied. Preliminary data in the Mahad (unpublished) lab shows that in DRG specific mitochondrial mutant mice there is a gradual decline in mitochondrial content in myelinated axons. Upon demyelination mitochondria deficient in respiratory chain enzymes appear in the demyelinated axonal segment in mutants, contrasting the findings in wild-type mice.

In summary, multiple sclerosis is characterized by inflammation, demyelination, but also mitochondrial changes in the neuronal cell body, namely deficiency of some respiratory chain subunits (Noseworthy et al., 2000; Compston and Coles, 2002; Dutta et al., 2006; Campbell et al., 2011; Broadwater et al., 2011; Witte et al., 2013; Kim et al., 2010; Hares et al., 2014; Fischer et al., 2013; Haile et al., 2017a; Mahad, Trapp, and Lassmann, 2015). In order to understand and model multiple sclerosis better, a disease model needs to address these changes, while most models currently in use, only reflect parts of the mentioned changes in multiple sclerosis, there are no models that adequately model oxidative damage or mitochondrial deficiency in the neurons (Schuh et al., 2014; Dutta et al., 2006; Campbell et al., 2011; Broadwater et al., 2011; Witte et al., 2013; Kim et al., 2010; Hares et al., 2014; Fischer et al., 2013; Haile et al., 2017a).

1.3 Hypothesis and Aim

1.3.1 Hypothesis

1. The axonal response of mitochondria to demyelination (ARMD), which helps the axon to cope with the increased energy demand after demyelination, is constituted by a) anterograde transport of mitochondria from the cell body into the demyelinated axon, b) fusion of motile mitochondria with the stationary mitochondria in the demyelinated axon

and c) biogenesis of mitochondria in the neuronal cell body

2. The ARMD is perturbed in neurons with complex IV deficiency by the lack of mitochondrial activity, reduction in mitochondrial numbers, reduction in fusion and reduced anterograde transport of mitochondria.

1.3.2 Aim

During my PhD thesis, I will use *in vitro* and *in vivo* techniques to look at fusion/fission dynamics and transport under basal and experimentally demyelinated conditions. I will use a cerebellar slice culture system to determine which mechanism drives the ARMD and where these additional mitochondria come from. I will analyse demyelinated axons and compare with them myelinated axons in mitochondrial mutant mice and controls to determine whether the ARMD is perturbed in mitochondrial mutants. Furthermore, I intend to test mitochondria targeted drugs as potential therapeutic agents to prevent axon degeneration.

Specific aims

1. Determine the timecourse of ARMD in cerebellar slice cultures to find the optimal time point for live imaging of mitochondria in the axon.

To determine the timecourse of the ARMD, cerebellar slice cultures will be demyelinated by using lysolecithin and then stained with immunohistochemistry at different timepoints after demyelination.

2. To assess the extent of transport and fusion dynamics in myelinated and unmyelinated axons of wildtype neurons.

To determine mitochondrial dynamics in myelinated and unmyelinated axons, I will tranduce purkinje-cells (PC) by using a lentivirus expressing a photoconvertible dye with mitochondrial targeting sequence, as PC have easy to follow axons and cerebellar slices are well established for myelination experiments.

3. To assess the extent of transport and fusion in demyelinated axons of wildtype neurons.

The ARMD is constituted by several aspects (increased numbers, activity, size and speed) and I will aim to identify the relative contribution of transport and fusion by using cerebellar slice cultures with lysolecithin-induced demyelination.

4. Manipulation of the ARMD using different compounds.

To assess the effect of blocking or enhancing certain aspects of the ARMD, I will use different compounds to either block mitochondrial fission and transport respectively, or enhance mitochondrial biogenesis.

5. To develop *in vitro* and *in vivo* systems to determine how the ARMD is affected in neurons lacking complex IV activity.

I will aim to determine what effect the presence of these non-functional mitochondria has on the ARMD using an *in vivo* and *in vitro* system. Preliminary data indicates that mitochondrial complex IV deficiency occurs in the cell body before it appears in the non-demyelinated axon and ARMD is perturbed in transgenic mice lacking cytochrome-c oxidase in neuronal cell body ($COX10^{fl/fl} - Thy1 - Cre - ERT2^{+-}$ mutants). The optimal timing for demyelinating the mutants is when there is no structural change but sufficient complex IV deficiency. I will therefore use the *in vivo* system ($COX10^{fl/fl} - Thy1 - Cre - ERT2^{+-}$) to determine which structural changes the deficiency of complex IV causes and to determine the optimal time point for demyelination. Because any observed change will be most pronounced at the end stage, I will start there and work my way back to earlier time points where there is no structural change apparent. I will check for signs of inflammation, synapse loss, effects on cell body or dendrites (axons have already been looked at in the Mahad lab). This *in vivo* data will then be compared to the situation in the slice culture system by inducing demyelination in a cerebellar brain slices derived from the $COX10^{fl/fl} - Thy1 - Cre - ERT2^{+-}$ mice. In the slice culture system, I will

manipulate mitochondrial fission/fusion, axonal transport and biogenesis to assess their effect on the ARMD.

Chapter 2

Timecourse of the ARMD

2.1 Introduction

2.1.1 Cerebellar slice culture and demyelinating agent

There are several recent publications about studying mitochondrial dynamics *in vivo* and *in vitro*, while *in vivo* offers the obvious advantage of seeing how the dynamics take place in the live animal, the possibility of easy manipulation is a key advantage that lies within the *in vitro* approach, especially in the organotypic brain slice culture which offers the best similarity to the *in vivo* situation is one of the most widely used *in vitro* techniques (Zambonin et al., 2011; Ohno et al., 2011; Kiryu-Seo et al., 2010; Ohno et al., 2014; Misgeld et al., 2007; Misgeld, Nikic, and Kerschensteiner, 2007). Organotypic brain slice cultures have been used to study areas from electrophysiology to assessing drug effects in a close to *in vivo* setting (Humpel, 2015; Suter, Smith, and Dudek, 1999; Miki, Hirai, and Takahashi, 2013; Miron et al., 2010). Another area that has been studied by using cerebellar brain slices is demyelination and remyelination and the most widely used demyelinating agent is lysolecithin (Miron et al., 2010; Birgbauer, Rao, and Webb, 2004; Zhang et al., 2011). Lysolecithin is, amongst the most widely used demyelinating agents, the one that affects mitochondrial function function the least, while also keeping the axons intact (Birgbauer, Rao, and Webb, 2004; Zhang et al., 2011; Komai, Hunter, and Takahashi, 1973; Keough, Jensen, and Yong, 2015; Jeffery and Blakemore, 1995; Wallace et al., 2003; Yu et al., 2007).

Cerebellar slice culture was chosen, not only because there are a lot of publications concerning demyelination, but also because the cerebellum has

a very distinct morphology and only a few different types of neurons, and the single output of the cerebellar cortex is coming from the purkinje cells, which are positioned between the molecular layer and granule cell layer in the cerebellar cortex (Sillitoe and Joyner, 2007; Mordel et al., 2013). The purkinje cells are one of the biggest neurons in the brain and have an easy to recognize morphology, because of their big dendritic tree (Kapfhammer, 2004). Furthermore, purkinje cells have easy to follow myelinated axons and have been used in previous studies of demyelination in organotypic brain slice culture (Miron et al., 2010; Birgbauer, Rao, and Webb, 2004; Zhang et al., 2011). Both the dendritic tree and the axons are preserved if the organotypic brain slices are cut in sagittal orientation (Miron et al., 2010; Birgbauer, Rao, and Webb, 2004; Zhang et al., 2011). Last but not least, the cerebellum is frequently affected in multiple sclerosis, often from the start of the disease (Tornes, Conway, and Sheremata, 2014; Weier et al., 2015). All these features make the cerebellum as well as the purkinje cell a reasonable good model to study mitochondrial dynamics in demyelinated axons.

2.1.2 Axonal response of mitochondria to demyelination (ARMD)

Previous studies have shown, that several mitochondrial parameters are changed in demyelinated axons of MS patients compared to healthy controls, this change has also been shown in animal models of the disease, as well as in tissue culture (Mahad et al., 2009; Witte et al., 2009; Zambonin et al., 2011; Ohno et al., 2011; Kiryu-Seo et al., 2010; Ohno et al., 2014). There is an increase in mitochondrial numbers, size, activity and speed of motile mitochondria in the demyelinated axon compared to the myelinated axon (Mahad et al., 2009; Witte et al., 2009; Zambonin et al., 2011; Ohno et al., 2011; Kiryu-Seo et al., 2010; Ohno et al., 2014). This ARMD, is an adaptive mechanism to deal with the increase in energy demand in the demyelinated axon, which is caused in part by the redistribution of sodium channels along the axon after demyelination, which in term needs more Na^+/K^+ pump activity to get rid of the excess sodium inside the axon (Craner et al., 2004b; Witte et al., 2014; Trapp and Stys, 2009; Kiryu-Seo et al., 2010; Ohno et al., 2014). The ARMD seems to be protective in the short term, as it was shown

by demyelinating snph-KO mice, in which the ARMD is not mounted. This lead to a higher number of alzheimer-precursor-protein (APP) positive bulbs in the snph-KO compared to the control, which indicates a short-term protective effect of the ARMD after demyelination (Ohno et al., 2014). Another study has shown the long-term effect of crossing a snph-KO with a *shiverer* mutant, which the authors claim to be a model for progressive multiple sclerosis (Joshi et al., 2015). In this case the disruption of the ARMD, by knocking out syntaphlin was protective, as the *shiverer*-snph-double-KO had a better survival rate than the *shiverer* (Joshi et al., 2015). The authors argue that over a long period, the mitochondria which are stuck in the axon, are more and more damaged and are subsequently damaging the axon via ROS and therefore argue that the increased content of mitochondria is harmful after a prolonged period of demyelination (Joshi et al., 2015).

2.1.3 Timecourse of the ARMD

While several studies described the different changes of mitochondrial parameters in the axon occurring as a response to demyelination in MS, as well as in different model systems, so far the timecourse of the ARMD and how it is mounted was not described (Mahad et al., 2009; Witte et al., 2009; Zambonin et al., 2011; Ohno et al., 2011; Kiryu-Seo et al., 2010; Ohno et al., 2014). To study the timecourse of the ARMD, I used an *in vitro* slice culture system with lysolecithin induced demyelination and immunohistochemistry (IHC) staining at different timepoints after demyelination. This approach also allowed me to determine the best time point to perform live imaging of the mitochondrial dynamics, which is shown in Chapter 4. The optimal time point for live imaging would be when the response is still strong in terms of dynamics and many mitochondria are transported to the axon.

2.2 Materials and methods

2.2.1 Cerebellar brain slice culture

Animals

All procedures were performed according to the 1986 Animals Act (scientific procedures) UK and were approved by the local ethics committee. For all the experiments C57BL/6 mice were used. For the generation of cerebellar organotypic slice cultures mice from P7 to P12 were used, because slice generated at this age ensures a good survival of purkinje cells, while already displaying many features of the adult structure of the cerebellum.

Dissection of the cerebellum

Every step was carried out on ice to minimize the tissue damage. For the dissection of the cerebellum, P7 to P12 C57BL/6 mice were decapitated with big scissors and placed into ice-cold dissection medium in a 60 mm petri dish. Medium sized bow scissors were used to cut the skin above the mid line of the skull. A curved forceps was used to pierce into the eyes to hold the head in place. Using small bow scissors the skull was penetrated above the middle of the mid line and cut along the mid line and to both sides of the skull. Using a forceps the skull pieces were peeled back and removed as much as possible. The connection between the cerebellum and the cerebrum was cut using a scalpel knife to cut in between the cerebellum and the cerebrum. Finally a curved spatula was used to remove the cerebellum and brain stem from the skull and immerse it into the ice-cold dissection medium, while the rest of the head was discarded. The whole dissection procedure was done in about 5 minutes.

Slicing with Leica VT1200S

The cerebellum with attached brain stem was then carried to the Leica VT1200S Vibratome, while immersed in dissection medium inside a petri dish placed in an icebox. For immobilizing the cerebellum on the magnetic stage cyanoacrylate superglue with gel control was used, for this several small drops of the superglue were placed in the middle of the magnetic

stage. The cerebellum was then picked up using a curved spatula and carefully placed sideways in the middle of the superglue drop to cut the cerebellum into sagittal slices. Sagittal orientation allows for the best preservation of purkinje cells, as their dendritic tree and the axon is orientated along the sagittal plane, only the axons of the granule cells are cut as they are orientated along the coronal plane. Before mounting the magnetic stage back into the Vibratome, the superglue was allowed to dry for a few seconds before immersion into the ice cold dissection medium which filled the cutting chamber of the Vibratome. On the Vibratome settings, the cutting thickness was set at $300\,\mu\mathrm{m}$, the cutting speed at $0.4\,\mu\mathrm{m}$ per second and the amplitude at 1.40mm. Using the automatic cutting mode, the front end rear cutting points were chosen. The wilkinson razor blade which was put in place before the procedure, was lowered as near as possible to the top plane of the slice before starting the cutting.

Each cut slice was transferred to a 6 well plate sitting on ice filled with a little of the ice cold dissection buffer, using a reversed broken glass pipette with an attached rubber bulb. If the slice was too attached to the rest of the brain, a forceps was used to sever the connection, without touching any region of interest. After the cutting was finished, the slices from the 6 well plate were transferred onto the Millicell® cell culture inserts (PICM0RG50) with $0.4\,\mu\mathrm{m}$ poresize, which were placed in another six well plate containing 1ml of slice culture medium per well. This plate with the Millicell® cell culture inserts and slice culture medium were put in an incubator at $37\,^{\circ}\mathrm{C}$ with 5% CO_2 at least 30 minutes before starting the slicing procedure. The membranes of the cell culture inserts allow the slices to get access to oxygen from the air above, while the slice culture medium supplies the slices with nutrients from below through the membrane. For the transfer of the slices the reversed broken glass pipette with attached rubber bulb was used. Because the slices need access to air and contact with the membrane for attachment, excess dissection medium from the membranes was carefully removed using a $1000\,\mu\mathrm{l}$ pipette with filter tips. Because the slices should not be to close to each other, the slices were moved around until the were placed roughly in the middle of the insert and far enough apart from each other by sucking and releasing medium with the pipette without touching the slices. The plate with the slices placed correctly was then put again into

the incubator, until the next round of slicing. The plate was labelled with date, mouse number and special procedures. After the last round of slicing was finished, the plates were put again into the incubator at $37\,^{\circ}\mathrm{C}$ with 5% CO_2 and the culture medium is changed one hour after slicing and thereafter every 2 days.

Reagents and Media

Dissection medium (for 200ml medium)
196ml HBSS (Life technologies)
2ml 450g/L D-glucose (5mg/ml; Sigma)
2ml Antibiotic/Antimycotic (Life technologies)
Keep on ice before dissection

Culture medium (for 40ml medium)
20ml MEM (Life technologies)
10ml HBSS (Life technologies)
10ml heat inactivated horse serum ((Life technologies)
0.41ml D-Glucose (5mg/ml; Sigma)
0.41ml GlutaMAX (Life technologies)
0.41ml Antibiotic/Antimycotic (Life technologies)

2.2.2 Demyelination with lysolecithin

In the literature lysolecithin concentrations ranging from 0.25mg/ml to 0.5mg/ml are most widely reported concentrations with incubation times reaching from 16 hours to 26 hours, with 0.5mg/ml for 17 hours being used in most studies (Miron et al., 2010; Ohno et al., 2014; Liu et al., 2010; Birgbauer, Rao, and Webb, 2004). Therefore for the demyelination of the slices 0.5mg/ml lysolecithin was added to the slice culture medium for 17 hours before replacing it with normal medium. The slices were then stained at several timepoints after demyelination to determine the timecourse of the ARMD. For this the slices were fixed with paraformaldehyde (PFA), after which antigen retrieval was performed, after which the slices were blocked before incubating them with the primary and secondary antibody.

2.2.3 Immunohistochemistry

For Immunohistochemistry slice culture tissue and frozen sections were used, the slides were labelled according to which antibodies, dilution and antigen-retrieval method would be used, and furthermore the date of the beginning of the current staining was indicated. After fixation with 4% paraformaldehyde (PFA) the slides or slices were washed and heat-induced antigen retrieval was performed by using a microwave. After the antigen retrieval step, the specimen were washed, before blocking with 2% NGS for 20 minutes on room temperature (RT). After the blocking step the primary antibody solution was directly applied on the slides or slices.

Frozen section staining

The frozen tissue was cut into whole brain sections, so that the cerebellum was readily observable. After cutting a piece of Whatman® paper and labelling it appropriately with date and type of tissue, a small drop of O.C.T. ™ compound (Tissue-Tek) was applied onto the paper. The tissue was put into that drop and put on fast freeze in a Leica CM1950 cryostat with a chamber temperature of $-20\,^{\circ}\mathrm{C}$ and the paper with the tissue on it was frozen onto a metal chuck. The chuck with the tissue on it was then fixed in the cutting chamber and the tissue was cut into $15\,\mu\mathrm{m}$ thick sections. The cut tissue was then put onto a coated glass slide, which was then labelled accordingly and left on room temperature to dry for about 60 minutes, before putting it into a $-80\,^{\circ}\mathrm{C}$ freezer for long term storage. Before the staining the slides were incubated 60 minutes on room temperature and then fixed in 4% PFA for 30 minutes. If needed the slides were blocked with 0.3% H_2O_2 in dH_2O for 30 minutes on room temperatures before antigen retrieval. For the frozen section a microwave was used to achieve antigen retrieval. For this the appropriate buffer was heated in the microwave on high setting until the solution began to boil, the slides were immersed into this hot solution for 1 minute. Afterwards the slides were briefly washed with dH_2O before washing them 3 times for a minimum of 2 minutes with TBS.

Antibody application

After the antigen-retrieval step, a PAP pen was used to make a hydrophobic circle around the sections for the following washing and incubation steps. The slides were then washed at least 3 times for 2 minutes with tris-buffered-solution (TBS) pH 7.6.

TABLE 2.1: Antibodies

Primary Antibody	Antibody type	Used concentration	Target	Source
COXI	mouse monoclonal IgG2a	1:200	Mitochondrially Encoded Cytochrome C Oxidase I	Abcam (ab14705)
MBP	Rat monoclonal IgG1	1:200	Myelin basic protein	AbD Serotec (MCA409S)
NF	Chicken polyclonal	1:2000	Neurofilament-(heavy)	EnCor Biotechnology (CPCA-NF-H)

Before the application of the primary antibodies, the sections were blocked for 20 minutes at room temperature using 2% normal goat serum (NGS) in TBS buffer. The primary antibodies were then also diluted in 2% NGS/TBS and after pipetting the antibody-solution on the sections the slides were incubated either over night at $4\,^{\circ}\mathrm{C}$ or for 1 hour and 30 minutes at room temperature. After the incubation with the primary antibody, the sections were washed at least 3 times for 2 minutes with TBS pH 7.6. The secondary antibodies were also diluted in 2% NGS/TBS, applied on the sections and incubated for 30 minutes at room temperature. For the double- or triple-labelling of different epitopes, primary antibodies from different species or different IgG subclasses were combined to prevent cross reaction of the secondary antibodies. The slides were then incubated with appropriate fluorescent secondary antibody diluted 1:200 in 2% NGS/TBS. After washing the slides again with TBS they were finally the mounted with

Vectashield mounting medium with DAPI (Vector) and put into a $-20\,^{\circ}\mathrm{C}$ freezer before analysis. Imaging was performed with a Zeiss LSM 710 confocal laser-scanning microscope.

Slice culture staining

The slices and a piece of surrounding membrane were cut out of the slice culture insert using a scalpel, the slices stayed attached to the membrane through the whole staining procedure. Similar to the frozen sections the slices were fixed in 4% PFA for 30 minutes before washing them with distilled water. The antigen retrieval was achieved by microwaving a 1mM EDTA (pH 8.0) solution until boiling and immersing the slices for 30 seconds. The transfer between different solutions was achieved by grabbing the membrane surrounding the slices with a flat forceps. The slices were then washed 3 times in TBS, by immersing them in a TBS filled well of a 24-well plate. After the washing steps, the slices were blocked for 20 minutes in another well filled with 2% NGS. During the blocking step, a wet chamber was prepared and the glass slides which was later used for the incubation of the slices with the different antibodies were labelled with slice culture information, used antibodies and date. Furthermore two circles were made on each glass slide by using a PAP pen, in which the antibody solution would be applied for the staining. After the blocking with 2% NGS, the primary antibody solution was slowly dropped into the PAP pen circles on the slides and the slices were transferred into the solution by using the flat forceps. The primary antibody was then incubated over night in the cold room at $4\,^{\circ}\mathrm{C}$, while the slices were free floating in the antibody solution. On the next day the slices were washed by removing the primary antibody solution by using a $200\,\mu\mathrm{l}$ pipette and applying TBS washing solution with a pasteur pipette. The washing step was repeated 3 times, before the secondary antibody solution, containing fluorescently labelled antibodies was applied and incubated for 90 minutes at room temperature, again the slices were free floating in the antibody solution to allow maximal access through the entire thickness. After the secondary antibody step the slices were washed again 3 times in TBS, after which a drop of Vectashield with dapi was added on the slides, before putting on the glass coverslip and nail polish to seal it. Before the Vectashield was added, the TBS washing

solution was completely removed and the slices were checked for orientation, by using the light reflection across the membranes and slices, which revealed a different reflection pattern when the slices were in the right orientation (top). The slides were then stored in the cold room at $4\,^{\circ}\mathrm{C}$ until imaging with the Leica LSM 710 confocal microscope.

Reagents and media

Citrate Buffer (pH 6.0)
1. Weigh out 1.47g citric acid per 500mL distilled water for a 15mM solution
2. Adjust to pH 6 using 0.1M Hydrochloric Acid or 0.1M Sodium Hydroxide solution

EDTA (pH 8.0)
1. Weigh out 210mg EDTA per 500mL distilled water for a 1mM solution
2. Adjust to pH 8 using 0.1M Hydrochloric Acid or 0.1M Sodium Hydroxide solution

PFA (4%)
1. Heat 500ml distilled water in a glass beaker to $65\,^{\circ}\mathrm{C}$ using a microwave and measuring the temperature using a thermometer between microwave cycles.
2. Weight out 40g of paraformaldehyde powder in a large weighing boat
3. Add paraformaldehyde to warmed distilled water in fume cupboard
4. Use hot plate and magnetic stirrer to mix the solution
5. Add a few drops of 1M NaOH to the solution and leave it on the stirrer until the solution has cleared
6. Add 500ml of Phosphate buffer pH 7.4
7. Adjust to pH 7.4 if needed using 0.1M Hydrochloric Acid or 0.1M Sodium Hydroxide solution
8. Make 40ml aliquots and freeze at $-20\,^{\circ}\mathrm{C}$ and store the rest in the cold room

Phosphate Buffer
1. Stock A: weight out 3.12g sodium dihydrogen orthophosphate and dissolve it in 50ml distilled water for a 500mM solution

2. Stock B: (500mM) weight out 14.15g disodium hydrogen orthophosphate and dissolve it in 250ml distilled water for a 500mM solution
3. Buffer composition: 47.5ml Stock A + 202.5ml Stock B, adjust to pH 7.4 using 0.1M Hydrochloric Acid or 0.1M Sodium Hydroxide solution and make up to 500ml with distilled water.

TBS-washing solution
Weigh out 300mg trizma base and 5g of NaCl per 500mL distilled water for a 5mM solution
1. Adjust to pH 7.6 using 0.1M Hydrochloric Acid or 0.1M Sodium Hydroxide solution

2.2.4 Confocal microscopy

The stained slices, as well as the frozen sections, were imaged using a Zeiss LSM 710 confocal microscope with a 63x NA 1.4 oil immersion objective. The microscope parameters were set to image Alexa fluor-488, Rhodamine-X-Red and Alexa fluor-633. The filters were set to catch the appropriate wavelengths and the laser power was at 6% for the green 35% for the red and 40% for the deep red channel. The images were captured by taking a z-stack at 2x zoom, a 1024x1024 pixel resolution and pixel dwell time of $1.06\,\mu s$ and saved as lsm files. For each image every plane of the z-stack was exported separately as a tif file for further analysis.

2.2.5 Image preparation

The tif files were then opened with photoshop to clean all non-axonal mitochondria from the images. For this the foreground and background colors were switched so that the white color rectangle is in the front and the black one in the back. Then the green channel, which contained the neurofilament staining for the axons, was selected, the colors were inverted and the threshold was set to get good shaped axons without having too much background. After the thresholding, the 'color range...' option in the panel 'select' was used to mark the whole image frame outside the axons that were selected by thresholding. After the selection was active, the blue

channel, which was the COX-I staining for the mitochondria, was activated and cut out to get rid of all non-axonal mitochondria. The cleared image was then saved as a tif in a new folder. The images with non-axonal mitochondria cleaned, were then opened in ImageJ (Fiji) and axons of a minimum size were selected randomly, marked with the freehand selection tool, cut out by using ctrl-x. The single axons were then copied into a new image file, created with the shortcut ctrl+n, and saved as a new tif file into a new folder.

2.2.6 Analysis of axonal mitochondrial parameters

To analyse the axonal mitochondrial parameters each single axon file was then again opened with ImageJ and analysed using several macros. First the macro was loaded via 'Plugins->Macro->Install...' in ImageJ and the first macro file named 'A1' was selected. After the macro was loaded the first image was added to ImageJ and the macro was started by pressing '1', which separated the three color channels. For the macro to work each channel was then thresholded, the threshold for the green channel (neurofilament for the axons) was always set to 128 automatically, the blue channel (COX-I for the mitochondria) was set automatically by using the default threshold setting and the red channel (MBP for myelin) was not used for analysis and thus closed. After threshold each of the used channels, the green channel was selected and with the macro shortkey 'a' the axonal area was automatically measured and inserted into an excel file sheet. The allocated axon number and the threshold for each channel was also inserted into the same excel file sheet. Then the length of the axon was measured by drawing a line along the axon, measured by pressing 'm' and also inserted into the excel file sheet. The green channel for the axon was then closed and the blue channel for the mitochondria was activated. By pressing the macro shortkey '2' the number of mitochondria and area sizes was measured by using the 'Analyse particle...' function of Fiji, which is integrated into the macro and measures pixel sizes from 5-infinity pixels to exclude very small particles. The results obtained from the measurements of the number of mitochondria and area sizes was then inserted into the excel sheet on another page, which automatically copied the number of mitochondria onto

summary sheet. The excel sheet also calculated the total mitochondrial area, which corresponded to the total measured area. The percentage of axonal area occupied by mitochondria was automatically calculated on the first sheet of the excel file sheet, by dividing the total mitochondrial area by the total axonal area and multiplying it by 100. Finally the average size of one mitochondrion was measured by dividing the total mitochondrial area by the number of mitochondria. This calculations were done separately for each axon, 40 axons per slice were done, and the average of each of the mitochondrial parameters was calculated and used for statistical analysis and graph creation in GraphPad Prism 6. In Graphpad Prism 6 'Enter and plot a single Y value' was selected and the calculated averages for each slice were inserted into the matrix. For creation of the graphs the dataset was selected in the 'Graphs' folder on the left and scatter plot from the 'Column' tab was selected, which automatically created a scatter plot from the dataset showing mean and error bars. For statistical analysis the 'Analyse' function was selected in the dataset matrix and 'Column analyses' was selected to compare two different datasets. Since the data is not expected to be normally distributed the 'Mann-Whitney-U' test was selected as a non-parametric test. Multiple column comparison was done by using the Kruskal-Wallis test. A p-value below 0.05 was regarded as being significant and assigned a '*' in the graphs.

2.3 Results

2.3.1 Comparison *in vitro - in vivo*

To check if the mitochondrial parameters (occupancy of the axons, number of mitochondria and size of single mitochondria) in the *in vitro* slice culture system is comparable to the *in vivo* situation, frozen sections from C57 mice and cerebellar slices were immunostained. For this slices from P10 mice were used and left in culture for 2 weeks before staining with Neurofilament (NF), Myelin Basic Protein (MBP) and COXI antibodies to visualize axons, myelin and mitochondria respectively. Also P24 frozen brain sections were stained with the same antibodies to compare the mitochondrial parameters of the axons in the brain sections to the mitochondrial parameters of the axons in the cerebellar slices; see Figure 2.1.

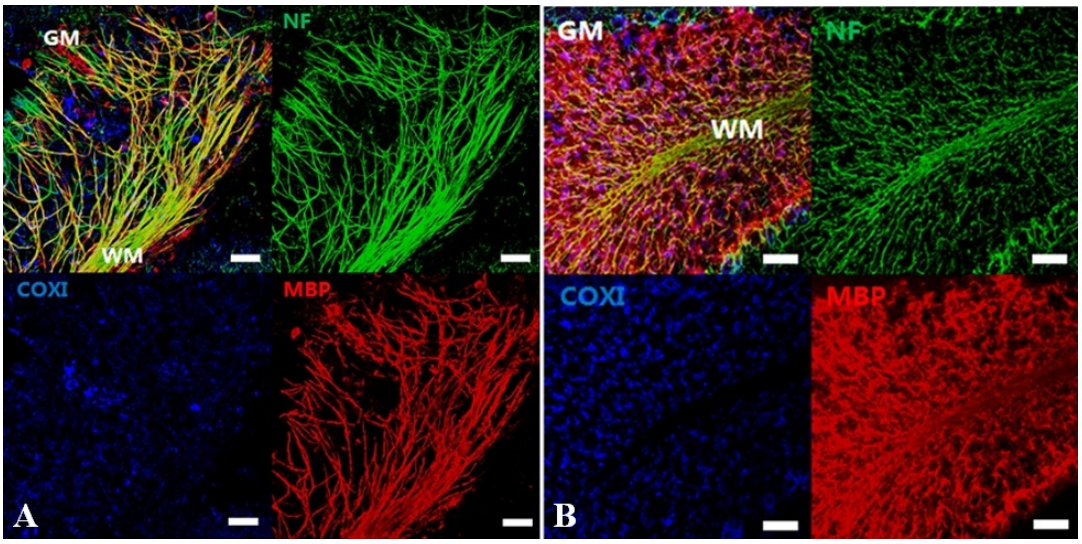

FIGURE 2.1: Comparison of mitochondrial parameters *in vivo* and *in vitro*, depicted by IHC staining for NF, MBP and COXI in a cerebellar brain slice (A) and a cryosection of mouse cerebellum (B), showing the overall similarity in appearance as well as myelination. Scalebar=50 µm; WM=white matter; GM=grey matter

Overall there was robust myelination in the cerebellar slice culture after two weeks in culture and in most slices several cerebellar foliae had healthy axons; see figure 2.1. The overall occupancy of the axons by mitochondria was very comparable between the slices and the *in vivo* situation, there was

a slight trend to lower number of mitochondria in the slices and the size of the single mitochondria showed a slight trend towards bigger mitochondria in the slices compared to the *in vivo* sections, but no significant difference was detected; see figure 2.2. This data indicates that the cerebellar slice culture after two weeks in culture is very comparable to the *in vivo* situation concerning myelination status and mitochondrial parameters inside the axon.

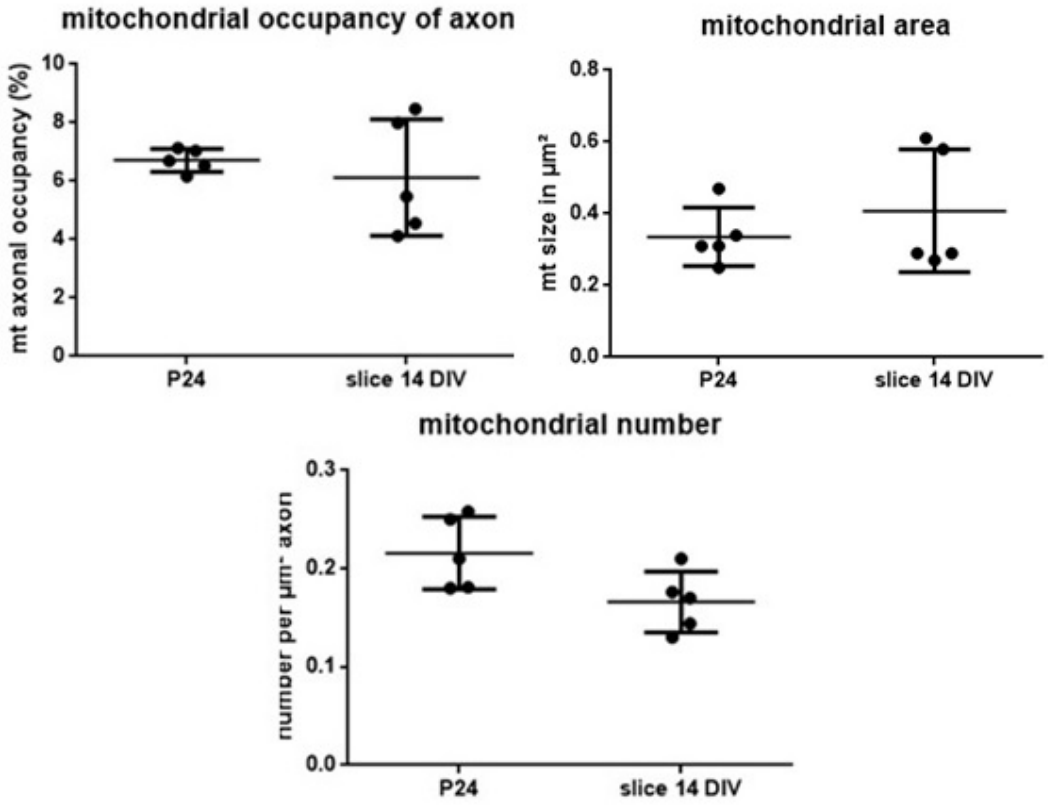

FIGURE 2.2: Similarity of mitochondrial axonal parameters between the cerebellar slice culture and cryosections of mouse cerebellum. There was no significant difference between *in vivo* and *in vitro* in the parameters measured. The slices from P10 mice have been in culture for two weeks. Each dot represents one slice or frozen brain section from one mouse and includes 40 analysed axons

2.3.2 Demyelination with lysolecithin

For the timecourse of the ARMD 0.5mg/ml lysolecithin was added to the slices after 1 week in culture for 17 hours as this is the most widely used

concentration of lysolecithin in demyelination experiments using organotypic brain slices. In my hands this concentration did not lead to complete demyelination of the cerebellar slices, but since only fixed immunohistochemistry stained slices were imaged for this chapter is was possible to randomly select demyelinated axons during the imaging process; see figure 2.3. After the lysolecithin was removed the slices were left in culture for another 24 hours, which was then the 24 hour timepoint after demyelination. The other timepoints were chosen accordingly 48, 72, 96, 120 and 144 hours after demyelination. The control slices were myelinated slices without lysolecithin after 1 or 2 weeks in culture.

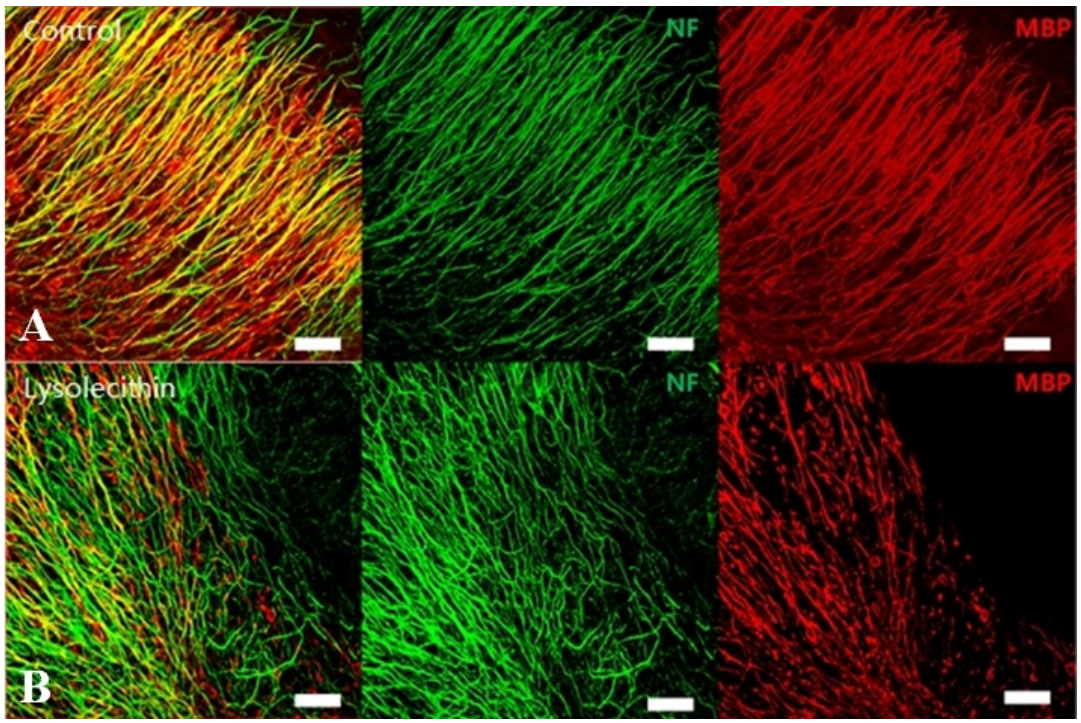

FIGURE 2.3: Demyelination of cerebellar slices cultures with lysolecithin using 0.5mg/ml lysolecithin for 17h. (A) Control after 1 week in culture stained for NF and MBP. (B) Lysolecithin added after 6 days in culture and stained the day after for NF and MBP. Scalebar=50 µm

This procedure resulted in sufficient demyelination in the cerebellar slices, so that is was possible to find at least 40 axons per slice that were demyelinated; see figure 2.3. The demylinated axons were then cut out in ImageJ and non-axonal mitochondria were cleared in Photoshop. The

mitochondrial occupancy, number and size was then analysed by using an ImageJ macro.

2.3.3 Timecourse of the ARMD

At all timepoints after demyelination with lysolecithin that were observed, the mitochondrial parameters were changed significantly compared to the myelinated control axons; see figure 2.4. The AMRD was mounted quick, with all parameters changed already after 24 hours, while some reaching the peak after 72 hours after demyelination.

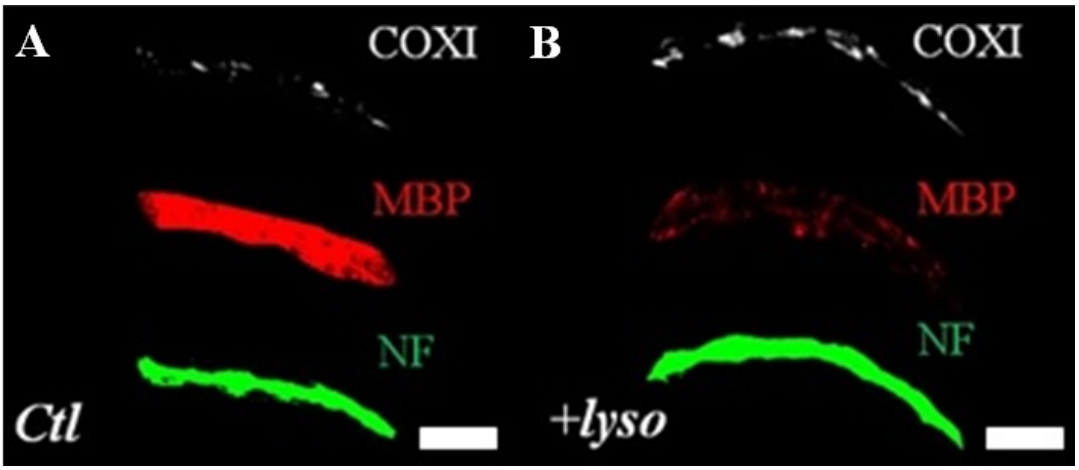

FIGURE 2.4: Impact of demyelination with lysolecithin on mitochondrial parameters in the axons, showing the comparison of control (A) and lysolecithin treated slices (B) after IHC staining for NF, MBP and COXI. Scalebar=5 µm

Mitochondrial occupancy

The percentage of mitochondrial occupancy of the axons increased sharply 24 hours after demyelination and continued to increase until it plateaued around 72 hours after lysolecithin treatment; see figure 2.5.

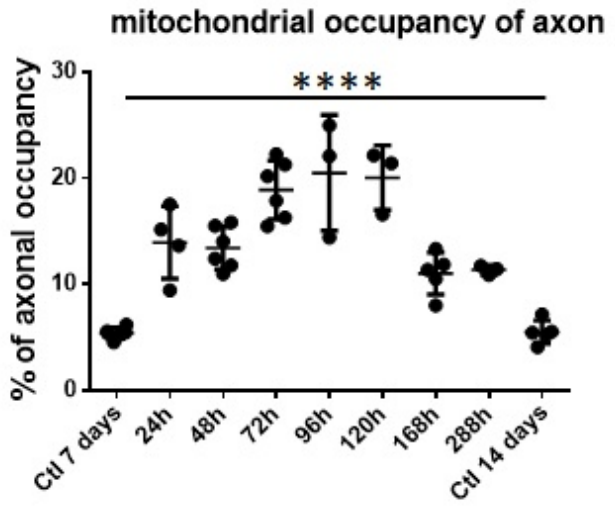

FIGURE 2.5: Impact of demyelination on the mitochondrial occupancy of the axons, depicting the mitochondrial occupancy of the axons (in percent) at different timepoints after demyelination. The multiple group comparison with the Kruskal-Wallis test showed a significant difference with a p-value <0.0001. Each dot represents one slice from one mouse and includes 40 analysed axons

The mitochondrial occupancy was still up 7 to 12 days after demyelination compared to baseline, but not as high as the peak at 72 hours after demyelination; see figure 2.5. At around 1 week after demyelination, remyelination starts to begin, but this was not sufficiently analysed in this thesis.

Mitochondrial size and numbers

The number of mitochondria in the axons increased even faster with the plateau already reached after 24 hours, with a slight increase at 72 hours after lysolecithin treatment; see figure 2.6. In contrast to the mitochondrial numbers, the size of the single mitochondria slowly increased over the timecourse, reaching the peak size at 96 hours after demyelination; see figure 2.6. All timepoints showed a significant increase in the size of the average single mitochondrion compared to the myelinated control.

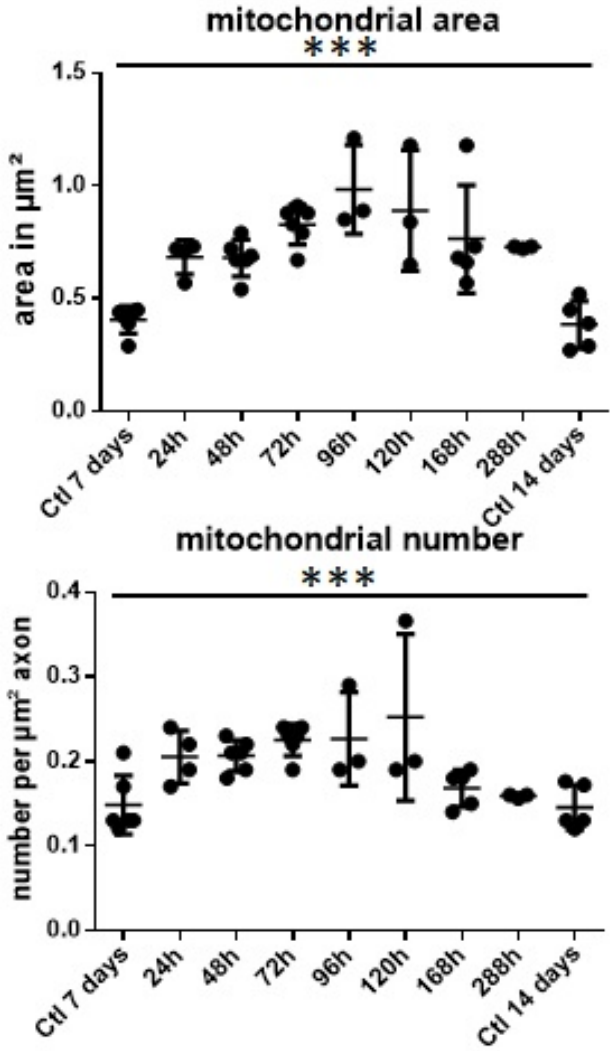

FIGURE 2.6: Top: Impact of demyelination on the mitochondrial size, depicting the size of single mitochondria in the axons (in μm^2) at different timepoints after demyelination. The multiple group comparison with the Kruskal-Wallis test showed a significant difference with a p-value of 0.0001. Bottom: Impact of demyelination on the mitochondrial numbers in the axons, depicting the mitochondrial numbers in the axons (per μm^2) at different timepoints after demyelination. The multiple group comparison with the Kruskal-Wallis test showed a significant difference with a p-value of 0.0004. Each dot represents one slice from one mouse and includes 40 analysed axons.

2.4 Discussion

2.4.1 The ARMD in cerebellar slice culture

This chapter showed that it is possible to get *in vitro* cerebellar slice cultures, that are comparable to the *in vivo* situation in terms of myelination, as well as mitochondrial parameters. Furthermore, we showed that the ARMD, which is readily observed in demyelinated axons in multiple sclerosis, can be modelled in this *in vitro* cerebellar slice culture model by using lysolecithin as a demyelinating agent.

Although all the parameters of the AMRD (increase in mitochondrial numbers, size, activity and speed in the demyelinated axon) have already been shown in multiple sclerosis and relevant disease models by using immunohistochemistry stainings of appropriate tissue sections, the timecourse of this ARMD has not been studied in detail yet (Mahad et al., 2009; Witte et al., 2009; Zambonin et al., 2011; Ohno et al., 2011; Kiryu-Seo et al., 2010; Ohno et al., 2014).

Here we show the ARMD timecourse over several days after demyelination, at several different timepoints. Already at 24 hours after demyelination the numbers of mitochondria in the axons was significantly higher than in myelinated control axons, this indicates a very fast response by transporting the mitochondria, presumably from the cell body, to the demyelinated axon. Over the following days the number of mitochondria in the axon remained increased. The size of the single mitochondria in the demyelinated axon increased steadily at every timepoint checked until reaching a peak at 4 days after demyelination. This indicates that mitochondrial fusion within the demyelinated axon is increased the days following demyelination.

The percentage of mitochondrial occupancy of the demyelinated axon reflects both of these mitochondrial parameters, as it increases quickly after 24 hours hours, where there is mostly transport of additional mitochondria into the demyelinated axon and increases steadily until reaching a peak at 4 days after demyelination, coinciding with the peak in mitochondrial size (fusion). This data shows that transport of additional mitochondria, presumably from the cell body, and mitochondrial fusion within the demyelinated axon are both important parameters for mounting the ARMD.

The mitochondrial occupancy going down after 7 to 12 days, could be a consequence of remyelination taking place, as remyelination typically starts one week after demyelination and is reported to be quite robust 14 days after. This change in mitochondrial occupancy also has been reported in multiple sclerosis autopsy cases, as the mitochondrial occupancy of remyelinated axon is reduced in comparison to demyelinated axons, but still elevated compared to the myelinated axon (Zambonin et al., 2011).

This ARMD is a consistent and robust reaction to demyelination of axons, which could be a response to the increased energy demand within the demyelinated axon, as a redistribution of sodium channels has been reported along demyelinated axons. This leads to an increased amount of sodium in the axon, which has to be transported out of the axon by the Na^+/K^+ ATPase (Craner et al., 2004b; Witte et al., 2014; Trapp and Stys, 2009; Mahad, Trapp, and Lassmann, 2015; Mohd, 2010; Albers and Siegel, 1998; Lores Arnaiz and Ordieres, 2014). There are several possibilities how this increased mitochondrial occupancy of the axon is mediated: Firstly, increased mitochondrial biogenesis in the perinuclear region of the cell and subsequent transport to the axon and fusion of newly transported mitochondria with the stationary mitochondria within the axon. Secondly, there could be increased transport from the soma to the axon without enhanced biogenesis, but this option would deplete mitochondrial content over time. The third option would be mitochondrial biogenesis in the axon, at the site where they are needed. Although there have been reports of mitochondrial biogenesis of mitochondria in the axon, this was shown only in developing regenerative stages of neurons, if axonal biogenesis of mitochondria in mature neurons takes place has yet to be shown (Amiri and Hollenbeck, 2008).

2.4.2 Optimal timepoint for live imaging mitochondrial dynamics

Besides determining the timecourse of the ARMD, which has been discussed in the previous section, this experiment was also used to find the optimal timepoint for performing live imaging of mEOS2 transduced purkinje cells (PC) to determine the mitochondrial dynamics in

demyelinated axons of PC in cerebellar slices cultures. To effectively perform live imaging on mitochondrial dynamics after demyelination, the different parameters of the ARMD should be at or near the peak.

Because our main goal for the mitochondrial dynamics experiment was to determine where these additional mitochondria in the demyelinated axon come from, it was important that the mitochondrial transport rate in the axon was at the peak. Since the 24h timepoint after demyelination already showed the peak in mitochondria numbers, indicating the peak in transport of mitochondria to the axon, it was decided the best timepoint for live imaging the mitochondrial dynamics was directly after the lysolecithin was removed from the medium.

Chapter 3

Mitochondrial dynamics in the myelinated axon

3.1 Introduction

3.1.1 Mitochondrial imaging *in vivo*

To study mitochondrial dynamics with live imaging, several mitochondrial proteins, as well as genetic models of mitochondrial targeted fluorescent proteins or transduction with a virus encoding a mitochondrial targeted fluorescent protein are the most widely used options (Zhou et al., 2016; Misgeld et al., 2007; Misgeld, Nikic, and Kerschensteiner, 2007). Mitochondrial dyes have the advantage of not needing any elaborate preparation, they are added to the tissue and stain the mitochondria after a short incubation period (Chazotte, 2011; Mitra and Lippincott-Schwartz, 2011). The most widely used mitochondrial dyes are cationic fluorophores, which means that their import into the mitochondria is dependant on membrane potential (Chazotte, 2011; Mitra and Lippincott-Schwartz, 2011; Kholmukhamedov, Justin M. Schwartz, and John J. Lemasters, 2014). One of the first mitochondrial targeted dyes was the Mitotracker, which is available in different fluorescent colors and stains all mitochondria in live tissue and, due to forming a covalent bond, is retained in the mitochondria even after the membrane is depolarized (Kholmukhamedov, Justin M. Schwartz, and John J. Lemasters, 2014). On the other hand dyes like TMRE, which do not form covalent bonds, are lost after the mitochondrial membrane is depolarized and therefore only labels mitochondria with intact membrane potential, while depolarized mitochondria are not labelled or will loose

labelling upon depolarization (Kholmukhamedov, Justin M. Schwartz, and John J. Lemasters, 2014). The main disadvantage of the mitochondrial dyes is they will stain mitochondria across all of the cell types in the tissue, so it is not possible to follow mitochondrial dynamics in a cell type of interest (Chazotte, 2011; Mitra and Lippincott-Schwartz, 2011; Kholmukhamedov, Justin M. Schwartz, and John J. Lemasters, 2014).

While the genetic models have the advantage of being independent of mitochondrial membrane potential and expressing the fluorophore only in the cells which express the selected promoter in a very reliable manner, it is very time and resource consuming to make a suitable genetic model. There are several publications of both *in vivo* and *in vitro* experiments using genetic models (Zhou et al., 2016; Misgeld et al., 2007; Misgeld, Nikic, and Kerschensteiner, 2007). Furthermore, it is possible to combine genetic labelling of mitochondria with mitochondrial dyes, for example Zhou et al (2016) looked at the effect of different manipulations on mitochondrial membrane potential and used a combination genetic labelling of all mitochondria (GFP-Mito) with TMRE, which is dependant on mitochondrial membrane potential (Zhou et al., 2016). This way mitochondria with intact membrane potential can be differentiated from mitochondria with depolarized membrane potential (Zhou et al., 2016).

The second possibilty of labelling only a subpopulation of cells is to use viral mediated transduction; see figure 3.1 (Zhou et al., 2016). There are several different virus types available for transducing cells *in vivo* and *in vitro*, with the most widely used being the lentiviruses and Adeno-associated viruses (AAV) (Kiryu-Seo et al., 2010; Ohno et al., 2014; Zhou et al., 2016; Stephen et al., 2015a). Both lentiviruses and AAV have been used previuosly *in vitro* to look at mitochondrial dynamics (Kiryu-Seo et al., 2010; Ohno et al., 2014; Zhou et al., 2016; Stephen et al., 2015a). Furthermore lentiviral constructs have been used previously to transduct PC in cerebellar slices and image mitochondrial dynamics (Kiryu-Seo et al., 2010; Ohno et al., 2014).

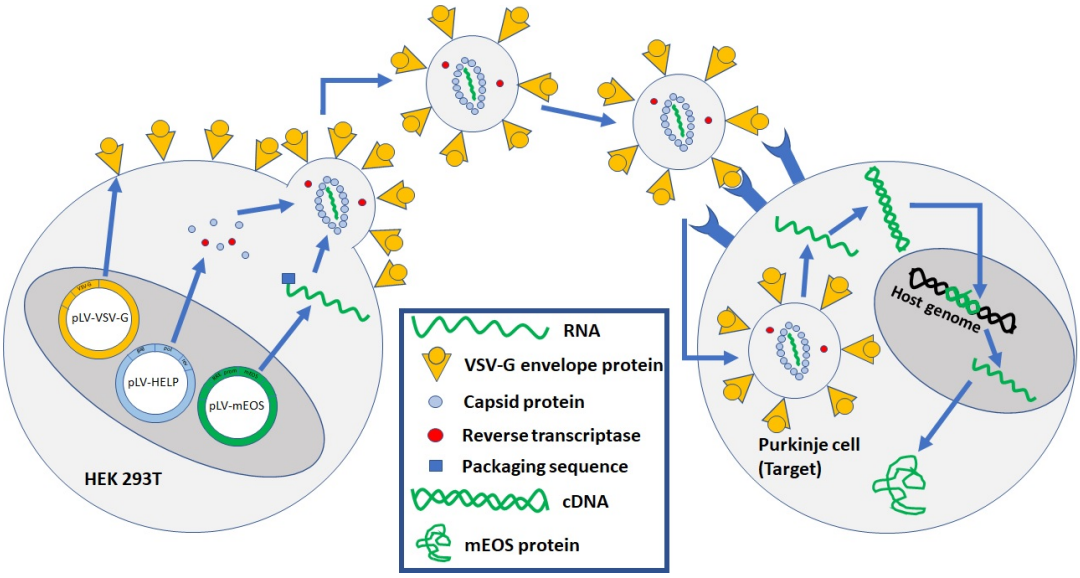

FIGURE 3.1: Lentiviral transduction of a target cell, depicting the HEK293T cells containing the packaging plasmid, transfer plasmid and envelope plasmid and the completely assembled lentivirus infecting the target cell, reverse transcribing the lentiviral RNA and integrating it into the target cell genome. Adapted from the short review Lentiviral vector production and cell transduction from Invivogen *http* : *//www.invivogen.com/docs/Insight*$_2$*01004.pdf*

Lentiviral vectors are single-stranded RNA plasmids derived from the HIV-1 virus. Lentiviruses belong to the family of retroviruses, which means that they are reverse transcribed from RNA into cDNA and inserted into the host genome for stable expression; see figure 3.1 (Escors and Breckpot, 2010; Sakuma, Barry, and Ikeda, 2012). Envelope proteins from several different viruses are available in combination with the usage of lentivirus, which allows for the infection of dividing as well as non-dividing cells (Cronin, Zhang, and Reiser, 2005). A lentiviral vector needs to contain several different protein coding sequences, which are spread across several plasmids, to allow the vector to transduce a target cell and integrate its genetic material into the host genome; see figure 3.1 (Kim et al., 2012; Durand and Cimarelli, 2011; Wollebo, Woldemichaele, and White, 2014). For the integration into the host genome, the lentivirus needs a packaging sequence (HIV-1 psi packaging signal), which is usually on the packaging plasmid, and long terminal repeats (HIV-1 5'LTR and 3'LTR), which are placed along the gene of interest on the transfer plasmid; see figure 3.1 (Kim

et al., 2012; Durand and Cimarelli, 2011; Wollebo, Woldemichaele, and White, 2014).

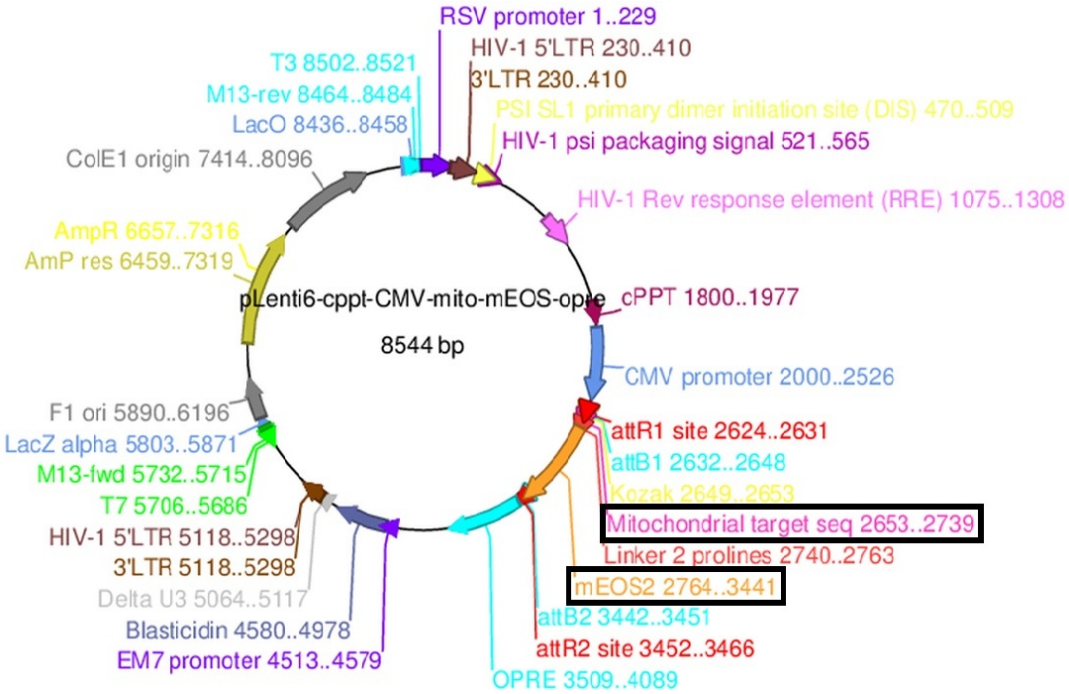

FIGURE 3.2: mEOS2 construct, depicting the transfer plasmid containing the mEOS2 (in orange) protein with attached mitochondrial targeting sequence (in pink). *Original graphic supplied by Pamela Brown and slightly modified for this thesis*

In the 3rd generation lentiviruses, the packaging plasmid is split into two packaging plasmid, encoding GAG (coding for the lentiviral core) and POL (codes for the reverse transcriptase) on one plasmid and REV (regulates viral protein expression) on another; see figure 3.1 (Dull et al., 1998; Cribbs et al., 2013). As mentioned above, envelope proteins from many different viruses are available to combine with lentiviruses, the envelope protein is located on the envelope plasmid (Cronin, Zhang, and Reiser, 2005; Dull et al., 1998; ; Cribbs et al., 2013). These plasmids are transfected into HEK 293T cells, which are left to grow for a few days with media changes in between (Cribbs et al., 2013; Merten, Hebben, and Bovolenta, 2016; ; Wang and McManus, 2009). The supernatant at harvest timepoint is collected and centrifuged to concentrate the virus and finally stored at $-80\,^{\circ}\mathrm{C}$ (Cribbs et al., 2013; Merten, Hebben, and Bovolenta, 2016; ; Wang and McManus, 2009). It is possible to integrate genes up to a size of 10kb into the transfer

plasmid, but with increase in size there is also a drop in viral titer, which leads to a lower transduction rate of cells (Holehonnur et al., 2015).

3.1.2 Visualizing mitochondrial dynamics in myelinated axons with mitochondrial targeted mEOS2

To determine the transport and fusion dynamics in the myelinated and unmyelinated PC axons, a lentivirus containing a construct with the photoconvertible protein mEOS2 with attached mitochondrial targeting sequence was used; see figure 3.2.

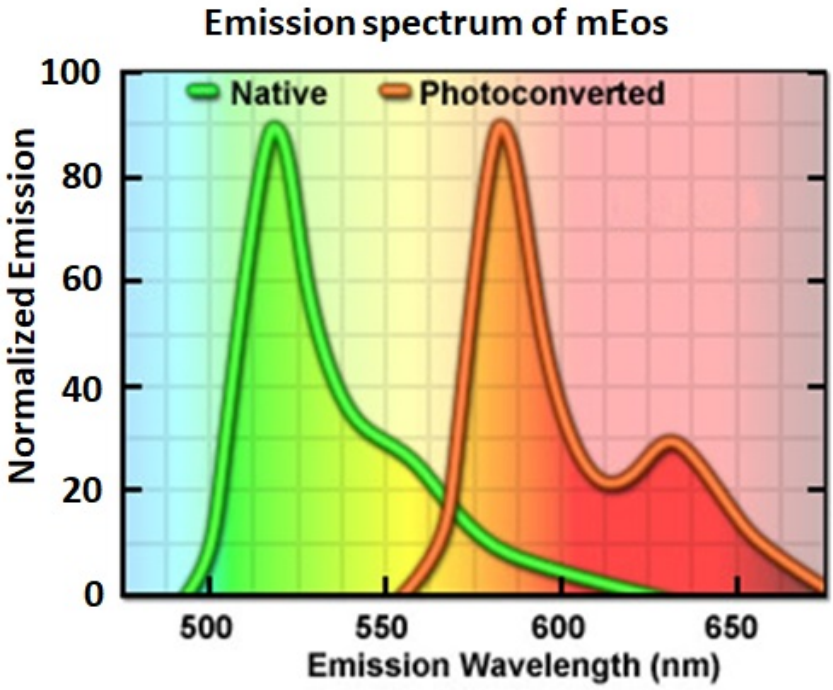

FIGURE 3.3: Spectrum of the mEOS2 protein, showing excitation spectrum of the unconverted green and converted red protein on the left and the emission spectra of both the unconverted and converted state of mEOS2 on the right. Graphic from: http://zeiss-campus.magnet.fsu.edu/articles/probes/highlighterfps.html

The mEOS2 is a monomeric protein derived from the coral *lobophyllia hemprichii*, which emits green light when excited with the 488nm laser; see figure 3.3 (McKinney et al., 2009). This photoconvertible protein can be irreversibly converted to a red emission spectrum by illuminating the

structure of interest with UV light; see figure 3.3 (McKinney et al., 2009). The emission spectrum of mEOS2 is very different between the unconverted green and converted red state, so that there is very little overlap between the two states, which allows for a good separation during imaging; see figure 3.3 (McKinney et al., 2009). There are several versions of the EOS protein available, with the monomeric version being the most widely used for protein labelling since its small size allows fusion proteins with single molecules; see figure 3.2 (McKinney et al., 2009). The advantage of mEOS2 is that it allows for maturation of the fluorescent protein at $37\,^{\circ}\mathrm{C}$, which is optimal when imaging cerebellar slices from mice (McKinney et al., 2009). One of the main advantages of using photoconvertible proteins is that it is possible to create two distinct mitochondrial populations according to their conversion status, unconverted green mitochondria and converted red mitochondria. This allows to more accurately follow mitochondria from one population (eg unconverted green) through another population of mitochondria (eg converted red). Another key advantage of differently labelled mitochondria is the ability to visualize and quantify mitochondrial fusion (Pham, McCaffery, and Chan, 2013; Owens and Walcott, 2012). There are both genetic models of photocovertible proteins available, as well as lentiviral construct expressing these photoconvertible proteins after transduction and both have been used to study mitochondrial fusion in different tissues both *in vivo* and *in vitro*, for example skeletal muscle and motor neurons in cell culture (Pham, McCaffery, and Chan, 2013; Owens and Walcott, 2012; Owens and Edelman, 2015).

3.2 Materials and methods

Animals

All procedures were performed according to the 1986 Animals Act (scientific procedures) UK and were approved by the local ethics committee. For all the experiments C57BL/6 mice were used. For the generation of cerebellar organotypic slice cultures mice from P7 to P12 were used, because slice generated at this age ensures a good survival of purkinje cells, while already displaying many features of the adult structure of the cerebellum.

3.2.1 Cerebellar brain slice culture

For the slicing protocol see methods section in chapter 2.

Injection using a Picospritzer III®

During the incubation of the plate with membranes, the Picospritzer III® from Parker was assembled and prepared. Glass capillaries (Harvard Apparatus, 1.5 OD x 1.86 ID x 75 L) were pulled and broken to a diameter between $3\,\mu\mathrm{m}$ and $15\,\mu\mathrm{m}$ by using a glass capillary puller model PP-830 by NARISHIGE Japan and breaking the needle tip with a Micro Forge MF-830 by NARISHIGE Japan. For the injection the plate with slices culture inserts was placed on a stereo microscope, besides which a metal plate with magnetic stand and attached micro-manipulator was placed. The needle was then fixed to the appropriate device of the Picospritzer III®, which was then in turn fixed onto the micro-manipulator. The concentrated virus solution was kept in $-80\,^{\circ}\mathrm{C}$ in $20\,\mu\mathrm{l}$ aliquots for long term storage and was defrosted on ice just before injection of the slices. To each aliquot $0.5\,\mu\mathrm{l}$ of Fast Green (FG) solution (1%) was added. The solution was then picked up with a pipette which had a long thin metal tip and transferred to the glass needle. The needle was then placed in a roughly 45° angle as close to the slice as possible. Using the micro-manipulator the needle was then manoeuvred to the purkinje cell layer (PCL) and the foot petal was used to inject the viral solution into the PCL, using a pressure of 12 psi and varying injection duration times (10-60ms) depending on the needle thickness. The applied pressure, needle thickness and injection duration times were each determined by trying many different combinations of these parameters in test experiments. For each slice 5-10 injection were made, visible by a distribution of the FG dye. After injection, the slices were put back into the incubator and after 2-3 hours the medium was changed, to prevent any possible detrimental effects of the FG dye on the PCs.

3.2.2 Media, reagents and devices

For the slice culture reagents see methods section in chapter 2.

3.2.3 Determine myelination status by using spectral confocal reflectance microscopy (SCoRe)

To determine the myelination status of the axons I used the spectral confocal reflectance microscopy (SCoRe) technique, which is a label free imaging method for myelin; see figure 3.4 (Schain, Hill, and Grutzendler, 2014).

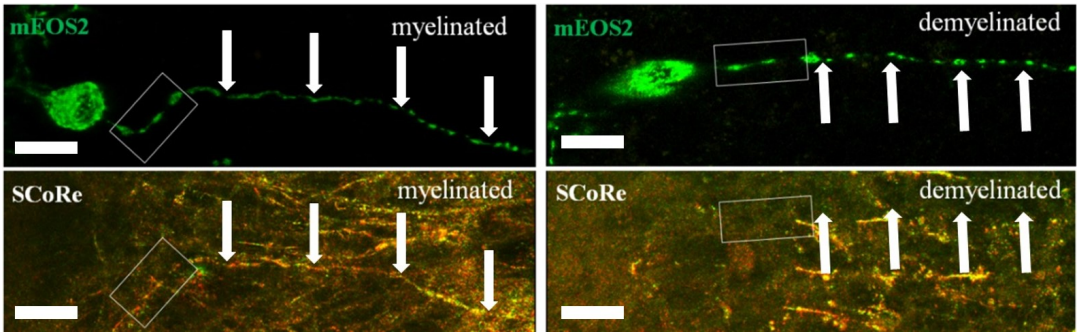

FIGURE 3.4: ScoRe technique depicting a myelinated (left panel) and demyelinated (right panel) mEOS2 positive axon. The white rectangle shows the area which was converted and used for live imaging. Scalebar=20 µm

Since the lipid rich myelin has such a high refractive index, which leads to a specific reflectance pattern when illuminated with different lasers (each laser has its own pattern), it is possible to visualize it while live imaging by collecting the reflectance of the laser with a very narrow collection spectrum in and around the lasers excitation wavelength; see figure 3.4 (Schain, Hill, and Grutzendler, 2014). The SCoRe imaging technique requires only very low laser power to create the characteristic reflectance pattern, so it does not excite any fluorescent proteins since the laser power is not high enough (Schain, Hill, and Grutzendler, 2014). The SCoRe image was taken in the same region and z-dimension as the fluorescent image of the mEOS2 positive cell, to allow overlapping of the two images; see figure 3.4.

3.2.4 Live imaging and conversion of mEOS2

The slices were imaged 14 days after the transduction with the lentivirus containing the mEOS2 construct. The lentivirus used for this study was supplied by Pamela Brown at the SURF facility of the University of Edinburgh, who cloned and created the construct. For live imaging of

mitochondria in the cerebellar brain slices an upright Zeiss LSM 880 airyscanner with a Zeiss 20x water dipping objective (NA 1.0) was used. The CO_2 independent Hibernate A was used as a live imaging solution and the slices were imaged in a heating chamber maintained at $37\,^{\circ}\mathrm{C}$. To convert the mEOS2 positive mitochondria from the basal green fluorescence to red fluorescence, selected parts of the neurons were illuminated with a 405nm laser with 3% laser power for 10 to 60 seconds, depending on the structure that was converted. The cell body required longer exposure time than the axon to be converted. To determine if the newly transported green mitochondria come from the cell body, a $50\,\mu\mathrm{m}$ segment adjacent to AIS was converted using the 405nm laser at 3% laser power for around 20 seconds. After the conversion a $85\,\mu\mathrm{m}$ segment was imaged, using a 20x water dipping objective from Zeiss (NA 1.0), every minute for 20 minutes. Newly incoming mitochondria were counted visually and on the kymograph, while their size was measured in ImageJ when they first appeared in the axon.

3.2.5 Analysis of movement and fusion

For the analysis of newly transported unconverted green mitochondria into the ROI each axon image series was manually analysed, for that each image of the series was checked for any new green mitochondria appearing either from the cell body direction or from the distal part of the axon.

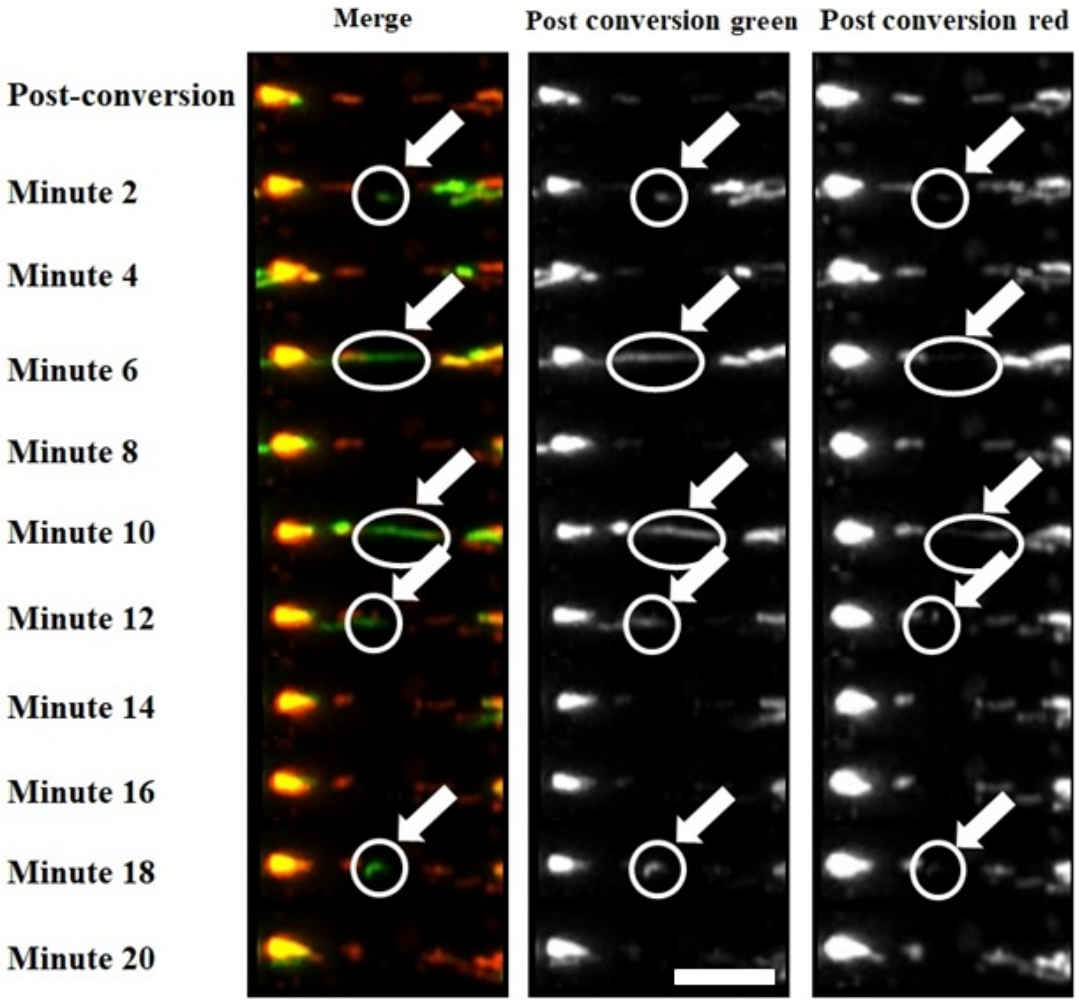

FIGURE 3.5: Newly transported mitochondria displaying only green fluorescence. Depicted is a timelapse image series showing several stationary red mitochondria with some green residue and newly transported mitochondria with green fluorescence only. Scalebar=10 µm

For each mitochondrion appearing, the direction of movement was noted, as well as the area of the mitochondrion was measured when it first appeared in the ROI.

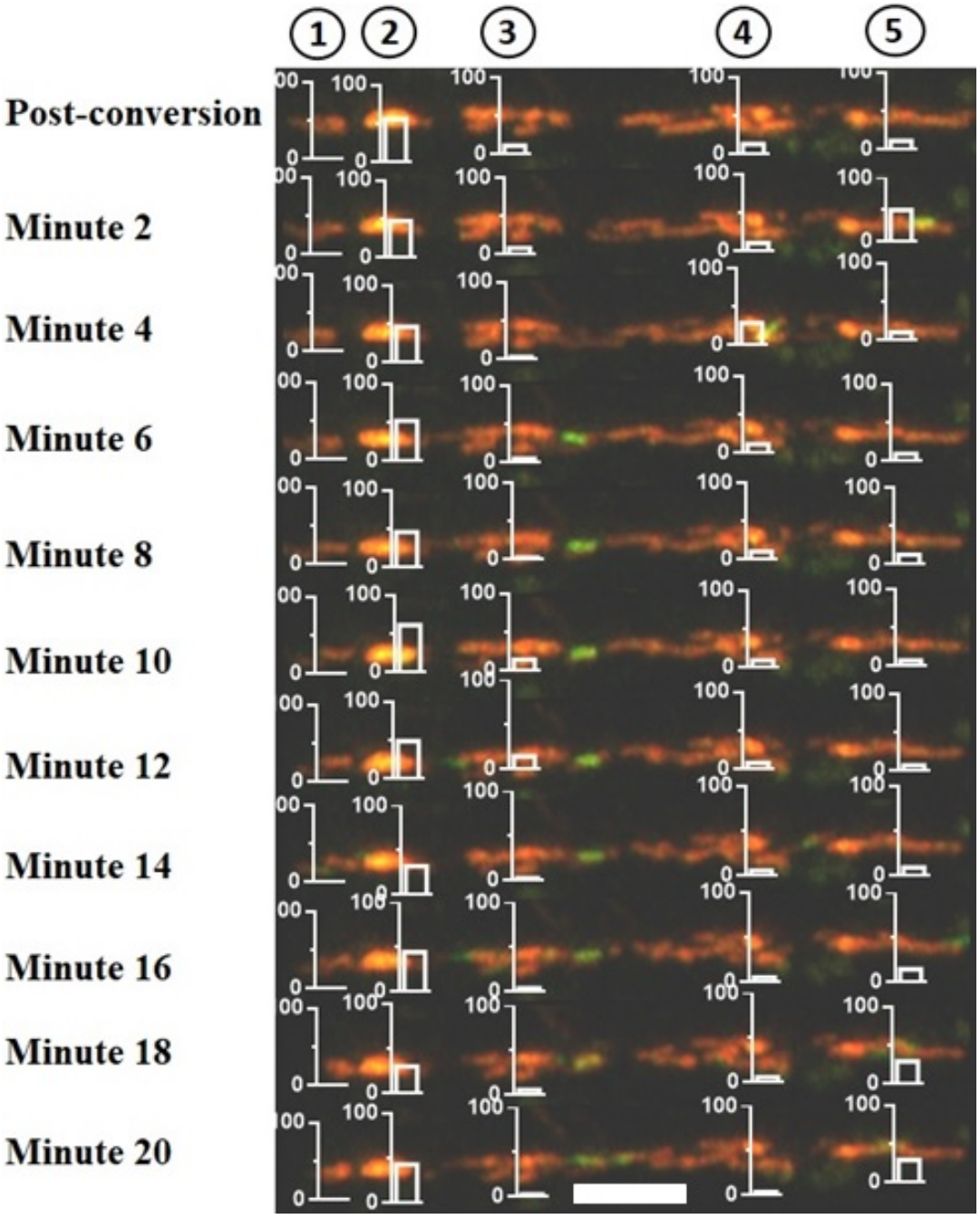

FIGURE 3.6: Fusion dynamics within a myelinated axon, shown in a timelapse image series with fusion data for 5 stationary red mitochondria within the ROI, increasing sharply in green fluorescence (bar graphs) after fusion events and loosing green fluorescence (bar graphs) after a fission event. Scalebar=10 µm

The newly transported mitochondria could be distinguished, because they displayed green fluorescence only, as opposed to the converted

mitochondria already present within the ROI, which were mostly red with some green residue inside. To calculate fusion of newly incoming unconverted (green) mitochondria with the stationary converted (red) mitochondria within the region of interest, an ImageJ macro to calculate the proportion of green in red fluorescence at different timepoints after conversion, corrected for the baseline green fluorescence right after conversion, was used. For this the baseline image was imported into ImageJ the channels were split into green and red, the red channel was thresholded using the default threshold and the green threshold was set to the same value. The first part of the macro was activated by pressing '2' on the red channel, which measured the area of the red mitochondria in the ROI by using the 'particle analysis' function of ImageJ. The second part of the macro was activated, after the two color channels were merged by using the 'Image->Color->Merge Channels...' option in Imagej, by pressing the macro shortcut '3', which calculated the green area inside the red area.

This process was done for the earliest timepoint after conversion and the 20 minute timepoint, and the baseline green in red percentage (earliest timepoint after conversion) was then substracted from the percentage of green in red at the 20 minute timepoint to calculate the increase in green inside red fluorescence, which represents the amount of fusion that took place during the imaging process, minus the amount of fission during that time. The green in red fluorescence increased sharply after fusion of an incoming green mitochondria with a stationary red mitochondria within the ROI, and decreased again after a fission event; see figure 3.6.

3.2.6 Kymograph generation and analysis of mitochondrial speed

Kymographs of the timelapse images were generated by using the ImageJ plugin KymographClear2.0, roughly this is done by performing a Z-projection of the hyperstack and registering the stack to the first image. Via the selected line tool the axon is traced, subsequently straightened by the macro and the width in pixels is selected, which was 20 pixels for these experiments. The linearized stack is then resliced and finally a z-projection

of the resliced image generates the kymograph (Pham and Chan, 2014; Mangeo, Prevo, and Peterman, 2016).

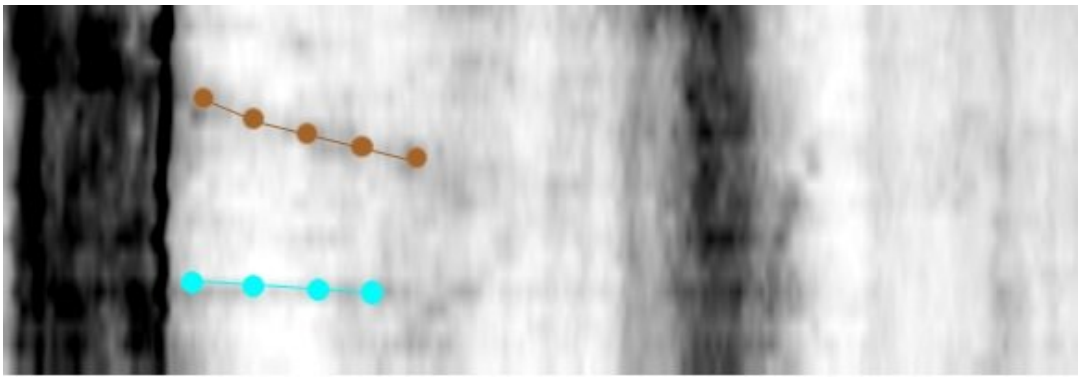

FIGURE 3.7: Kymograph of a myelinated axon showing the tracing of individual movements of mitochondria in the kymograph, which were subsequently used for the calculation of the mitochondrial movement speed.

Mitochondrial speeds were subsequently measured by using the Kymotoolbox Imagej plugin (designed by Fabrice Cordelieres), this was done by tracing the single lines in the kymographs with the segmented line tool and calculating the speed with the "analyze kymo" function of the Kymotoolbox plugin, which calculates the displacement amount of a traced particle over time; see figure 3.7 (Mangeo, Prevo, and Peterman, 2016; Zala et al., 2013). Since the ROI was only imaged every minute, it was not possible to measure 'real' mitochondrial movement speed, but rather a relative speed, which can be compared between different axons. The mitochondrial number, entering from anterograde or retrograde direction, was represented by the number and slope direction of tracks in the kymograph.

3.2.7 Immunohistochemistry

For Immunohistochemistry protocol see methods section in chapter 2.

Antibody application

For Immunohistochemistry protocol see methods section in chapter 2.

TABLE 3.1: Antibodies

Primary Antibody	Antibody type	Used concentration	Target	Source
COXI	mouse monoclonal IgG2a	1:200	Mitochondrially Encoded Cytochrome C Oxidase I	Abcam (ab14705)
MBP	Rat monoclonal IgG1	1:200	Myelin basic protein	AbD Serotec (MCA409S)
NF	Chicken polyclonal	1:2000	Neurofilament-(heavy)	EnCor Biotechnology (CPCA-NF-H)
Calbindin	Rabbit polyclonal	1:1000	calbindin D-28k	Swant

3.3 Results

3.3.1 Validation of SCoRe technique

To validate if the SCoRe technique really shows the myelin reflectance pattern it was used in combination with IHC antibody staining against MBP; see figure 3.8. Since this technique also works on fixed brain sections, PFA fixed brain sections were stained with NF (for axons) and MBP (for myelin) and subsequently imaged on a Zeiss LSM 710 confocal microscope to visualize axons and their myelin; see figure 3.8. On the same region the SCoRe technique was then applied by changing the confocal microscope settings and the resulting SCoRe imaging was then overlapped with the IHC staining from before; see figure 3.8.

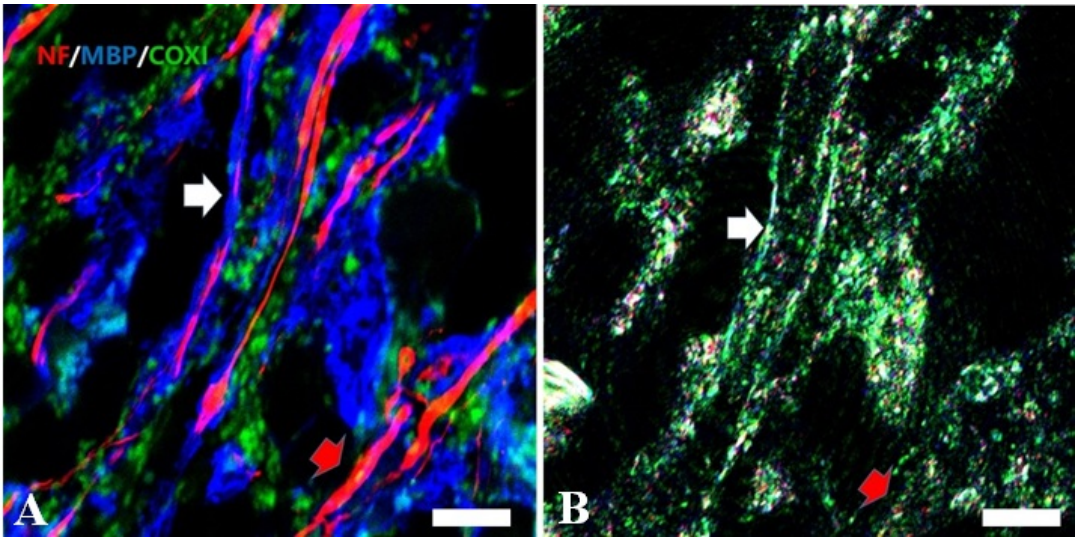

FIGURE 3.8: Validation of SCoRe technique. (A) IHC staining for NF and MBP to validate the SCoRe technique. (B) SCoRe image of same area as in (A). White arrow=myelinated axon which can also be seen in the SCoRe image. Red arrow=demyelinated axon, which is missing from the SCoRe image on the right. Scalebar=10 µm

3.3.2 Stability of mEOS2 protein and viability of cerebellar slices

To test the stability of the converted mEOS2 protein and the slice culture viability, cerebellar slices were injected with the Picospritzer III® to get

mEOS2 positive cells, at this point it was not important which cell type would be transduced, as this was just to evaluate the stability of the converted protein in general, as well as the slice viability.

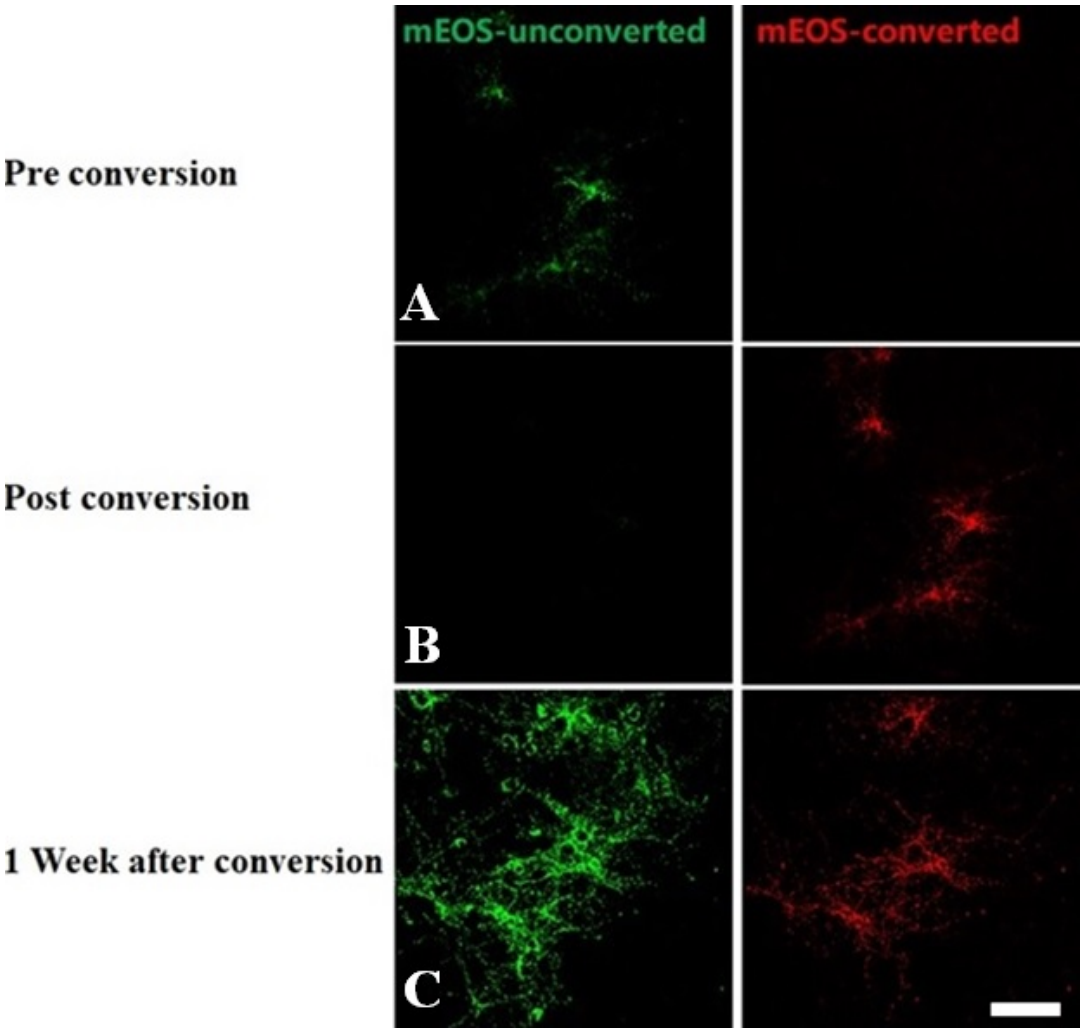

FIGURE 3.9: Stability of mEOS2 protein, shown in several different fluorescence images before, directly conversion after and 1 week after conversion. (A) Fluorescent images of cells before conversion displaying only green fluorescence. (B) After conversion mEOS2 is displaying only red fluorescence. (C) The same region 1 week after conversion with the red fluorescence being still stable, while a lot of new green mitochondria appeared over time. Scalebar=40 µm

After 2 weeks in culture a complete field of view was converted using the UV laser on the confocal microscope and the same region was observed 1 week after conversion; see figure 3.9. The red converted protein was still

observable and seemed to be stable even one week after conversion, while the converted cells were still alive and overall the slice culture appeared to be intact; see figure 3.9. Apart from the converted cells from the week before, many other cells that started expressing mEOS2 after the conversion and were visible by harbouring only unconverted green mEOS inside their mitochondria; see figure 3.9. An issue of the mEOS2 protein is the bleaching after laser exposure, which is quite significant after imaging every 30 seconds over 30 minutes, with the green being strongly affected by photobleaching and the red being relatively stable over this time frame. Because of this issue the imaging was limited to 20 minutes with 1 z-stack imaging per minute, to reduce the bleaching of the green.

3.3.3 Transduction of PC

To transduce cells within the cerebellar slice culture $5\,\mu l$ of the lentiviral solution containing the mEOS2 construct was pipetted on top of the slices right after the slicing procedure. This only lead to a transduction of cells on the outer rim of the cerebellar slices, while all the inner parts, including the PCL were not transduced at all. To get the lentiviral solution into the deeper layers of the cerebellar slice culture a pressure controlled Picospritzer III® system was used.

To image the transport and fusion dynamics in myelinated and unmyelinated axons in cerebellar PC, several different optimization steps were necessary to get mEOS2 positive PC in the cerebellar brain slices. The first step was to test several different viral envelope proteins, among them the WE, MLV-AMPHO and MLV-ecotrophic (murine leukemia virus), Rabies, MOK (Mokola virus) and the widely used VSV-G (Vesicular stomatitis virus glycoprotein) envelope proteins to test which of these give the best neuronal transduction efficiency; see figure 3.10. Indeed the VSV-G envelope protein resulted in the greatest number of positive cells, which was the reason for using this envelope for all future experiments; see figure 3.10.

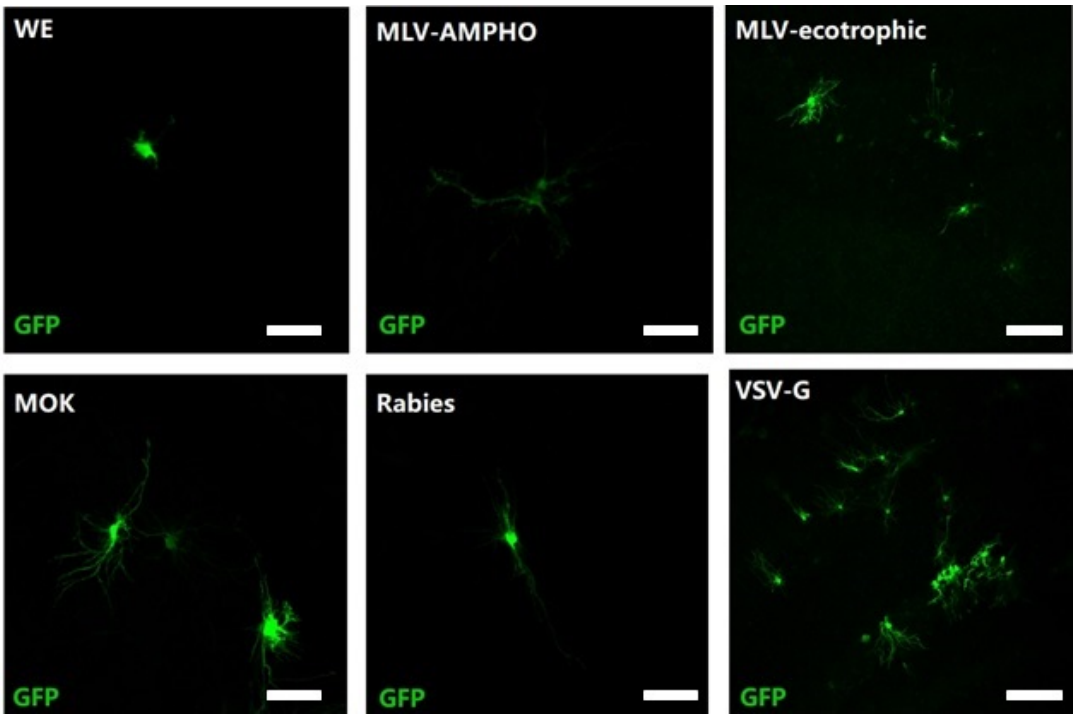

FIGURE 3.10: Lentivirus with different envelope proteins, showing transfected cells in green at different magnifications. Scalebar=20 µm for WE, MOK, Rabies and MLV-AMPHO and Scalebar=40 µm for MLV-ecotrophic and VSV-G

But, as revealed by IHC staining for calbindin, which in the cerebellum is specifically expressed in the PC, it did not result in any positive PC; see figure 3.11. Also, all the other envelope proteins did not transduce any cerebellar PC, while giving a lot less positive transduced cells overall. Since non of the envelope proteins lead to a transduction of PC in the cerebellar brains slices, an intense literature research was performed to find possible reasons. The japan based group lead by Hirokazu Hirai reported that a shorter (after 40 hours) harvest of lentivirus lead to a better transduction of PC *in vivo* and later showed in another publication that the reason behind this was the change in pH over time and the subsequent change in cathepsin K expression, as this was responsible for the switch from the neuron-preferential transduction at the earlier harvest timepoint (after 40 hours) to a glia-preferential transduction at the later harvest timepoint (after 64 hours) and this effect could be reversed by treating the HEK cells with cathepsin K inhibitor before harvesting the virus (Torashima et al., 2006; Goenawan and Hirai, 2012).

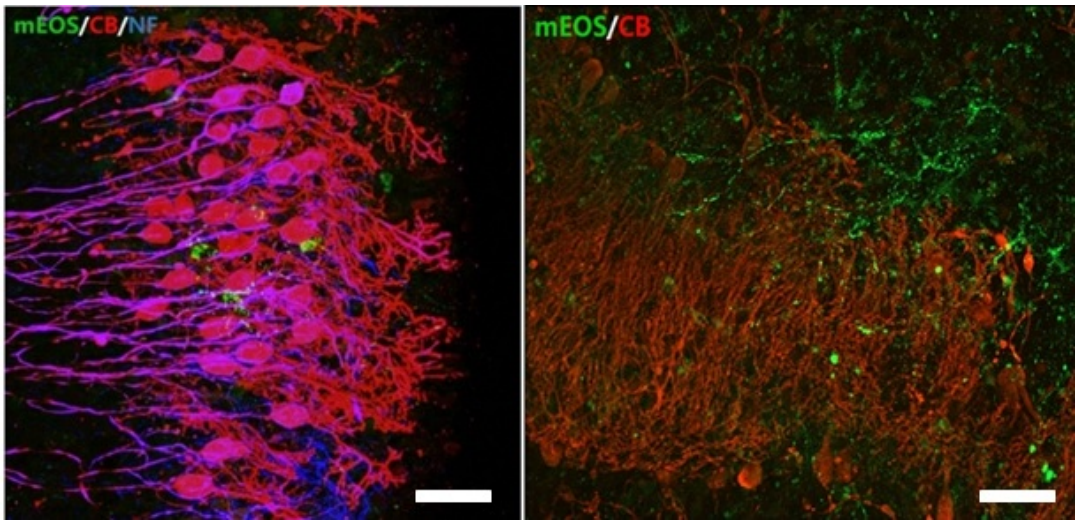

FIGURE 3.11: Lenti-CMV-mEOS2 not able to transduce purkinje cells in cerebellar slices. mEOS2 (green) transfected slices stained for PC (calbindin) in red showing no overlap between the two. Scalebar=left $40\,\mu m$ right $50\,\mu m$

This treatment with cathepsin-K inhibitor leads to a stronger transduction of neurons, as opposed to mostly glial cell transduction by lentivirus without cathepsin K inhibitor (Goenawan and Hirai, 2012). The treatment of the HEK cells with cathepsin K inhibitor still did not lead to transduction of PC in the cerebellar slices, but it did show mEOS2 positive neuronal cells in dorsal root ganglion (DRG) culture. Some more literature research showed some reports that stated that the CMV promoter, which is the promoter driving the mEOS2 construct, is not effective in some *in vitro* experiments and it was hypothesized that the CMV is silenced in the PC *in vitro* (Li et al., 2010; Kumar et al., 2015). It was shown by Wheeler et al that the CMV promoter is activated by neuronal depolarization and that this can be mimicked by adding forskolin, therefore forskolin was added to the medium one day after slicing and renewed two days later (Wheeler and Cooper, 2001). Around 12 to 14 days after the slicing procedure and adding forskolin, mEOS2 positive purkinje cells could be found in the slices; see figure 3.12.

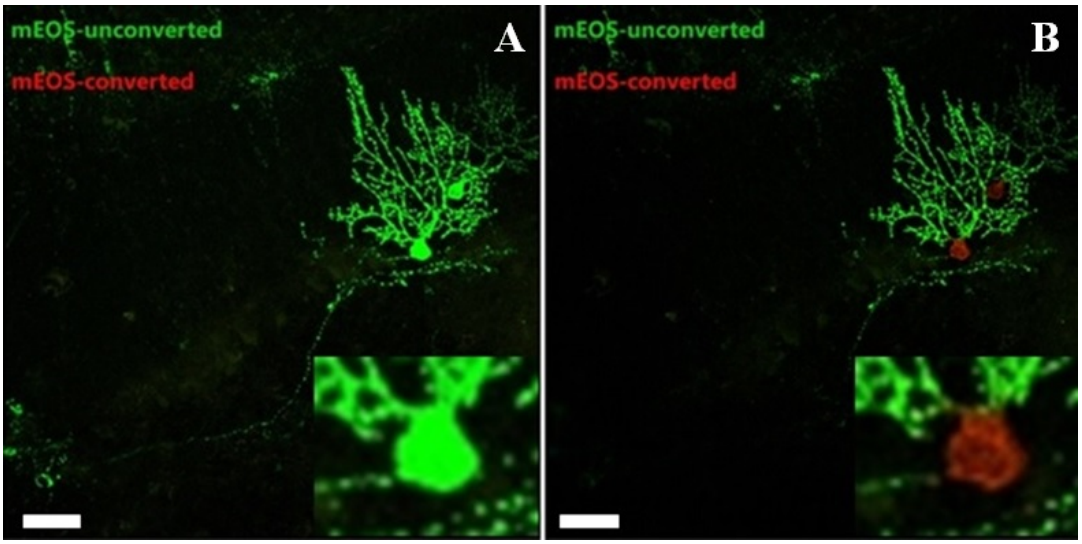

FIGURE 3.12: Transduction with mEOS2 in cerebellar purkinje cells and conversion with 405nm laser. mEOS2 positive PC unconverted (A) and with converted cell body (B). The inlets showing a magnification of the cell body before (A) and after (B) conversion with the 405nm laser. Scalebar=40 µm

Two different structures were converted to determine the mitochondrial dynamics in the axons of cerebellar PC, namely the cell body and the axon, which both lead to the axonal mitochondria fluorescing differently from mitochondria in the cell body; see figure 3.12. The conversion of the cell body resulted in the cells dying 1 day later. This could be a result of damage to the DNA by the strong UV illumination, because of the big number of mitochondria in the cell body it needed longer UV illumination than other structures of the cell.

In contrast to the conversion of the cell body, converting the axon lead to cells with converted axonal mitochondria that were still healthy 2 days after the conversion with UV laser. The ROI for the conversion with the 405nm laser was chosen so that the mitochondria in the axon are converted as complete as possible, while minimizing the conversion of the mitochondria in the cell body; see figure 3.13. This was achieved by converting the first part of the axon just after the AIS, as there was a spill-over conversion outside the ROI. This lead to the axonal mitochondria in the ROI being red, while the cell body mitochondria and the axonal mitochondria outside the ROI were mostly green fluorescent; see figure 3.13.

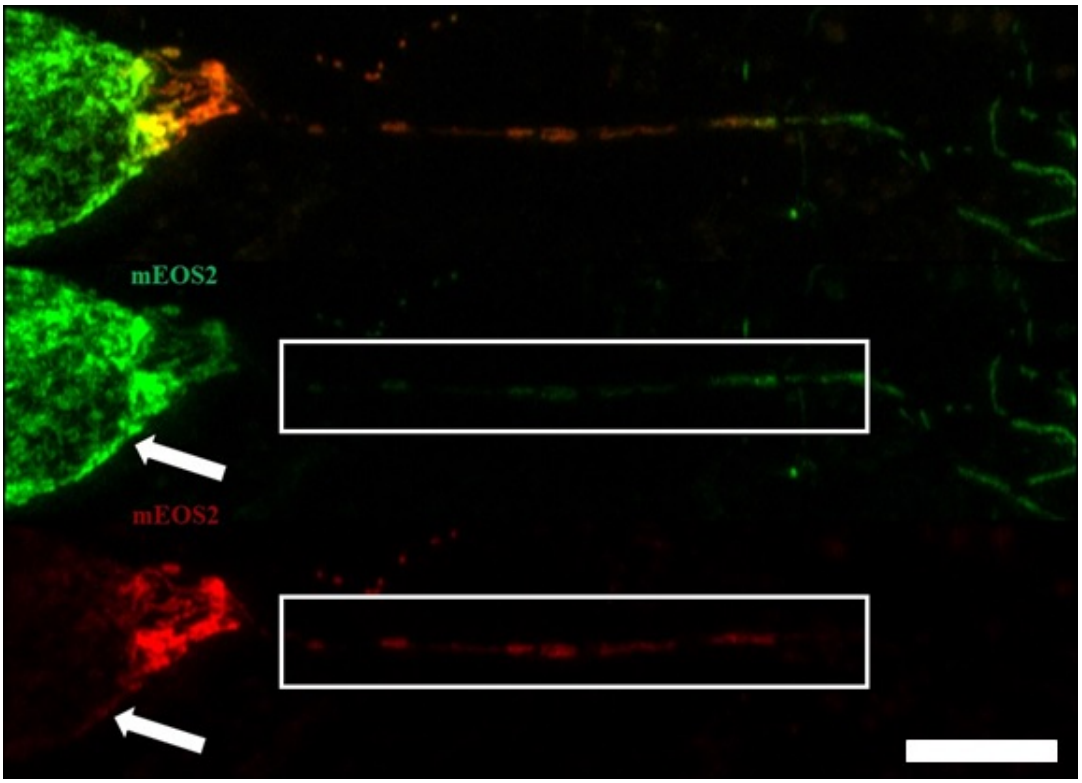

FIGURE 3.13: Conversion of mEOS2 in purkinje cells, depicted in fluorescence images showing a converted PC. The mitochondria in the cell body are still mostly green (arrow), while the mitochondria in the ROI (box) are fully converted to red fluorescence. Scalebar=10 µm

3.3.4 Mitochondrial dynamics of newly transported mitochondria

Mitochondrial movement in myelinated and unmyelinated axons

To check the dynamics of mitochondrial movement in the myelinated and unmyelinated axon, slices were injected with a lentivirus containing the mEOS2-construct and were imaged 14 days later; see figure 3.14. In the unconverted cell body and axon, all mitochondria displayed green fluorescence and only minor background red fluorescence was visible before conversion; see figure 3.13. Axons with sufficient positive SCoRe reflection in the field of view were counted as myelinated, whereas axon without any myelin in the field of view were counted as unmyelinated. Axons with uncertain SCoRe reflection were not included.

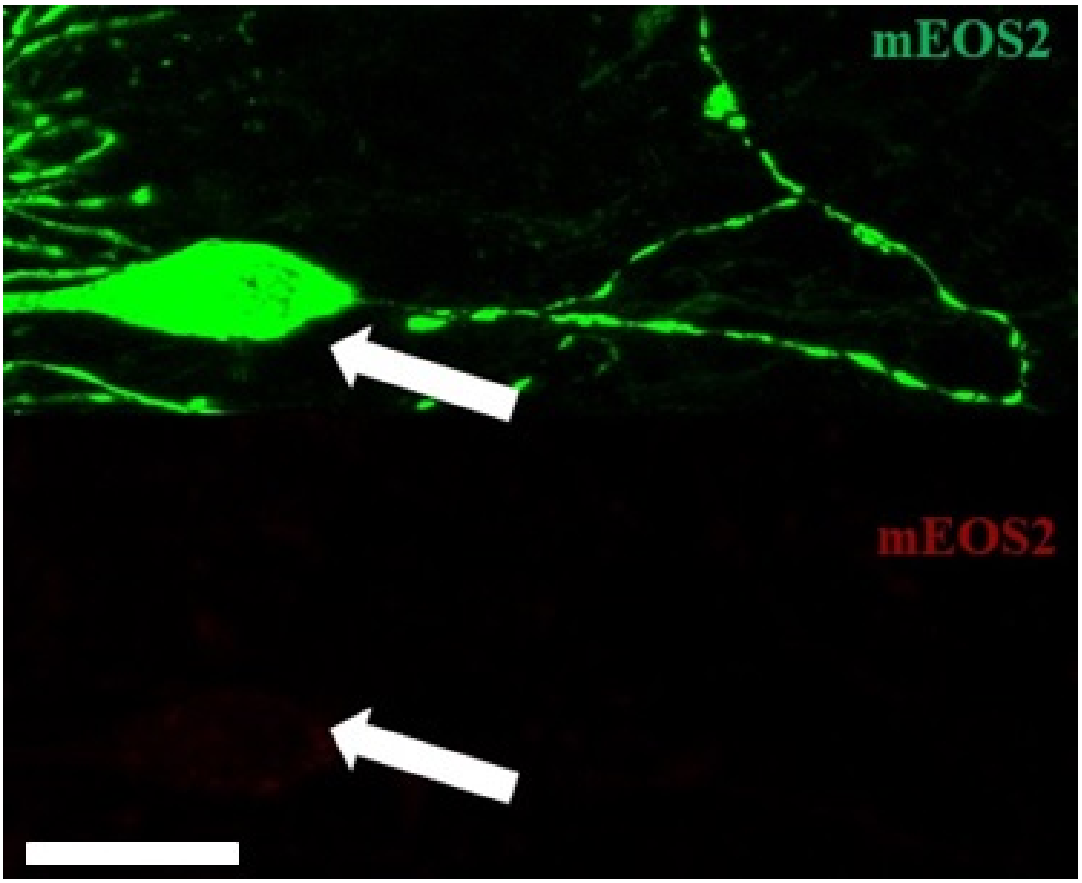

FIGURE 3.14: Fluorescence image of a pre conversion mEOS2 positive PC, showing that all mitochondria in the cell body and axon are green fluorescing before conversion and only minor red background fluorescence is visible. The arrows mark the cell body in the green and red channel images. Scalebar=20 µm

Since the axonal mitochondria in the ROI were all converted to red and all mitochondria outside the ROI (including the cell body and axon) were unconverted green fluorescent, newly transported green mitochondria could readily be observed and counted; see figure 3.15. Fusion of the newly transported green mitochondria with the converted red mitochondria in the axon lead to yellow fluorescent mitochondria in the ROI. This enabled the analysis of mitochondrial movement and fusion in the ROI. Overall there was a trend of more newly transported green mitochondria entering the converted part of the axon in the unmyelinated compared to the myelinated axon from the anterograde direction and significantly more newly transported mitochondria entering from the retrograde direction; see figure 3.16.

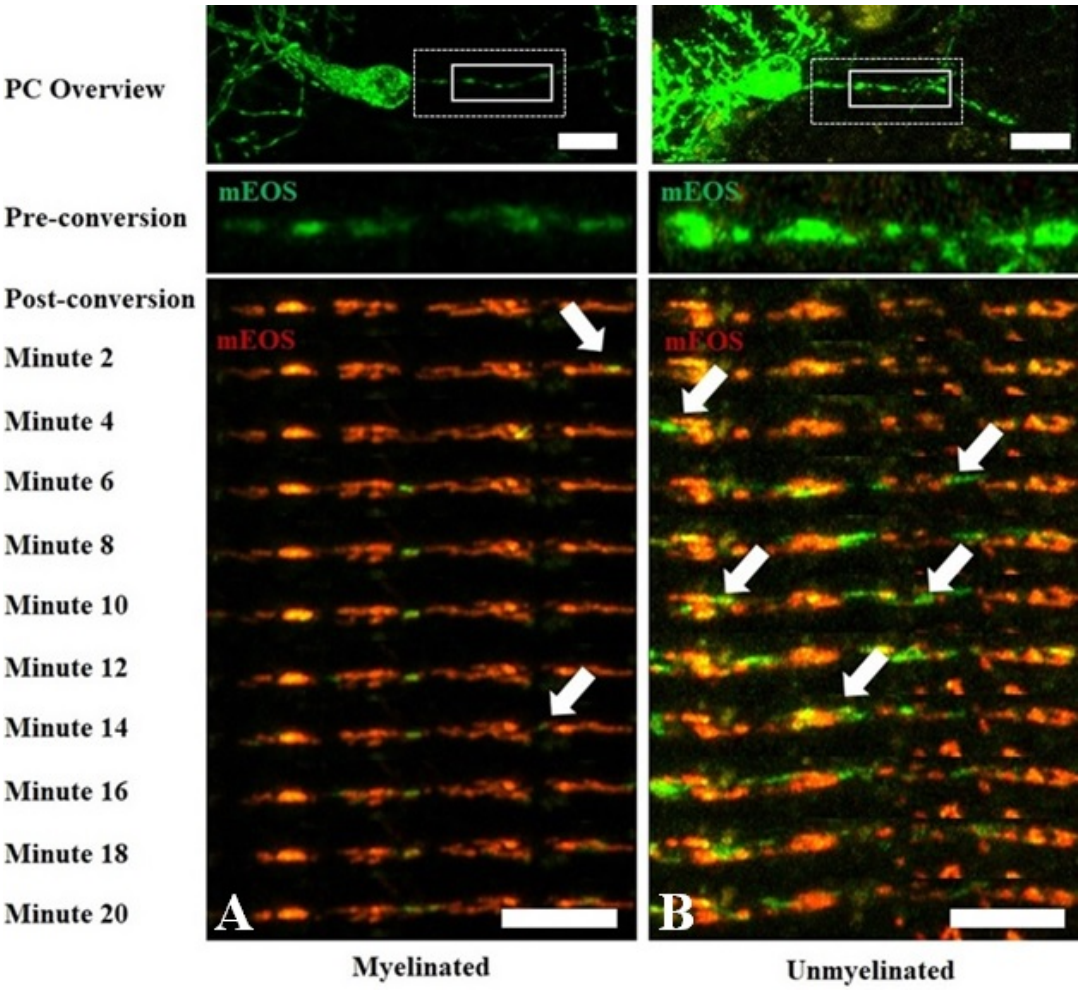

FIGURE 3.15: Mitochondrial transport dynamics in myelinated and unmyelinated axons. Depiction of a converted segment of a myelinated (A) and unmyelinated (B) axon, showing newly transported green mitochondria moving into the converted part (white arrows). The continuous box represents the converted part of the axon, while the dashed box indicates the ROI for imaging. Scalebar=20 µm for low magnification and 10 µm for high magnification images

The size of the newly transported mitochondria was significantly bigger in the anterograde direction and in the retrograde direction in the unmyelinated compared to the myelinated axons; see figure 3.16.

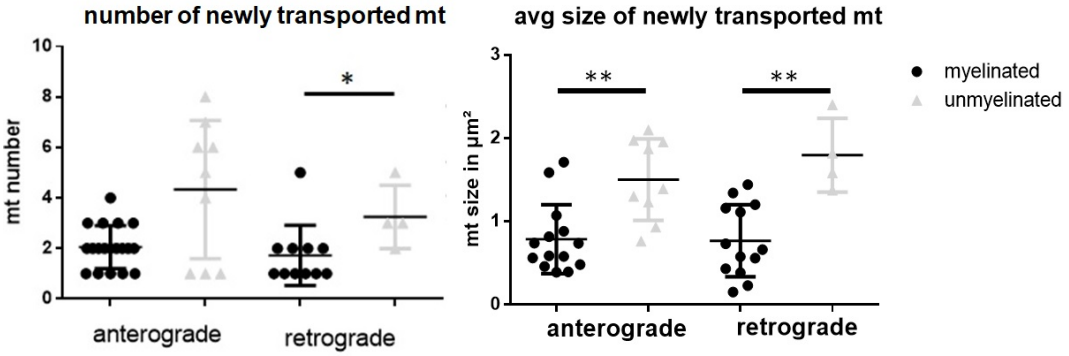

FIGURE 3.16: Mitochondrial transport dynamics in myelinated and unmyelinated axons, showing the number of newly transported green mitochondria into the converted axon and their respective sizes. There was a significant increase in number of newly transported mitochondria in the retrograde direction and a significant increase in size of newly transported mitochondria moving in the anterograde and retrograde direction in the unmyelinated compared to the myelinated axon. Each dot represents the average of all mitochondria from one axon; the total n-number for the myelinated axons is 16 slices from 12 different mice and for the unmyelinated 8 slices from 6 different mice. **=p-value <0.01; *=p-value <0.05

Mitochondrial speed in the myelinated axon

Kymographs of the timelapse images, every minute imaged was included, were generated with the ImageJ plugin KymographClear2.0 and mitochondrial speeds were subsequently measured by using the Kymotoolbox Imagej plugin (designed by Fabrice Cordelieres), this was done by tracing the single lines in the kymographs with the segmented line tool and calculating the speed with the "analyze kymo" tool; see figure 3.17 (Mangeo, Prevo, and Peterman, 2016; Zala et al., 2013). The anterogradely moving newly transported mitochondria displayed a significantly greater speed in the unmyelinated axons compared to the myelinated axons, while the retrograde moving speed of newly transported mitochondria showed a trend towards an increase in the unmyelinated compared to the myelinated axons, which might become significant with higher n-numbers; see figure 3.18.

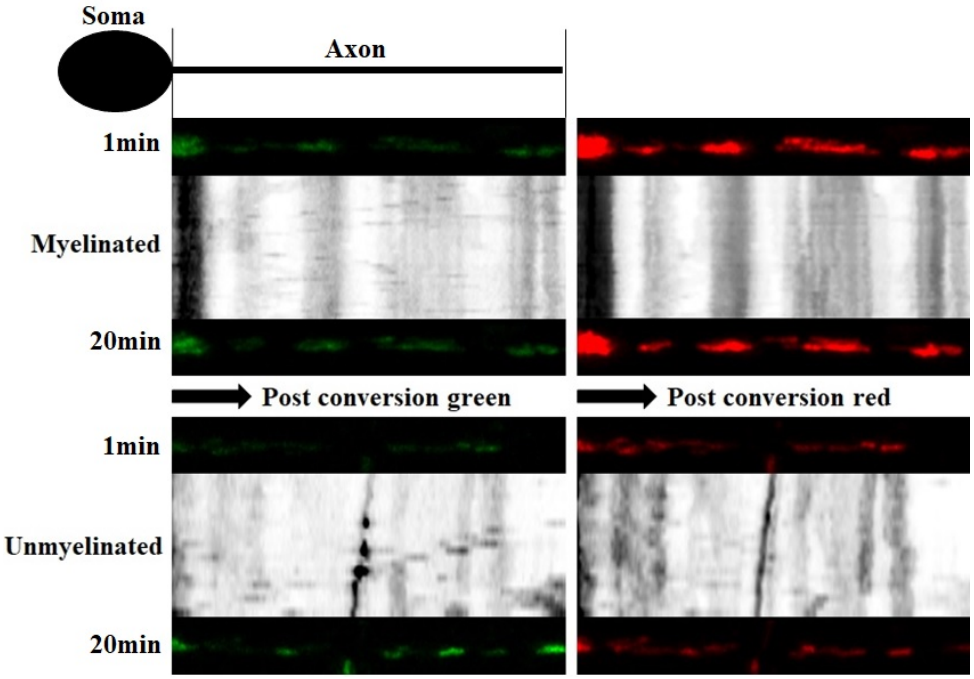

FIGURE 3.17: Kymographs of a myelinated (top panel) and unmyelinated (bottom panel) axon, the black arrows pointing in the anterograde direction. The left panels shows the movement of newly transported green mitochondria, while the right panels show converted red mitochondria within the axon of myelinated (top) and unmyelinated (bottom) axons.

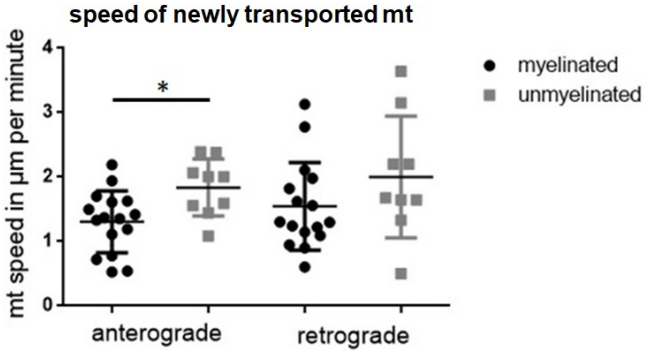

FIGURE 3.18: Mitochondrial movement speed in the unmyelinated and myelinated axons. There was a significant increase of mitochondrial anterograde movement speed in the unmyelinated compared to the myelinated axon. Each dot represents the average of all mitochondria from one axon; the total n-number for the myelinated axons is 16 slices from 12 different mice and for the unmyelinated 8 slices from 6 different mice. *=p-value <0.05

Mitochondrial fusion in the myelinated and unmyelinated axon

To determine the fusion rate of newly transported green mitochondria with the stationary red mitochondria inside the axon, the percentage of green in red fluorescence in the ROI was determined at different timepoints after conversion and corrected for the baseline green in red fluorescence.

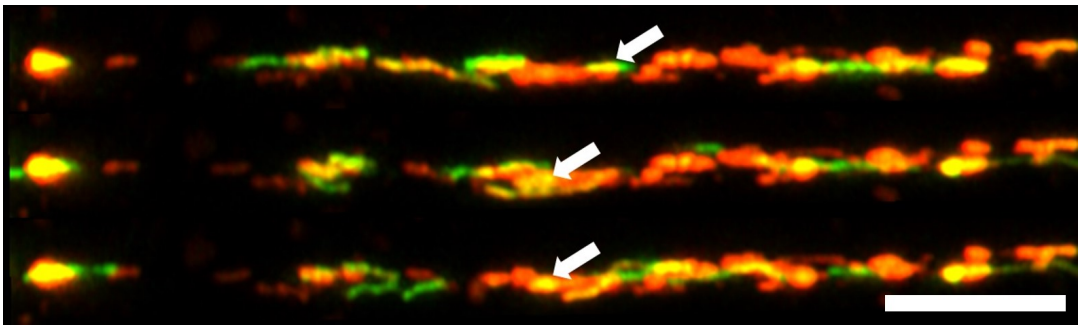

FIGURE 3.19: Mitochondrial fusion event, depicted in a timelapse image series, which shows a fusion event and subsequent increase in green fluorescence in the stationary red mitochondria over 3 minutes. Scalebar=8 µm

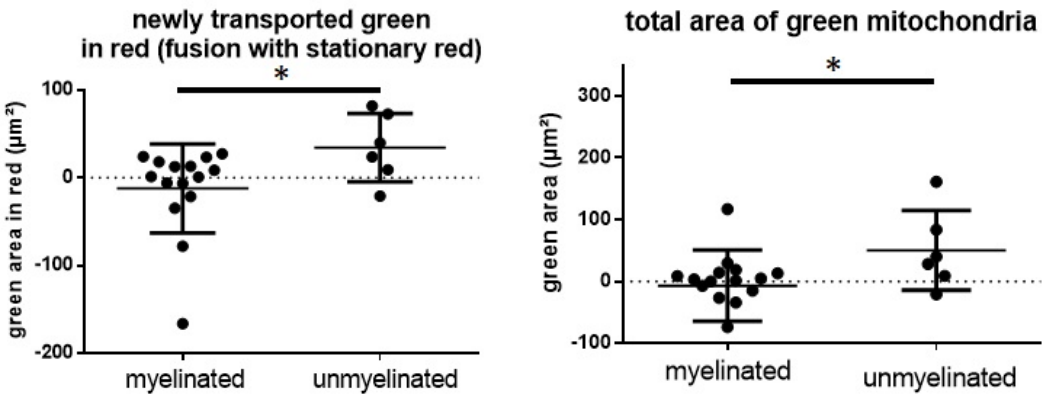

FIGURE 3.20: Fusion of newly transported mitochondira with the stationary converted mitochondria within the ROI. There was a significant increase of mitochondrial fusion, as well as significantly more newly transported green mitochondria that have not (yet) fused with the converted mitochondria in the unmyelinated compared to the myelinated axon. Each dot represents the average of all mitochondria from one axon; the total n-number for the myelinated axons is 16 slices from 12 different mice and for the unmyelinated 8 slices from 6 different mice. *=p-value <0.05

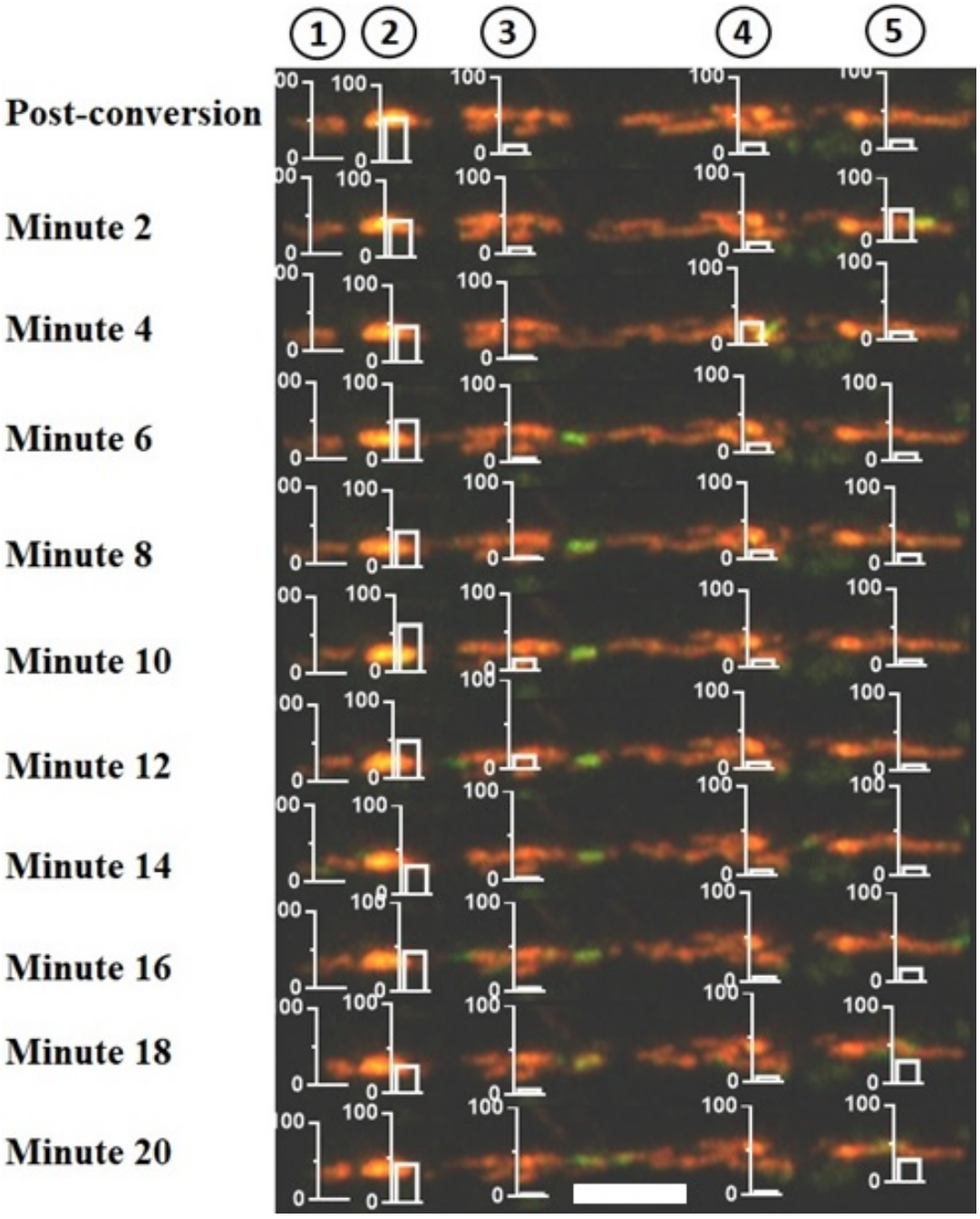

FIGURE 3.21: Mitochondrial fusion and fission dynamics, depicted in a timelapse series which shows a sharp increase in the green in red fluorescence (bar graphs) after a fusion event and decreasing (bar graphs) after a fission event over the imaged time in a myelinated axon. Scalebar=8 µm

The green in red fluorescence increased sharply after fusion of an incoming green mitochondria with a stationary red mitochondria within the

ROI, and decreased again after a fission event. In some instances it was also possible to observe single fusion events; see figure 3.19.

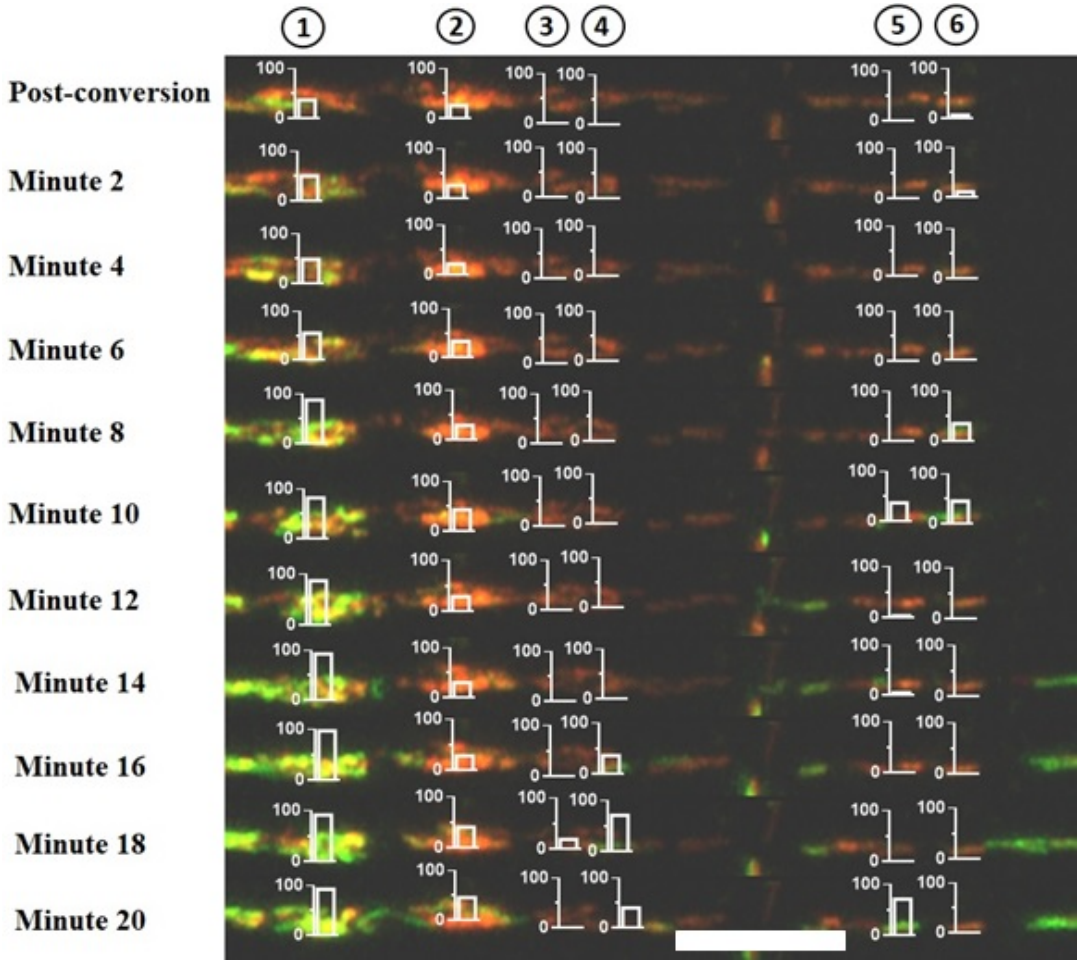

FIGURE 3.22: Mitochondrial fusion and fission dynamics, depicted in a timelapse series which shows a sharp increase in the green in red fluorescence (bar graphs) after a fusion event and decreasing (bar graphs) after a fission event over the imaged time in an unmyelinated axon. Scalebar=10 µm

The analysis showed an increase in mitochondrial fusion in the unmyelinated axon compared to the myelinated axon, while most of the newly incoming mitochondria did not fuse with the stationary red mitochondrial pool over the imaged time; see figure 3.20. The measurements for the fusion data were done at the end of the imaging process by determining the green in red fluorescence and correcting it for the baseline green in red fluorescence. The fusion and fission events

however are very dynamic processes and during the imaging time several fusion/fission events can take place, so the fusion data effectively underestimates the fusion events taking place during that time. Green in red fluorescence increases sharply after a fusion event and decreases after a fission event; see figure 3.21. Apart from the overall greater increase of green in red fluorescence over the imaged time, the single fusion and fission events also displayed a higher dynamic in the unmyelinated compared to the myelinated axon; see figure 3.22.

3.3.5 Mitochondrial dynamics of converted mitochondria

Mitochondrial movement in myelinated and unmyelinated axons

To determine the movement of mitochondria already present in the myelinated and unmyelinated axons of PC, the red converted mitochondria were analysed for anterograde/retrograde movement and size of mitochondria. Overall there was no significant difference in the number of converted moving mitochondria between the myelinated and unmyelinated; see figure 3.23. Furthermore, the average size of the moving converted mitochondria did not differ between the two conditions.

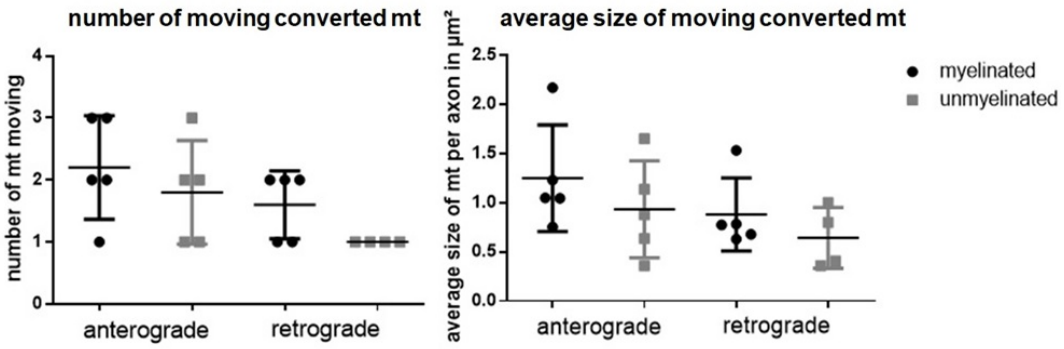

FIGURE 3.23: Dynamics of converted mitochondria within the ROI, depicting the number of moving converted mitochondria on the left and the average size of these moving converted mitochondria (in μm^2) per axon on the right. Each dot represents the average of all mitochondria from one axon. There was no significant difference in both parameters between the unmyelinated and myelinated axon; the total n-number for the myelinated axons is 5 slices from 5 different mice and for the unmyelinated 5 slices from 4 different mice.

Mitochondrial speed in the myelinated and unmyelinated axon

While most of the converted mitochondria did not move great distances, the speed of the ones moving was analysed in myelinated and unmyelinated axons. To measure the speed of the unconverted red mitochondria, the according lines in the red kymographs were traced and speed was calculated by using the Kymotoolbox 'analyse kymo' function. The speed of mitochondria in myelinated axons did not differ significantly from the speed of mitochondria in the unmyelinated axons, neither in anterograde, nor retrograde direction; see figure 3.24.

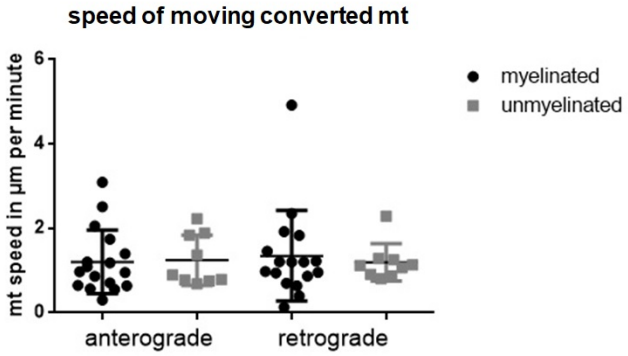

FIGURE 3.24: Mitochondrial movement speed of the converted mitochondria within the ROI, showing no significant difference in mitochondrial movement between the myelinated and unmyelinated axons. Each dot represents the average of all mitochondria from one axon; the total n-number for the myelinated axons is 5 slices from 5 different mice and for the unmyelinated 5 slices from 4 different mice.

3.4 Discussion

3.4.1 Transduction of PC in cerebellar slices and conversion of mEOS2 protein

To analyse the mitochondrial transport and fusion dynamics in the myelinated and unmyelinated axon, the green to red photoconvertible protein mEOS2 was used for live imaging of PC axon in cerebellar slices (McKinney et al., 2009). As discussed in the introduction, the mEOS2 protein can be irreversibly converted from the unconverted green to the converted red state and as shown in Figure 3.9 the converted state remains stable at least a week in culture (McKinney et al., 2009). Furthermore, the protein does not seem have a toxic effect on the cells, leaving them growing even 3 weeks after transduction with the lentivirus expressing the photoconvertible protein, which also shows that the lentivirus is not harming the cerebellar slices to a significant extent. The transduction of PC in the cerebellar slices was a major challenge during this project, as several different steps are necessary to get mEOS2 positive PC by using the lentiviral construct with CMV promoter. Firstly it was necessary to use a pressure controlled system, like the Picospritzer III® to get the viral solution into the deeper layers of the slices, as pipetting the solution on top only leads to transduction of cells in the outer rim of the cerebellar slices. An optimization of pressure strength, duration of injection and needle thickness was done and the tracer dye FG was used to give visual feedback during injections. The test series of several different viral envelope glycoproteins, showed that the widely used VSV-G envelope protein is the most suitable one to get a high transduction rate in the cerebellar slices (Cronin, Zhang, and Reiser, 2005). By using a shorter harvest timepoint, 40 hours after the setting up of the HEK293T cell culture instead of 64 hours, and by adding the Cathepsin K Inhibitor to the HEK293T cell culture, the transduction of neurons with the lentivirus containing the mEOS2 construct was increased (Torashima et al., 2006; Goenawan and Hirai, 2012). This could be observed in DRG culture, were the transduction of DRG was much more efficient with the short 40 hour harvest and the Cathepsin K Inhibitor treatment compared to the 64 hours harvest without Cathepsin K Inhibitor.

The activation of the activity dependant CMV promoter, was achieved by depolarizing the PC by adding forskolin to the slice culture medium (Wheeler and Cooper, 2001). Using this method mEOS2 positive PC can be observed in culture 12-14 days after the injection of the lentivirus. It is possible to photoconvert single structures of a cell by illuminating a region of interest with UV laser, this ROI can be very small, even conversion of single mitochondria is possible if neighbouring mitochondria are not too close. If converting bigger structures, the conversion gradient has to be taken into consideration, as illuminating a ROI for complete photoconversion, will results in a partial conversion of the adjacent structures, structures further away will not be converted. Another important finding is that strong illumination of the cell body leads to the cells degeneration within 24 hours, one reason for this could be extensive DNA damage due to the long exposure to the UV laser. The conversion of the axonal mitochondria, adjacent to the AIS to prevent conversion of the cell body mitochondria, did not lead to the degeneration of the PC even after 48 hours. The SCoRe technique proved to be a valuable tool by revealing the myelination status of the axons during live imaging (Schain, Hill, and Grutzendler, 2014).

3.4.2 Mitochondrial dynamics in myelinated and unmyelinated axons

The mitochondrial movement dynamics in myelinated and unmyelinated axons were measured by manual counting and kymograph analysis. The manual analysis also allowed to measure the size of any incoming mitochondrion. Despite having some residual green fluorescence in myelinated axons, there was not much mitochondrial movement observed compared to the unmyelinated axons. This phenomenon of residual green within the converted part of the axon was observed in both myelinated and unmyelinated axons, but since only completely green mitochondria were counted as being newly transported, it is still clear that this set of mitochondria is coming in from the cell body or distal part of the axon respectively. The movement analysis showed a trend toward more mitochondria moving into the ROI from the anterograde direction and a

significant increase in retrograde movement in the unmyelinated axons compared to the myelinated axons. This increased mitochondrial transport, could be due to an increase in energy demand in the unmyelinated compared to the myelinated axon, possibly due to more sodium channels being placed along the unmyelinated axon, leading to increased sodium influx and demand the more ATP driven Na^+/K^+ ATPase activity to get rid of excess sodium (Craner et al., 2004b; Witte et al., 2014; Mahad, Trapp, and Lassmann, 2015; Mohd, 2010; Albers and Siegel, 1998; Lores Arnaiz and Ordieres, 2014). Concerning the size, significantly bigger mitochondria were entering from the distal axonal part via retrograde transport and as well as from the cell body direction via anterograde transport in the unmyelinated axon opposed to the myelinated axon. In this system it is not possible distinguish between unmyelinated and demyelinated axon, so it is entirely possible that some of these axons were demyelinated following the slicing procedure or other stress factors during the *in vitro* culture process. Interestingly, there was quite a spread of numbers of mitochondria moving in either direction, especially in the anterograde direction, in the unmyelinated axons. So it could be speculated that some of these axons really were unmyelinated from the start, while others have been demyelinated after being already myelinated, and that these two populations of axons have a distinct mitochondrial transport profile.

When determining the rate of mitochondrial fusion of the newly transported unconverted (green) mitochondria with the stationary converted (red) mitochondria within the ROI, by measuring the increase of the green inside red fluorescence from the timepoint after conversion to the 20 minute timepoint, a significant increase of fusion was observed in the unmyelinated axons compared to the myelinated axons. As with the transport, the increase in fusion, could be an adaptive mechanism to an increase in energy demand in the unmyelinated, or possibly demyelinated axons, as bigger mitochondria produce ATP more efficiently. Most importantly the observations made in the mitochondrial transport and fusion dynamics in the myelinated axon set the baseline for further experiments in the which the cerebellar slices were treated with a demyelinating agent and made it possible to assess any effect demyelination might have on mitochondrial dynamics in PC axons in cerebellar slices.

Chapter 4

Mitochondrial dynamics in the demyelinated axon

4.1 Introduction

4.1.1 Live imaging of mitochondria in demyelinated axons

Mitochondrial pathology has been implicated in axon degeneration in multiple sclerosis and relevant disease models. It has also been reported that mitochondrial damage, without demyelination, is sufficient to lead to axonal death, showing the importance of mitochondrial function in disease (Dutta et al., 2006; Campbell et al., 2011; Campbell and Mahad, 2012; Mahad et al., 2009; Mahad, Trapp, and Lassmann, 2015; Nikić et al., 2011; Sorbara et al., 2014). There have been already several studies that involved live imaging of mitochondrial dynamics in axons either *in vivo* or *in vitro* (Ohno et al., 2011; Kiryu-Seo et al., 2010; Misgeld et al., 2007; Misgeld, Nikic, and Kerschensteiner, 2007). Misgeld et al developed two mouse lines that express either CFP (Thy1-mitoCFP) or YFP (nse-mitoYFP) under the control of the neuron specific Thy1 or nse promoter respectively, both targeted to mitochondria by a mitochondrial targeting sequence (Misgeld et al., 2007; Misgeld, Nikic, and Kerschensteiner, 2007). These mouse lines can be used to image mitochondrial dynamics both *in vivo* or in acutely explanted nervous tissue. The labelling by mitoCFP or mitoYFP seems to leave mitochondrial physiology mostly intact, as Misgeld et al show that the mitochondria are still co-stained by membrane potential-sensitive mitochondrial dyes (Misgeld et al., 2007; Misgeld, Nikic, and Kerschensteiner, 2007). The authors also checked for mitochondrial changes

after the transection of intercostal nerves *in vivo* and reported that already by 3 hours after transection the distal axonal segment showed 2-3 fold reduction in mitochondrial anterograde transport and more than 20-fold after 6 hours (Misgeld et al., 2007). In contrast to the distal axon, the proximal part of the axon showed an increase in anterograde transport by 12 hours after the injury, which was maintained at 24 and 48 hours, before declining over the following weeks (Misgeld et al., 2007). This increase in anterograde transport could be a sign of injury response, which contributes to regeneration (Misgeld et al., 2007).

Several publications on mitochondrial dynamics in myelinated and demyelinated axons were made by the Trapp Group from Cleveland and the Mahad Group. In the first publication the Trapp group used an *in vitro* rat DRG myelinating culture and infected it with a mito-DsRed2 expressing lentivirus to follow any changes in mitochondrial dynamics via live imaging. They found an increase in size of the mitochondrial stationary sites after demyelination with lysolecithin, as well as an increase in mitochondrial transport speed (Kiryu-Seo et al., 2010). These changes returned to baseline after remyelination of the DRG axons. However they did not look at the number of stationary sites or moving mitochondria in the remyelinated axon, which was checked by Zambonin et al and they reported an increase in the number of stationary sites in remyelinated axon (Zambonin et al., 2011). Kiryu-Seo et al furthermore reported that lysolecithin had no apparent effect on unmyelinated axons, so the changes after demyelination can be attributed to the loss of myelin rather than an effect of lysolecithin on mitochondria (Kiryu-Seo et al., 2010). In the second publication the Trapp group used cerebellar slice culture to look at the difference of mitochondrial stationary sites and transport in the nodal/paranodal and juxtaparanodal/internodal axoplasm and reported juxtaparanodel/internodal increase of mitochondrial stationary sites and activity dependant modulation of mitochondrial motility (Ohno et al., 2011). These effects were not observed in slices of the md-mutant, which lacks compact myelin and subsequently does not form paranodal specializations (Ohno et al., 2011). In the third publication from the Trapp group, again a cerebellar slice culture system was used, both from wild-type and *syntaphilin*-KO mice to look at the difference in the ARMD and the effect on

axonal health (Ohno et al., 2014). They reported that the ARMD is not mounted in the *syntaphilin*-KO, namely that there is no increase in mitochondrial stationary sites, but an increase in the number and speed of motile mitochondria in the KO compared to the wildtype (Ohno et al., 2014).

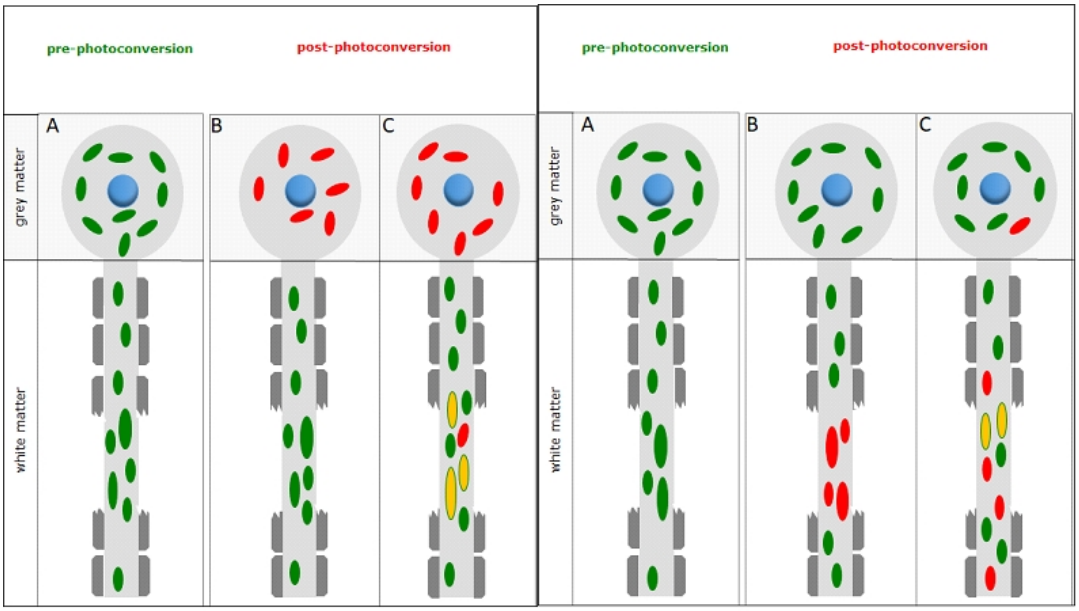

FIGURE 4.1: Method for the conversion of mitochondria within different cellular compartments. Left: conversion of cell body and movement of converted red mitochondria into the axon where fusion with stationary unconverted green mitochondria gives rise to yellow mitochondria in the axon. Right: conversion of axon and movement of newly transported unconverted green mitochondria into the axon where fusion with stationary converted red mitochondria gives rise to yellow mitochondria in the axon.

Furthermore, they showed that there is a significant increase in Alzheimer-precursor-protein (APP) positive axons in the KO, which indicates increase degeneration of axons in the KO (Ohno et al., 2014). This finding points towards a protective effect of the ARMD in the short term. (Ohno et al., 2014). Although these studies provide insight into the changes of mitochondrial parameters after demyelination, none of the mentioned studies looked at the fusion dynamics of the ARMD, nor was it determined where these additional mitochondria come from. To study the dynamics of the ARMD in more detail, namely to determine were the additional mitochondria that are responsible to mount the ARMD come from and to

assess the fusion dynamics in the demyelinated PC axons, cerebellar slices were transduced by injecting the mEOS2 containing lentivirus into the PCL of the slices by using the Picospritzer III®. By using the photoconvertible protein mEOS2, it is possible to convert a subset of mEOS2 (green in basal state) expressing mitochondria (red in converted state) and determine the rate of fusion with non-converted green mitochondria, by assessing the green in red fluorescence; see figure 4.1 (McKinney et al., 2009). Furthermore, by converting the first part of the axon adjacent to the AIS it can be determined from which direction newly transported (unconverted green) mitochondria come into the converted (red) segment of the axon; see figure 4.1.

4.2 Materials and methods

Animals

All procedures were performed according to the 1986 Animals Act (scientific procedures) UK and were approved by the local ethics committee. For all the experiments C57BL/6 mice were used. For the generation of cerebellar organotypic slice cultures mice from P7 to P12 were used, because slice generated at this age ensures a good survival of purkinje cells, while already displaying many features of the adult structure of the cerebellum.

4.2.1 Demyelination with lysolecithin

To determine the fusion and transport dynamics of mitochondria in demyelinated axons, lysolecithin (L-α-Lysophosphatidylcholine powder from egg yolk; L4129 Sigma) was used as the demyelinating agent, as Lysolecithin has, as mentioned in chapter 2, the least effect on mitochondria among the most widely used demyelination agents (Birgbauer, Rao, and Webb, 2004; Zhang et al., 2011; Komai, Hunter, and Takahashi, 1973; Keough, Jensen, and Yong, 2015; Jeffery and Blakemore, 1995; Wallace et al., 2003; Yu et al., 2007). Right before the demyelination timepoint, the L-α-Lysophosphatidylcholine powder was dissolved in slice culture medium to the appropriate concentration, heated in the $37\,^{\circ}\mathrm{C}$ water bath and mixed by using a Vortex Genie®. After the lysolecithin was completely

dissolved, 800 µl of the lysolecithin solution was added to each well of a six well plate and the membranes with the slices on top were transferred from the previous six well plate into the lysolecithin containing plate by using a forceps. To find out the optimal concentration of lysolecithin to ensure complete demyelination, while keeping the morphology of the axons intact, several different lysolecithin dilutions were tested. The most widely used concentration, which was also used in chapter 2, 0.5mg/ml lysolecithin left on for 17 hours did not lead to significant demyelination (Birgbauer, Rao, and Webb, 2004). Alternatively 0.5mg/ml was left on for 24 hours, 0.75mg/ml was tested for 17 hours and 24 hours, as well as 1mg/ml for 17 hours and 24 hours and 2mg/ml for 17 hours.

4.2.2 Determining mitochondrial dynamics in the demyelinated axon

In chapter 2 the timecourse of the ARMD was determined by examining the mitochondrial parameters at different timepoints after demyelination.

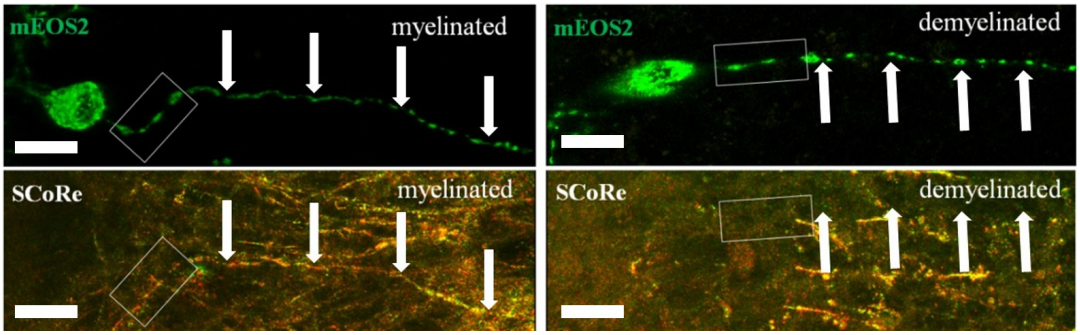

FIGURE 4.2: ScoRe technique depicting a myelinated (left panel) and demyelinated (right panel) mEOS2 positive axon. The white rectangle shows the area which was converted and used for the subsequent live imaging experiment. Scalebar=20 µm

Furthermore, as the analysis in chapter 2 showed, that the ARMD is mounted very fast after demyelination and this suggests that it would be possible to observe any changes in mitochondrial dynamics soon after demyelination with lysolecithin. Because of these findings, the first part of the axon near to the cell body was converted by using UV laser and imaged every minute over 20 minutes, right after the lysolecithin was removed from

the slice culture. Like in chapter 3, SCoRe was used to determine the myelination status of the axons; see figure 4.2. Mitochondrial movement direction, size and numbers, as well as mitochondrial speed and fusion dynamics were determined. Like in chapter 3, the fusion of newly transported unconverted (green) mitochondria with the converted (red) mitochondria into the ROI was determined by measuring the increase of green in red fluorescence over the imaged time, this was corrected for the baseline fluorescence right after conversion. For the mitochondrial transport of unconverted green into the converted red ROI two different methods were used. The first method, as used in chapter 3, was to determine the newly transported unconverted green mitochondria by manual analysis and to measure the size of each of these mitochondria. The second method, which also allowed to compare the relative transport speed between different axons, was to create kymograph by using the KymographClear 2.0 Plugin for Imagej and to use the kymotoolbox plugin function to measure the number and speed of green mitochondria being transported within the ROI (Wallace et al., 2003; Zala et al., 2013). For the analysis of speed the 'analyse kymo' function of the kymotoolbox plugin was used and, after the individual tracks were traced by using the 'segmented line' tool, the movement speed of traced mitochondria was calculated. Since the ROI was only imaged every minute, it was not possible to measure 'real' mitochondrial movement speed, but rather a relative speed, which can be compared between different axons. The mitochondrial number, entering from anterograde or retrograde direction, was represented by the number of tracks in the kymograph.

4.3 Results

4.3.1 Determination of the myelination extent in cerebellar slices

Since the lentiviral transduction of PC in organotypic brain slices of the cerebellum is quite sparse and random, it was important to determine the myelination ratio in the cerebellar slices.

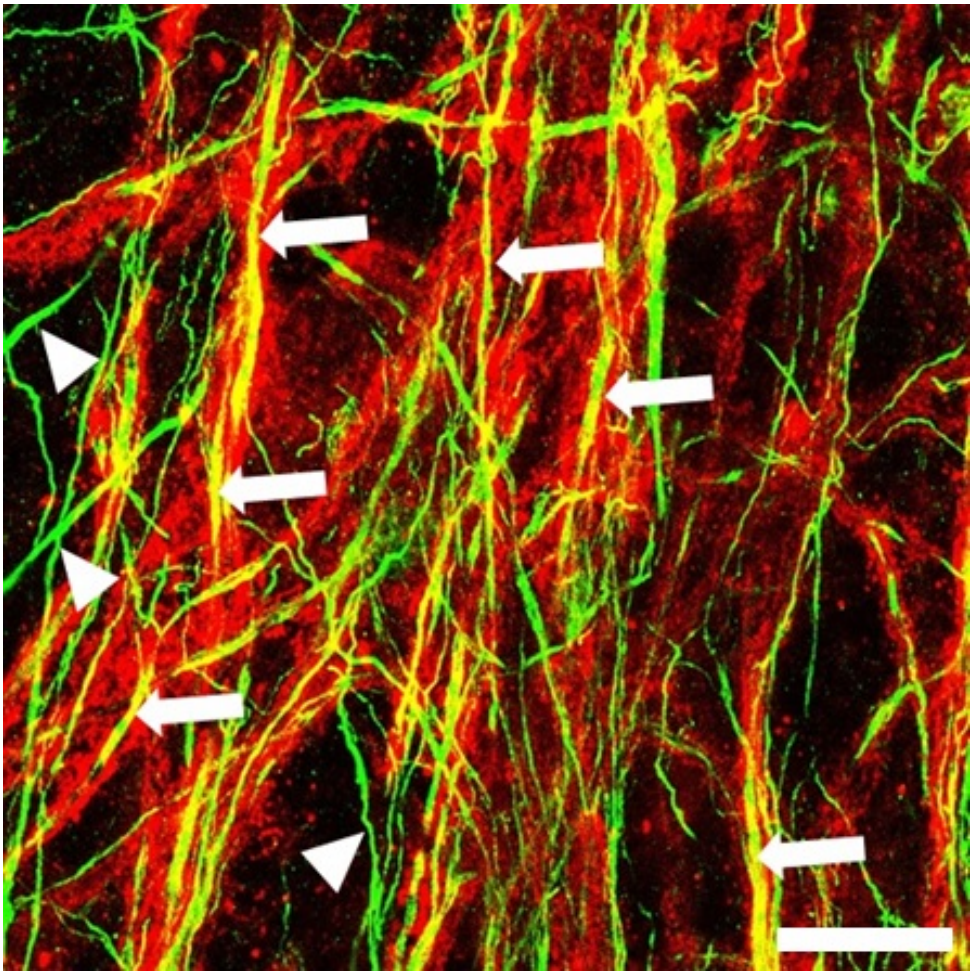

FIGURE 4.3: Amount of myelinated and unmyelinated axons within cerebellar slices. Fluorescent image showing myelinated and unmyelinated axons with IHC staining for NF and MBP in cerebellar slices. The arrow depicting some of the myelinated axons, while the arrowheads point at unmyelinated axons. Scalebar=15 µm

For this the slices were left in culture for 14 days, the same amount of time as they would be in culture for demyelination and live imaging, and stained with IHC for NF and MBP to determine the amount of myelinated axons; see figure 4.3. Axons with sufficient continuous myelination in the field of view were counted as myelinated, whereas axons without myelin or with very little myelin in the field were counted as being unmyelinated; see figure 4.3. The ratio of unmyelinated to myelinated axons was 1:5, which amounts to about 80% of axons being myelinated after 2 weeks in culture; see figure 4.4. Another possibility would be that those axons were actually demyelinated by an unknown process at some time point during or after the slicing procedure.

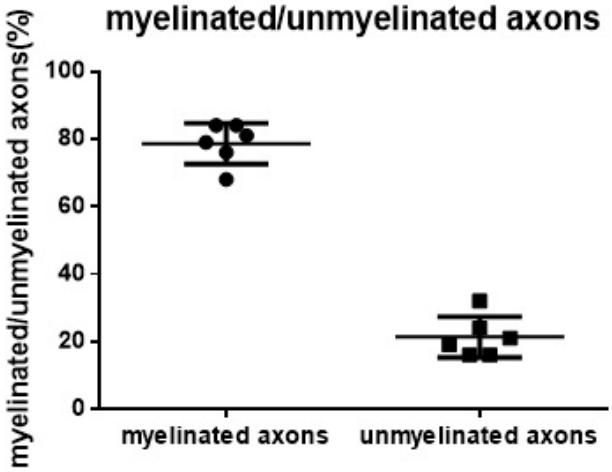

FIGURE 4.4: Proportion of myelinated axons in cerebellar slices after 14 days in culture, showing that about 20% of axons on cerebellar slices were either unmyelinated after 2 weeks in culture or demyelinated at some time after the slicing procedure by an unknown factor. Each dot represents one slice from one mouse and includes at least 40 analysed axons

4.3.2 Determination of the optimal lysolecithin concentration

The dose of 0.5mg/ml lysolecithin for 17h turned out not to be sufficient to demyelinate most of the axons in the slices, despite being suitable for IHC staining analysis, like used in chapter 2, since only demyelinated axons can be selected for analysis, it was not sufficient for live imaging as there is no

guarantee that the mEOS2 positive cells were demyelinated. Therefore, a lysolecithin concentration experiment was done, testing different concentrations of lysolecithin left on for different amount of times, to check which concentration gives enough demyelination and still leaves the axons healthy and intact. 24 hours after removing lysolecithin, the slices were fixed and stained for NF and MBP.

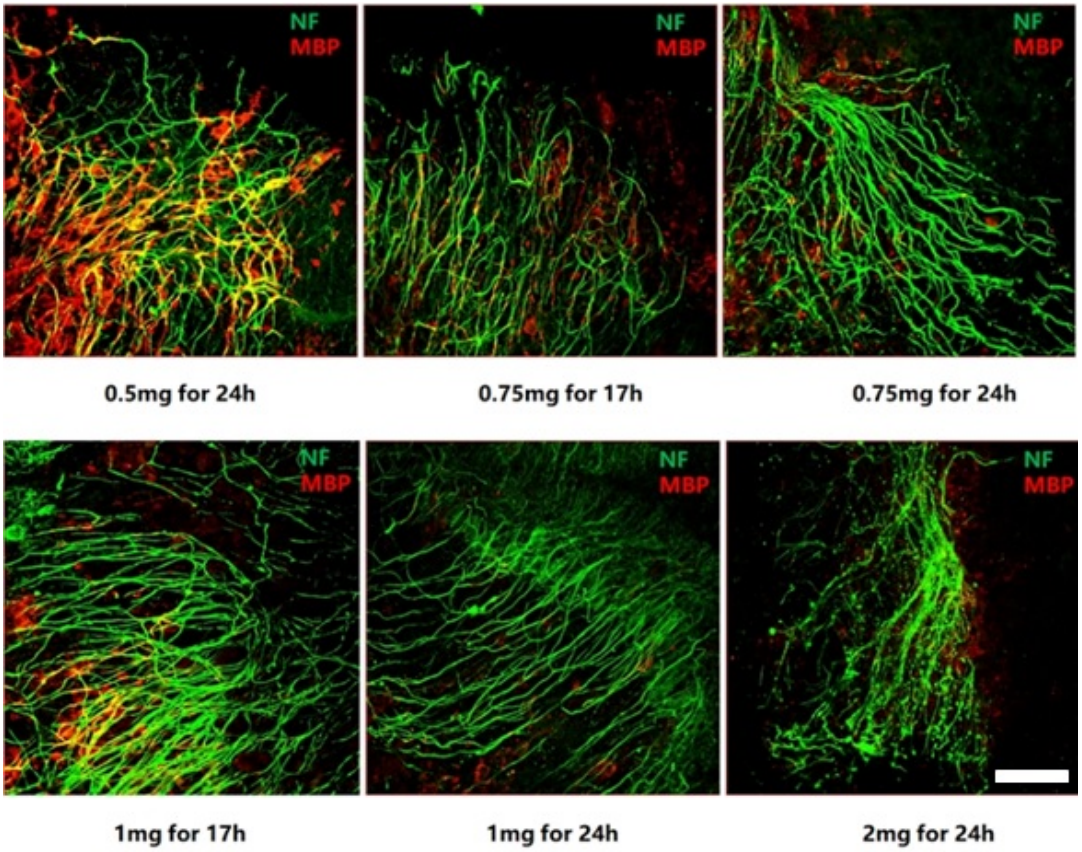

FIGURE 4.5: Effect of different lysolecithin concentrations on demyelination efficiency and axonal health. The aim was to determine the optimal concentration which leads to nearly complete demyelination, while still keeping the axonal integrity intact. 2mg/ml lysolecithin lead to a deterioration of the axonal health, which can be seen as extensive beading of the NF stained axons. 0.5mg/ml lysolecithin did not lead to sufficient demyelination, while 0.75mg/ml and 1mg/ml lysolecithin lead to enough demyelination with the axonal integrity still being intact. Scalebar=30 µm

As mentioned before and shown in 4.5 the most widely used concentration of 0.5mg/ml lysolecithin, even when left on for 24 hours, did

not lead to sufficient demyelination; see figure 4.5. The next higher concentration 0.75mg/ml already prompted a better demyelination ratio at 17 hours exposure time, while the 24 hour exposure lead to an even better demyelination efficiency, with the axonal integrity still intact; see figure 4.5. The 1mg/ml concentration lead to sufficient demyelination both after 17 hours and 24 hours of lysolecithin treatment with normal axonal morphology. Finally, the 2mg/ml concentration, which was only used for 17 hours, did demyelinate the axons completely, but also seemed to have a detrimental effect on the axonal health, as their morphology was clearly affected; see figure 4.5. The most fitting concentration and timing, which was subsequently used in all live imaging experiments, was 0.75mg/ml lysolecithin left on for 24h, because it was the lowest concentration that showed an overall good demyelination efficiency, while still keeping the axons intact; see figure 4.5.

4.3.3 Mitochondrial dynamics of newly transported mitochondria

Direction of movement, number and size of newly transported mitochondria

As in Chapter 3, the part of the axon adjacent to the AIS was converted and imaged every minute over 20 minutes, to determine the difference in mitochondrial transport and fusion dynamics between the myelinated and demyelinated axons; see figure 4.6. Each newly transported green mitochondrion was counted and the direction was noted, also the size of each newly transported mitochondrion was calculated by using ImageJ; see figure 4.6. Furthermore, the rate of fusion was calculated by the fraction of green reappearing in the stationary red mitochondria over the imaged time. Axons with sufficient positive SCoRe reflection in the field of view were counted as myelinated, whereas axon without any myelin in the field of view were counted as demyelinated. Axons with only minimal SCoRe reflection were not included, which was a rare finding, because the lysolecithin concentration used was determined as being high enough for nearly complete demyelination of axons in the slices.

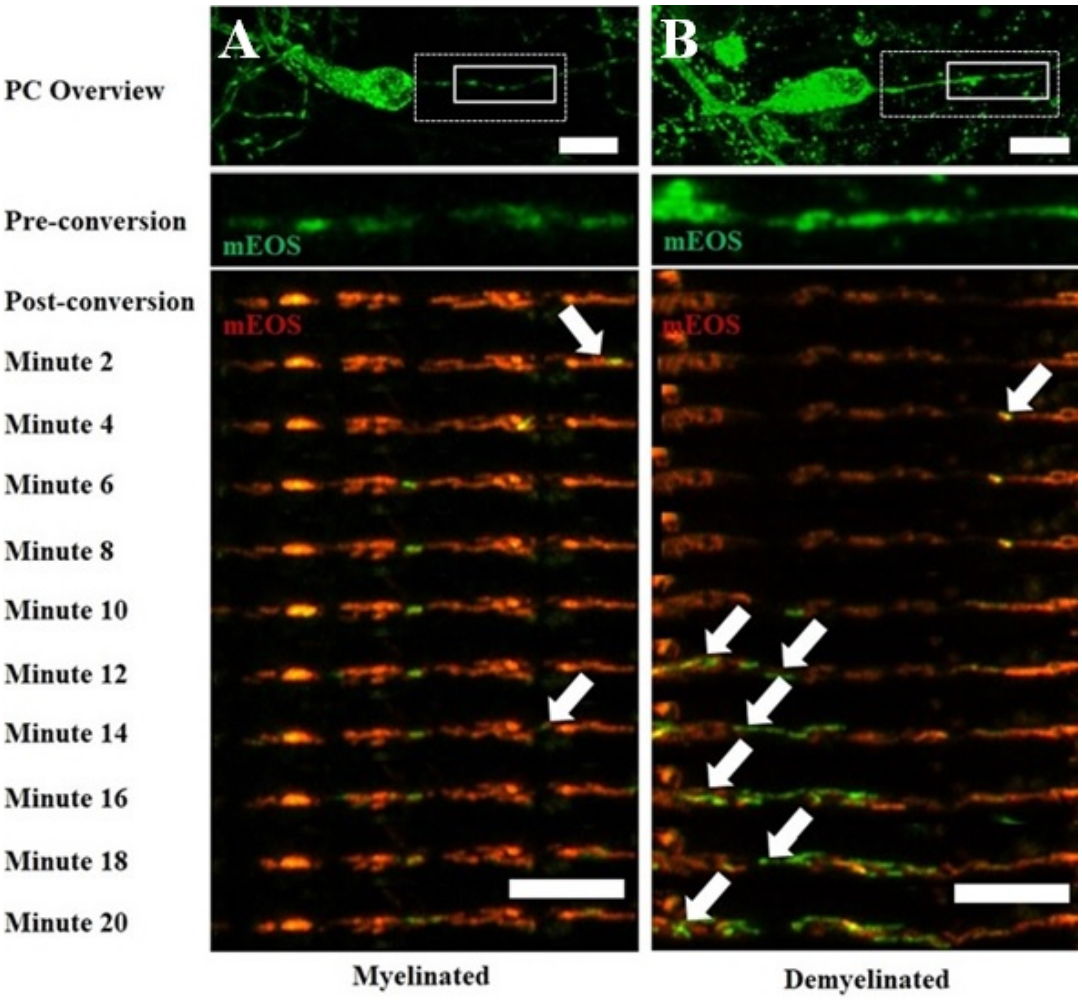

FIGURE 4.6: Mitochondrial transport and fusion dynamics in demyelinated axons, showing a converted segment of a myelinated (A) and demyelinated (B) axon, showing newly transported green mitochondria moving into the converted part (white arrows). The continuous box represents the converted part of the axon, while the dashed box indicates the ROI for imaging. Scalebar=20 µm for low magnification and 10 µm for high magnification images.

Overall there were significantly more new green mitochondria being transported into the demyelinated axon compared to the myelinated axon. This mirrored the observation made in the unmyelinated axons compared to the myelinated axons as shown in chapter 3.

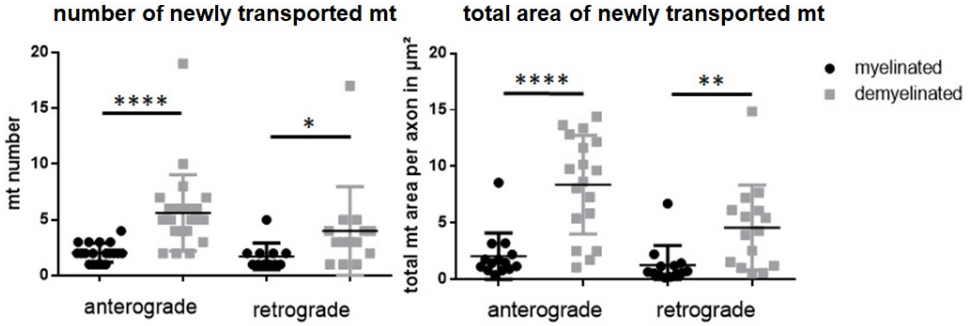

FIGURE 4.7: Mitochondrial transport dynamics in demyelinated axons depicting the number of newly transported green mitochondria and total area of incoming mitochondria into the converted axon. There were significantly more newly transported mitochondria moving in the anterograde and retrograde direction in terms of numbers and total area in the demyelinated compared to the myelinated axon. Each dot represents the average of all mitochondria from one axon; the total n-number for the myelinated axons is 16 slices from 12 different mice and for the demyelinated 18 slices from 13 different mice. *=p-value <0.05 ;**=p-value <0.01; ****=p-value <0.0001

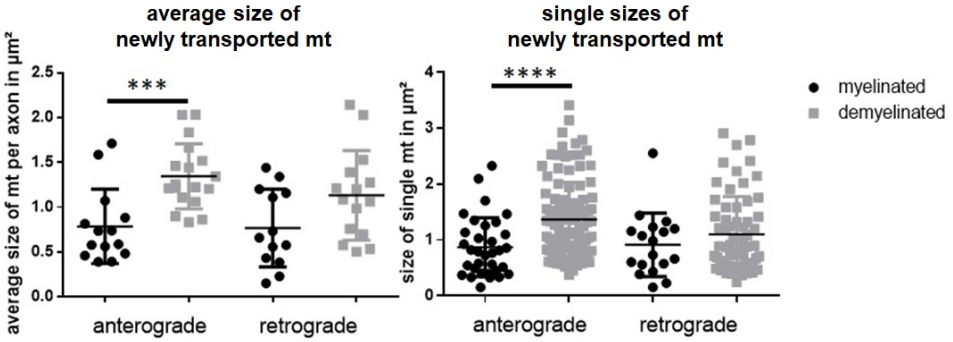

FIGURE 4.8: Mitochondrial transport dynamics in demyelinated axons depicting depicting the sizes of newly transported green mitochondria into the converted axon. Left: average sizes in μm^2; Right: sizes of single mitochondria in μm^2. There were significantly bigger newly transported mitochondria moving in the anterograde direction, measured as average and single sizes, in the demyelinated compared to the myelinated axon. Each dot represents the average of all mitochondria from one axon; the total n-number for the myelinated axons is 16 slices from 12 different mice and for the demyelinated 18 slices from 13 different mice. ***=p-value <0.001; ****=p-value <0.0001

This change was observed in both directions, while there were significantly more mitochondria coming in from the anterograde direction as compared to the retrograde direction in the demyelinated axon (not shown); see figure 4.7. The significant increase in transported mitochondria was reflected both in numbers as well as in total area. The size of the newly transported green mitochondria was significantly greater in the anterograde moving mitochondria of demyelinated axons compared to myelinated axons, both the average sizes of mitochondria per axon and all single sizes of all mitochondria; see figure 4.8. The size of retrograde moving mitochondria did not differ between the two conditions.

Fusion of newly transported mitochondria with post-conversion mitochondria

To determine the fusion rate of the newly transported green mitochondria with the converted red mitochondria within the ROI, an Imagej macro was used to calculate the green inside red ratio for each image-series and corrected for the baseline green fluorescence.

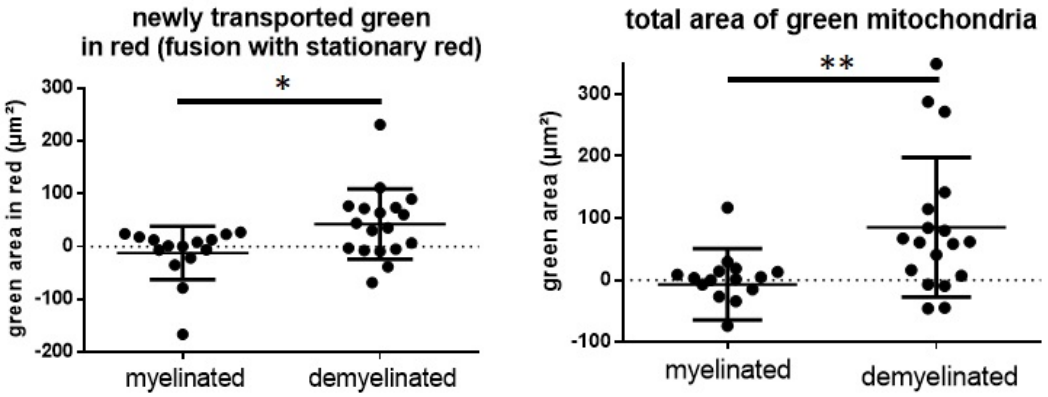

FIGURE 4.9: Mitochondrial fusion dynamics depicting the fusion of newly transported mitochondria with the converted mitochondria in the axon. There was significantly more fusion of mitochondria, as well as significantly more green only mitochondria in the demyelinated compared to the myelinated axon. Each dot represents the average of all mitochondria from one axon; the total n-number for the myelinated axons is 16 slices from 12 different mice and for the demyelinated 18 slices from 13 different mice. **=p-value <0.01

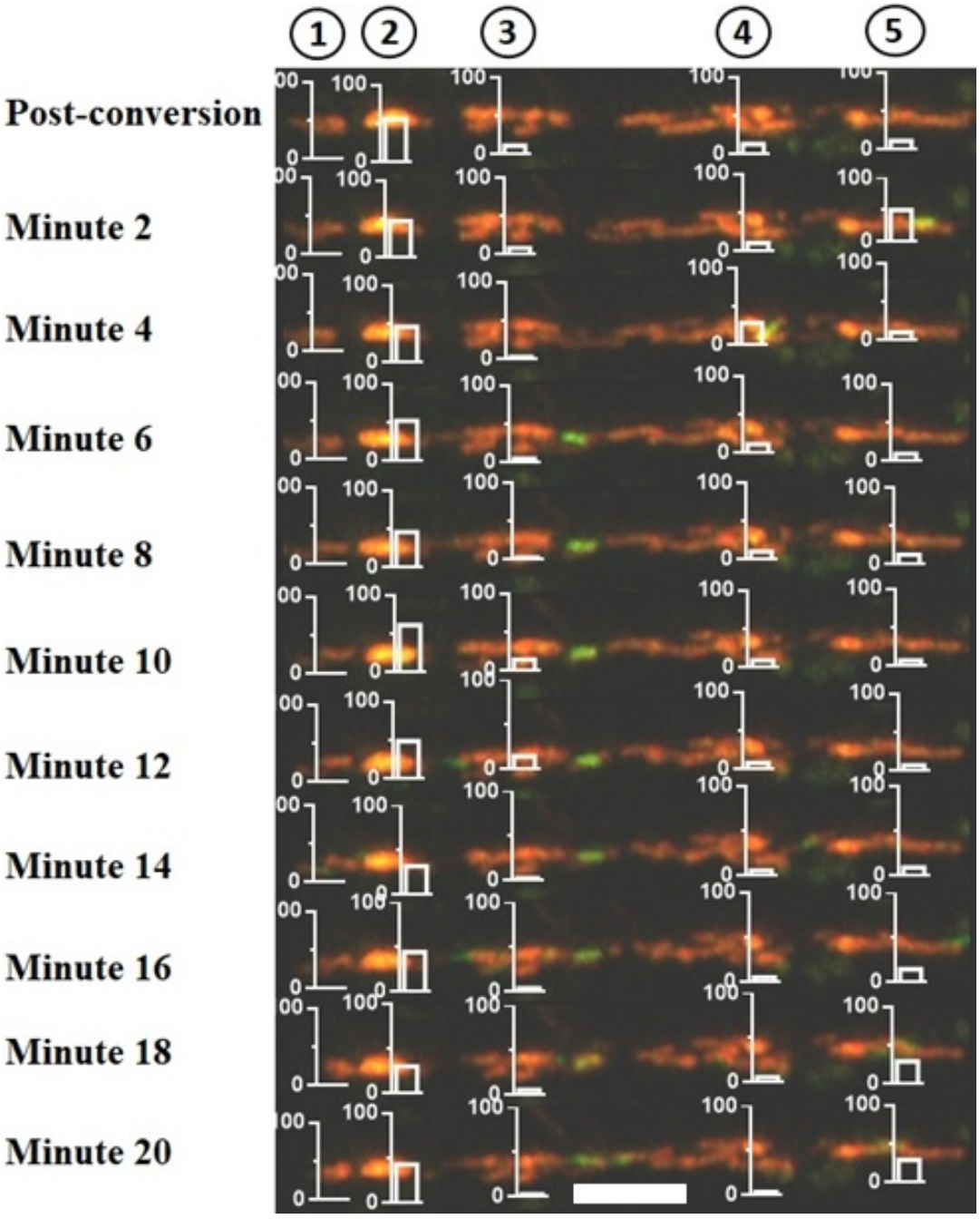

FIGURE 4.10: Mitochondrial fusion dynamics of a myelinated axon depicting a timeseries showing the fusion and fission dynamics over the imaged time in a myelinated axon, sharply increasing the green in red fluorescence after a fusion event and decreasing after a fission event. Scalebar=10 µm

Overall there was significantly more fusion taking place in the demyelinated axon compared to the myelinated axon, although the majority

of the newly transported mitochondria did not (yet) fuse with the converted stationary mitochondrial sites in the axon; see figure 4.9.

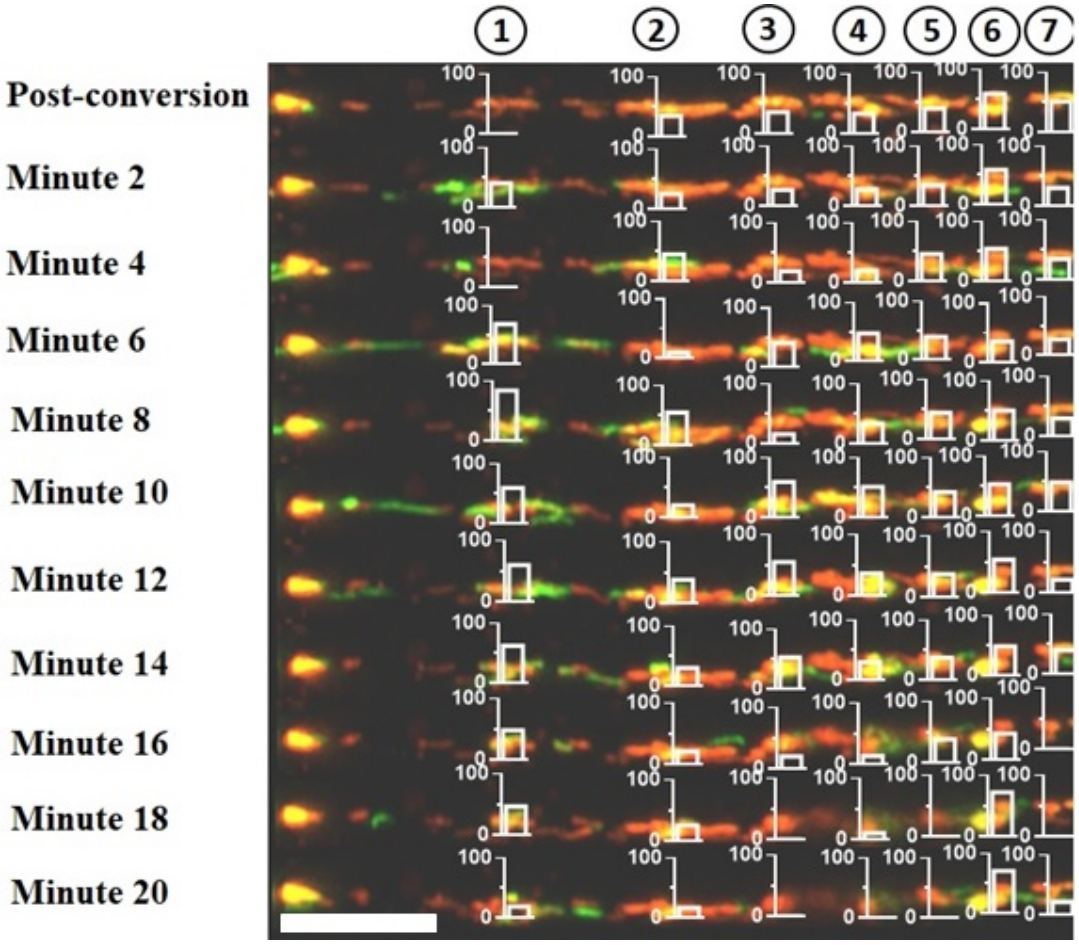

FIGURE 4.11: Mitochondrial fusion dynamics of a demyelinated axon depicting a timeseries showing the fusion and fission dynamics over the imaged time in a demyelinated axon, sharply increasing the green in red fluorescence after a fusion event and decreasing after a fission event. Scalebar=10 µm

As the data for the fusion was determined by measuring the green in red fluorescence at the end of the timelapse imaging and correcting it for the green in red fluorescence at baseline, it underestimates the fusion events taking place during that time. This is because there are many fusion and fission events in between that increase the green in red fluorescence or decrease it again respectively; see figure 4.10. The fusion dynamics were not only increased when measuring the total green in red fluorescence at the

end of the imaging process, but also the number of single fusion and fission events seemed to be increased in the demyelinated compared to the myelinated axon when looking at fusion/fission events in a single axons, although this would need further analysis; see figure 4.11.

Mitochondrial speed in the demyelinated axon

For calculating the mitochondrial movement speed, kymographs of the timelapse images were generated by using the KymographClear2.0 ImageJ plugin, while every minute imaged was included. The Kymotoolbox Imagej plugin was then used to calculate the mitochondrial speed by tracing the single lines in the kymographs with the segmented line tool and using the "analyze kymo" function; see figure 4.12 (Mangeo, Prevo, and Peterman, 2016; Zala et al., 2013).

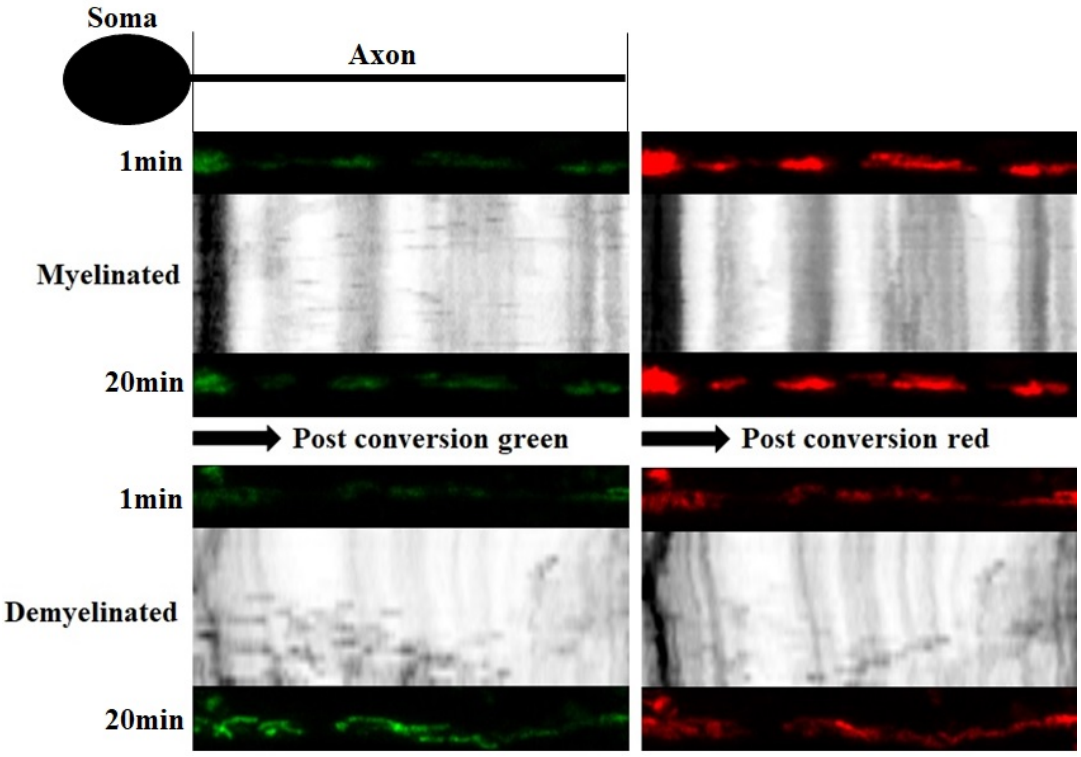

FIGURE 4.12: Kymographs of moving mitochondria within a myelinated (top panel) and demyelinated (bottom panel) axon, the black arrows pointing in the anterograde direction. The left panels shows the movement of newly transported green mitochondria, while the right panels show converted red mitochondria within the axons.

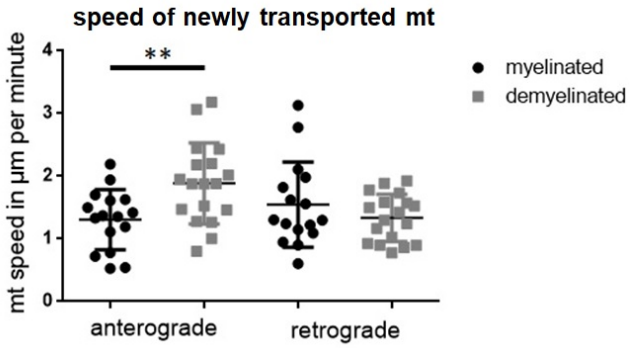

FIGURE 4.13: Mitochondrial movement speed in demyelinated axons, showing significantly faster anterograde movement of newly transported mitochondria in the demyelinated axons compared to myelinated axons. The movement speed in retrograde direction did not show any statistical difference between the demyelinated and myelinated axons. Each dot represents the average of all mitochondria from one axon; the total n-number for the myelinated axons is 16 slices from 12 different mice and for the demyelinated 18 slices from 13 different mice. **=p-value <0.01

The speed of the newly transported mitochondria moving in anterograde direction was significantly greater in the demyelinated axon compared to the myelinated axon, while the retrograde speed of movement was not different between the two conditions; see figure 4.13.

4.3.4 Mitochondrial dynamics of converted mitochondria

Mitochondrial movement in myelinated and demyelinated axons

To check the dynamics of the mitochondria already present in the axon at the time of conversion, the movement directionality and respective sizes of the converted red moving mitochondria was measured. There was no significant difference between the myelinated and the demyelinated axons in terms of number or average size of the converted moving mitochondria; see figure 4.14. However only the size of the moving converted mitochondria was measured and as there were many stationary red mitochondria with bigger size in the ROI, which were not taken into account in this analysis.

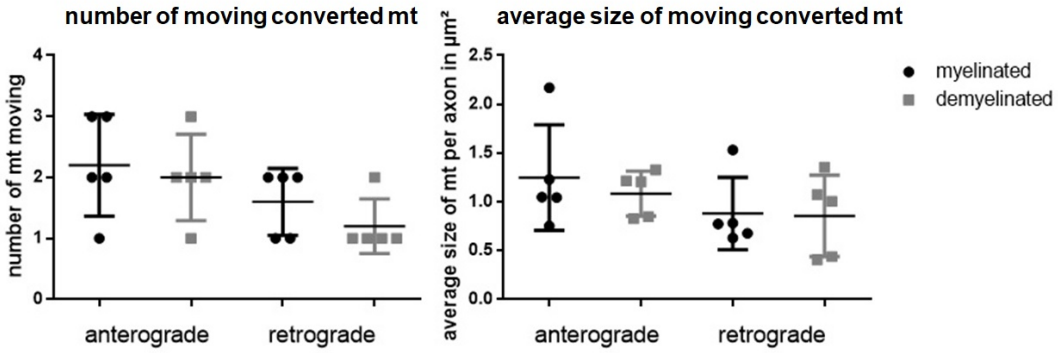

FIGURE 4.14: Mitochondrial dynamics of the converted mitochondria within the ROI, showing the number and directionality of moving mitochondria and their respective average sizes in both myelinated and demyelinated axons. There was no significant difference in the parameters measured between the myelinated and demyelinated axon. Each dot represents the average of all mitochondria from one axon; the total n-number for the myelinated axons is 5 slices from 5 different mice and for the demyelinated 5 slices from 4 different mice.

Mitochondrial speed in the myelinated axon

To measure the speed of the converted mitochondria within the ROI, lines were traced on the kymographs created for the red converted mitochondria and the speed was calculated with the 'analyse kymo' function of the kymotoolbox plugin in ImageJ (Mangeo, Prevo, and Peterman, 2016; Zala et al., 2013). The speed of the converted mitochondria was not different between the myelinated and demyelinated axons, neither in anterograde nor retrograde direction; see figure 4.15. As mentioned above only the moving converted red mitochondria were taken into account during this analysis and slight movement of the stationary red mitochondria, which represents the biggest part of the converted red mitochondria, were not analysed. Overall the speed of the converted red mitochondria was similar to the unconverted green mitochondria in the myelinated axons, while the anterograde transport in demyelinated axons showed a trend towards decreased speed in the transport of converted mitochondria.

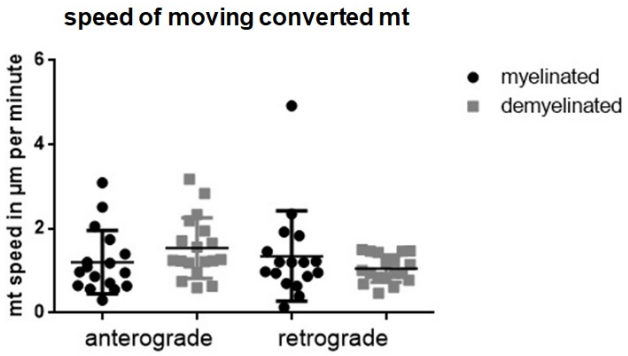

FIGURE 4.15: Mitochondrial movement speed of post conversion mitochondria in demyelinated and myelinated axons. No significance difference between myelinated and demyelinated axons was detected, neither in anterograde or retrograde movement speed. Each dot represents the average of all mitochondria from one axon; the total n-number for the myelinated axons is 5 slices from 5 different mice and for the unmyelinated 5 slices from 4 different mice.

4.3.5 Cerebellar slice culture of the *shiverer* mutant

To determine if the greater number of mitochondria moving into the demyelinated axon is a direct effect of the lysolecithin treatment rather than demyelination, slices of the *shiverer* mutant were used to examine the effect of lysolecithin on dysmyelinated axons; see figure 4.16 (Chernoff, 1981). The dynamics of newly transported mitochondria coming into the ROI in the *shiverer* mutant was similar to the demyelinated and unmyelinated wild-type slices, with significantly increased anterograde transport of mitochondria compared to the myelinated slices; see figure 4.17.

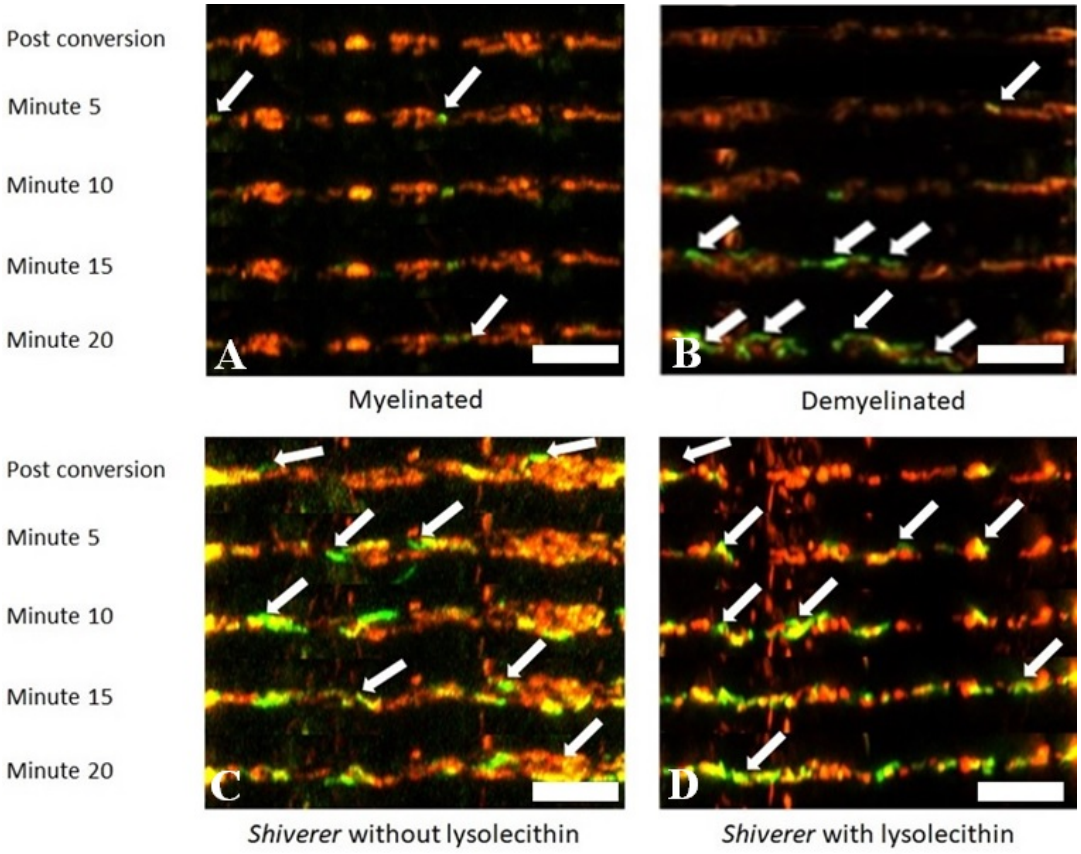

FIGURE 4.16: Mitochondrial dynamics in the *shiverer* mutant with and without lysolecithin treatment. Timeseries of axons in *shiverer* mutant slices with (D) and without (C) lysolecithin, compared with myelinated (A) and demyelinated (B) axons of wildtype slices. Scalebar=10 µm

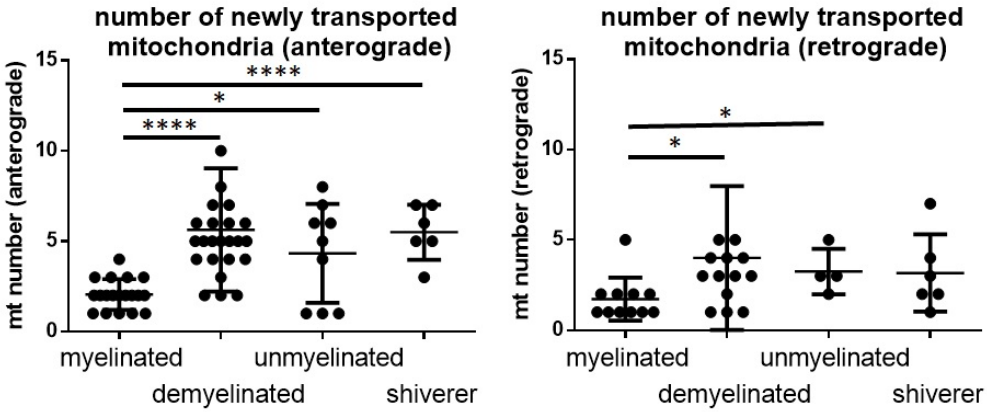

FIGURE 4.17: Mitochondrial transport in the *shiverer* slices without lysolecithin treatment compared to wildtype slices in different conditions, showing an increase in anterograde moving newly transported mitochondria compared to the myelinated wildtype, while the retrograde transport was not different to the myelinated control. Each dot represents the average of all mitochondria from one axon; the total n-number for the *shiverer* axons without lysolecithin treatment is 5 slices from 3 different mice.****=p-value < 0.0001; *=p-value < 0.05

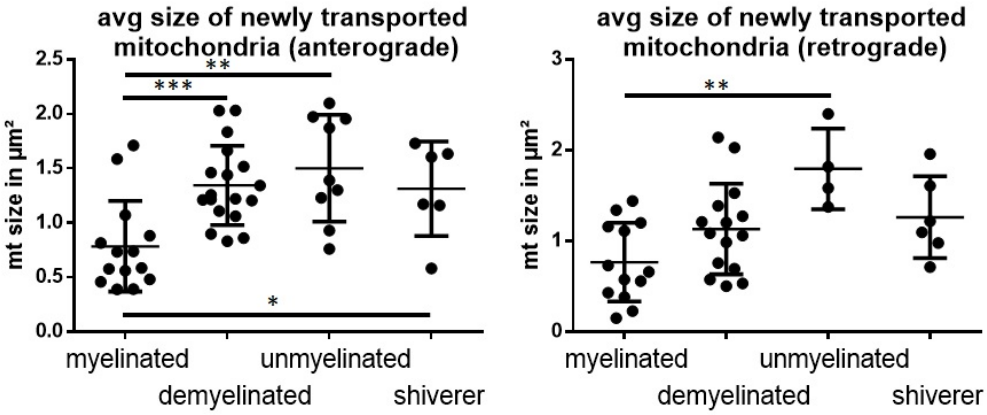

FIGURE 4.18: Mitochondrial average sizes in the *shiverer* slices without lysolecithin treatment compared to wildtype slices in different conditions. There was a statistical significant increase in mitochondrial size in anterograde moving mitochondria in the *shiverer* mutant compared to the myelinated control. Each dot represents the average of all mitochondria from one axon; the total n-number for the *shiverer* axons without lysolecithin treatment is 5 slices from 3 different mice. ***=p-value < 0.001; **=p-value < 0.01; *=p-value < 0.05

The retrograde transport number of newly transported mitochondria however was not increased in the *shiverer* compared to myelinated control; see figure 4.17. There was a statistical significant increase in mitochondrial sizes of the anterograde moving mitochondria in the *shiverer* compared to myelinated control, while the retrograde moving mitochondria did not differ in size between the two conditions; see figure 4.18. However the transport between the *shiverer* slices with and without lysolecithin treatment was not significantly different, as both displayed increased anterograde transport, with a slight decreasing trend in the lysolecithin treated slices; see figure 4.19.

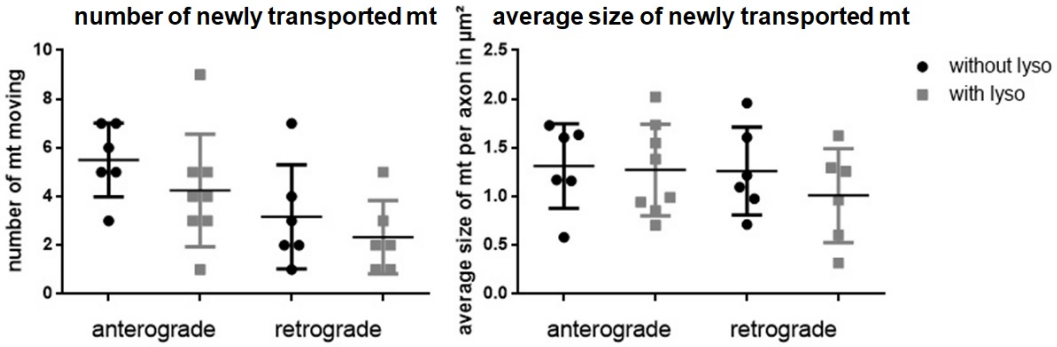

FIGURE 4.19: Mitochondrial dynamics in the *shiverer* mutant with and without lysolecithin treatment, showing the number of newly transported mitochondria on the left and their respective average sizes on the right. There was no significant difference between the *shiverer* mutant with and without lysolecithin treatment, neither in number or size of newly transported mitochondria. Each dot represents the average of all mitochondria from one axon; the total n-number for the *shiverer* axons without lysolecithin treatment is 5 slices from 3 different mice and for the *shiverer* with lysolecithin treatment 8 slices from 6 different mice.

To determine the speed of moving mitochondria in the *shiverer* mutant, kymographs were created with the Kymoclear 2.0 ImageJ plugin; see figure 4.20 (Mangeo, Prevo, and Peterman, 2016). The speed was calculated by tracing individual lines in the kymographs and using the 'analyse kymo' function of the kymotoolbox ImageJ plugin; see figure 4.20 (Zala et al., 2013).

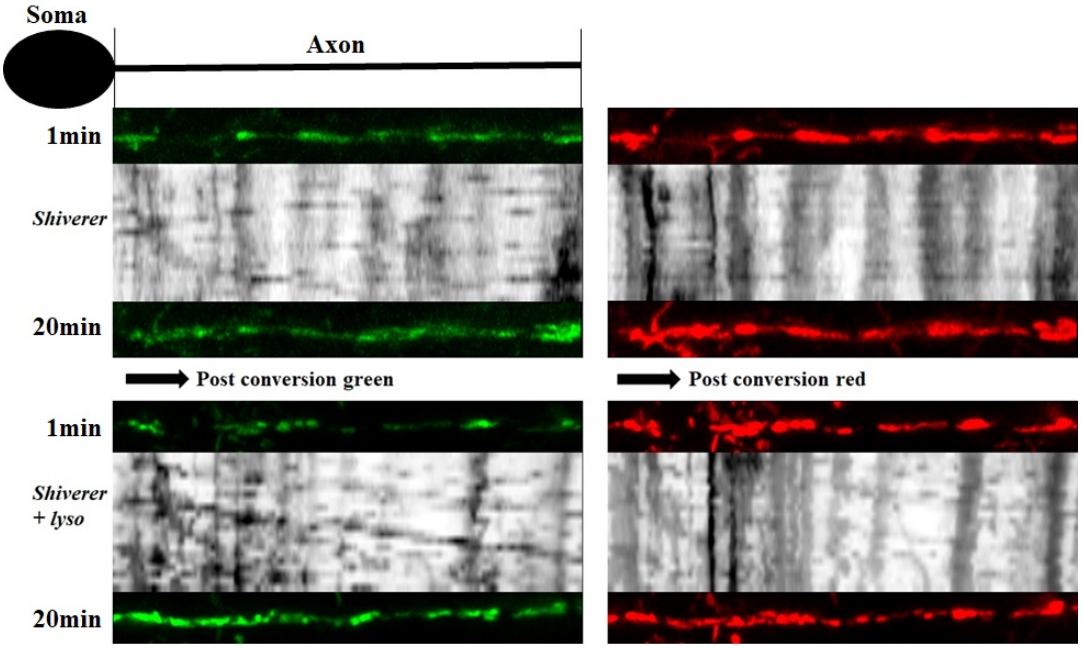

FIGURE 4.20: Kymographs for axons of the *shiverer* mutant without lysolecithin (top panel) and *shiverer* mutant with lysolecithin (bottom panel) treatment, the black arrows pointing in the anterograde direction. The left panels shows the movement of newly transported green mitochondria, while the right panels show converted red mitochondria within the axons, showing significant movement in both conditions.

The mitochondrial movement speed in the anterograde direction was similar to demyelinated and unmyelinated wild-type, with a statistical significant increase of mitochondrial anterograde transport speed in the *shiverer* compared to the wild-type axons; see figure 4.21. The analysis of the mitochondrial speed in the *shiverer* mutant showed no significant different between the *shiverer* slices with or without lysolecithin, although there was a clear trend towards decreased anterograde and retrograde speed of newly transported mitochondria in the *shiverer* slices with lysolecithin treatment; see figure 4.22.

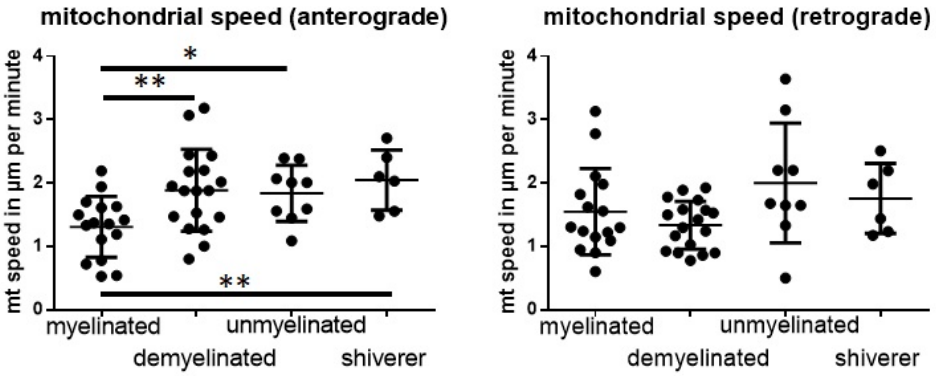

FIGURE 4.21: Mitochondrial movement speed comparison between the *shiverer* slices without lysolecithin treatment and different wt conditions. There was a statistical significant increase of mitochondrial transport speed in the anterograde direction in the *shiverer* axons compared to myelinated control. There was however no significant different in the retrograde movement speed. Each dot represents the average of all mitochondria from one axon; The total n-number for the *shiverer* axons without lysolecithin treatment is 5 slices from 3 different mice. **=p-value < 0.01; *=p-value < 0.05

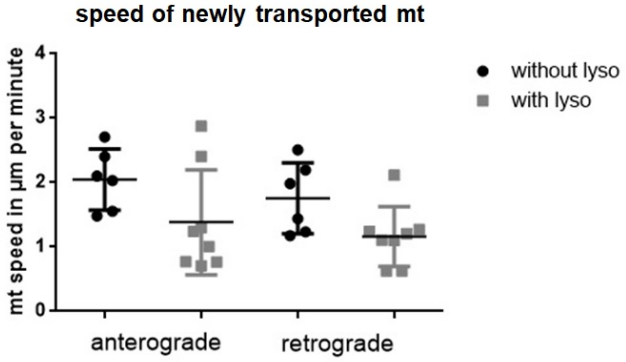

FIGURE 4.22: Movement speed of newly transported mitochondria in the *shiverer* mutant with and without lysolecithin treatment, showing no significant difference in either anterograde or retrograde movement speed, but with a trend towards decreased mitochondrial speed in the *shiverer* with lysolecithin treatment compared to *shiverer* without lysolecithin. Each dot represents the average of all mitochondria from one axon; the total n-number for the *shiverer* axons without lysolecithin treatment is 5 slices from 3 different mice and for the *shiverer* with lysolecithin treatment 8 slices from 6 different mice.

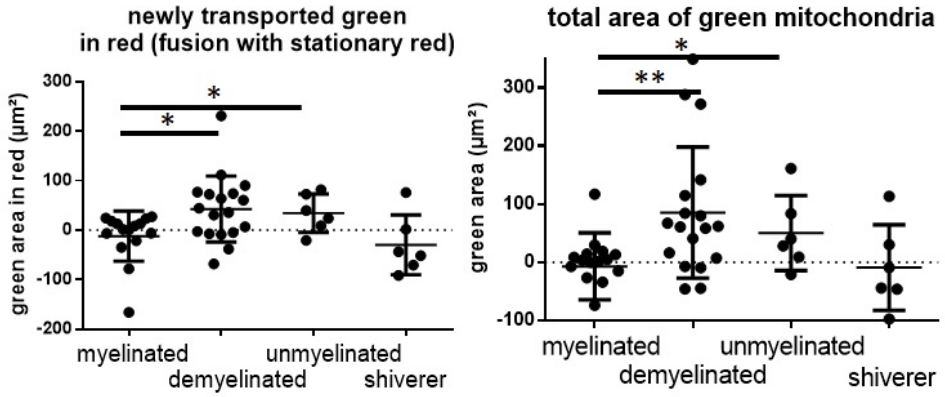

FIGURE 4.23: Mitochondrial fusion in the *shiverer* axons compared to wild-type axons in different conditions. There was no statistical significant difference in mitochondrial fusion between the myelinated control and the *shiverer* and neither was there a statistical significant difference in the total green area between the two conditions. Each dot represents the average of all mitochondria from one axon; The total n-number for the *shiverer* axons without lysolecithin treatment is 5 slices from 3 different mice. **=p-value < 0.01; *=p-value < 0.05

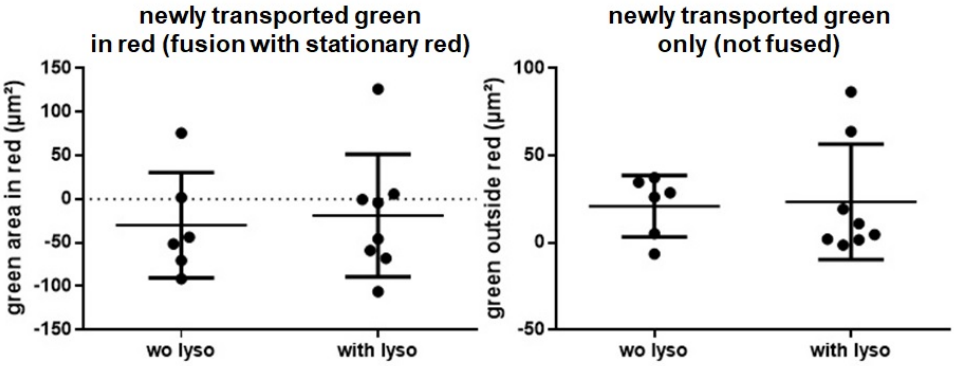

FIGURE 4.24: Fusion dynamics of the *shiverer* mutant with and without lysolecithin treatment, showing no significant difference in fusion rate and both conditions display surprisingly low fusion rates. Each dot represents the average of all mitochondria from one axon; the total n-number for the *shiverer* axons without lysolecithin treatment is 5 slices from 3 different mice and for the *shiverer* with lysolecithin treatment 8 slices from 6 different mice.

To analyse the fusion dynamics of the *shiverer* mutant slices, green in red

fluorescence was measured at minute 20 and corrected for the baseline green-in-red fluorescence at minute 0.

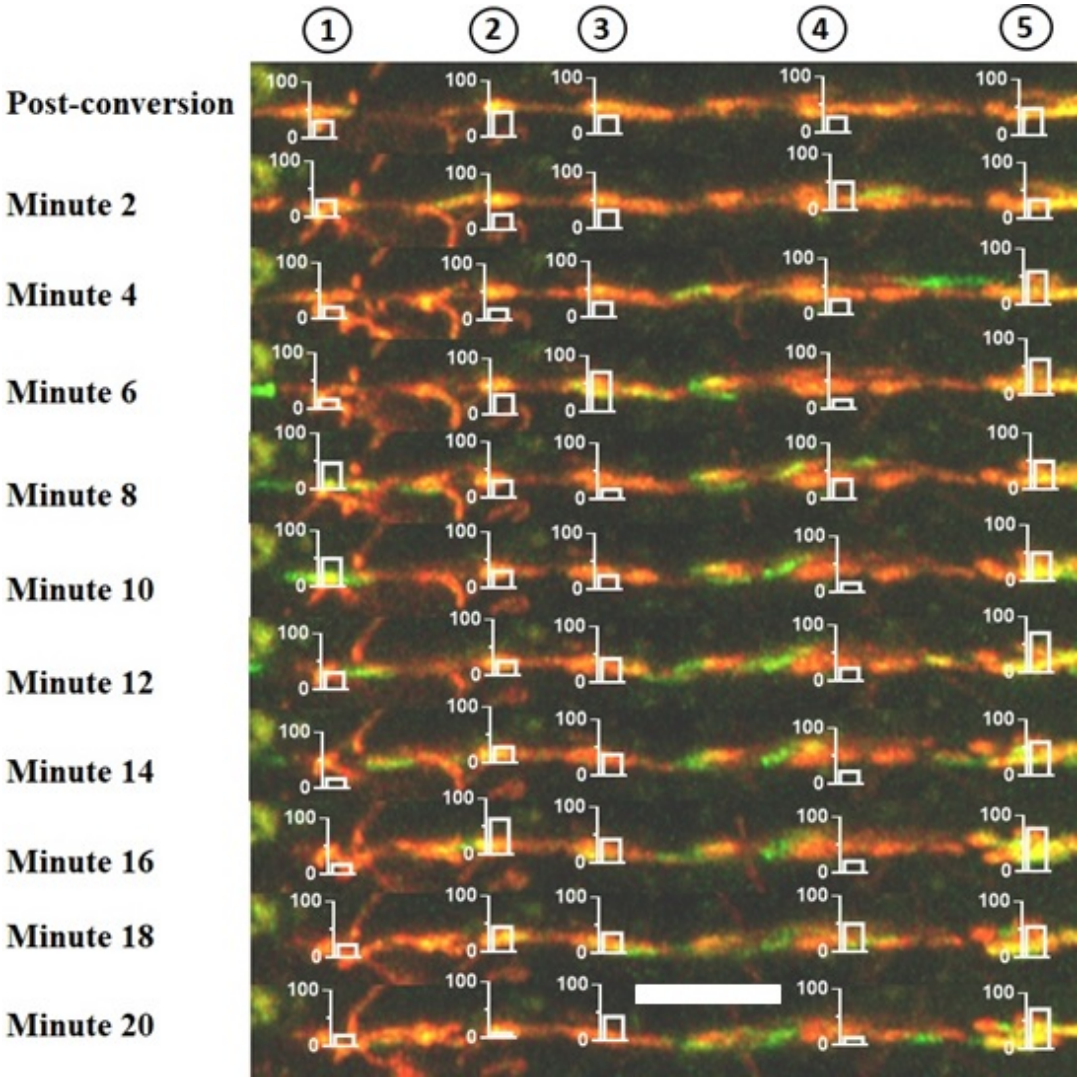

FIGURE 4.25: Fusion dynamics at the level of single fusion and fission events, depicted by a timelapse image series showing several stationary converted mitochondria in a *shiverer* mutant without lysolecithin treatment, that display an increase and decrease in green fluorescence after fusion and fission events respectively. Scalebar=8 µm

The comparison to the myelinated control showed no statistical significant difference in the amount of mitochondrial fusion in the *shiverer* slices also when comparing the total green area there was no significant difference in the *shiverer* and myelinated axons; see figure 4.23. The

comparison of *shiverer* with or without lysolecitiin treatment showed that most of the mitochondria being transported to the converted region of the axon, did not fuse with the converted stationary mitochondria and only exhibited green fluorescence; see figure 4.24. When looking at the fusion and fission dynamics in detail in single axons, it becomes clear that the fusion data underestimates the number of fusion and fission events in the *shiverer* axons without or with lysolecithin treatment; see figures 4.25 and 4.26.

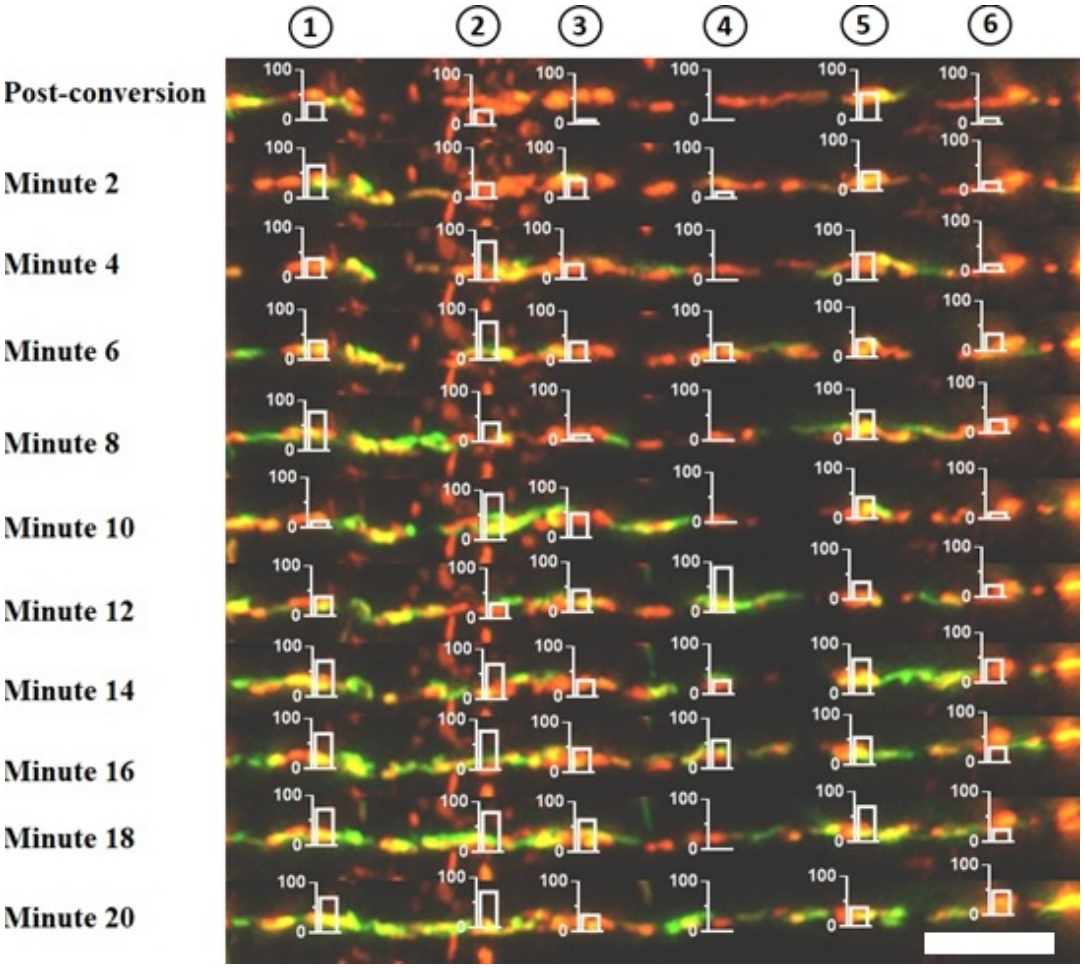

FIGURE 4.26: Fusion dynamics at the level of single fusion and fission events, depicted by a timelapse image series showing several stationary converted mitochondria in a *shiverer* mutant with lysolecithin treatment, that display an increase and decrease in green fluorescence after fusion and fission events respectively. Scalebar=8 µm

This data set indicates that lysolecithin treatment does not increase

mitochondrial transport, speed or fusion dynamics and the increase in mitochondrial dynamics, seen after lysolecithin treatment of wildtype slices, is an effect of the demyelination of the PC axons. There was however a slight trend towards decrease in numbers and a trend towards decreased mitochondrial transport speed in the lysolecithin treated *shiverer* slices compared to the *shiverer* slices without lysolecithin treatment.

4.4 Discussion

4.4.1 Mitochondrial dynamics in demyelinated axons

The timecourse experiment of the ARMD (Chapter 2) has shown that already 24 hours after demyelination with lysolecithin there are significantly more mitochondria in the demyelinated axon compared to the myelinated axon, this is reflected in an increase in overall occupancy of the axon by mitochondria and increased mitochondrial numbers. There is also an increase in the area of single mitochondria, which increases even further 72 hours post demyelination. This increase in size indicates increased mitochondrial fusion within the demyelinated axon. To assess the mitochondrial dynamics in the demyelinated axon, mEOS2 positive PC were demyelinated by using lysolecthin. To get sufficent demyelination of PC axons, a lysolecithin concentration experiment was performed, since the most widely used lysolecithin concentration did not result in complete demyelination of the axons in the cerebellar slice culture. The relatively low transduction rate of PC cells after injection with the lentivirus containing the mEOS2 photoconvertible protein (roughly 1 positive cell per 3 slices) made it necessary to ensure complete demyelination of the PC axons with lysolecithin. A slightly higher concentration of 0.75mg/ml lysolecithin left for 24 hours on the cerebellar slices, lead to sufficient demyelination while still preserving the axonal structure. Subsequently only axons completely without SCoRe signal in the field of view were counted as being demyelinated, while axons with sufficient myelination in the field of view were counted as being myelinated. However with the techniques used it can not be ruled out that the rest of the axon is different from the observable part, since some axons could not be imaged over the whole length.

The demyelinated, mEOS2 positive PC axons were then used to study the mitochondrial transport and fusion dynamics in live cerebellar slices by imaging every minute over 20 minutes and analysed for any changes in mitochondria parameters. This analysis revealed an increase in mitochondrial transport to the demyelinated axon, both from the anterograde and retrograde direction. Since the converted axonal segment was adjacent to the AIS, it can be assumed that the anterograde moving green unconverted mitochondria are coming into the demyelinated axon

from the unconverted cell body. Despite having some residual green fluorescence in myelinated axons, there was not much movement observed compared to the demyelinated axons. This phenomenon of residual green in the ROI was observed in both myelinated and demyelinated axons that were not fully converted, but since only completely green mitochondria were counted as being newly transported, it is still clear that this set of mitochondria is coming in from the cell body or distal part of the axon respectively. The rate of anterograde transport into the observed region was significantly higher than the rate of retrograde transport, so the increased number of mitochondria in the axon and the overall increased occupancy of the axon by mitochondria after demyelination, can be explained by a net increase of anterograde transport. Mitochondrial fusion, which was assessed by measuring the increase of green fluorescence within the stationary red mitochondria, also was more frequent in the demyelinated axon. This lead to an overall increase in the green to red ratio in the demyelinated axon compared to the myelinated axon. This increased fusion rate during the live imaging could explain the overall increase in size in the ARMD timecourse experiment in chapter 2, as increased fusion leads to bigger mitochondria. To assess mitochondrial movement speed in both anterograde and retrograde direction, a kymograph of each axon was generated and the kymograph tracks were analysed using different ImageJ plugins (Mangeo, Prevo, and Peterman, 2016; Zala et al., 2013).

There was a significant increase in the speed of anterograde moving newly transported mitochondria in the demyelinated axon, while the speed of retrograde transport was not different between the demyelinated and myelinated axons. This indicates an overall increase in anterograde speed, which, like the increase in the number of mitochondria being transported in the anterograde direction, eventually will lead to an accumulation of mitochondria in the demyelinated axon over time. In summary the changes in mitochondrial dynamics in the demyelinated axon, namely the increase of anterograde movement, the faster speed of anterograde moving mitochondria and the increased fusion rate of mitochondria within the demyelinated axon compared to the myelinated axon are sufficient to explain the increased mitochondrial content, which can be observed at different timepoints after demyelination (see chapter 2).

4.4.2 Mitochondrial dynamics in the *shiverer* mutant

To determine if the increase in mitochondrial dynamics after demyelination with lysolecithin is not an effect of lysolecithin, but of demyelination itself, cerebellar brain slices of the dysmyelination *shiverer* mutant were used. Like the wild-type slices, the *shiverer* slices were injected with the lentivirus just after the slicing procedure and 2 weeks afterwards live imaging was performed to determine changes in mitochondrial dynamics. Similar to the demyelinated slices, the *shiverer* slices without lysolecithin treatment showed an increase in anterograde transport and speed of anterograde movement. In contrast to the demyelinated axons, the mitochondria in the *shiverer* slices, retrograde transport was not higher than in the myelinated slices.

TABLE 4.1: Change of mitochondrial dynamics between the different conditions: '+' marks baseline. '++' marks a statistical significant increase <2x compared to baseline. '+++' marks a statistical significant increase >2x. A=anterograde; R=retrograde

	Transport number		Speed		Size		Fusion
	A	R	A	R	A	R	
Myelinated	+	+	+	+	+	+	+
Unmyelinated	+	++	++	+	++	++	+++
Demyelinated	+++	+++	++	+	++	+	+++
Shiverer without lysolecithin	+++	+	++	+	++	+	+
Shiverer with lysolecithin	+++	+	+	+	++	+	+

Furthermore, mitochondrial fusion events were also similar to myelinated axons, which could be a explained by the longer time of increased mitochondrial dynamics in the *shiverer* compared to the wild-type demyelinated slices and fusion being already at the maximum and most of the newly transported mitochondria just passing the stationary sites, although this would result in bigger stationary sites compared to wild-type demyelinated axons which was not observed, so the more likely explanation is stronger bleaching of the green fluorescence during the *shiverer* experiments. Between the *shiverer* slices with or without lysolecithin

treatment, there was no significant difference in any of the mitochondrial dynamics parameters measured, although there was a trend towards decrease mitochondrial transport speed in the lysolecithin treated slices. This experiment shows that the increase in mitochondrial dynamics in the previous experiment, is not due to a secondary effect of lysolecithin, but due to demyelination itself.

4.4.3 Future directions

As we only looked at the first part of the PC axon adjacent to the AIS, the dynamics in the axon further away from the cell body could be completely different. Most of the previous studies that were reporting about the ARMD in demyelinated axons, were looking at axonal parts far away from the cell body, mostly white matter tracts, in a different type of neurons and mitochondrial dynamics might be different between cell types (Ohno et al., 2011; Kiryu-Seo et al., 2010; Zhou et al., 2016; Misgeld et al., 2007; Misgeld, Nikic, and Kerschensteiner, 2007). The *in vivo* situation might also be different than *in vitro* and the dynamics might be different depending on the demyelinating agent. In this case lysolecithin was used because its effect on mitochondria is less pronounced than other commonly used agents, furthermore, the *shiverer* experiment of this thesis showed no direct effect of lysolecithin on mitochondrial dynamics (Birgbauer, Rao, and Webb, 2004; Zhang et al., 2011; Komai, Hunter, and Takahashi, 1973; Keough, Jensen, and Yong, 2015; Jeffery and Blakemore, 1995; Wallace et al., 2003; Yu et al., 2007).

At this point it can only be speculated what the signal for this change in mitochondrial dynamics in response to demyelination could be. Firstly, the loss of the oligodendrocyte wrapped around the axon could either set a signalling cascade in motion to respond to demyelination, since the trophic support for the axon is lost, or it may be the other way around and the oligodendrocyte is constantly signalling to the neuron and the loss of the signalling pathway activates the ARMD (Nave, 2010;Morrison, Lee, and Rothstein, 2013; Saab, Tzvetanova, and Nave, 2013). Another possibility could be that the increase in energy demand of demyelination, the subsequent change in the ADP/ATP ratio and change in ionic balance

within the axon is enough to bring in more mitochondria from the cell body and lead to a higher stopping probability in the axon (Trapp and Stys, 2009; Mahad, Trapp, and Lassmann, 2015; Mohd, 2010; Albers and Siegel, 1998; Lores Arnaiz and Ordieres, 2014). The increased mitochondrial content in the *shiverer* mutant, which also shows similar changes in the mitochondrial transport dynamics to the demyelinated axon, favours the latter hypothesis, as in the *shiverer* mutant there is still some myelin wrapped around the axon and it was shown that there is an increase in mitochondrial activity inside the *shiverer* axons (Andrews et al., 2006). But since the myelin wrap around the axon is not tight in the *shiverer* mutant, because the MBP is missing, it could still be enough to signal a loss of myelin to the neuron (Barbarese, Nielson, and Carson, 1983). To elucidate the mechanism behind the ARMD, further experiments are necessary. Microfluidic chambers would offer the possibility to separately manipulate and analyse the axonal and cell body compartment, this would offer significant advantages over the cerebellar slices for certain experiments, as every manipulations in the slice culture always affects the complete neuron as well as the glia cells around it (Taylor et al., 2005).

Chapter 5

Manipulations of the ARMD

5.1 Introduction

5.1.1 Manipulating mitochondrial dynamics

Some of the most widely studied neurodegenerative diseases, among them Alzheimer's, Huntington's and Parkinson's disease, display gene and protein changes that imply that mitochondrial dynamics are involved, namely fusion/fission and transport dynamics, which shows the importance of the dynamic nature of these cellular organelles (Chan, 2006a; Su et al., 2010; Bonda et al., 2011). The constant fusion and fission of mitochondria leads, over time, to a complete mixing of mitochondrial lipids and content, including the mtDNA (Chan, 2006a; Chan, 2006b; Chan, 2012a; Chen et al., 2010). As every mitochondrion contains multiple nucleotids, which contain mtDNA, a single mitochondrion can contain wild-type as well as mutant DNA, called heteroplasmy (Chan, 2006b; Wallace, 2005; Dimauro and Davidzon, 2005; DiMauro and Schon, 2003; Hayashi et al., 1991; Nakada et al., 2001; Nakada, Inoue, and Hayashi, 2001). Via mitochondrial fusion mutant mtDNA is diluted and via mitochondrial fission, mitochondria containing only mutant mtDNA, called homoplasmy, can be degraded via mitophagy (Chan, 2006b; Wallace, 2005; Dimauro and Davidzon, 2005; DiMauro and Schon, 2003; Hayashi et al., 1991; Nakada et al., 2001; Nakada, Inoue, and Hayashi, 2001; Bingo and Sheng, 2016; McWilliams and Muqit, 2017; Whitworth and Pallanck, 2017). This is an important part of mitochondrial quality control, as defective mitochondria can be selectivity degraded via fission followed by mitophagy and if that is not sufficient for maintaining mitochondrial health, fragmentation of

mitochondria can also promote apoptosis (Bingo and Sheng, 2016; McWilliams and Muqit, 2017; Whitworth and Pallanck, 2017; Wang, 2001; Mao and Klionsky, 2013).

Another important part of mitochondrial dynamics is the mitochondrial transport along microtubules, especially in neurons with their highly polarized morphology mitochondrial transport is essential to supply distant parts of the neuron with this vital organelle (Schwarz, 2013; Britt et al., 2016; Sheng, 2014; Lin and Sheng, 2015; Cai and Sheng, 2009; Saxton and Hollenbeck, 2012; Sheng and Cai, 2012). As described in chapter 1 mitochondria are coupled to the kinesin motor proteins via specific adapter proteins, among them Miro1, which, with its EF hands, halts mitochondria at sites with high Ca^{2+} concentration (Lin and Sheng, 2015; Cai and Sheng, 2009; Saxton and Hollenbeck, 2012; Sheng and Cai, 2012; Morris and Hollenbeck, 1995; Stephen et al., 2015b; Guo et al., 2005). It is also reported that disruption of Miro1 can greatly influence mitochondrial shape (Yamaoka and Leaver, 2008). Furthermore, defects in dynein, which is required for the retrograde transport of mitochondria, can lead to elongated mitochondria in the perinuclear region, which shows that defects in the mitochondrial transport machinery can affect mitochondrial fusion/fission (Varadi et al., 2004; Chen and Chan, 2009a). Conversely, defects in mitochondrial fusion and fission have been shown to affect mitochondrial transport, showing that the different aspects of mitochondrial dynamics are interconnected and interdependent (Chen and Chan, 2009a; Verstreken et al., 2005; Li et al., 2004).

As mentioned above several neurodegenerative diseases are linked to defects in mitochondrial dynamics. The inherited form of Parkinson's disease shows a defect in the Pink1 and Parkin genes, which have been shown to be important for mitochondrial quality control (Bingo and Sheng, 2016; McWilliams and Muqit, 2017; Whitworth and Pallanck, 2017; Winklhofer and Haass, 2010). Interestingly, overexpression of Drp1 or down regulation of Marf/Mfn2 in drosophila *pink1* or *parkin* mutants leads to an amelioration of symptoms, which points to a connection to mitochondrial fusion/fission dynamics (Chen and Chan, 2009a). Parkin has also been implicated in mitochondrial turnover, by marking mitochondria with low membrane potential for mitophagy (Chen and Chan, 2009a; Narendra et al.,

2008). Apart from defects in mitochondrial fusion/fission, defects in mitochondrial transport have been linked to many neurodegenerative diseases and it was reported that genes affecting mitochondrial transport can cause neurodegeneration (Chan, 2006a; Sheng and Cai, 2012; Sorbara et al., 2014; Chang and Reynolds, 2006; Schon and Przedborski, 2011). Furthermore, recently it was shown that mitochondrial transport deficits precede axonal degeneration, which is the main correlate of clinical disability, in mouse models of multiple sclerosis (Sorbara et al., 2014). These mitochondrial transport deficits can be ameliorated by treatment with redox scavengers or glucocorticoids, which suggests that inflammatory mediators including ROS/RNS are the main mediators of these transport deficits (Sorbara et al., 2014).

Manipulations of mitochondrial dynamics are possible through genetic mutation of fusion/fission or transport proteins, leading to mutant lines with different expression of the targeted mitochondrial proteins or knock-out of the gene of interest (Ohno et al., 2014; Chen et al., 2003; Zhou et al., 2016). Furthermore, genetic manipulations can be done by viral transduction, either enhancing expression of a gene of interest or by a targeted knock-down via shRNA (Zhou et al., 2016). It was recently shown that *syntaphilin*-KO, which leads to enhanced mitochondrial transport in axons, can aide axonal regeneration after axotomy *in vitro* and *in vivo*, this effect was also replicated by overexpressing Miro1 *in vitro* (Zhou et al., 2016). Another study reported that *shiverer* crossed with *syntaphilin*-KO results in an increased lifespan compared to *shiverer* alone (Joshi et al., 2015). The third possibility is manipulations via small compounds targeting mitochondrial dynamics. The small molecular compound mdivi-1 (mitochondrial division inhibitor 1) is reported as being a specific inhibitor of Drp1 and thus preventing mitochondrial fission, although a recent publication claims that mdivi-1 does not have a specific effect on mitochondrial fission and instead is a reversible complex I inhibitor (Cassidy-Stone et al., 2008; Bordt et al., 2017). Another small molecule compound available for manipulating mitochondrial dynamics is oligomycin, which is an ATPase inhibitor and acts by blocking the F0-subunit of the mitochondrial ATPase (Zala et al., 2013; Shchepina et al., 2012). As mitochondrial transport is dependant on ATP production, the

inhibition of the ATPase by oligomycin completely blocks mitochondrial transport, while leaving the fast axonal transport of vesicles intact (Zala et al., 2013). Pioglitazone, another small molecule compound, is a licensed diabetes drug and was reported to increase mitochondrial biogenesis *in vivo* and *in vitro* (Desouza and Shivaswamy, 2010; Skov et al., 2008; Bogacka et al., 2005; Ghosh et al., 2007). Pioglitazone enhances mitochondrial biogenesis by increasing the expression of peroxisome proliferator-activated receptor (PPAR)-gamma coactivator-1alpha (PGC-1α) and mitochondrial transcription factor A (TFAM), which are both regulators of mitochondrial biogenesis (Corona and Duchena, 2016; Miglio et al., 2009). To manipulate mitochondrial dynamics and test the effect on axonal health after demyelination, the aim of this chapter was to test several small molecule compounds in cerebellar slices after lysolecithin mediated demyelination.

5.2 Materials and methods

Animals

All procedures were performed according to the 1986 Animals Act (scientific procedures) UK and were approved by the local ethics committee. For all the experiments C57BL/6 mice were used. For the generation of cerebellar organotypic slice cultures mice from P7 to P12 were used, because slice generated at this age ensures a good survival of purkinje cells, while already displaying many features of the adult structure of the cerebellum.

5.2.1 Demyelination with lysolecithin

For the demyelination of the slices 0.5mg/ml lysolecithin was added to the slice culture medium for 17 hours before replacing it with normal medium. Several different compounds were added to the slice culture medium before, during and after lysolecithin mediated demyelination was performed and the slices were then stained at 24 hours or 3 days after removing the lysolecithin. For this the slices were fixed with paraformaldehyde (PFA), after which antigen retrieval was performed. The slices were then blocked before incubating them with the primary and secondary antibody; for detailed IHC protocol see chapter 2.

Oligomycin live imaging experiment

Because the increase of green fluorescence inside red fluorescence described in chapter 3 & 4 could stem from the green protein being transported back into the stationary red mitochondria, with no need for fusion events to increase the green in red fluorescence. To address this issue oligomycin was used to block all mitochondrial transport and check if the green in red fluorescence would still increase over time (Zala et al., 2013). If the green protein is transported back into the stationary red mitochondria over the time observed, an increase in green in red fluorescence would be expected despite there being no mitochondrial transport. If the increase of green in red fluorescence is due to fusion of newly transported unconverted green mitochondria with the stationary converted red mitochondria, no increase of green in red fluorescence would be expected in the absence of mitochondrial transport. For the live imaging experiment the slices were injected with the lentivirus expressing mEOS2 (see chapter 3) and after 14 days in culture $20\,\mu M$ oligomycin was added to the slice culture 30 minutes before imaging them on a Zeiss LSM 880 Airyscanner, with the oligomycin solution staying on during the image acquisition. The $20\,\mu M$ concentration of oligomycin was enough to bring mitochondrial movement to a complete stop. For analysis the green in red ratio was measured at baseline and at 5 minutes, 10 minutes, 15 minutes and 20 minutes respectively. The green in red ratio was measured by using ImageJ with the previously described macro (chapter 2), with the addition of a macro for calculating the percentage of green inside the red area.

5.2.2 Inhibiting mitochondrial transport with oligomycin

For inhibition of mitochondrial transport the ATPase inhibitor oligomycin was used (Zala et al., 2013; Shchepina et al., 2012). Oligomycin works by blocking the F0-subunit (proton channel) of the ATPase and thus inhibiting oxidative phosphorylation (Shchepina et al., 2012). In 2013 it was shown by Zala et al that by adding $20\,\mu M$ for 5 minutes was enough to completely block mitochondrial transport, while vesicular fast axonal transport was still intact due to having onboard glycolysis (Zala et al., 2013). In another publication it was shown that a concentration of $0.25\,\mu M$ of oligomycin was the lowest

dose that significantly inhibits oxidative phosphorylation in several cancer cell lines (Hao et al., 2010). Therefore $0.25\,\mu M$ oligomycin was added to the slices destined for treatment for either 6 hours or 24 hours. During that time lysolecithin was added as well for 24 hours to achieve demyelination of the slices and 24 hours after removing lysolecithin from the slices, all slices were stained for neurofilament (NF), myelin basic protein (MBP) and complex IV subunit (COXI). The stained slices were then imaged on a Zeiss LSM 710 confocal microscope using a 63x oil immersion objective with 2x zoom and analysis was done in ImageJ by using the macro described in chapter 2.

5.2.3 Inhibiting mitochondrial fission with mdivi-1

For the inhibition of mitochondrial fission, the Drp1 (dynamin-related protein 1) selective inhibitor mdivi-1 was used (Cassidy-Stone et al., 2008). Slices were prepared and cultured as described in chapter 2 and kept in culture at least seven days before any manipulations were done. After 7 days mdivi-1 was diluted in slice culture medium either $50\,\mu M$ or $100\,\mu M$, before removing the medium from the slices and replacing it with the diluted mdivi-1 solution. After 2 days the mdivi-1 solution was renewed with the appropriate concentration of mdivi-1 again diluted in slice culture medium and lysolecithin was added to the solution at a concentation of 0.5mg/ml. The lysolecithin containing solution was then added to the slices that were going to be demyelinated, while mdivi-1 solution without lysolecithin was added to the myelinated treated slices and lysolecithin without mdivi-1 to the demyelinated control slices. Furthermore, some slices neither received mdivi-1 nor lysolecithin and were used as myelinated control slices. After 17 hours lysolecithin was removed from the slices were it was added before, while adding mdivi again. At 24 hours after removing the lysolecithin, a final renewal of mdivi-1 was done and all slices were stained 2 days later for neurofilament (NF), myelin basic protein (MBP) and complex IV subunit (COXI). The stained slices were then imaged on a Zeiss LSM 710 confocal microscope using a 63x oil immersion objective with 2x zoom and analysis was done in ImageJ by using the macro described in chapter 2.

5.2.4 Increasing mitochondrial biogenesis with pioglitazone

To examine the effect of increased mitochondrial biogenesis on the ARMD and on axonal health after demyelination with lysolecithin, the licensed diabetes drug pioglitazone was used, which is an activator of (PPAR)-gamma-coactivator-1-alpha (PGC-1α) and mitochondrial transcription factor A (TFAM) and thus increases mitochondrial biogenesis. Like with the other small molecule compounds the slices were prepared and cultured as described in chapter 2 and kept in culture for a week, before adding pioglitazone to the culture medium in either $10\,\mu M$ or $40\,\mu M$ concentration. Two days later pioglitazone was renewed and lysolecithin 0.5mg/ml was added to the culture medium. After 17 hours the lysolecithin was removed and pioglitazone added again until staining the slices 3 days after the removal of lysolecithin. Pioglitazone was also added to slices that did not receive lysolecithin and some slices were demyelinated without pioglitazone treatment, and finally some slices received neither lysolecithin nor pioglitazone. All slices were stained 3 days after removing lysolecithin from the slices for neurofilament (NF), myelin basic protein (MBP) and complex IV subunit (COXI) and subsequently imaged on a Zeiss LSM 710 confocal microscope using a 63x oil immersion objective with 2x zoom and analysis was done in ImageJ by using the macro described in chapter 2.

5.2.5 Immunohistochemistry

For Immunohistochemistry protocol see methods section in chapter 2.

TABLE 5.1: Antibodies

Primary Antibody	Antibody type	Used concentration	Target	Source
COXI	mouse monoclonal IgG2a	1:200	Mitochondrially Encoded Cytochrome C Oxidase I	Abcam (ab14705)
MBP	Rat monoclonal IgG1	1:200	Myelin basic protein	AbD Serotec (MCA409S)
NF	Chicken polyclonal	1:2000	Neurofilament-(heavy)	EnCor Biotechnology (CPCA-NF-H)

For Immunohistochemistry protocol see methods section in chapter 2.

Reagents and Media

For slice culture reagents see methods section in chapter 2.

5.3 Results

5.3.1 Live imaging after inhibition of mitochondrial transport with oligomycin

To show that the increase of green in red fluorescence is not an effect of the green protein simply being transported back into the stationary red mitochondria over time, but real fusion events of newly transported unconverted (green) mitochondria with converted stationary (red) mitochondria, mitochondrial transport was inhibited by adding 20 µM oligomycin to the culture medium 30 minutes before imaging and left on during image acquisition (Zala et al., 2013); see figure 5.1.

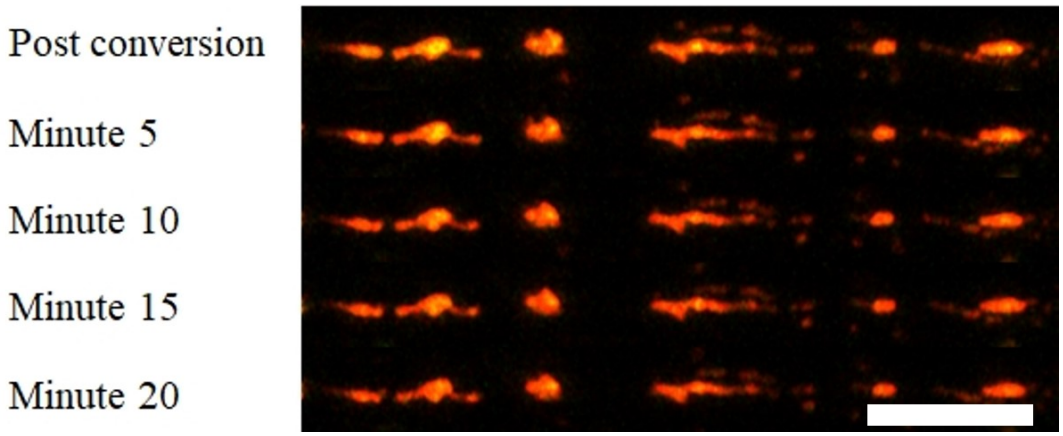

FIGURE 5.1: Impact of high dose oligomycin on mitochondrial movement shown in a timelapse series, illustrating the stop of mitochondrial movement and fading of green inside red fluorescence over time. Scalebar=10 µm

This concentration completely stopped mitochondrial transport, so if the green fluorescence coming back in the converted red mitochondria is an effect of the protein being transported back in, the green in red fluorescence would still be expected to increase over time; see figure 5.1. But if the green coming back in the red fluorescence is due to green mitochondria moving in and fusing with the stationary red mitochondria, inhibition of mitochondrial transport with oligomycin should get rid of this effect. After inhibiting mitochondrial transport, the green in red was constantly declining in comparison to the baseline, which suggest that there is no transport back in of the green fluorescent protein and the bleaching of the

green fluorescence constantly reduces the green in red fluorescence; see figure 5.2.

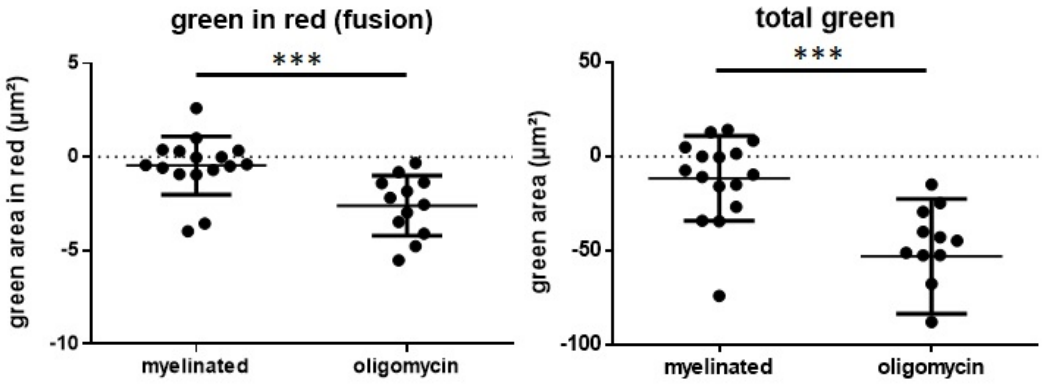

FIGURE 5.2: Impact of high dose oligomycin on mitochondrial movement and fusion, showing the decrease of the green in red and total green fluorescence over the time imaged. There was a significant decrease of green in red fluorescence, as well as significantly decreased green overall in the oligomycin treated slices compared to control. Each dot represents the average of all mitochondria from one axon; the total n-number for the untreated control axons is 16 slices from 12 different mice and for the oligomycin treated slices 8 slices from 4 different mice. ***=p-value <0.001

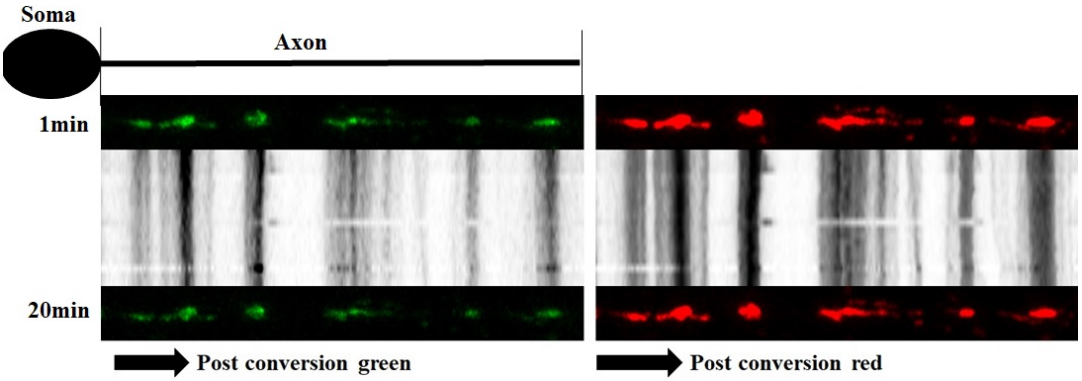

FIGURE 5.3: Mitochondrial speed after high dose oligomycin treatment shown on a kymograph and depicting the complete stop of mitochondrial movement in the green in red channel respectively. Above the kymograph the first images after conversion, while below the kymograph the last frame of the timeseries are placed, to illustrate the changes over time. The black arrow is pointing in the anterograde direction.

This decline of green in red was a constant decline over time, without fusion or fission events in between, bleaching the green fluorescence during the imaging process, due to the lack of transported of new mitochondria to the axon; see figure 5.4.

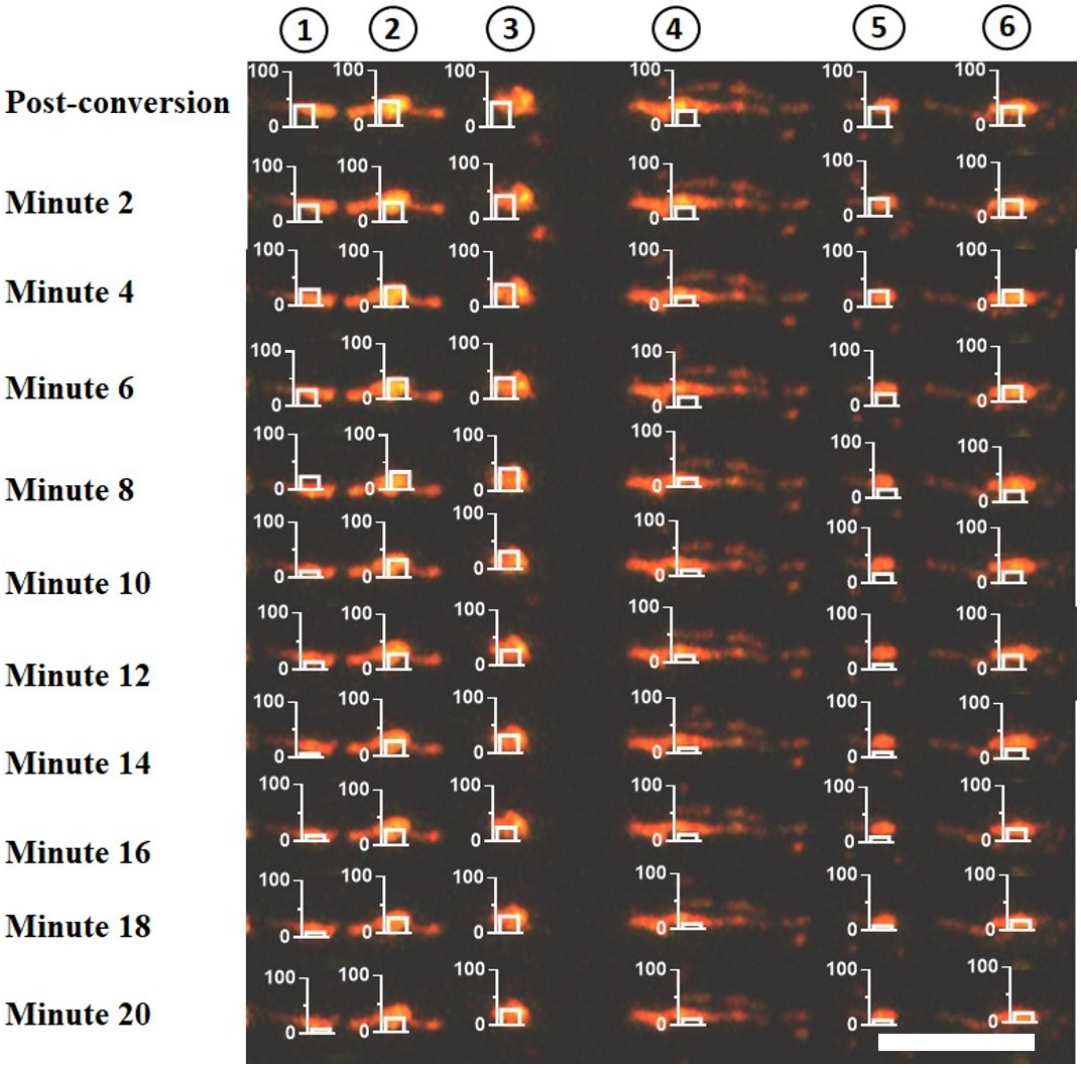

FIGURE 5.4: Mitochondrial fusion dynamics after high dose oligomycin treatment depicting the total stop of mitochondrial transport and fusion and fission events, which leads to a constant decline in green in red fluorescence over time without any sharp increases or decreases in between shown by the constant decrease of the bar graphs over time. Scalebar=10 µm

The complete stop of mitochondrial movement was further examined by creating the kymographs for green and red channels of the oligomycin

treated axons with the Kymoclear 2.0 ImageJ plugin. Like expected neither in green or red kymograph any significant movement was detected, apart from a general drift of the axon over time; see figure 5.3.

5.3.2 Manipulation of mitochondrial transport by the ATPase inhibitor oligomycin

By using the ATPase inhibitor oligomycin, which was shown to inhibit mitochondrial transport, the effect of reducing mitochondrial transport after demyelination was determined (Zala et al., 2013). Using a concentration of $0.25\,\mu M$ oligomycin, which was either added together with lysolecithin (for a total of 24h) or 6 hours before the removal of lysolecithin (6h), the effect of reduced mitochondrial transport on the ARMD was tested; see figures 5.5.

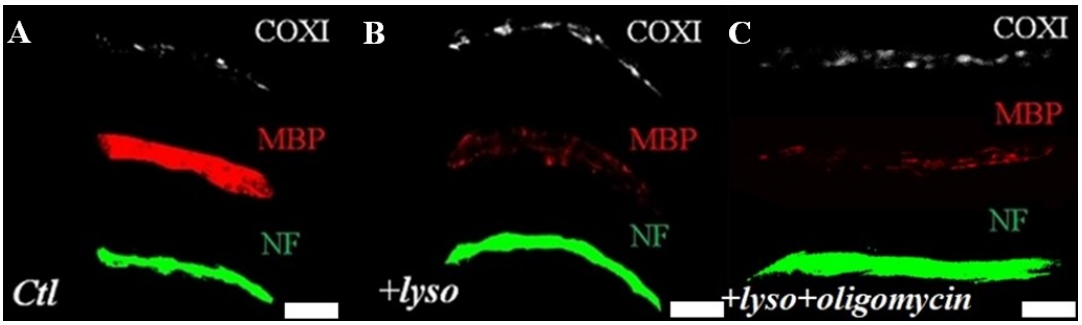

FIGURE 5.5: Effect of oligomycin on axonal mitochondria shown in confocal images of untreated control (A), lysolecithin demyelinated axon (B) and lysolecithin demyelinated axon treated with $0.25\,\mu M$ oligomycin for 24h (C). Scalebar=$5\,\mu m$

For this experiment the total lysolecithin exposure was 24 hours and the slices were stained at 24 hours after removing lysolecithin from the slice culture medium. Already the shorter exposure time of 6 hours oligomycin showed a trend towards decrease of the mitochondrial occupancy of the axon, indicating that hindering transport of new mitochondria to the axon potentially may diminish the ARMD, the same effect was observed by using the longer exposure time of 24 hours of oligomycin; see figure 5.6.

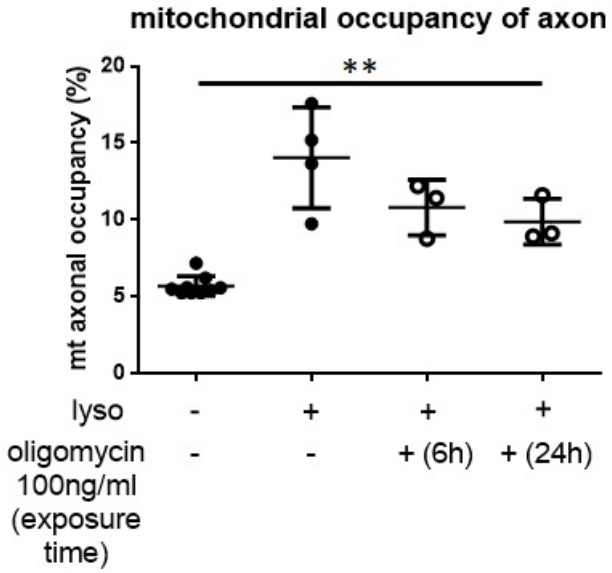

FIGURE 5.6: Impact of oligomycin on the mitochondrial occupancy of the axon after demyelination with lysolecithin, depicting the difference of mitochondrial occupancy (in percent) with and without adding oligomycin and lysolecithin. There was a significant increase of mitochondrial occopancy of the axon in all demyelinated conditions compared to the myelinated conditions. Although there was no significant different between the demyelinated control and the demyelinated oligomycin treated, there was a trend towards decreased mitochondrial occupancy in the oligomycin treated axons. Each dot represents one slice from one mouse and includes 40 analysed axons. **=p-value <0.01

It must be noted that neither exposure time lead to a significant reduction in mitochondrial occupancy, which could be due to the low concentration of oligomycin used. But since oligomycin significantly inhibits ATP production, exposure to high oligomycin concentrations was not desired, as it would interfere with many cellular processes. There was however a significant difference in mitochondrial occupancy of the axon between the myelinated control and oligomycin untreated and treated demyelinated slices. There was a trend to a decrease of mitochondrial area and increase in mitochondrial numbers observed in the oligomycin treated slices compared to the lysolecithin control without oligomycin treatment; see figure 5.7.

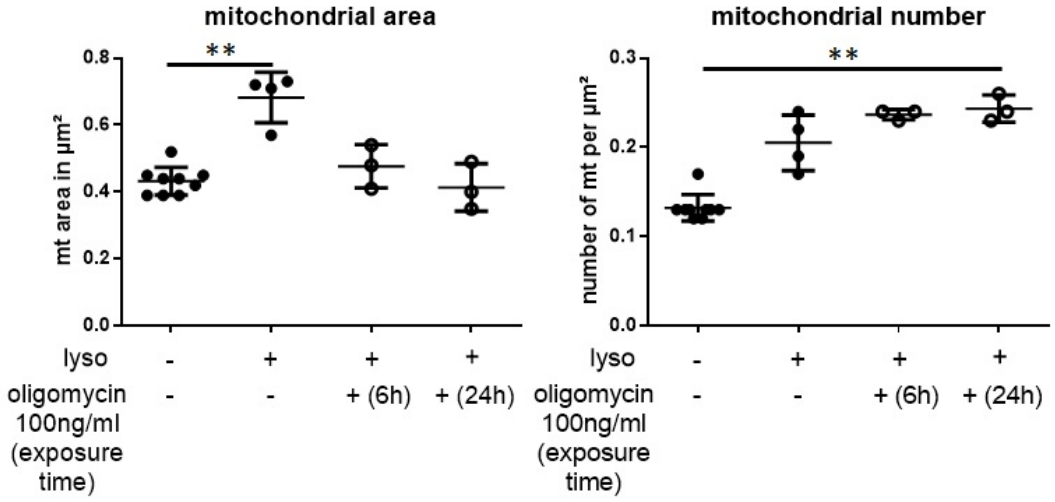

FIGURE 5.7: Impact of oligomycin treatment on mitochondrial numbers and size after demyelination with lysolecithin. Left: average mitochondrial area of single mitochondria in μm^2. Right: the mitochondrial number per μm^2. There was a significant increase of mitochondrial size of the axon in the demyelinated control compared to the myelinated control. Although there was no significant difference between the demyelinated control and the demyelinated oligomycin treated, there was a trend towards decreased mitochondrial size in the oligomycin treated axons. There was a significant increase of mitochondrial number in all the demyelinated conditions compared to the myelinated condition. Although there was no significant difference between the demyelinated control and the demyelinated oligomycin treated, there was a trend towards increased mitochondrial number in the oligomycin treated axons. Each dot represents one slice from one mouse and includes 40 analysed axons. **=p-value <0.01

This observation could indicate a fragmentation of the mitochondrial networking inside the axon, which could be due to the blockage of mitochondrial electron transport chain (ETC) by oligomycin, although not used in high dose, is still able to inhibit the mitochondrial ATPase to a significant proportion (Hao et al., 2010). There was a significant difference in mitochondial numbers between the myelinated control and oligomycin untreated and treated slices and also the mitochondrial area was significantly different between the myelinated and demyelianted control.

Effect of inhibition of mitochondrial transport on axonal health

To determine to effect of oligomycin on axonal health, the area of the axonal bulbs was divided by the total axonal area to get the percentage of axonal bulb area; see figure 5.8. Since oligomycin is an ATPase inhibitor, several other detrimental possibilities on axonal health apart from inhibition of mitochondrial transport are possible. Although a relatively low dose of oligomycin was used, the inhibitory effect on the ATPase and subsequently on the ETC function is still expected to be substantial (Hao et al., 2010).

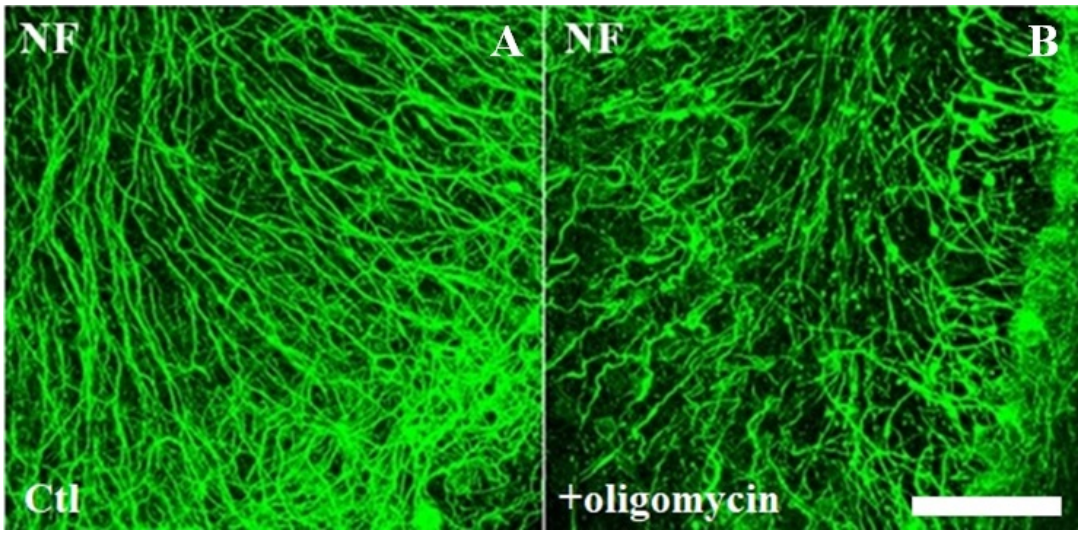

FIGURE 5.8: Impact of oligomycin on axonal health judged by confocal images of demyelinated axons stained for NF, showing axonal bulbs in demyelinated slices without (A) and with oligomycin treatment (B). Scalebar=$50\,\mu m$

The reduction of mitochondrial transport and ATPase activity in general, lead to a significant increase of axonal bulbs with the 24 hours exposure to oligomycin, indicating a detrimental effect on axonal health; see figure 5.9. Already the 6 hour treatment of demyelinated axons with oligomycin showed a trend towards an increased number of axonal bulbs; see figure 5.9.

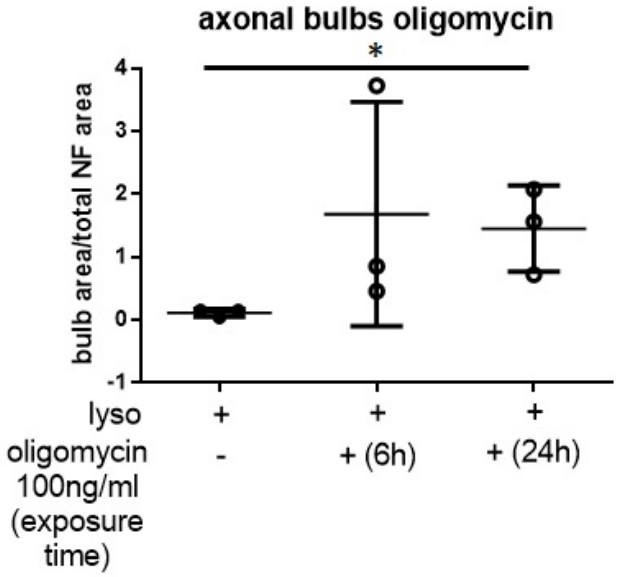

FIGURE 5.9: Effect of oligomycin treatment on axonal health after demyelination, showing the area of axonal bulbs corrected for the total axonal area in demyelinated slices with or without oligomycin treatment. There was a significant increase of axonal bulbs in the slices treated with oligomycin for 24 hours compared to control, there was however no difference between the 6 hour oligomycin treatment and control. Each dot represents one slice from one mouse and includes at least 40 analysed axons. *=p-value <0.05

5.3.3 Manipulation of the ARMD by blocking mitochondrial fission

By using mdivi-1, a putative selective inhibitor of Drp1 and thus mitochondrial fission, the effect of blocking mitochondrial fission during the ARMD was examined (Cassidy-Stone et al., 2008). For this experiment, two different concentrations of mdivi-1 (50 µM and 100 µM) were added to the slice culture medium 2 days before demyelinating with lysolecithin for 17 hours or without adding lysolecithin at all, mdivi-1 was renewed when adding lysolecithin and the slices were stained for Neurofilament (NF), myelin basic protein (MBP) and complex IV subunit (COX-I) 3 days after lysolecithin was removed from the slice culture medium; see figure 5.10. It was reported previously that mdivi-1 can inhibit mitochondrial

fragmentation and exert neuroprotective effects on hippocampal neurons (Xie et al., 2013).

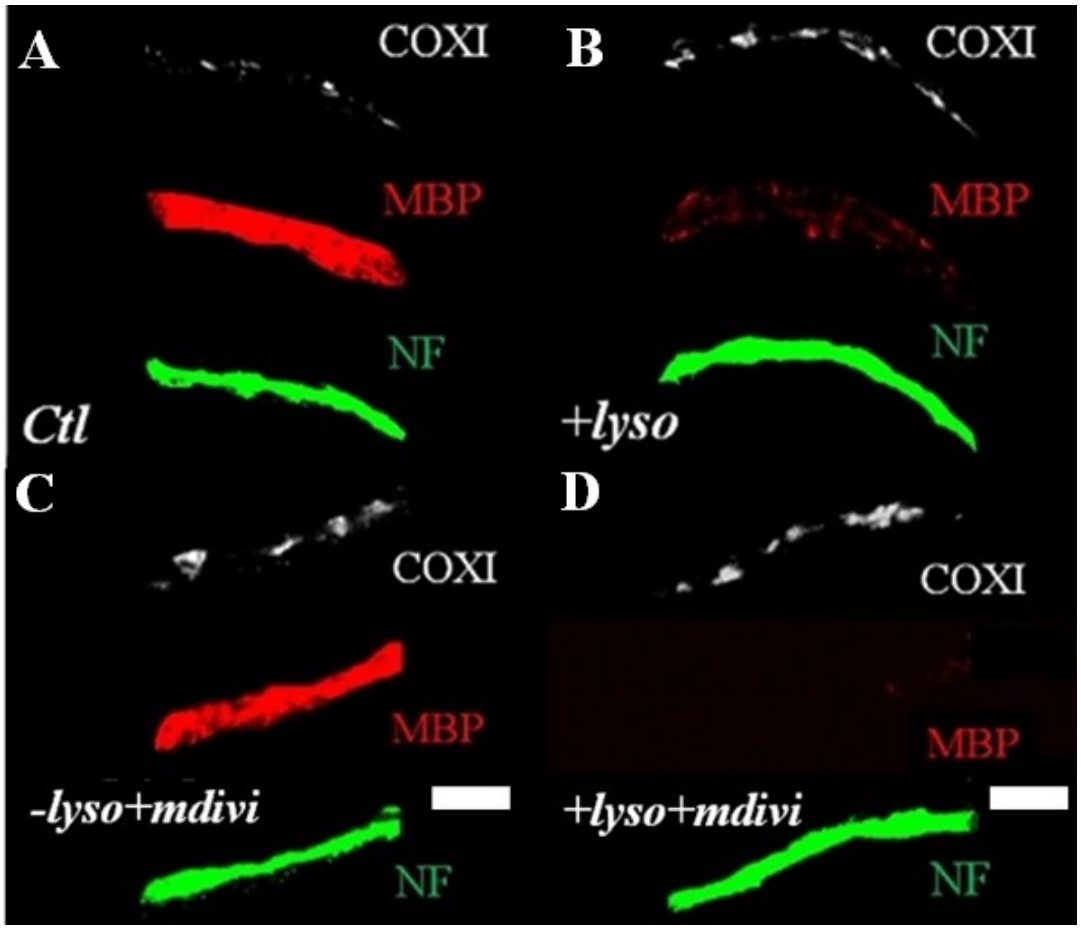

FIGURE 5.10: Impact of mdivi-1 treatment on mitochondria in the axon with or without lysolecithin mediated demyelination, showing the mitochondrial occupancy of axons in (from left to right) myelinated control (A), lysolecithin (B), mdivi (C) and lysolecithin+mdivi (D) treated slices. Scalebar=5 µm

Mdivi-1 caused an increase in the mitochondrial occupancy of the myelinated axons, while it increased the mitochondrial occupancy of the axons even more in the demyelinated axons compared to demyelinated axons without mdivi-1 treatment, with no difference between the 50 µM and 100 µM mdivi-1 concentration; see figure 5.11. There was a significant difference in mitochondrial occupancy of the axon between the myelinated control and mdivi-1 untreated/treated demyelinated slices.

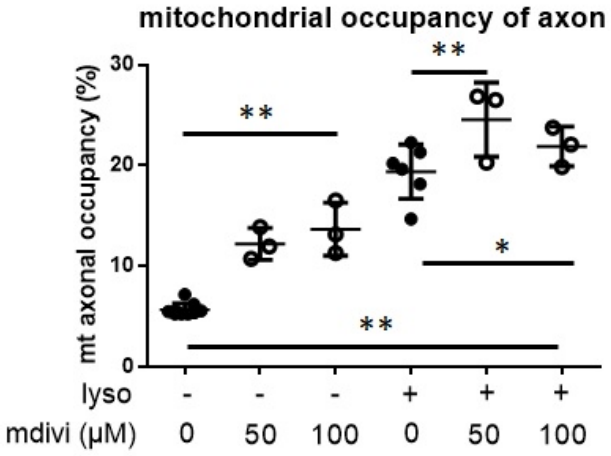

FIGURE 5.11: Effect of mdivi-1 on the mitochondrial occupancy, showing the mitochondrial occupancy of the axons (in percent) with and without adding mdivi and lysolecithin. There was a significant increase in mitochondrial occupancy in the axon with both concentrations of mdivi-1 compared to control, in the myelinated as well as demyelinated axon. Each dot represents one slice from one mouse and includes 40 analysed axons. *=p-value <0.05 ;**=p-value <0.01

As a putative specific Drp1 inhibitor and therefore inhibitor of mitochondrial fission, mdivi-1 was expected to enhance the average area of single mitochondria and indeed the mitochondrial size was increased in both the myelinated and demyelinated axons after mdivi-1 treatment, again no significant difference between the 50 µM and 100 µM mdivi-1 concentration was observed; see figure 5.12. Furthermore, there was a significant difference in mitochondrial size between the myelinated control and mdivi untreated/treated demyelinated slices.

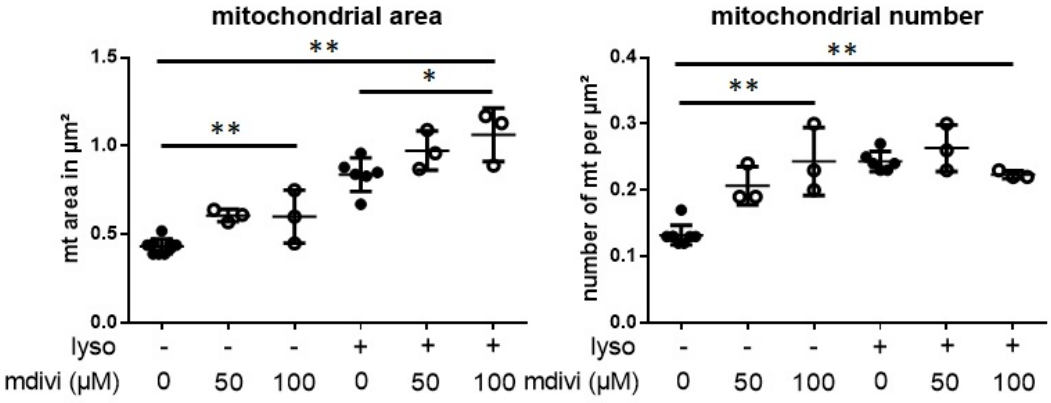

FIGURE 5.12: Effect of mdivi-1 on the mitochondrial size and number, showing a significant increase in mitochondrial size with both concentrations of mdivi-1 compared to control, in the myelinated as well as demyelinated axon. The number of mitochondria was significantly increased in the myelinated axon treated with mdivi-1 compared to myelinated control, there was however no difference in the demyelinated axon. Average mitochondrial area of single mitochondria in μm^2; number of mitochondria per μm^2. Each dot represents one slice from one mouse and includes 40 analysed axons. *=p-value <0.05 ;**=p-value <0.01

An unexpected observation was the increase in mitochondrial number in the myelinated axons treated with mdivi-1, there seemed to be a trend of even further increase of mitochondrial numbers in the $100\,\mu M$ compared to the $50\,\mu M$ mdivi-1 samples; see figure 5.12. In the demyelinated axons mdivi-1 did not increase the mitochondrial number any further, compared with the already increased numbers of mitochondria after demyelination with lysolecithin alone; see figure 5.12. There also was a significant difference in mitochondrial numbers between the myelinated control and mdivi-1 untreated/treated demyelinated slices.

Effect of inhibition of mitochondrial fission on axonal health

To test whether the inhibition of mitochondrial fission with mdivi-1 is promoting axonal health or is detrimental to it, the area of the axonal bulbs was divided by the total axonal area to get the percentage of axonal bulb area. In the $100\,\mu M$ mdivi-1 treated samples, a lot of axonal bulbs in the neurofilament (NF) staining were observed; see figure 5.13.

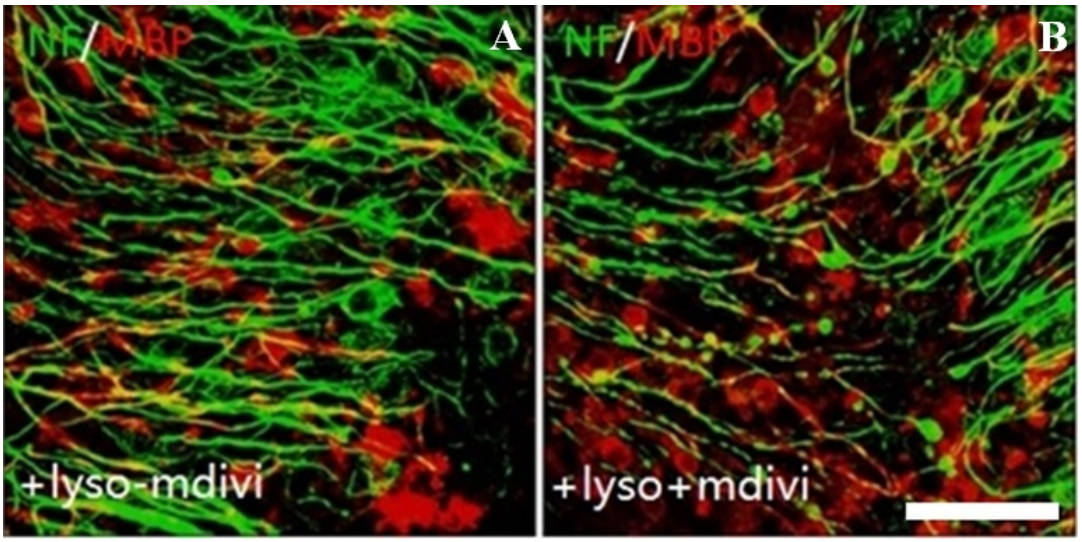

FIGURE 5.13: Impact of mdivi-1 on axonal health as judged by confocal images of demyelinated axons stained for NF and MBP, showing axonal bulbs in demyelinated slices without (left) and with mdivi-1 100 µM treatment (right). Scalebar=50 µm

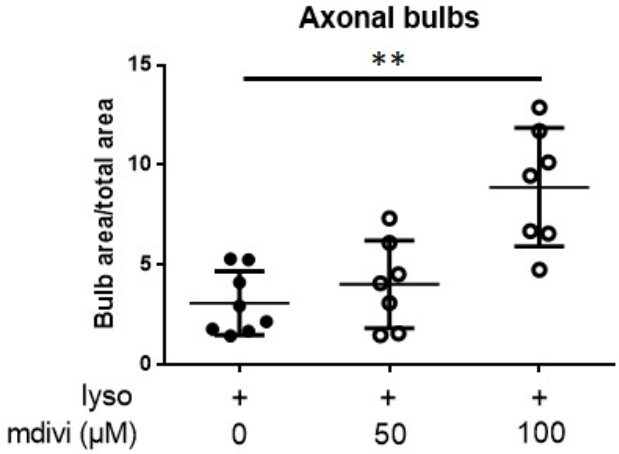

FIGURE 5.14: Effect of mdivi-1 on axonal health, shown by the axonal bulb area corrected for the total axonal area in demyelinated slices with or without mdivi-1 treatment. There was a significant increase of axonal bulbs in the 100 µM mdivi treatment compared to control, there was however no difference between the 50 µM concentration and control. Each dot represents one slice from one mouse and includes at least 40 analysed axons. **=p-value <0.01

The analysis of axonal bulb area as a fraction of total axonal area, showed a slight trend in increasing axonal bulbs with $50\,\mu M$ concentration of mdivi-1 in the demyelinated axons and a substantial increase of axonal bulbs at $100\,\mu M$ mdivi, compared to the axons demyelinated with lysolecithin alone; see figure 5.14.

5.3.4 Manipulation of mitochondrial biogenesis with pioglitazone

By using the licensed diabetes drug pioglitazone, which was shown to increase mitochondrial biogenesis by increasing the expression of peroxisome proliferator-activated receptor (PPAR)-gamma coactivator-1alpha (PGC-1α) and mitochondrial transcription factor A (TFAM), the effect of increasing mitochondrial biogenesis on the ARMD was tested; see figure 5.15 (Desouza and Shivaswamy, 2010; Skov et al., 2008; Bogacka et al., 2005; Ghosh et al., 2007). For this experiment two different concentrations of pioglitazone were used ($10\,\mu M$ and $40\,\mu M$) and renewed two days after the first addition together with the addition of lysolecithin and a final renewal 24 hours after removing the lysolecithin. The total lysolecithin exposure time was 18 hours and the slices were stained at 3 days after removing the lysolecithin from the culture. The ScoRe imaging technique was used to determine the myelination status of the axons in this experiment.

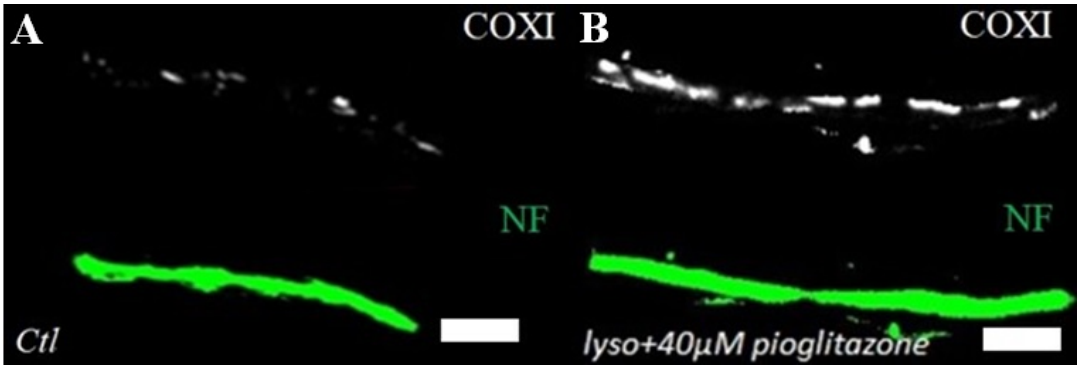

FIGURE 5.15: Effect of pioglitazone on axonal mitochondria, depicted in fluorescent images of myelinated axons in slices with (B) or without (A) pioglitazone treatment. Scalebar=$5\,\mu m$

Although the n-number for this experiment was not high enough to reach statistical significance, there was a clear trend towards increased mitochondrial occupancy of myelinated axons in pioglitazone treated slices without lysolecithin treatment compared to slices not treated with pioglitazone; see figure 5.16.

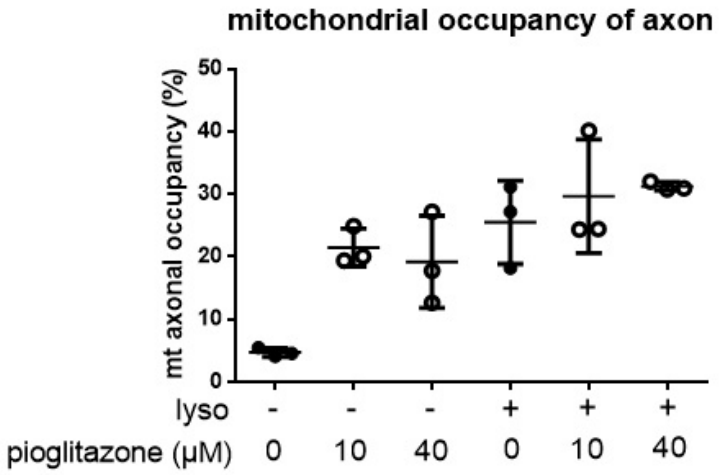

FIGURE 5.16: Impact of pioglitazone treatment on the axonal occupancy of mitochondria, showing a trend towards increased occupancy in the myelinated axons. Although there was no significant different between the myelinated control slices and the pioglitazone treated slices, in both the myelinated and demyelinated axons, there was a clear trend towards increased mitochondrial occupancy of the axon in the pioglitazone treated slices. A higher n-number would be needed to reach statistical significance. Each dot represents one slice from one mouse and includes 40 analysed axons.

There was a slight trend towards an increase in mitochondrial occupancy in the lysolecithin-demyelinated slices treated with the 40 µM pioglitazone concentration, compared to the untreated demyelinated slices, but higher n-number would be required to confirm a possible difference between the two; see figure 5.16.

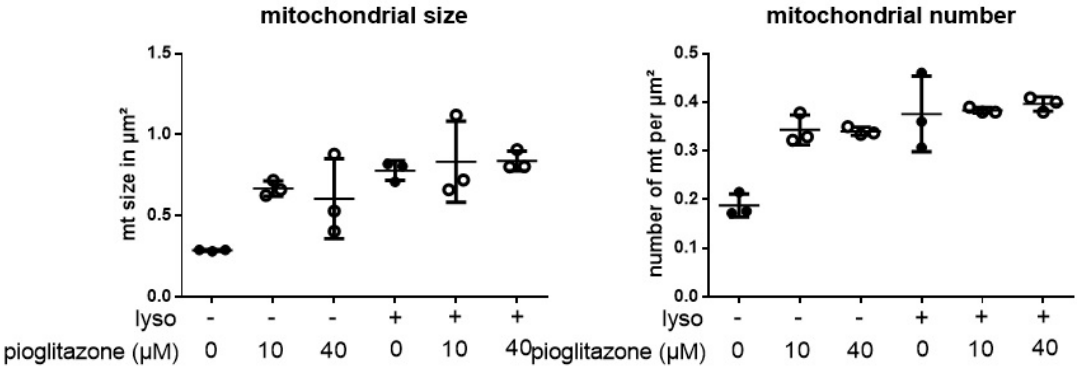

FIGURE 5.17: Impact of pioglitazone on mitochondrial size and number in axons. Like the occupancy, size and number, showed an increasing trend in the myelinated axons. Although there was no statistical significant difference between the myelinated control slices and the pioglitazone treated slices, there was a clear trend towards increased mitochondrial size and number in the myelinated pioglitazone treated slices. A higher n-number would be needed to reach statistical significance. There was no difference in the demyelinated axons between control and pioglitazone treated slices. Each dot represents one slice from one mouse and includes 40 analysed axons.

Like the occupancy, the mitochondrial number in the axons and the area of the average single mitochondrion showed an increasing trend in the pioglitazone treated myelinated slices compared to myelinated control. In the demyelinated slices, the number and average size of single mitochondria did not differ between the pioglitazone treatment and the control; see figure 5.17.

Effect of increasing mitochondrial biogenesis on axonal health

To check the effect of pioglitazone treatment on axonal health after demyelination with lysolecithin, pioglitazone treated and untreated slices were demyelinated with lysolecithin and stained 3 days after removing lysolecithin. The slices were then stained for NF to compare the percentage of axonal bulbs between the groups; see figure 5.18.

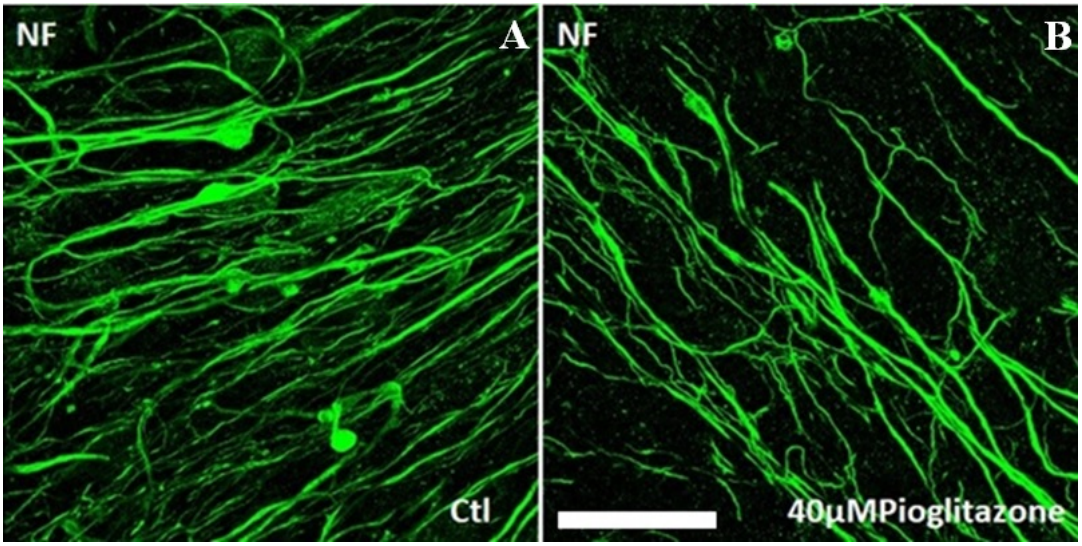

FIGURE 5.18: Impact of pioglitazone on axonal health as shown by fluorescent images of NF staining in demyelinated slices with (B) or without (A) pioglitazone treatment. Scalebar=50 µm

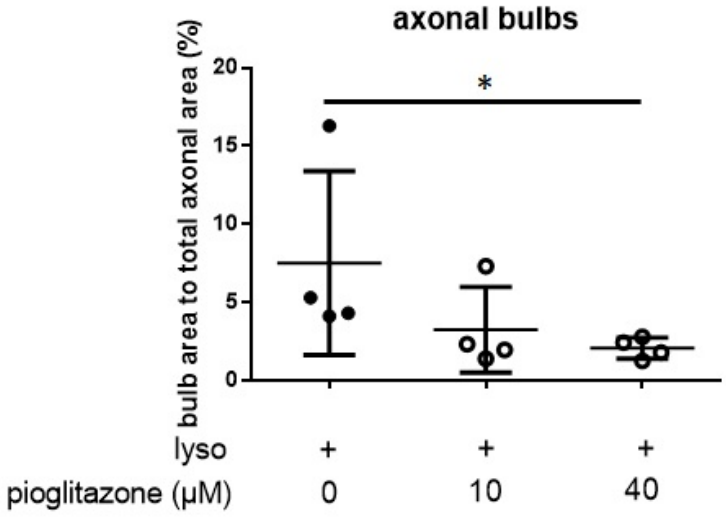

FIGURE 5.19: Effect of pioglitazone on axonal health as judged by the percentage area of axonal bulbs of the total axonal area in demyelinated slices with or without pioglitazone treatment. There was a significant decrease of axonal bulbs, when the size of bulbs was taken into account, in the 40 µM pioglitazone treated slices compared to demyelinated control. Each dot represents one slice from one mouse and includes at least 40 analysed axons. *=p-value <0.05

The analysis of the axonal bulb area as a percentage of the total axonal area showed a significant reduction of axonal bulb area with the $40\,\mu M$ pioglitazone concentration compared to the control; see figure 5.19. The $10\,\mu M$ as well showed a slight trend towards reduced axonal bulbs compared to the control; see figure 5.19. This significant difference however was lost when the total number of axonal bulbs, which was corrected for the total axonal area, was measured; see figure 5.20.

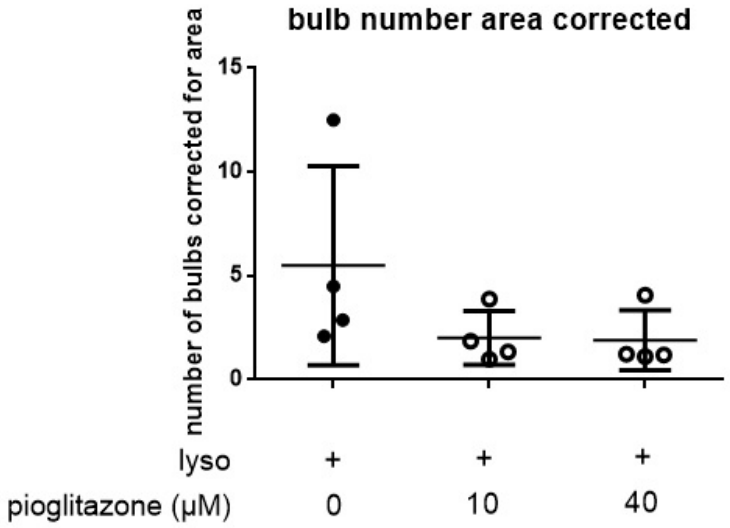

FIGURE 5.20: Impact of pioglitazone treatment on axonal health as judged by the number of axonal bulbs corrected for the total axonal area in pioglitazone treated and untreated slices after demyelination with lysolecithin. There was no significant difference of axonal bulbs, when just counting the numbers, between the pioglitazone treated slices compared to demyelinated control. Each dot represents one slice from one mouse and includes at least 40 analysed axons.

5.4 Discussion

As several neurological diseases show protein alterations that imply involvement of mitochondrial dynamics, either in fusion/fission dynamics or mitochondrial transport dynamics, targeting mitochondrial dynamics is of great interest to possibly modify the clinical outcomes of these diseases (Chan, 2006a; Su et al., 2010; Bonda et al., 2011). Although genetic manipulations of mitochondrial dynamics are widely used in experiments *in vitro* as well as *in vivo*, genetic manipulations are not used in the clinical setting, were small molecular compounds are warranted to target specific molecular processes (Ohno et al., 2014; Chen et al., 2003; Zhou et al., 2016).

5.4.1 Manipulation of mitochondrial transport

The ATPase inhibitor oligomycin, which targets the F0-subunit of complex V of the ETC, was reported to completely inhibit mitochondrial transport *in vitro* (Zala et al., 2013; Shchepina et al., 2012). Two separate experiments were done using oligomycin in specific concentrations for each experiment. The first experiment was done to determine the effect of decreasing mitochondrial transport, with a low dose of oligomycin, has on the ARMD and subsequently on axonal health after demyelination with lysolecithin. For this oligomycin was added together with lysolecithin, or 18 hours after adding lysolecithin to the medium, while keeping it in the medium until lysolecithin was removed, the slices were then stained 24 hours after removing lysolecithin. This lead to a total oligomycin exposure time of 6 or 24 hours with a concentration of $0.25\,\mu M$, which represents a relatively low dose compared to the one used by Zala et al, which was shown to completely inhibit mitochondrial transport (Zala et al., 2013). Compared to the 24 hour timepoint after demyelination without treatment, the oligomycin treatment lead to a trend in decreased mitochondrial occupancy of the axon at 24 hours after removing lysolecithin from the medium, although no statistical significant difference was observed.

The size of single mitochondria in the axon also showed a trend towards decreased size in the oligomycin treated group compared to lysolecithin alone, again no statistical significant difference was observed. At the same time the number of mitochondria in the axon showed a trend towards an

increase in mitochondrial numbers after treatment with oligomycin, with no statistical difference. The increase in mitochondral numbers and decrease in size of single mitochondria, although not significant, could point towards mitochondrial fragmentation following oligomycin treatment. As oligomycin is an inhibitor of the F0-subunit of complex V of the ETC and thus inhibits ATP production, it would not surprising be to observe mitochondrial fragmentation after oligomycin treatment (Shchepina et al., 2012). Overall the trend towards a decrease in mitochondrial occupancy of the axon and decrease in size of single mitochondria after demyelination, points towards a disturbance of the ARMD after blocking mitochondrial transport by oligomycin treatment. This decrease in the ARMD after blocking mitochondrial transport, hints at the importance of mitochondrial transport to the axon from other parts of the cell. Although is has to be noted, that these findings were not statistical significant and oligomycin, as an ATPase inhibitor, has many other effects on cellular health besides blocking mitochondrial transport.

To check the effect of oligomycin treatment on axonal health after demyelination, the area of axonal bulbs was measured and corrected for the total axonal area. There was a significant increase in axonal bulbs with the oligomycin treatment over 24 hours, with a trend of increase in axonal bulbs after 6 hours of oligomycin exposure. This increase in axonal bulbs after oligomycin and lysolecithin treatment indicates that mitochondrial transport is an important part of the ARMD in protecting the axon from degeneration. Again it has to be noted, that oligomycin has many other effects on cellular health apart from blocking mitochondral transport, so it can not be ruled out that some other effect of blocking ATP production lead to the increase in axonal bulbs. As noted above the main caveat of this oligomycin experiment, is that the blockage of the ATPase leads to many different detrimental effects on cellular health besides inhibiting mitochondrial transport, so a lower concentration of oligomycin was used which did not lead to significant impact on the ARMD and instead blunted the response. To further test the effect of oligomycin on the ARMD a concentration titration of oligomycin should be done to determine the optimal dose for inhibition of mitochondrial transport, while keeping the cells alive. Another possibility to check the effect of mitochondrial transport

on the ARMD, without affecting the ATP production, would be to use genetic manipulations of the mitochondrial transport machinery. It was already reported in the literature that overexpression of syntaphilin, a mitochondrial docking protein in the axon, leads the decreased mitochondrial transport, while a knock-out of syntaphilin leads to an increase of mitochondrial transport in the axon (Ohno et al., 2014; Zhou et al., 2016). Also overexpression of Miro1, an adapter protein that indirectly links mitochondria the kinesin and dynein motor proteins, was reported to increase mitochondrial transport significantly (Stephen et al., 2015b; Zhou et al., 2016).

The second experiment with oligomycin, which was a live imaging experiment, was done to exclude any transport of the unconverted green mEOS2 protein back into the stationary converted red mitochondria. For this a higher dose of oligomycin (20 µM), which is reported in the literature to completely block mitochondrial transport, was added to the slices 30 minutes before imaging and was left on during the imaging procedure (Zala et al., 2013). This brought mitochondrial movement to a nearly complete stop. The ROI was converted and imaged every minute for 20 minutes and the overall movement as well as the green in red fluorescence was measured. If the green protein would be transported back into the stationary red mitochondria within the ROI, it would be expected to see an increase of green in red fluorescence over the imaged time, on the other hand if the green in red fluorescence only increase when fusion of newly transported unconverted green mitochondria fuse with the stationary converted red mitochondria, no increase of green in red fluorescence would be expected. There was a significant decrease of green in red fluorescence measured over time, which indicates that there is no transport back of the green protein into the converted red mitochondria. That there was a decrease of green in red fluorescence, instead of just stable levels, can be explained by the bleaching of the green fluorescence over the imaged period. This effect was also seen in the total green fluorescence, again a significant decrease over the imaged 20 minutes. This clearly shows that the increase of green in red fluorescence observed in chapter 3 and 4, is a product of newly transported unconverted green mitochondria to the ROI and subsequent fusion with the stationary converted red mitochondria.

5.4.2 Manipulation of mitochondrial fission

To manipulate mitochondrial fission and to measure the effect on the ARMD or axonal health after demyelination, the putative Drp1 specific inhibitor mdivi-1 was used to inhibit mitochondrial fission in cerebellar brain slices with or without lysolecithin (Cassidy-Stone et al., 2008). As mentioned in chapter 1, mitochondrial fission is mediated by the GTPase Drp1, which interacts with surface proteins on the mitochondrial outer membrane, potential candidates are for example Mff (mitochondrial fission factor) and Fis1 (mitochondrial fission 1 protein) (Liu and Chan, 2015; Losón et al., 2013; Otera et al., 2010). A reduction in mitochondrial fission would lead to enlarged mitochondria, emulating increased mitochondrial fusion, which was reported to be protective under stress conditions, as elongated mitochondria were shown to have increased ATP production and better protection against ROS/RNS (Tondera et al., 2009; Redpath et al., 2013; Chiang et al., 2015). Furthermore, mitochondrial fusion allows for complementation of damaged mitochondria with healthy mitochondria, thus diluting mitochondrial defects (DiMauro and Schon, 2003; Chan, 2012a; Scott and Youle, 2010; Chan, 2012b; Nakada, Inoue, and Hayashi, 2001).

For this experiment two different concentrations of mdivi-1 were added to the slices ($50\,\mu M$ and $100\,\mu M$) and the effect on the size and number of mitochondria in the axon and subsequently on axonal health was measured after demyelination with lysolecithin. Interestingly, mdivi-1 already significantly increased mitochondrial content in the myelinated axons, with both concentrations. Furthermore, mdivi-1 significantly increased the mitochondrial occupancy in the lysolecithin treated axons even more than with lysolecithin alone. The effect seen in the myelinated axons, can be attributed to the increase in mitochondrial size, which was significantly greater in the mdivi-1 treated axons compared to control. There was also an increase in mitochondrial number, which was an unexpected finding, since mdivi-1, as an inhibitor of mitochondrial fission, is expected to increase mitochondrial size, but not numbers. On the contrary, it would be expected that the bigger mitochondria, which are an effect of the decrease in fission, are more difficult to transport to the axon. In the demyelinated axon there was also an increase in mitochondrial occupancy of the axon with the mdivi-1 treatment compared to the demyelinated axons treated with

lysolecithin alone. This effect was significant with both used concentrations of mdivi-1. In the case of the demyelinated axon this increase in mitochondrial occupancy is not driven by the number of mitochondria in the axon, as there was no increase in mitochondrial numbers compared to the mdivi-1 untreated demyelinated axons. There was however an increase in mitochondrial size, which was observed with both concentrations of mdivi-1.

To check the effect of mdivi-1 treatment on axonal health after demyelination, the area of axonal bulbs was calculated by using ImageJ and was substracted from the total axonal area to correct for any differences in axonal numbers between the images taken. There was no protective effect on axons by treating the slices with $50\,\mu M$ mdivi-1 when demyelinating them with lysolecithin. With the $100\,\mu M$ concentrations of mdivi-1 there was even a significant increase of axonal bulbs compared with the mdivi-1 untreated slices. This detrimental effect of mdivi-1 on axonal health was unexpected, since an increase in elongated mitochondria is supposed to be protective in stress environments. Recently, it was reported that mdivi-1 is not a specific inhibitor of Drp1 (and thus mitochondrial fission), since it only poorly inhibits the GTPase activity (K_i > 1.2 mM), but a reversible NADH Coenzyme Q oxidoreductase (complex I of the ETC) inhibitor; (Bordt et al., 2017). This inhibitory effect on complex I could explain the detrimental effect on axonal health, furthermore the increase in mitochondrial size, despite being significant, was only marginal in terms of absolute size of single mitochondria. If mdivi-1 was inhibiting mitochondrial fission efficiently, the size of single mitochondrial would be expected to increase by a substantial amount, which is not observed with the concentrations used, in line with the report of mdivi-1 being a weak Drp1 inhibitor (Bordt et al., 2017).

To really assess the effect of decreasing mitochondrial fission or increasing mitochondrial fusion, a different approach should be used, either by using different compound or by manipulating mitochondrial fusion/fission dynamics by genetic manipulation. The peptide P110 was reported to decrease mitochondrial fission efficiently *in vitro* by interacting with Drp1, also under oxidative stress conditions (Qi et al., 2013; Filichia et al., 2016). Furthermore, P110 was found to be neuroprotective in a model

of Parkinson's disease *in vitro*, by reducing excessive mitochondrial fission and ROS production (Qi et al., 2013; Filichia et al., 2016). Dynasore is another candidate to reduce mitochondrial fission, which was also reported to be protective against ischemia/reperfusion injury in the mouse heart (Reddy, 2014; Tanaka and Youle, 2008; Gao et al., 2013).

5.4.3 Manipulation of mitochondrial biogenesis

To measure the effect increasing mitochondrial biogenesis on the ARMD and axonal health after demyelination, the licensed diabetes drug pioglitazone was used to increase mitochondrial biogenesis in cerebellar brain slices with or without lysolecithin treatment (Desouza and Shivaswamy, 2010). Pioglitazone has been shown to increase expression of PGC-1α and TFAM, two regulators of mitochondrial biogenesis (Skov et al., 2008; Bogacka et al., 2005; Ghosh et al., 2007; Corona and Duchena, 2016). While TFAM binds to mitochondrial promoters in the DNA and enhances transcription of mitochondrial genes, PGC-1α is the master regulator of mitochondrial biogenesis and is responsible for the activation of cAMP response-element-binding-protein (CREB) and nuclear-respiraty-factor-1 and 2 (NRF1& 2), which in term increases the transcription of genes responsible for mitochondrial biogenesis (Alam et al., 2003; Campbell, Kolesar, and Kaufman, 2012; Liang and Ward, 2006). Increasing mitochondrial biogenesis is reported to be neuroprotective and protects neurons from mitochondrial insult (Stetler et al., 2012; Hasegawa et al., 2016).

Two different concentrations of pioglitazone were used for this experiment ($10\,\mu M$ and $40\,\mu M$) and the mitochondrial occupancy of the axons, as well as the size and number of mitochondria in the axon was analysed and compared between treated and untreated slices. Furthermore, the effect of pioglitazone on axonal health was measured after demyelination with lysolecithin. There was a trend towards increased mitochondrial occupancy of myelinated axons in pioglitazone treated slices compared to untreated slices. In the lysolecithin treated demyelinated slices, pioglitazone did not increase the mitochondrial occupancy any further than with lysolecithin treatment alone. The increase in mitochondrial occupancy

in the myelinated axons, seemed to stem from the increase in mitochondrial numbers, as well as the increase in the average size of the single mitochondrion. In the demyelinated slices there was neither a change in mitochondrial number nor size of the average mitochondrion compared to slices only treated with lysolecithin. To confirm the trend seen in the myelinated axons and examine the effect of pioglitazone on mitochondrial parameters after demyelination in more detail a higher n-number is warranted.

To determine the effect of pioglitazone treatment on axonal health after demyelination, the area of each axonal bulb was calculated by using ImageJ, added together and the percentage of axonal bulb area to the total axonal area was calculated. There was already a slight trend toward a decrease in percentage of axonal bulb with the $10\,\mu M$ pioglitazone concentration, while the $40\,\mu M$ concentration lead to a significant decrease in axonal bulb area. This effect however was not observable when measuring the number of bulbs corrected for the total axonal area, which means that there is only a reduction in size of the axonal bulbs, not in numbers.

5.4.4 Summary manipulating mitochondrial parameters

In summary, inhibition of mitochondrial fission, and possible inhibition of complex I, with mdivi-1 leads to an increase in axonal bulbs compared to untreated demyelinated axons (Cassidy-Stone et al., 2008; Bordt et al., 2017). Also, the inhibition of mitochondrial transport, as well as the reduction of ATP synthesis, with oligomycin has a detrimental effect on axonal health as shown by the increase in axonal bulb area (Shchepina et al., 2012). The increase of mitochondrial biogenesis with pioglitazone might have a protective effect on axonal health after demyelination with lysolecithin, although this protective effect was only significant when taking the bulb size into account, while the total number of axonal bulbs was not significantly lower than in untreated control slices. (Skov et al., 2008; Bogacka et al., 2005; Ghosh et al., 2007; Corona and Duchena, 2016).

Chapter 6

Modelling mitochondrial deficiency

6.1 Introduction

6.1.1 Mitochondrial deficiency in MS

The previous chapters were looking at mitochondrial dynamics after demyelination with lysolecithin, to study the effect of demyelination, which is a hallmark feature of multiple sclerosis, on this dynamic organelle (Noseworthy et al., 2000; Ferguson et al., 1997; Fawcett and Asher, 1999; Bitsch et al., 2000a; Stichel and Muller, 1998; Popescu, Pirko, and Lucchinetti, 2013; Lassmann, 2013; Kutzelnigg and Lassmann, 2014). In all these experiments, only wild-type neurons of the cerebellum were analysed, but many neurons in multiple sclerosis show mitochondrial dysfunction and DNA defects, as shown in MS autopsy cases. This defects can lead to deficiency in one or more subunits of the ETC, which has negative consequences for the neuronal mitochondria and is likely to contribute to neurodegeneration seen in MS (Dutta et al., 2006; Campbell et al., 2011; Broadwater et al., 2011; Witte et al., 2013; Kim et al., 2010; Hares et al., 2014; Fischer et al., 2013; Haile et al., 2017a). To model the effect of this mitochondrial deficiency on the ARMD and ultimately axonal health after demyelination, slices from mutants with mitochondrial DNA deletions were used. Because these mtDNA deletions lead to embryonic lethality, a Cre-lox system with an ERt site was used to induce a conditional knock-out with tamoxifen after the mice reached a certain age (Agostino et al., 2003). There

are several transgenic mouse models used in the Mahad laboratory that have distinct mitochondrial defects.

$COX10^{fl/fl} - Thy1 - Cre - ERT2^{+-}$

The $COX10^{fl/fl} - Thy1 - Cre - ERT2^{+-}$ mouse line is, after activation of the Cre-recombinase with tamoxifen, lacking the mitochondrial scaffolding protein COX10 in a subpopulation of neurons expressing the Thy1.2 promoter. Since COX10 is needed for the assembly of complex IV of the mitochondrial respiratory chain, these mice completely lack complex IV; see figure 6.1. This mouse line was generated by Graham Campbell in the Mahad lab by crossing a mouse line in which the CreERT2 cassette is driven by the Thy1.2 promoter (TCE) with a $Cox10^{flox/flox}$ mouse line (Zonta et al., 2011; Fünfschilling et al., 2012).

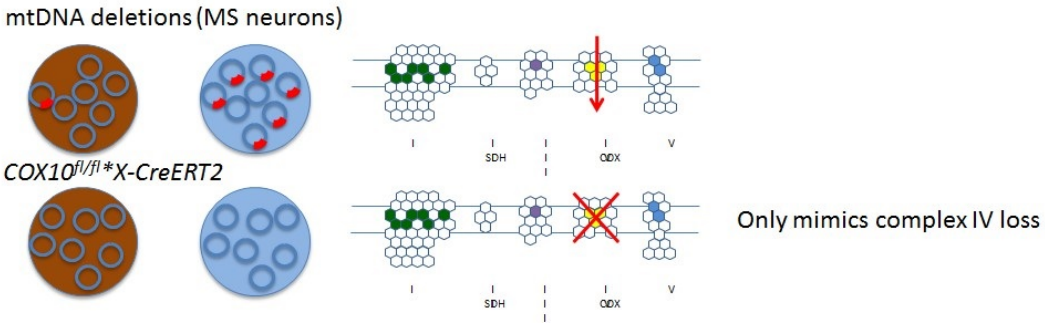

FIGURE 6.1: Effects of different mitochondrial DNA defects. The top panel shows the situation in MS, where an expansion of mitochondrial DNA deletions over time is observed, which leads to a reduction in complex IV activity. The bottom panel show the effect of a COX10 deletion, which leads to a complete loss of complex IV.

6.2 Timeline of $COX10^{fl/fl} - Thy1 - Cre - ERT2^{+-}$ mouse

$COX10^{fl/fl} - Thy1 - Cre - ERT2^{+-}$ mice which were injected (by Graham Campbell) on five consecutive days two weeks apart, show widespread complex IV deficient neurons in the CNS four weeks after the last injection; see figure 6.2. Six weeks later the mice present with severe clinical signs e.g.

flat profile and severe hind limb disturbance; see figure 6.2. It was also shown by Graham Campbell and other members of the Mahad lab, that the ARMD is perturbed in the complex IV deficient axons, displaying an even greater increase of mitochondrial occupancy compared to wild-type shortly after demyelination, followed by a depletion over time. These mitochondria appearing in the axon lack complex IV as opposed to wild type neurons with are complex IV efficient. To determine any structural changes following loss of mitochondrial complex IV in neurons, paraffin embedded tissue of the mutant mice was stained for different cellular markers, including synapses, and compared to litter mate control tissue ($COX10^{fl/fl} - Thy1$). Because any observed change will be most pronounced at the end stage, every staining was first done at 10 weeks after the last tamoxifen injection and thereafter earlier time points were stained. This is done to determine the optimal time point for demyelination *in vivo*, when there is no structural change but sufficient complex IV deficiency found in the neurons.

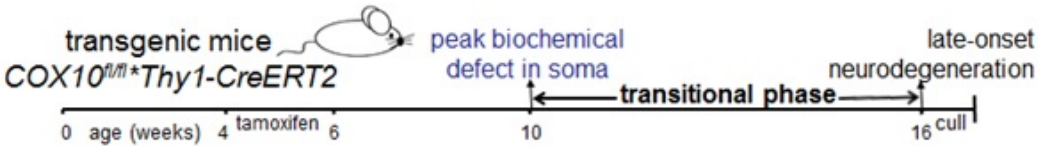

FIGURE 6.2: Timeline of the $COX10^{fl/fl} - Thy1 - Cre - ERT2^{+-}$ transgenic mouse line, depicting the onset of biochemical deficiency and late onset neurodegeneration.

6.3 Materials and methods

6.3.1 Mutant mouse lines

All procedures were performed according to the 1986 Animals Act (scientific procedures) UK and were approved by the local ethics committee. The mutant mouse lines used for this experiments were created before my arrival by Graham Campbell in the Mahad lab, with the $COX10^{fl/fl} - Thy1 - Cre - ERT2^{+-}$ being generated by crossing a mouse line in which the CreERT2 cassette is driven by the Thy1.2 promoter (TCE) with a $Cox10^{flox/flox}$ mouse line (Zonta et al., 2011; Fünfschilling et al., 2012).

6.3.2 Immunohistochemistry

For Immunohistochemistry slice culture tissue and paraffin embedded sections were used, the slides were labelled according to which antibodies, dilution and antigen-retrieval method would be used, furthermore the date of the beginning of the staining was indicated. For Immunohistochemistry protocol see methods section in chapter 2.

6.3.3 Paraffin sections

For the paraffin sections four distinct steps followed, which are different depending on the staining, 1. Deparaffination of the slides and blocking of the endogenous peroxidase, 2. Antigen retrieval step, 3. Incubation with the Antibodies and optional 4. development of the staining with DAB.

Reagents

For reagents see methods section in chapter 2.

Antibody application

For Immunohistochemistry protocol see methods section in chapter 2.

TABLE 6.1: Antibodies

Primary Antibody	Antibody type	Used concentration	Target	Source
COXI	mouse monoclonal IgG2a	1:200	Mitochondrially Encoded Cytochrome C Oxidase I	Abcam (ab14705)
MBP	Rat monoclonal IgG1	1:200	Myelin basic protein	AbD Serotec (MCA409S)
NF	Chicken polyclonal	1:2000	Neurofilament-(heavy)	EnCor Biotechnology (CPCA-NF-H)
Porin	Mouse monoclonal IgG2b	1:400	Voltage-Dependent Anion Channel 1	Abcam (ab14734)
VGlut1	Mouse monoclonal IgG1	1:200	Vesicular glutamate transporte r 1	UC Davis/NIH NeuroMab Facility

COX/SDH assay

1. Frozen slides thawed on room temperature for 1 hour
2. DAB and Cytochrome C are thawed and combined
3. 1 Spatula of bovine catalase (Sigma) per thawed tube is added
4. Vortexed
5. Slides labelled accordingly PAP pen circle is drawn
6. Tissue is covered with DAB+Cytochrome C Solution
7. Slides/slices put into incubator for 30 minutes at $38\,^{\circ}\mathrm{C}$

8. Slides/slices washed 2 times for 2 minutes with PBS
9. NBT, PMS (light sensitive), Succinate and Azide are thawed
10. 100 µl of PMS and 100 µl of Succinate added to NBT
11. 10 µl of Azide added and vortexed
12. Tissue covered with SDH Solution
13. Slides/slices put into incubator for 30 minutes at 38 °C
14. Slides/slices washed 2 times for 2 minutes with PBS
15. Slides/slices put into 100% Ethanol for 10 minutes
16. Immersed into Histoclear 20 times
17. Mounted with DPX and glass coverslip

6.3.4 Imaging methods

VGlut1 synaptic staining

For the VGlut1 synaptic staining paraffin sections of different time points after tamoxifen induction of complex IV deficiency were stained according to the paraffin protocol and incubated over night at 4 °C with the VGlut1 antibody.

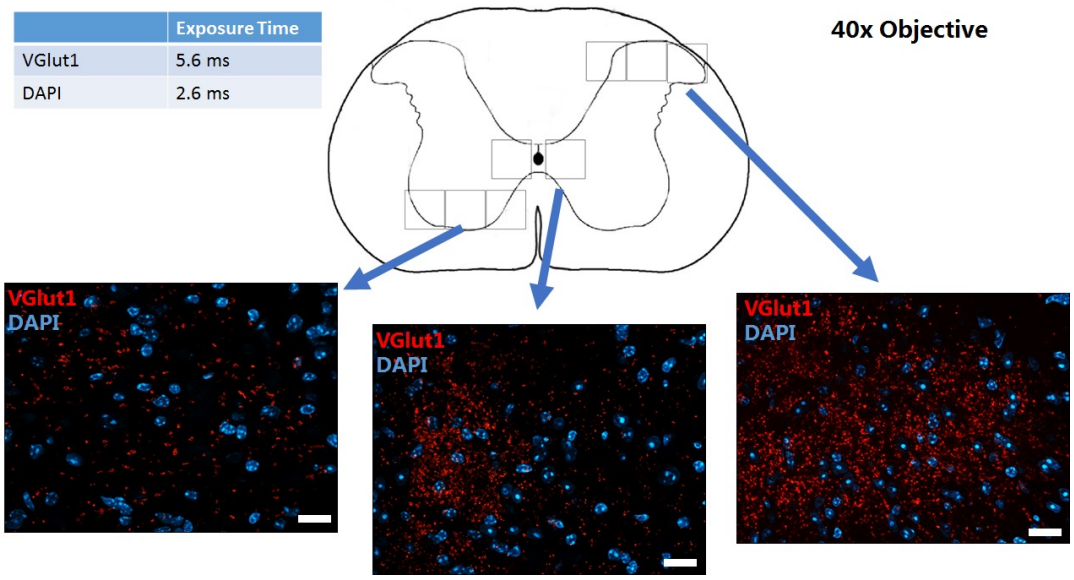

FIGURE 6.3: Overview of the imaging method of VGlut1 positive synapses (red) and nuclei (blue), scalebar $20\,\mu m$. Images of the whole dorsal and ventral areas, as well as the central (not analysed) region were taken with a 40x oil objective on a Zeiss ApoTome2.

Anti-IgG1 coupled to Rhodamine-Red-X was used as the secondary antibody. The imaging of the sections was done on a Zeiss ApoTome2 with a 40x oil objective and 5.6ms exposure time for the Rhodamine and 1.6ms for the DAPI. Pictures from the dorsal, central and ventral area were taken, although the central area was not included in the following analysis; see figure 6.3. For each area a z-stack of $6\,\mu m$ thickness was taken with $0.5\,\mu m$ intervals between z-planes. After the imaging the pictures were converted into 8-bit using ImageJ and adjusted for actual area of VGlut1 staining; see figure 6.4. The quantification was done using the analyse particles tool in ImageJ with a threshold of 8-255 and a selected pixel size of 10-500; see figure 6.5.

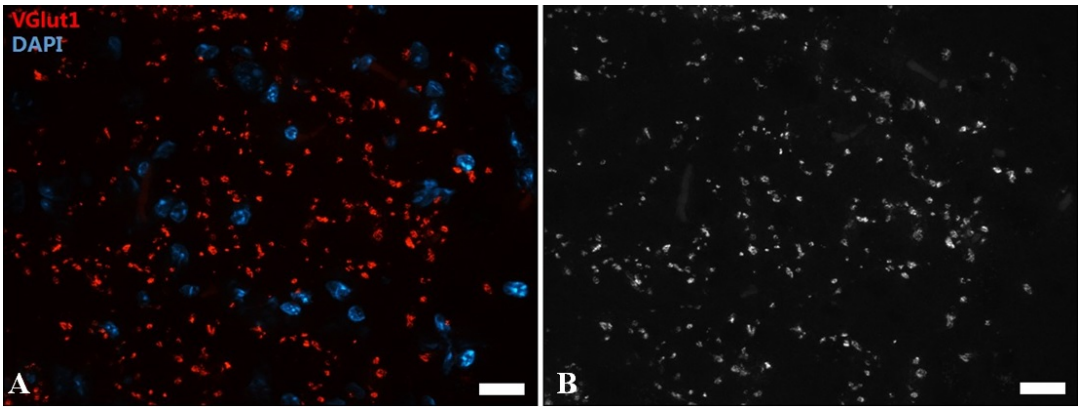

FIGURE 6.4: Conversion of images for quantitative analysis in ImageJ. The pictures (A) had to be converted to 8-bit black and white (B), this was done with ImageJ using the batch->convert option. VGlut1 (red) and DAPI (blue), scalebar 20 µm

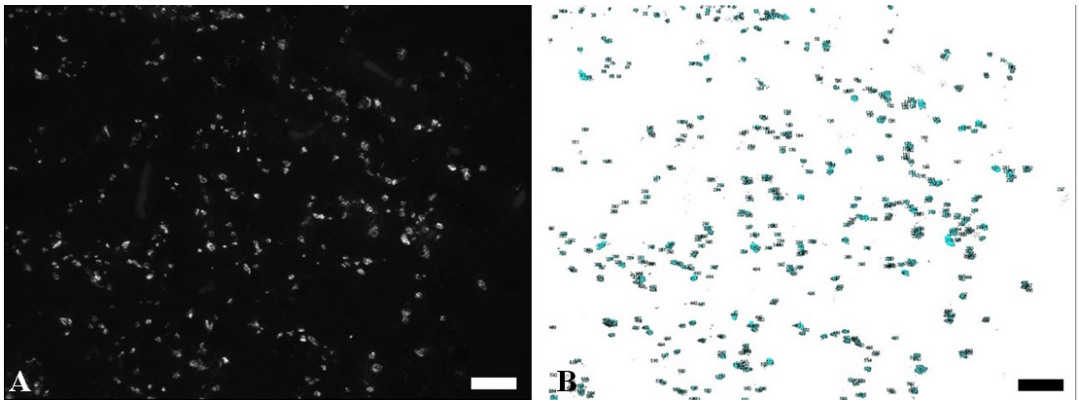

FIGURE 6.5: Calculation of number of synapses was done in ImageJ. To measure the number of VGlut1 positive synapses the analyse particles tool in ImageJ was used. On the left (A) a black and white 8-bit picture of VGlut1 positive synapses is shown, on the right (B) the counted dots. Scalebar 20 µm

Dendritic mitochondria (MAP2/Porin/COXI)

To determine the amount of deficient mitochondria in the dendrites a fluorescent triple labelling with MAP2 (dendrites), Porin (mitochondrial transmembrane protein present in all mitochondria) and COXI (subunit of Complex IV, which is not present in COX10 knock-out cells) was done on paraffin sections of controls and mutants at different timepoints after the induction of deficiency with tamoxifen.

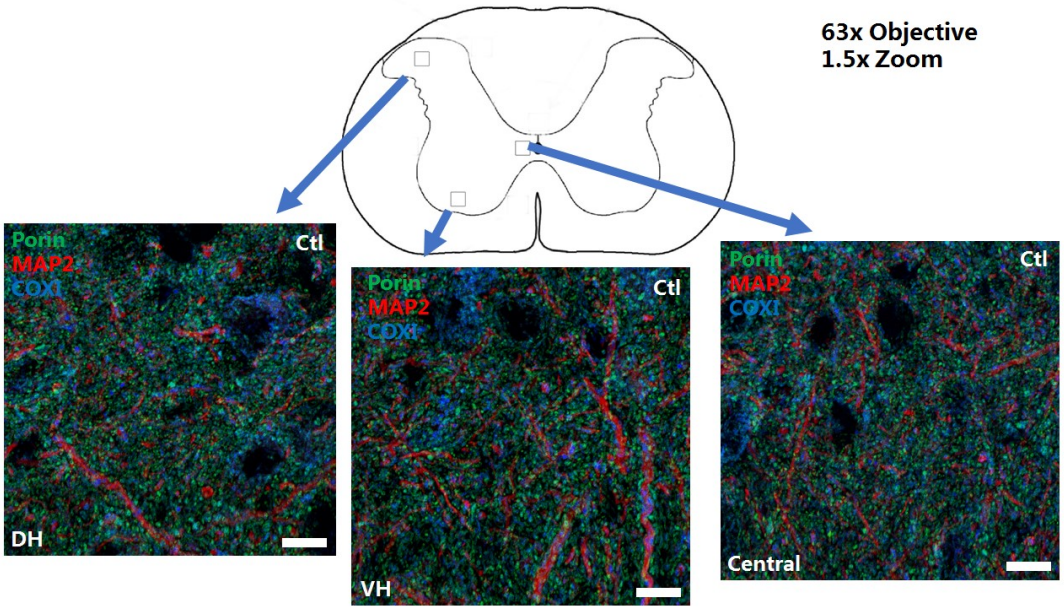

FIGURE 6.6: Overview of the imaging method of dendritic mitochondria, showing dendrites (red), mitochondria (green) and mitochondrial COXI (blue; subunit of mitochondrial complex IV). Images of the whole dorsal and ventral areas, as well as the central region were taken with a 63x oil objective with 1.5x zoom on a Zeiss LSM710 laser scanning confocal microscope. Scalebar $10\,\mu m$

For the MAP2/Porin/COXI staining paraffin sections of different time points after tamoxifen injection were stained according to the paraffin protocol and incubated for 1 hour and 30 minutes on room temperature with the MAP2, Porin and COXI antibodies. For the secondary antibody, anti-IgG1 Rhodamine, anti-IgG2b Alexa Fluor 488 and anti-IgG2a Alexa Fluor 633 antibody was used. The analysis of the sections was done on a Zeiss LSM 710 confocal scanning microscope using a 63x oil objective and 1.5x zoom. Pictures from the dorsal, central and ventral area were taken, although the central area was not included in the following analysis; see figure 6.6. For each area a z-stack of $4.29\,\mu m$ thickness was taken with $1.07\,\mu m$ intervals between z-planes.

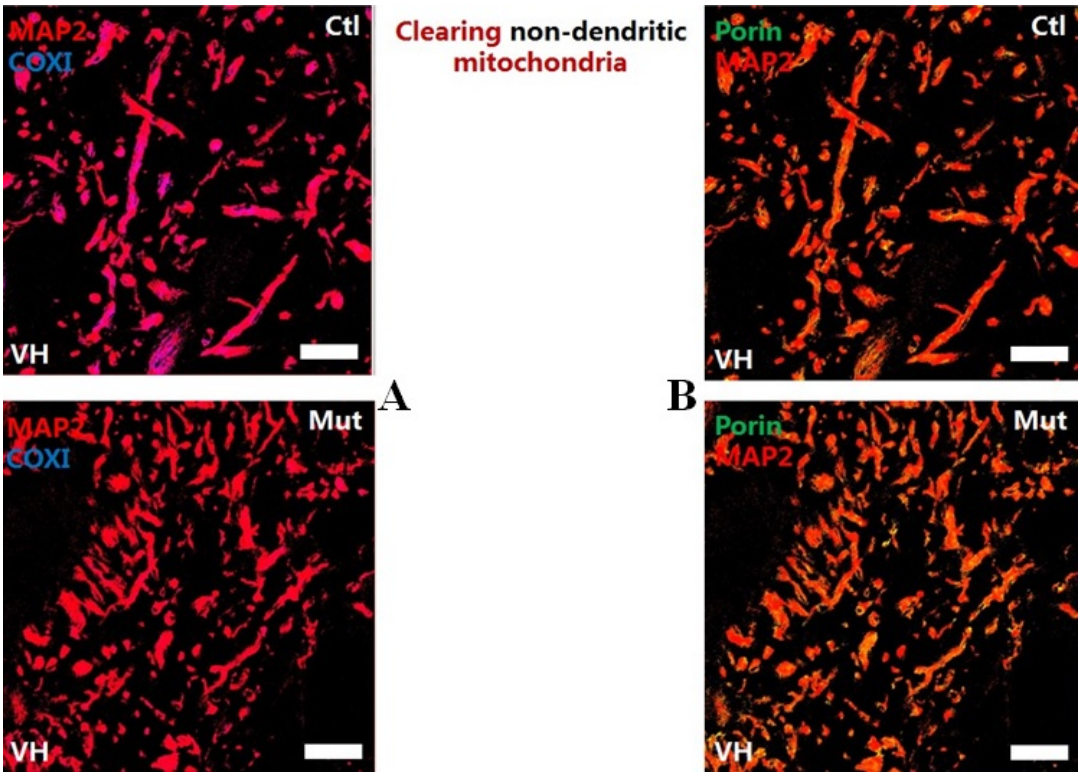

FIGURE 6.7: Determining the amount of deficient mitochondria in the dendrites. To assess the COXI deficiency of dendritic mitochondria, non-dendritic mitochondria were cleared from the images using Photoshop. The left panel (A) shows a control (top) and mutant (bottom) with dendrites (red) and dendritic COXI protein (blue), which is lacking in the mutant. The right panel (B) shows a control (top) and mutant (bottom) with dendrites (red) and all dendritic mitochondria (green). Scalebar 10 µm

The images were then cleared of all non-dendritic mitochondria using Photoshop; see figure 6.7. To clear non dendritic mitochondria, the red channel (MAP2 for dendrites) was set to a threshold with no cell bodies but most of the dendrites selected; see figure 6.7. The area outside of the dendritic area was selected, the channel changed to the green (Porin for mitochondria) and the selected area was cut out; see figure 6.7. The same procedure was done for the blue channel (COXI for complex IV) and the two separate channels were combined into one composite using ImageJ; see figure 6.7. Dendritic area, percentage of dendritic area occupied by mitochondria, average percentage of deficient mitochondria, mitochondrial area, number of mitochondria and average area of single mitochondria were

determined by using 3 different ImageJ macros (1. to measure dendritic area, 2. area and number of Porin/CoxI signal as well as 3. overlap between Porin and CoxI areas). An excel sheet was used to calculate the sums and average of different values gained from the macros (see Chapter 2 methods for the first 2 macros). After the first two macros have calculated the mitochondrial occupancy of the dendrites and other mitochondrial parameters, the two images depicting the porin staining for all mitochondria and the COX-I staining for mitochondria with complex IV were merged in ImageJ. After the images were merged the third macro was activated by pressing '3', which subsequently measured the percentage of blue (COXI) in green (Porin) staining and thus calculated the complex IV deficiency. This data was also inserted into the excel sheet, were the mean of all analysed dendrites was calculated, giving the total mean deficiency for the mitochondria in the dendrites from a specific region.

6.4 Results

6.4.1 Induction of COX10 deficiency in slices

To induce complex IV deficiency in cerebellar purkinje cells in $COX10^{fl/fl} - Thy1 - Cre - ERT2^{+-}$ slices, $10\,\mu M$ tamoxifen or $1\,\mu M$ 4-OHT was added to the slice culture medium and left on for 4 days, with one renewal at 2 days.

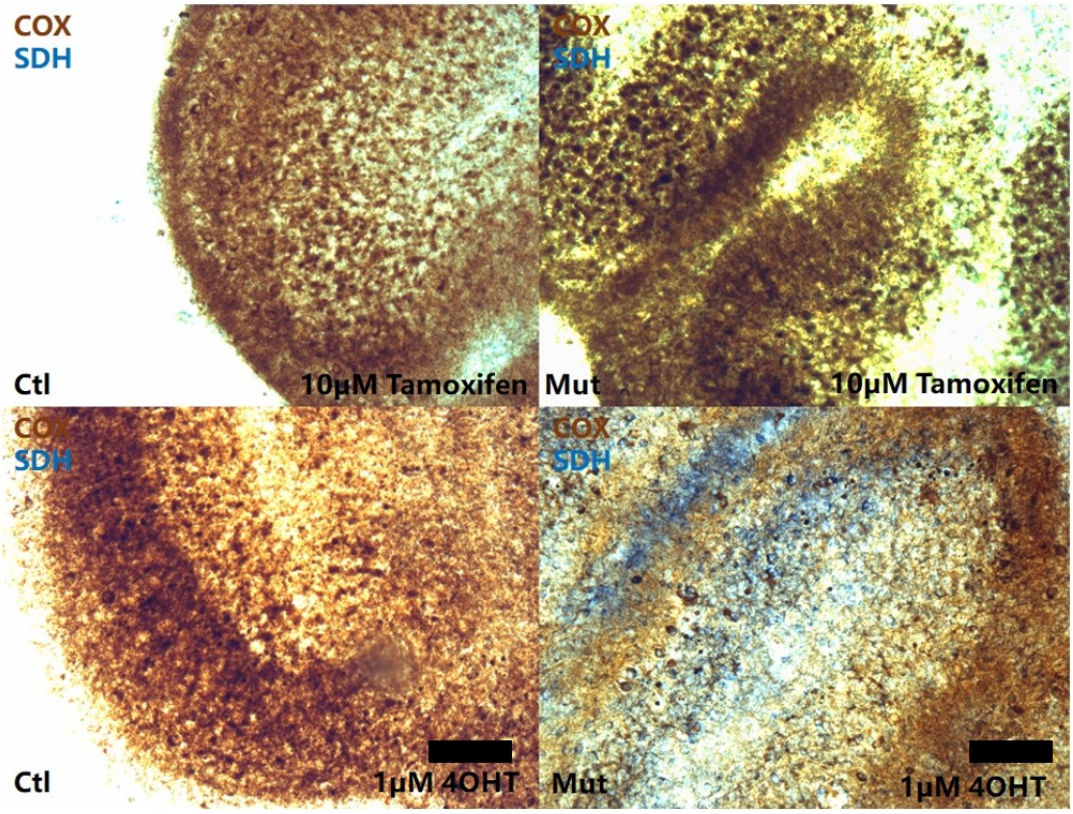

FIGURE 6.8: Mitochondrial complex IV deficiency in cerebellar slices. Bright field image showing cells that are deficient for mitochondrial complex IV in blue, while cells with complex IV activity are brown. Scalebar $100\,\mu m$

After the induction with tamoxifen or 4-OHT the slices were left in culture for another 3-4 weeks to allow sufficient time for the deletion to take effect. After this 3-4 week period a COX/SDH assay was performed on the slices to determine if there was successful COX10 deletion within the cerebellar purkinje cells; see figure 6.8. Although blue cells were visible in the slices, which is an indicator that complex II (completely nuclear-encoded) is active, but complex IV is not, non of these cells appeared to be purkinje cells as

judged by visual appearance; see figure 6.8. 4-OHT treatment lead to more deficient cells compared to tamoxifen, but no deficient PC could be observed by morphological features even 4 weeks after the induction with 4-OHT; see figure 6.9.

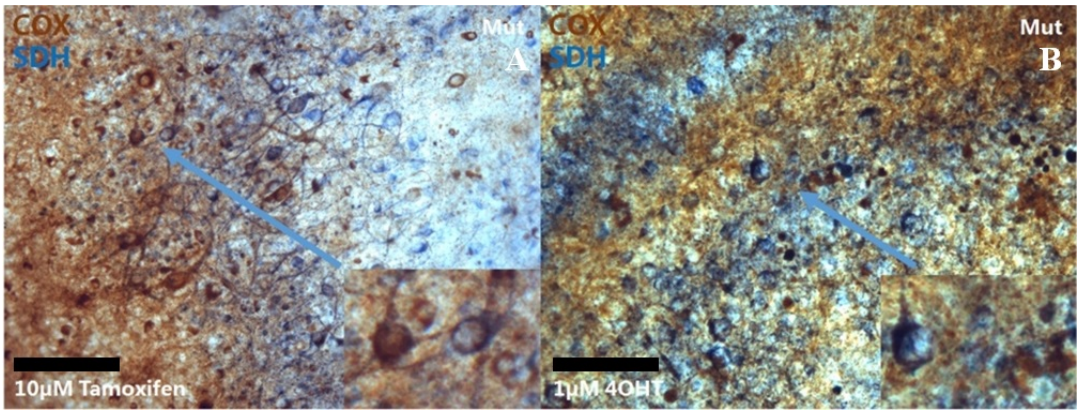

FIGURE 6.9: Mitochondrial complex IV deficiency in cerebellar slices. Bright field image showing complex IV deficient cells 4 weeks after treatment with either Tamoxifen (A) or 4-OHT (B). Scalebar 40 µm

Deficient PC in slices

To determine if the PC in the slices still have complex IV activity an IHC staining for calbindin with subsequent COX assay was performed and the appropriate regions were overlapped in Photoshop to determine complex IV activity in purkinje cells; see figure 6.10.

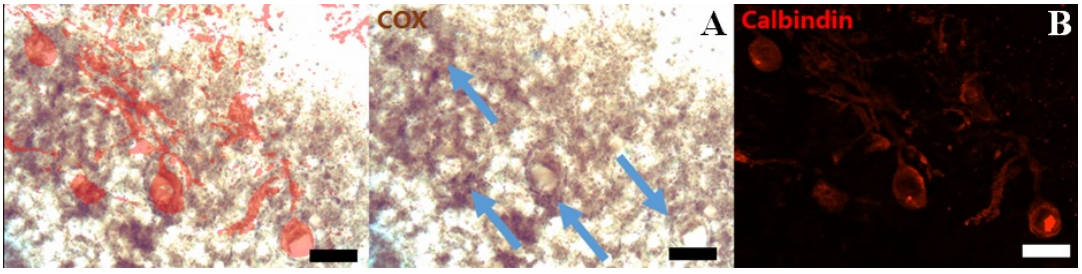

FIGURE 6.10: Mitochondrial complex IV deficiency in cerebellar slices. Fluorescence image of calbindin antibody (B) mediated fluorescence IHC and bright field image of COX assay (A) in a cerebellar slice overlapped to show the activity of mitochondrial complex IV in purkinje cells. Scalebar 20 µm

Furthermore, a triple staining for calbindin, porin (a mitochondrial outer membrane protein on all mitochondria) and COXI (complex IV subunit) was performed to determine the presence of complex IV in PC mitochondria; see figure 6.11.

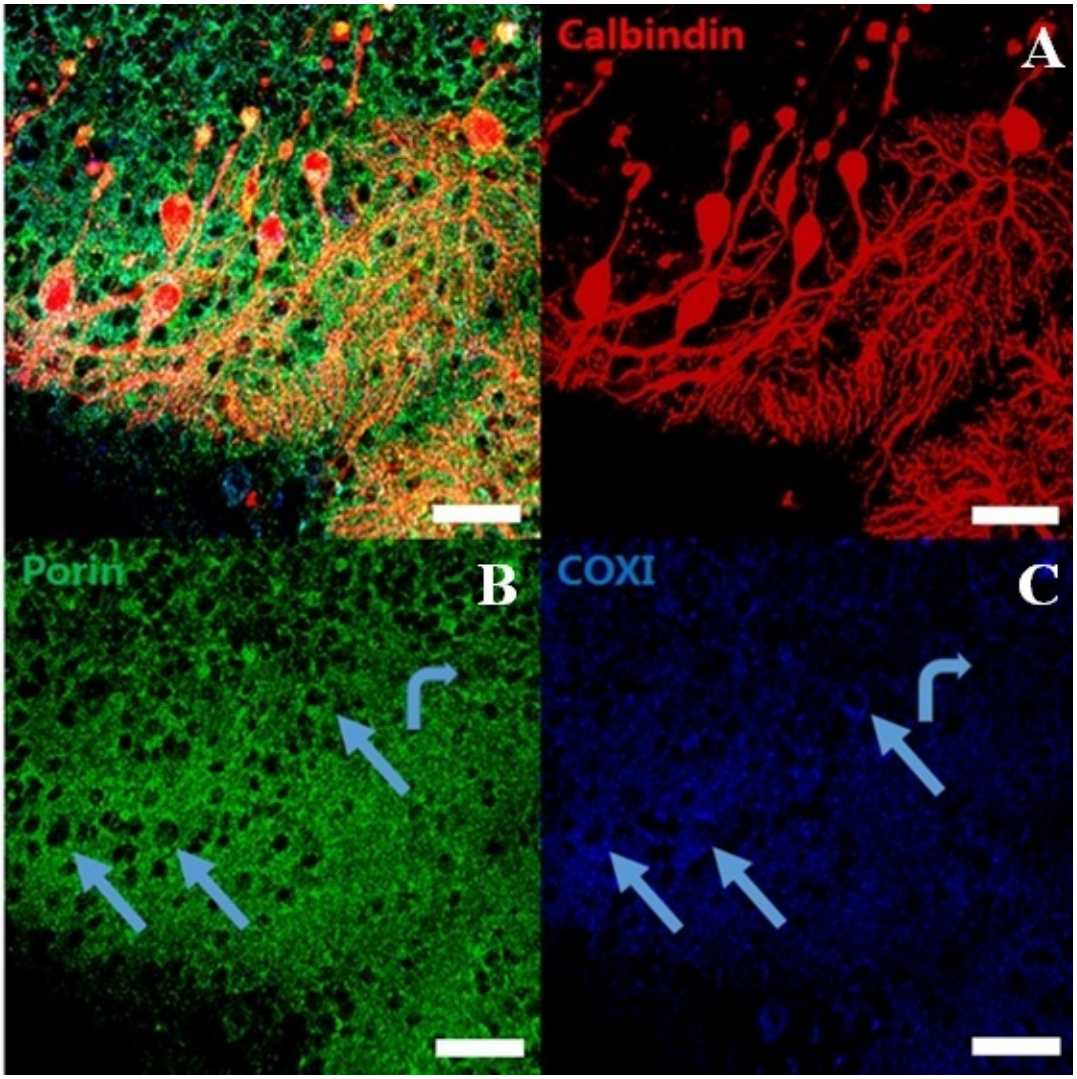

FIGURE 6.11: Mitochondrial complex IV deficiency in cerebellar slices. Fluorescence image of calbindin (A), porin (B) and COXI (C) triple-staining, to determine the presence of complex IV in purkinje cells in cerebellar slices. Scalebar $50\,\mu\mathrm{m}$

The COX assay combined with IHC, as well as the triple immunofluorescence staining, both showed that the PC mitochondria in the mutant slices still contain complex IV and maintain complex IV activity; see figure 6.10 and figure 6.11. A possible explanation for this lack of deficient

mitochondria after the induction with 4-OHT or tamoxifen, could be that the turnover for mitochondria in purkinje cells is too slow, so that the lifetime of healthy slices is too short to successfully get deficient PC in slice culture.

6.4.2 *In vivo* model $COX10^{fl/fl} - Thy1 - Cre - ERT2^{+-}$

Because it was not possible to get deficient PC in the slice culture system during this experiment, the determination of the effect of a mitochondrial complex IV defect on the ARMD had to be tested *in vivo*, where complex IV deficient cells can be found at 4 weeks after induction with tamoxifen.

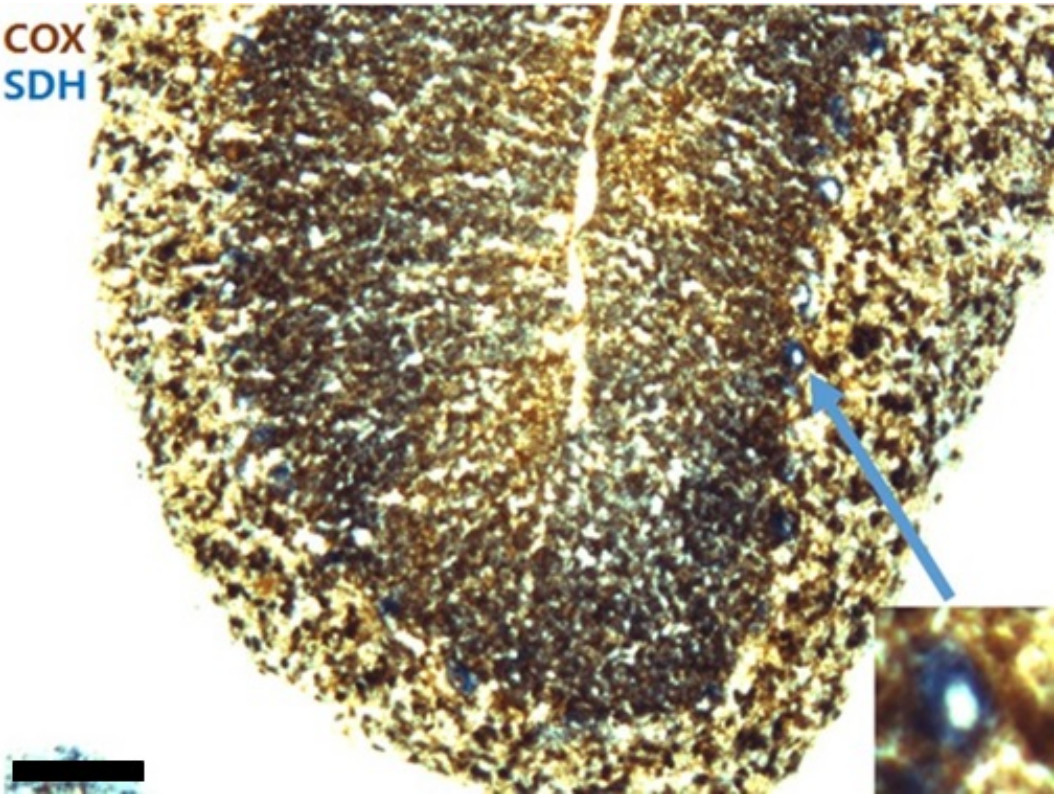

FIGURE 6.12: Complex IV deficient Purkinje cells in the cerebellum of $COX10^{fl/fl} - Thy1 - Cre - ERT2^{+-}$ mice 4 weeks after induction with tamoxifen. COX/SDH assay was done to visualize complex IV deficient cells in blue, while complex IV efficient cells are stained brown. Scalebar $100\,\mu m$

While the greatest part of this experiment was done by Graham Campbell, at the time post-doc in the Mahad lab, my contribution was to

determine the optimal timepoint for demyelination, where there is significant complex IV deficiency in the neurons, but no structural change. For this experiment IHC stainings for several different cellular markers were performed on paraffin emdedded sections at different timepoints after the induction of deficiency with tamoxifen.

VGlut1 in the spinal cord of $COX10^{fl/fl} - Thy1 - Cre - ERT2^{+-}$ mutants

Previous data from the lab has indicated that there is no neuronal loss or structural change at the neuromuscular junction, despite a strong motor function related phenotype in the mutant mice. It has been shown that glutamatergic synapses of neurons lacking complex IV in the hippocampus show signs of dysfunction (Booker et al., 2017). After testing several different cellular markers by doing IHC stainings, VGlut1 in the spinal cord turned out to be the marker most affected by the complex IV deficiency; see figure 6.13. Therefore, VGlut1 synapses were used as a marker to determine the earliest timepoint, with overt deficiency of complex IV, where there is no structural change in the ventral or dorsal spinal cord of the mutant mice.

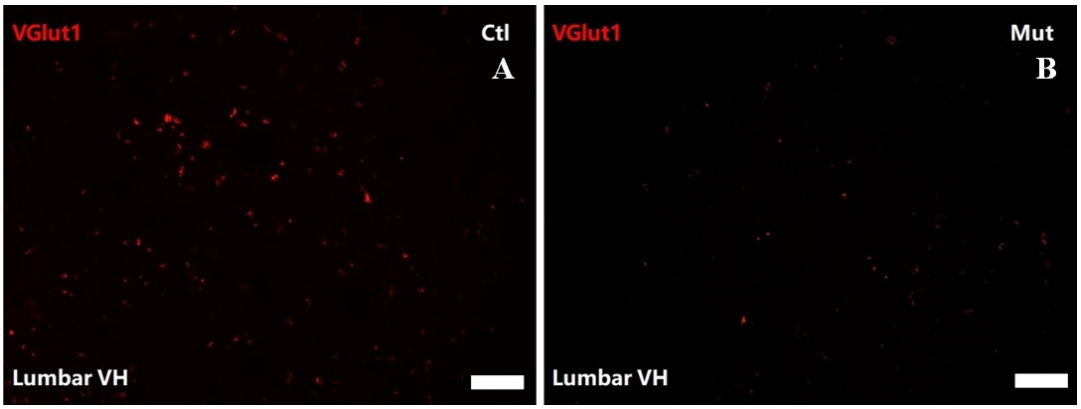

FIGURE 6.13: Loss of VGlut1 positive synapses in the ventral horn of $COX10^{fl/fl} - Thy1 - Cre - ERT2^{+-}$ mutants (B) compared to control (A), shown by IHC staining for VGlut1 in the ventral horn of control mice and mutant mice with complex IV deficiency 10 weeks after induction with tamoxifen. Scalebar 20 µm

At 10 weeks post induction of deficiency with tamoxifen the $COX10^{fl/fl} - Thy1 - Cre - ERT2^{+-}$ mutant mice showed a significant loss of VGlut1 in

the ventral horn of the cervical, thoracic and lumbar region of the spinal cord; see figure 6.13 and figure 6.14.

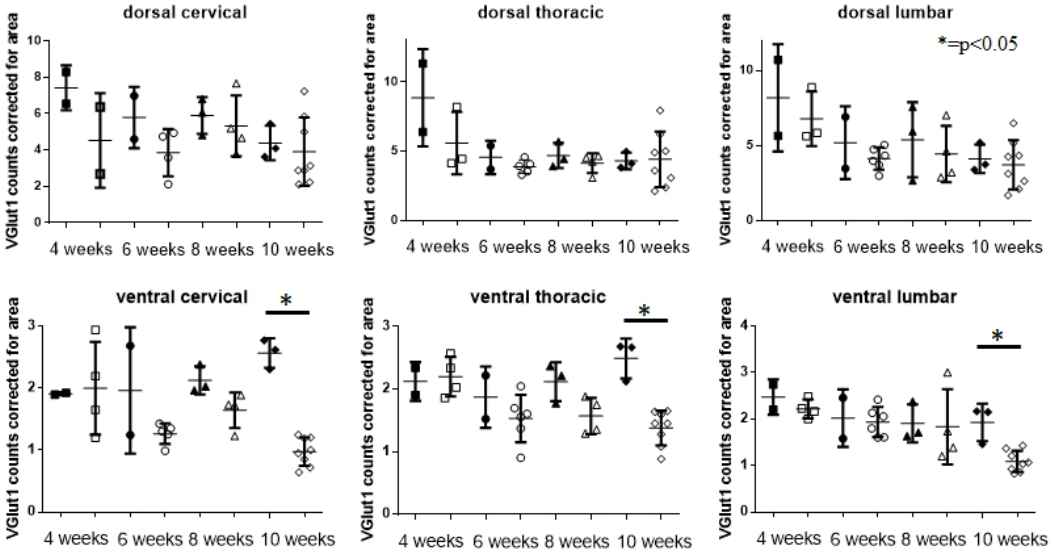

FIGURE 6.14: Impact of complex IV deficiency on the integrity of VGlut1 positive synapses, showing a significant synapse loss in the ventral horn of the cervical, thoracic and lumbar region of the spinal cord at 10 weeks post induction with tamoxifen. All other areas and timepoints were not significantly different, although there was a decreasing trend in several. Each dot represents the mean value from at least 4 different slides from one mouse. *=p-value <0.05

To check the VGlut1 loss at earlier timepoints, IHC staining for VGlut1 were done at 4, 6 and 8 weeks past induction with tamoxifen; see figure 6.14. Although at none of the other timepoints showed a significant loss of VGlut1 in the ventral horn either in the cervical, thoracic or lumbar region of the spinal cord, there was a slight trend towards decreasing synapse number at 6 and 8 weeks, while at 4 weeks post induction there was no indication of a possible VGlut1 reduction in the ventral horn of the spinal cord in $COX10^{fl/fl} - Thy1 - Cre - ERT2^{+-}$ mutant mice; see figure 6.14.

Mitochondrial deficiency in the dendrites of $COX10^{fl/fl} - Thy1 - Cre - ERT2^{+-}$ mutants

To determine the mitochondrial deficiency in the dendrites of $COX10^{fl/fl} - Thy1 - Cre - ERT2^{+-}$ mutants at different timepoints after

the induction of deficiency, a triple IHC staining for MAP2 (for neuronal dendrites), porin (labelling all mitochondria) and COXI (labelling mitochondrial complex IV) was performed. It was previously shown in the Mahad lab (unpublished data), that the complex IV deficiency is already present at 4 weeks post induction in the cell body, but takes much longer to manifest inside the axon. As with the VGlut1 staining the timepoint 10 weeks post tamoxifen induction was stained first, as this stage is near the end stage and the biggest effect is to be expected. The IHC triple staining at 10 weeks post induction revealed a significant amount of complex IV deficient mitochondria in the mutant compared to the control; see figure 6.15.

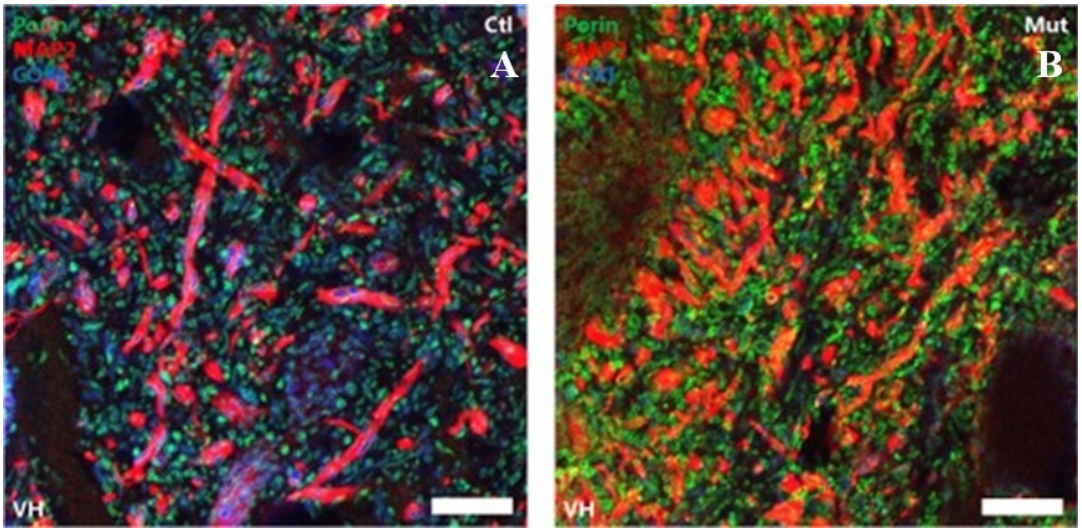

FIGURE 6.15: Loss of complex IV in dendrites of $COX10^{fl/fl} - Thy1 - Cre - ERT2^{+-}$ mutants (B) compared to control (A), shown in a IHC fluorescence triple staining at 10 weeks post tamoxifen. Depicted are the dendrites (red), all mitochondria stained by porin antibody (green), and complex IV efficient mitochondria stained with COXI antibody (blue), while complex IV deficient mitochondria are lacking COXI staining. Scalebar $10\,\mu m$

In the dorsal as well in the ventral horn of the spinal cord a significant higher percentage of mitochondria were deficient in the mutant compared to the control at 10 weeks post induction; see figure 6.16 and figure 6.17. Furthermore, there was a trend towards decreased mitochondrial and dendritic area, although not significant.

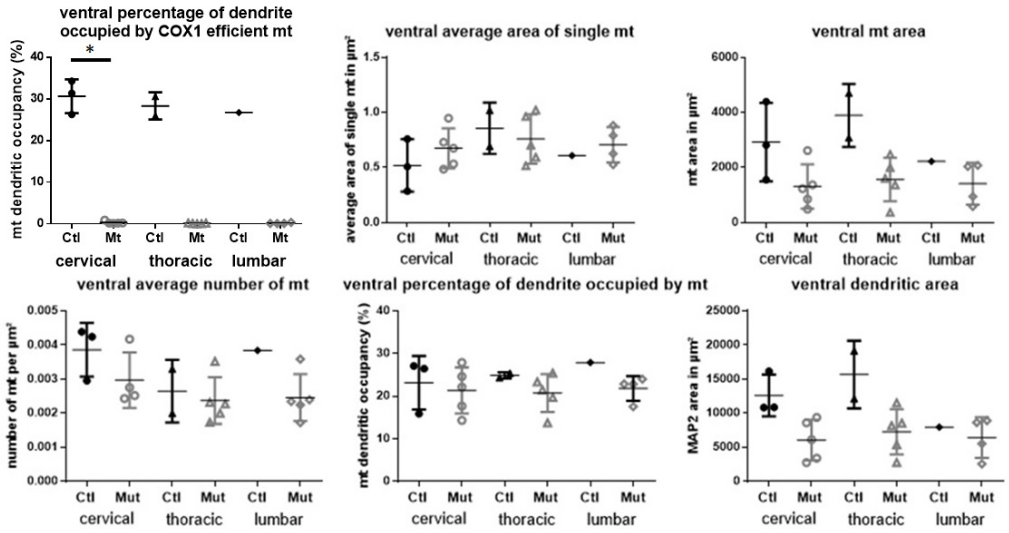

FIGURE 6.16: Loss of complex IV in dendrites of $COX10^{fl/fl} - Thy1 - Cre - ERT2^{+-}$ mutants, showing the significant increase in mitochondrial complex IV deficiency in the mutant ventral horn 10 weeks after induction with tamoxifen. Each dot represents the mean value from 2-4 different slides from one mouse. *=p-value <0.05

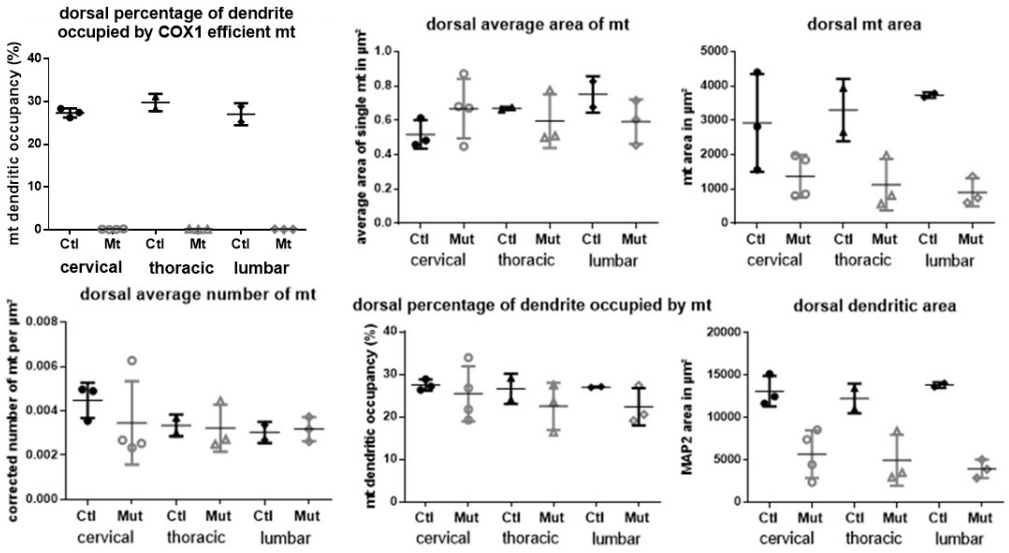

FIGURE 6.17: Loss of complex IV in dendrites of $COX10^{fl/fl} - Thy1 - Cre - ERT2^{+-}$ mutants, showing the significant increase in mitochondrial complex IV deficiency in the mutant dorsal horn 10 weeks after induction with tamoxifen. Each dot represents the mean value from 2-4 different slides from one mouse. *=p-value <0.05

The earliest timepoint stained for MAP2 was 4 weeks post induction with tamoxifen and at this time the dendrites in the cervical ventral spinal cord already showed a significant increase of complex IV deficiency compared with non-induced control cases; see figure 6.18. This determines 4 weeks after induction of deficiency as the earliest timepoint with significant deficiency and no structural change in the spinal cord of $COX10^{fl/fl} - Thy1 - Cre - ERT2^{+-}$ mutant mice.

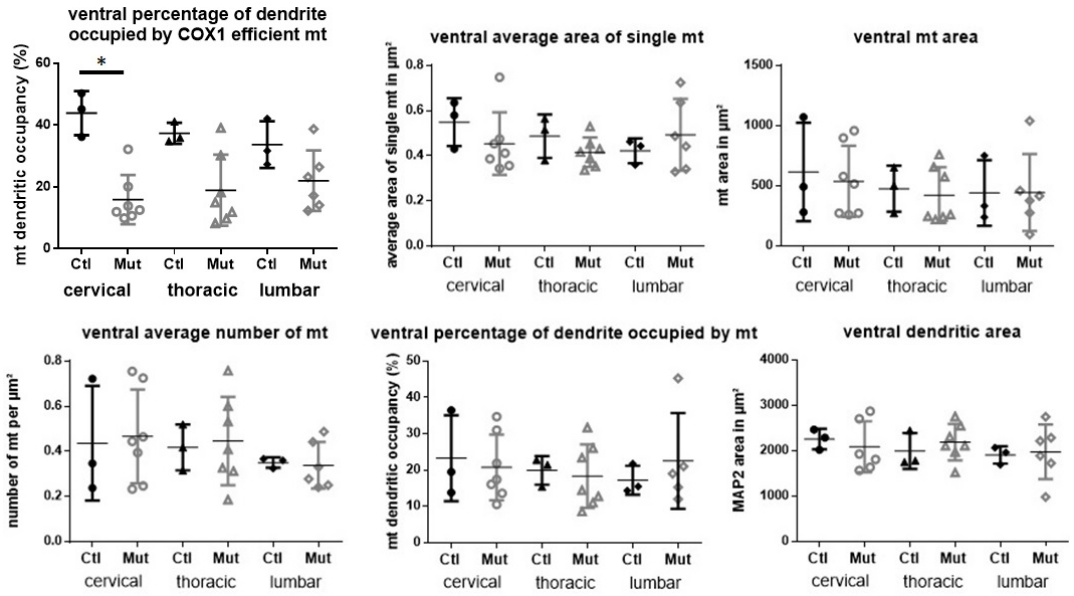

FIGURE 6.18: Loss of complex IV in dendrites of $COX10^{fl/fl} - Thy1 - Cre - ERT2^{+-}$ mutants, showing the increase in mitochondrial complex IV deficiency in the mutant cervical ventral horn 4 weeks after induction with tamoxifen. Other parameters show a slight decreasing trend in the mutant, although non of them are significant. Each dot represents the mean value from 2-4 different slides from one mouse. *=p-value <0.05

6.5 Discussion

Recently it was shown by several independant research groups that many neurons in multiple sclerosis show a deficiency in at least one of the complexes of the mitochondrial electron transport chain. These deficiencies are a consequence of mitochondrial DNA deletions, which have also been shown in multiple sclerosis autopsies (Dutta et al., 2006; Campbell et al., 2011; Broadwater et al., 2011; Witte et al., 2013; Kim et al., 2010; Hares et al., 2014; Fischer et al., 2013; Haile et al., 2017a). Data from the Mahad lab (unpublished data) shows that none of the currently used animals models of multiple sclerosis harbour these mitochondrial DNA deletions, so there is a need to model this MS phenomenon *in vivo* and *in vitro*. These models would allow test the effect of mitochondrial DNA deficiencies on demyelinated axons and to test different treatment strategies for this mitochondrial deficiencies. Ultimately these models may be useful in finding a treatment for progressive multiple sclerosis, which only has one licensed treatment thus far (Montalban et al., 2017). For this purpose several different mouse mutant lines have been established in the Mahad lab over the past years. For this thesis, the $COX10^{fl/fl} - Thy1 - Cre - ERT2^{+-}$ mutant line was used, firstly to make cerebellar slices and induce complex IV deficiency by using Tamoxifen or 4-OHT, and secondly to determine to optimal timepoint for demyelination *in vivo*, which is characterized by a significant complex IV deficiency without structural changes of cellular markers.

6.5.1 Induction of mitochondrial deficiency in cerebellar slices

To determine the effect of mitochondrial DNA deletions on the ARMD, cerebellar brain slices from $COX10^{fl/fl} - Thy1 - Cre - ERT2^{+-}$ mice were created and the Cre-recombinase was induced by adding either $10\,\mu M$ of Tamoxifen or $1\,\mu M$ of 4-OHT to the slice culture medium and left on for 4 days. After leaving the slices in culture for 3 to 4 weeks, either a COX/SDH assay or IHC triple staining for COXI, a complex IV subunit, was performed to check for complex IV deficiency. The COX/SDH assay, which tests for

complex II (blue) and complex IV activity (brown), showed complex IV deficient cells in the slices after 4 weeks of induction with tamoxifen/4-OHT. These blue cells were however, judging by morphology and confirmed by IHC staining for calbindin, not purkinje cells. Because the cerebellar brain slice health began to deteriorate after 3 to 4 weeks it was not possible to keep the slice culture long enough to obtain complex IV deficient purkinje cells with the induction of tamoxifen or 4-OHT. An alternative approach would be to use a lentivirus expressing Cre-recombinase and inject it into the slices right after making the slice culture, which might be a more effective way of inducing complex IV deficiency.

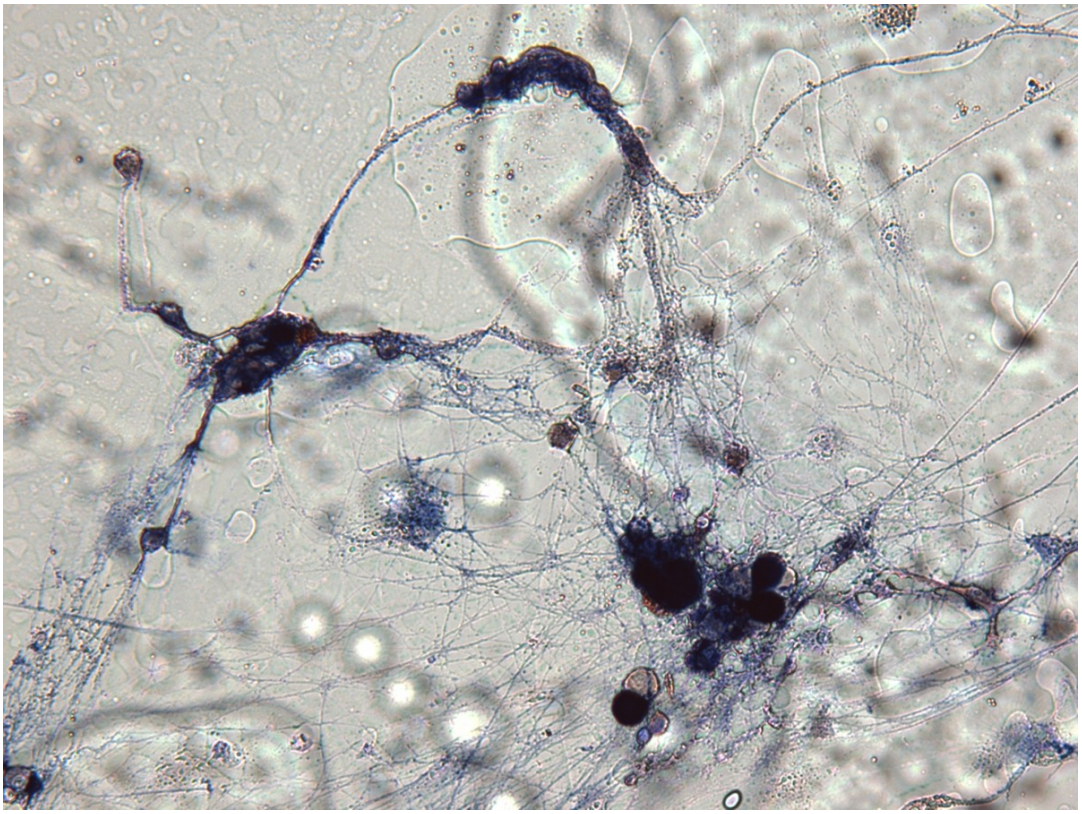

FIGURE 6.19: Complex IV deficient cells in DRG culture, depicted by the COX/SDH assay which labels complex IV deficient cells in blue, while complex IV efficient cells are stained brown.

Another possibility to model mitochondrial deficiency *in vitro* would be to use neuronal culture, for example dorsal root ganglia culture. In DRG culture it is possible to get mitochondrial complex IV deficient cells around

14 days after adding a lentivirus expressing Cre-recombinase into the culture medium. DRG culture can also be used in microfluidic chambers, which would allow the assessment of directionality of mitochondrial movement and the possibility to treat cell body and axon separately, to study the effects different drugs might have on the mitochondrial deficiency (Taylor et al., 2005).

6.5.2 Structural changes and mitochondrial deficiency in the $COX10^{fl/fl} - Thy1 - Cre - ERT2^{+-}$ mutant

The mitochondrial complex IV deficiency can also be modelled *in vivo*, where it is much easier to get complex IV deficient neurons. Another advantage of the *in vivo* approach is that the phenotype of the mitochondrial defect in question can be studied and different drugs can be tested to determine if they ameliorate the phenotype. The phenotype analysis, different drug treatments and injection of lysolecithin for demyelination *in vivo* was done by Graham Campbell and other members of the Mahad lab.

For this thesis, the structural integrity of several different cellular markers was tested to find the earliest timepoint where there is no structural change, but significant mitochondrial complex IV deficiency. For this, paraffin embedded sections of induced mutants were first stained near the endstage to ensure that any possible change in markers would be significant enough to observe. Most of the cellular markers tested (not shown), did not show a significant change in the induced $COX10^{fl/fl} - Thy1 - Cre - ERT2^{+-}$ mutant compared to the control, only the VGlut1 synapses did show a reliable marker of structural change after induction of deficiency. In general the loss of synapses was strongest in the cervical area, followed by the thoracic region of the spinal cord, while the lumbar region had the least dramatic reduction. At 10 weeks post induction of deficiency with tamoxifen, there was a significant reduction of VGlut1 positive synapses in the cervical, thoracic and lumbar ventral horn of the $COX10^{fl/fl} - Thy1 - Cre - ERT2^{+-}$ mutant spinal cord. This significant reduction was not observed at any earlier timepoint tested, although there was a trend towards a reduction of synapses at 8 weeks and a slight trend at 6 weeks post induction, only in the cervical region. At 4 weeks after

induction of deficiency, none of the regions analysed showed any reduction in VGlut1 positive synapses in the $COX10^{fl/fl} - Thy1 - Cre - ERT2^{+-}$ mutant. The conclusion from this experiment was that 4 weeks after induction of deficiency was the earliest timepoint with no structural change.

To determine the earliest timepoint with significant complex IV deficiency in the dendrites of the spinal cord a IHC triple staining with MAP2 for dendrites, porin for all mitochondria and COXI for complex IV efficient mitochondria was performed on paraffin embedded section of the $COX10^{fl/fl} - Thy1 - Cre - ERT2^{+-}$ mutant at different timepoints after induction of deficiency. Near the end-stage at 10 weeks post induction of deficiency there was a significant percentage of mitochondria deficient of complex IV in the mutant in the cervical region of the spinal cord. In the thoracic and lumbar region there was significant tissue damage in some of the cases, so the n-number in this regions was not high enough to reach statistical significance, but a clear trend was observable. As the earliest timepoint analysed, because there was no structural change found at this timepoint, 4 weeks post induction already showed a significant increase in mitochondrial complex IV deficiency in the dendrites of the cervical ventral horn. All the other parameters analysed, as well as VGlut1, did not show any significant change at this stage. Therefore, 4 weeks post-induction of deficiency was determined as the earliest timepoint with significant deficiency without any structural change.

Chapter 7

Discussion

7.1 Recap of the literature review and aims

The brain is the most energy demanding organ of the human body, using about 20% of the bodies energy reserves, while representing only about 2% of the total body mass (Raichle and Gusnard, 2002). The brain in turn uses about half of its energy budget for maintaining a transmembrane ionic balance of sodium and potassium with ATP powered ion-pumps (Fei et al., 2008). The myelination of axons, besides enhancing the signal transmission speed, is improving the energy efficiency of maintaining this ionic balance, with the ion channel and pumps being concentrated at the nodes of Ranvier between the myelinated segments of the axon (Neishabouri and Faisal, 2011; Saab, Tzvetanova, and Nave, 2013). At these nodes of Ranvier stationary sites of mitochondria supply the ATP necessary to maintain this ionic balance (Ohno et al., 2011; Chiu, 2011). Demyelinating diseases of the CNS and PNS destroy this energy efficiency by disrupting the ordered ion channel distribution, followed by a diffuse ion channel redistribution along the demyelinated axon (Craner et al., 2004b; Waxman, 1992; Craner et al., 2004a). To meet this increase in energy demand, mitochondria respond with an increase in numbers, speed and size in the demyelinated axon, termed the axonal response of mitochondria to demyelination (ARMD).

The phenomenon of the ARMD is described in the literature and observed in demyelinated axons in MS autopsy tissue as well as *in vitro* neuronal cell culture (Mahad et al., 2009; Witte et al., 2009; Zambonin et al., 2011; Ohno et al., 2011; Kiryu-Seo et al., 2010; Ohno et al., 2014). This increase in mitochondrial parameters seems to be a compensatory mechanism to deal with the increase in energy demand in the demyelinated

axon, which stems from the loss of trophic support from the oligodendrocyte and increased sodium influx caused by the redistribution of Nav1.2 and Nav1.6 along the axon (Craner et al., 2004b; Waxman, 2006; Mohd, 2010; Albers and Siegel, 1998; Lores Arnaiz and Ordieres, 2014). The literature on the details of mitochondrial dynamics in the context of demyelination is limited, with only the increase in the speed of mitochondrial transport after demyelination being reported so far (Kiryu-Seo et al., 2010). Where these additional mitochondria in the demyelinated axon come from, whether it is by transport from the cell body, biogenesis directly in the axon or transport from another part of the axon to the demyelinated site, has not been studied. Furthermore, the dynamics of mitochondrial fusion, which can be assumed to be different, judging from the change in mitochondrial morphology in demyelinated axons, has not been studied so far (Mahad et al., 2009; Witte et al., 2009; Zambonin et al., 2011; Ohno et al., 2011; Kiryu-Seo et al., 2010).

Another important aspect of neuronal mitochondria in multiple sclerosis is that they harbour mtDNA deletions, which lead to changes in the activity of the complexes of the mitochondrial electron-transport-chain (ETC) (Dutta et al., 2006; Campbell et al., 2011; Broadwater et al., 2011; Witte et al., 2013; Kim et al., 2010; Hares et al., 2014; Fischer et al., 2013; Haile et al., 2017a). These mtDNA deletions were found in the cell bodies of neurons in the cortex of MS autopsy tissue, which were also deficient for complex IV activity (Campbell et al., 2011). Furthermore, it has been reported, that neurons in the MS cortex display a decrease in expression of genes responsible for mitochondrial upkeep (Witte et al., 2013). As dysfunctional mitochondria display an increase in ROS production and are not able to efficiently generate ATP to meet the required energy demands, the question is raised what consequence it might have on the demyelinated axon if these deficient mitochondria from the cell body would be transported to the site of demyelination (Brand and Nicholls, 2011; Wang et al., 2013). To study the effect of mitochondrial DNA deletions and complex IV deficiency, mouse models with complex IV knock-out were created in the Mahad lab. Preliminary data shows, that there is a decrease of mitochondrial content in myelinated axons in these mutants, and that mitochondria deficient in complex IV activity appear in the axon following demyelination with

lysolecithin.

For the determination of the timecourse of the ARMD, how it develops over time after demyelination, a cerebellar slice culture system with lysolecithin mediated demyelination was used in this study. These cerebellar slices were then stained with IHC to determine mitochondrial occupancy, size and numbers at different timepoints after demyelination. To study the transport and fusion dynamics of mitochondria after demyelination and to determine where these additional mitochondria after demyelination come from, a lentivirus expressing a green-to-red photoconvertible protein was used, which allowed to differentiate between mitochondria being transported from either direction and to study the amount of fusion in the demyelinated axons of PC in cerebellar slices. Furthermore, different small molecule compounds that are able to manipulate mitochondrial dynamics were to used to study their effect on the ARMD and axonal health following demyelination (Cassidy-Stone et al., 2008; Bordt et al., 2017; Shchepina et al., 2012; Desouza and Shivaswamy, 2010; Skov et al., 2008; Bogacka et al., 2005; Ghosh et al., 2007; Corona and Duchena, 2016; Miglio et al., 2009; Hao et al., 2010). To model the mitochondrial deficiency found in MS neurons, cerebellar brain slices from $COX10^{fl/fl}$-$Thy1-Cre-ERT2^{+-}$ mutant mice were used, to study the impact of a COX10 deletion, which leads to complex IV deficiency, has on the ARMD *in vitro*. The effect of the COX10 deletion on the ARMD *in vivo* was studied in parallel by Graham Campbell and other members of the Mahad lab, my contribution to this was to determine to earliest timepoint after the induction of deficiency with tamoxifen, where there is significant deficiency, but no structural change within the neurons of the $COX10^{fl/fl}-Thy1-Cre-ERT2^{+-}$ mutant mice.

7.2 Major findings of this thesis

7.2.1 Timecourse of the ARMD

The timecourse experiment of the ARMD after demyelination with lysolecithin and IHC staining at different timepoints after demyelination, showed a bell shaped curve of increase and decrease of mitochondrial

parameters over the time analysed. The mitochondrial occupancy of the axon in percent increased sharply 24 hours after demyelination and continued to rice until reaching a peak at 4 days after lysolecithin was removed from the slice culture medium. After the peak the mitochondrial occupancy decreased again at 7 and 12 days after demyelination, while never reaching the control level of myelinated axons. The mitochondrial number in the axon after demyelination already reached its peak at 24 hours after removing lysolecithin, with only marginal but non-significant increase at 5 days after demyelination. Like the mitochondrial occupancy, the mitochondrial number in the axon decreased again at 7 and 12 days after removing lysolecithin. The average size of the single mitochondrion followed a similar change after demyelination, with significant increase at 24 hours after demyelination and reaching its peak at 4 days, and finally decrease again at 7 and 12 days after removing lysolecithin. These observations hint at either a transport of mitochondria from the cell body to the demyelinated axon, or local biogenesis in the axon, following demyelination. The second conclusion that can be drawn from this data set is that the ARMD is mounted soon after demyelination by enhancing mitochondrial numbers and there is an increase in mitochondrial fusion over the days following demyelination.

This bell shape curved increase and decrease of mitochondrial parameters in the demyelinated axon, shows that the mitochondria in the cell need a certain amount of time to adequately respond to the increase in energy demand after the loss of myelin. This leaves the axon in a vulnerable state until the ARMD is fully mounted and possibly beyond that point. In MS there is the additional component of inflammation, which most likely damages the axons in this vulnerable state even more than axons that have already mounted a sufficient response to the increase in energy demand after demyelination. This means that the ARMD can potentially be enhanced or sped up to decrease the timespan during which the demyelinated axons are in this vulnerable state and possibly lead to axonal protection. Another observation that can be made from this bell shaped curve is that the mitochondrial occupancy goes down again after a certain amount of time, which could indicate remyelination of the axons leading to a decrease in energy demand. The mitochondrial occupancy however does

not return to the baseline level during the timepoints measured, indicating that the energy demand is not (yet) in a normal range, this observation was also reported in a study of remyelinated axons in MS autopsy tissue (Zambonin et al., 2011). To determine where this additional mitochondria seen in the ARMD come from and how much greater the fusion rate in the demyelinated axon is compared to the myelinated axon, a lentivirus with photoconvertible protein was used in the following experiments.

7.2.2 Mitochondrial dynamics in myelinated axons

For the mitochondrial dynamics experiment first myelinated and unmyelinated axons of Purkinje cells in cerebellar slices were analysed. For this a lentivirus expressing mEOS2, a photoconvertible protein with attached mitochondrial targeting sequence, was injected into the Purkinje cell layer using a picospritzer 1 hour after the slicing procedure (McKinney et al., 2009). At 14 days after injection of the virus, the slices were used for living imaging on a Zeiss LSM 880 with airyscan module, mitochondrial transport speed and direction of transport as well as fusion dynamics were analysed by using ImageJ. Unmyelinated axons did either not myelinate during the 14 days until live microscopy or were demyelinated by an unknown event after the slicing procedure. In the unmyelinated axons a trend of increased anterograde transport of mitochondria and a significant increase in retrograde transport was found. There was also a significant increase of mitochondrial transport speed both in anterograde and retrograde direction in the unmyelinated compared to the myelinated axons, as well as a significant increase in fusion rate in the unmyelinated axons of PC. Apart from comparing the mitochondrial fusion and transport dynamics in unmyelinated and myelinated axons, this experiment set out to determine the 'baseline' mitochondrial dynamics in myelinated PC axons in cerebellar slices to compare it with axons demyelinated with lysolecithin in the next experiment.

7.2.3 Mitochondrial dynamics in demyelinated axons

The main aim of this thesis was to determine the transport and fusion dynamics in demyelinated PC axons and to determine if the additional

mitochondria in the demyelinated axon are transported from the cell body or another part of the axon to the demyelinated site. For this experiment the same experimental procedure as in the analysis of mitochondrial dynamics in myelinated PC axons was used, except that demyelination with lysolecithin was done for 17 hours at 13 days after the slicing procedure and imaging was done right after removing the lysolecithin. The analysis of the demyelinated axons show a significant increase of mitochondrial anterograde transport, as well as a significant increase of anterograde transport speed. Retrograde mitochondrial transport was also significantly enhanced in the demyelinated compared to the myelinated axons, while the retrograde speed not was different between the two groups. There was also significantly more fusion taking place in the demyelinated axons compared to control. Because the axon area converted was right next to the AIS, it was possible to show that the newly transported mitochondria coming in from the anterograde direction are being transported from the cell body.

Another part of this experiment was to determine if this observed increase in mitochondrial transport and fusion is caused by the process of demyelination and not some other effect of lysolecithin on the neurons. For this experiment cerebellar brain slices of the *shiverer* mutant were used, as it is reported in the literature that there is an increase of mitochondrial number and activity in this dysmyelination mutant (Andrews et al., 2006). *Shiverer* slices were cultured for 14 days until imaging and lysolecithin was either added the day before imaging or not. None of the parameters measured showed a significant difference between the *shiverer* with or without lysolecithin treatment, suggesting that the increase in mitochondrial parameters after lysolecithin is an effect of the demyelination rather than a secondary effect of the lysolecithin on the neurons. The number of mitochondria transported in anterograde direction as well as the anterograde mitochondrial speed of the *shiverer* slices without lysolecithin was very similar to the wild-type demyelinated slices, while the fusion rate and number of mitochondria being transported in retrograde direction was more similar to the myelinated axons. The *shiverer* with lysolecithin treatment showed slightly, although not significantly, lower movement speed of mitochondria, but otherwise no difference to the *shiverer* without lysolecithin treatment.

In summary this experiment showed that there is a significantly increased anterograde transport of mitochondria from the cell body to the demyelinated part of the axon, with an increase in transport speed and enhanced fusion of the newly transported mitochondria with the stationary mitochondrial sites within the axon. The mitochondrial dynamics in the *shiverer* were not increased with lysolecithin treatment, which suggests that this effect was due to demyelination itself and not some other effect of lysolecithin on the axons. This finding implies that the mitochondria deficient for complex IV found in neuronal cell bodies in the MS cortex, will be transported to the demyelinated axon upon demyelination. The already injured axon might not be able to cope with the increased energy demand, since the dysfunctional mitochondria are not able to produce ATP efficiently and might increase the ROS mediated damage to the axon.

7.2.4 Manipulations of the ARMD

Manipulation of mitochondrial dynamics has been reported to be neuroprotective, as it was shown that enhancing mitochondrial transport aides in the regeneration of axons after axotomy, inhibition of mitochondrial fission ameliorates axonal damage after capsaicin treatment and increasing mitochondrial biogenesis was shown to be protective in a model of parkinson's disease (Zhou et al., 2016; Chiang et al., 2015; Scholpa et al., 2018a). To test the effect that manipulating several mitochondrial parameters has on the axonal health after demyelination with lysolecithin, different compounds were added to the slice culture medium before demyelination (Cassidy-Stone et al., 2008; Bordt et al., 2017; Shchepina et al., 2012; Desouza and Shivaswamy, 2010; Skov et al., 2008; Bogacka et al., 2005; Ghosh et al., 2007; Corona and Duchena, 2016; Miglio et al., 2009; Hao et al., 2010).

The first experiment was the inhibition of of mitochondrial transport with the ATPase inhibitor oligomycin, which is reported to completely inhibit mitochondrial transport at a concentration of $20\,\mu M$ (Zala et al., 2013). To not cause too severe ATPase inhibition, as this would be detrimental on axonal health in itself, a lower concentration of $0.25\,\mu M$ was used for the axonal health experiment. This lower concentration already decreased the

mitochondrial occupancy of the axons after demyelination compared to lysolecithin treatment alone, although not significantly. The average size of an mitochondrion was decreased after treatment with oligomycin and the number of mitochondria increased, again no statistical significance in both cases. The greater number of smaller mitochondria after ATPase inhibition could be explained by the fragmentation and subsequent degradation of mitochondria, which is to be expected after ATP depletion. The effect of oligomycin treatment after demyelination on axonal health was detrimental, as the axonal bulb area increase significantly 24 hours after treatment. This negative effect can be explained by both inhibition of mitochondrial transport, shown by the decrease of mitochondrial occupancy, as well as the expected reduced ATP production after oligomycin treatment. Oligomycin was also used for a live imaging experiment, to determine if the increase of green in red fluorescence over time is really a consequence of mitochondrial fusion rather than transport back of the green mEOS2 protein into the stationary red mitochondria. For this a $20\,\mu M$ concentration of oligomycin was used to completely block mitochondrial transport and assess the green in red fluorescence change over 20 minutes. This experiment showed that without mitochondrial transport there is a constant decrease of the green in red fluorescence, which demonstrates that the green in red increase observed in the mitochondrial dynamics experiments is really a consequence of ongoing mitochondrial fusion, rather than transport back of green mEOS2 protein into the stationary red mitochondria.

The second manipulation was the inhibition of mitochondrial fission with the supposedly Drp-1 specific inhibitor mdivi-1 lead to a significant increase of mitochondrial occupancy, already in the myelinated axon and an even further increase of mitochondria in the demyelinated axons (Cassidy-Stone et al., 2008; Bordt et al., 2017). The size of an average mitochondrion was significantly increased as well in both myelinated and demyelinated slices. A curious observation was the increase in mitochondrial number in the myelinated slices, which is not expected after treatment with an inhibitor of mitochondrial fission. Another unexpected observation was the increase of axonal bulbs in the mdivi-1 treated slices compared to the untreated control, as it was expected for the inhibition of mitochondrial fission to be protective, or at least not detrimental, to axonal

health. Recently however, it was reported that mdivi-1 is not a very good inhibitor of mdivi-1, but instead a very efficient inhibitor of complex I of the ETC (Bordt et al., 2017). This could explain the negative effect on axonal health, as inhibition of complex I decreases the ATP production of mitochondria as well increased production of ROS, as well as the mediocre effect on mitochondrial area. The increased occupancy in the myelinated axons, could be a consequence of the decrease in energy production of the inhibited mitochondria and compensatory reaction in form of transport of additional mitochondria to the axon, as well as the subtle but significant increase in mitochondrial area due to the (unspecific) inhibition of drp1.

Lastly the effect of increased mitochondrial biogenesis on axonal health after demyelination with lysolecithin was tested. Pioglitazone, which was used in this experiment, was shown to increase mitochondrial biogenesis by enhance the expression of PGC-1α and TFAM (Desouza and Shivaswamy, 2010; Skov et al., 2008; Bogacka et al., 2005; Ghosh et al., 2007; Corona and Duchena, 2016; Miglio et al., 2009). Similar to mdivi-1 pioglitazone increased the mitochondrial occupancy, number and size in the myelinated axons compared to control, although the n-number used was too low to reach significance. In the demyelinated axons the mitochondrial parameters only showed a slight trend towards an increase with pioglitazone treatment compared to demyelinated control. The axonal health after pioglitazone demyelinated slices was significantly better when taking into account the bulb size, but lost significance when only comparing total bulb number, both values were corrected for total axonal area. Increasing mitochondrial biogenesis seems to be the most promising manipulation tested during this thesis, as it was the only manipulation showing a significant reduction of axonal bulbs after treatment. Increasing mitochondrial transport is another neuroprotective treatment, which was not tested within this thesis and could be a promising target, as it was reported to be protective in models of axonal damage (Zhou et al., 2016).

7.2.5 Modelling mitochondrial deficiency

Previous research from the Mahad lab, as well as several other independent research groups around the world, showed that neurons in MS harbour

mtDNA defects and display a down regulation of important mitochondrial genes, which subsequently lead to deficiencies of the ETC (Dutta et al., 2006; Campbell et al., 2011; Broadwater et al., 2011; Witte et al., 2013; Kim et al., 2010; Hares et al., 2014; Fischer et al., 2013; Haile et al., 2017a). As the experiment of this thesis were done on wild-type neurons of the cerebellum, the aim of this experiment was to model mitochondrial complex IV deficiency in cerebellar slices. For this cerebellar slices of $COX10^{fl/fl} - Thy1 - Cre - ERT2^{+-}$ mutant mice were generated and mitochondrial complex IV deficiency was induced by the addition of tamoxifen or 4-OHT to the slice culture medium. Even after 4 weeks in culture PC in the slices did not show any deficiency of mitochondrial complex IV. A possible explanation for this finding could be that the mitochondrial turnover in PC is too slow to induce any significant deficiency in that time frame, but since the health of the slices started to deteriorate after 3 to 4 weeks, it was not possible to produce complex IV deficient PC in cerebellar slices during this thesis.

In parallel to the experiments conducted for this thesis, Graham Campbell and other members of the Mahad lab performed *in vivo* experiments with the $COX10^{fl/fl} - Thy1 - Cre - ERT2^{+-}$ mutant mice. My contribution to this set of experiments was to determine the earliest timepoint where significant deficiency can be found in the neurons, but no structural change has occurred yet, as this would be the optimal timepoint for demyelination. The analysis of several different cellular markers determined VGlut1 positive synapses as the most sensitive marker for structural change after the induction of deficiency. Subsequently different timepoints after the induction of deficiency with tamoxifen were analysed by IHC staining for VGlut1 and showed a significant decrease of VGlut1 positive synapses in the ventral horn of the spinal cord at 10 weeks post induction of deficiency. There was still a trend to decreased number of VGlut1 synapses at 8 weeks and a slight trend at 6 weeks post induction of deficiency. As the earliest timepoint stained, $COX10^{fl/fl} - Thy1 - Cre - ERT2^{+-}$ mutant mice 4 weeks after tamoxifen injection, no loss of VGlut1 positive synapses was observed. The second part of this *in vivo* analysis, was to determine the mitochondrial complex IV deficiency in the dendrites of neurons in the spinal cord at 10 weeks and 4

weeks after induction of mitochondrial complex IV deficiency. At 10 weeks post tamoxifen injection there was significant increase in mitochondrial deficiency in the cervical ventral horn, while the n-number in other regions, due to significant tissue damage in the paraffin sections, was not high enough to reach statistical significance. Other mitochondrial parameters measured were not significantly different between mutant and control, only the mitochondria area showed a trend towards reduced area in the mutant. This observation, altough not signifcant, was similiar in another model of mitochondrial deficiency used in the Mahad lab, which showed a reduction of mitochondrial mass in the myelinated axons over time. Already at 4 weeks post induction of deficiency the complex IV deficiency in the cervical ventral horn could be observed, while other parameters measured were not different between mutant and control. These findings indicate week 4 after the induction of deficiency with tamoxifen as the earliest timepoint were there is significant deficiency in the neurons of the cervical ventral horn, while there is no significant structural change in the VGlut1 positive synapses. Therefore, 4 weeks after injection of tamoxifen would be the ideal timepoint for demyelination with lyoslecithin to study the effect of demyelination on neurons with complex IV deficiency.

7.3 Conclusion

MS was long regarded primarily as a white matter disease, although the involvement of the grey matter in the pathology of MS is known for well over a century, only in recent decades the interest in the grey matter came more into focus (Love, 2006; Popescu and Lucchinetti, 2012a). Now it is widely accepted that MS is a multi focal disease affecting both white matter and grey matter in varying amount, but are mostly dealt with like they are separate aspects of this disease (Love, 2006; Popescu and Lucchinetti, 2012a; Mahad, Trapp, and Lassmann, 2015). The neuron however connects these two aspects as it is affected both at the soma in the grey matter, as well as in the distal axon residing in the white matter and damage to the neuronal cell body affects the health status of the axon and vice versa. The axons in MS are compromised by inflammation, which affect axonal transport and energy production (Sorbara et al., 2014; Mahad, Trapp, and Lassmann,

2015). Demyelination of the axon further worsens the situation by increasing the energy demand in the axon via the redistribution of sodium channels along the axon and the excess sodium that has to be pumped out of the axolemma (Craner et al., 2004b; Waxman, 2006; Mohd, 2010; Albers and Siegel, 1998; Lores Arnaiz and Ordieres, 2014). To combat this increase in energy demand and decrease in local energy production, the amount of mitochondria in the axon is increased in demyelinated axons in MS (Mahad et al., 2009; Witte et al., 2009; Zambonin et al., 2011; Ohno et al., 2011). It is not known how this ARMD comes about or where these additional mitochondria observed in the demyelinated axons come from.

The aim of this thesis was to determine the mitochondrial dynamics in cerebellar brain slices after demyelination with lysolecithin, manipulate mitochondrial dynamics to preserve axonal health and to model mitochondrial deficiency *in vitro*. The timecourse experiment of the AMRD, revealed a bell shaped curve of mitochondrial occupancy of the axon over time, with sharp increase until reaching a plateau, before decreasing again. This response is mediated by fast transport of mitochondria into the axon and fusion of newly transported mitochondria with stationary mitochondria over time. These newly transported mitochondria are coming from the cell body and their movement speed is increased compared to the myelinated axon, while fusion rate within the demyelinated axon is also enhanced. Blocking mitochondrial transport with oligomycin showed that the increase of green-in-red fluorescence is truly an effect of fusion and not mediated by the transport back into the stationary mitochonria of the mEOS2 protein. The fact that the additional mitochondria, observed after demyelination, are coming into the axon from the cell body further stresses the important connection between cell body and axon, as the health status of the mitochondria in the cell body is of vital importance for the future health status of the axon, which with inflammation and demyelination is already in a state of virtual hypoxia (Trapp and Stys, 2009). The increased energy demand in the axon also puts stress on the cell body as increased transport of mitochondria from the cell body to the axon is needed to meet this increase in demand. Furthermore, it was shown that in models of MS the transport of mitochondria is already affected in non-demyelinated axons, leading to axonal structural changes and sparsity of mitochondria in the

distal part of the axon, stressing the importance of mitochondrial transport in MS (Sorbara et al., 2014). This sparsity of mitochondria in the distal axonal part, along with the increase in syntaphilin along the axon, which stops the newly transported mitochondria in the axon, could potential lead to drastic reduction in mitochondria in the synapses and consequently synapse loss, which was shown to be widespread in MS.

To determine if this increase of mitochondrial dynamics seen in the demyelinated axons is not an effect of the lysolecithin *shiverer* mutant slices with or without lysolecithin treatment were used, as it was reported that there is an increase of mitochodnrial content in the *shiverer* mutant. Lysolecithin treatment of *shiverer* mutant slices showed that the effect seen in the wild-type demyelinated slices is not a secondary effect of lysolecithin, but a consequence of demyelination, as the mitochondrial dynamics did not differ between treated and untreated *shiverer* mutant slices. Proper myelination seems to 'put the brakes on' mitochondrial dynamics as it not only increases the speed in propagation of action potentials, but also decreases the amount of energy needed to keep up neuronal communication and therefore decreases the need for an increase in mitochondrial dynamics (Neishabouri and Faisal, 2011; Saab, Tzvetanova, and Nave, 2013).

Several experiments with different small molecule compound demonstrated that the inhibition of mitochondrial fission, with mdivi-1 increases mitochondrial content of the axon and is detrimental to axonal health, but it is more likely that the detrimental effect on axonal health is caused by the inhibition of complex I which is supposed to be significant with mdivi-1 treatment (Cassidy-Stone et al., 2008; Bordt et al., 2017). It was reported earlier that decreasing excessive mitochondrial fission is protective in an *in vitro* model of Parkinson's disease, but a different compound, which is a specific inhibitor of mitochondrial fission (P110) without effect on complex I, was used, which could explain the different findings (Qi et al., 2013). Similarly to the inhibition of mitochondrial fission, the blockage of mitochondrial transport, and reduction of ATP synthesis, with oligomycin was found to be detrimental on axonal health, while decreasing the mitochondrial content in the treated axons (Zala et al., 2013; Shchepina et al., 2012). This detrimental effect on axonal health however was expected and confirms the importance of mitochondrial transport for the axon. Only

the increase of mitochondrial biogenesis with pioglitazone showed a significant improvement of axonal health after demyelination, when taking the size of axonal bulbs into account (Desouza and Shivaswamy, 2010; Skov et al., 2008; Bogacka et al., 2005; Ghosh et al., 2007; Corona and Duchena, 2016). Increasing mitochondrial biogenesis, as the decrease of mitochondrial fission, was shown to be protective in an *in vitro* model of Parkinson's disease, but none of these substances was used in the context of demyelination or MS (Scholpa et al., 2018b). Another possible manipulation for rescuing axonal health after demyelination is the acceleration of mitochondrial transport, which was shown to enhance axonal regeneration after transection, but was not used in a model of demyelination thus far (Zhou et al., 2016). The hypothesis for this experiment would be that the ARMD is accelerated and would reach its peak earlier than the 4 days after demyelination observed. This acceleration of ARMD potentially is also taking place in the pioglitazone experiment as the increase in mitochondrial biogenesis supplies more mitochondria to be transported into the demyelinated axon. But further investigation of the pioglitazone treatment as well as experiments involving increased mitochondrial transport are needed to test this hypothesis.

The experiments conducted for this thesis demonstrate that the health status of mitochondria in the cell body is important for the fate of the axon after demyelination, since the mitochondria from the cell body are the ones supplying the additional organelles after demyelination. If the cell body harbours dysfunctional mitochondria, which was demonstrated in the MS cortex, demyelination leads to an influx of dysfunctional mitochondria into the already damaged axon and subsequently will lead to energy deficiency, enhanced oxidative damage and eventual death of the axon (Dutta et al., 2006; Campbell et al., 2011; Broadwater et al., 2011; Witte et al., 2013; Kim et al., 2010; Hares et al., 2014; Fischer et al., 2013; Haile et al., 2017a). This deficiency of cell body mitochondria has to be modelled in a disease relevant model and needs to be addressed in potential therapies. Although mitochondrial deficiency is difficult to target, it was recently shown that deficiency in different complexes of the ETC, can be treated by hypoxia and compounds activating the hypoxia responsive pathways (Jain et al., 2016; Russell, Lightowlers, and Turnbull, 2016). Although contra intuitive at first

sight, the decrease of dependence, maybe via an increase of glycolosis, on these deficient mitochondria could lead to decreased ROS and subsequently improved cellular health (Jain et al., 2016; Russell, Lightowlers, and Turnbull, 2016). The artificial upregulation of hypoxia induced pathways, could be even more relevant to MS as it was shown that mitochondrial deficiency impairs the ability of up regulation of the hypoxia involving pathways (Jain et al., 2016; Russell, Lightowlers, and Turnbull, 2016). However, if this principal is of use in the treatment of MS and relevant disease models, where a state of virtual hypoxia is present, has yet to be investigated. One of the caveats of this thesis is that the model and methods used represent a reductionist view of the problem on hand, as there are many more components playing a role in MS, which include inflammation and various types immune cells that are present in the MS lesions, focal instead of total demyelination, as well as mitochondrial deficiencies in the neurons, which all play a significant part in MS pathology and were not addressed in the experiments conducted for this thesis. There is also chronic demyelination going on in MS, especially in the progressive phase of the disease, as opposed to the acute demyelination used for the experiments of this thesis.

The next step would be to determine if interventions that already showed a protective effect in wild type demyelinated axons, can also rescue demyelinated axons of neurons that contain a significant number of dysfunctional mitochondria. The ideal experimental setup for this would be a microfluidic chamber system, which not only allows to have a pre determined directionality of axons, but also offers the possibility to treat the cell body and axon separately. This enables to inhibit different complexes of the ETC in the cell body compartment and demyelinate the axonal chamber with lysolecithin to determine the effect of mitochondrial dysfunction on demyelinated axons and to test if different treatments of the cell body have an effect on axonal health. It was shown that there is only around 20% neuronal loss even at later stages of MS, while axonal loss very profound with 60-70% and there is also a very significant loss of synapses (Magliozzi et al., 2010; Papadopoulos, Pham-Dinh, and Reynolds, 2006; Peterson et al., 2001; Bitsch et al., 2000b; Jürgens et al., 2016; Trapp et al., 1998). This makes MS a very good target disease for neuroprotective therapies, as there is very

little neuron cell body loss for a long time, as opposed to other neurodegenerative diseases. There is still a relatively low rate of neuronal cell loss even when the disease becomes symptomatic, because the symptoms are not necessarily caused by neuronal death, but rather by the loss of synapses, myelin, axon connection disturbances and inflammation. This leaves a long window of opportunity in treating the neuronal cell bodies and disease progression.

One future difficulty will be to translate the findings into the clinical use, as these experiments are done on a very basic level without taking into account that treatment can have effects on many different part of the patients body, on different tissue types and finally on different cell types within the tissue, because mitochondria play a vital role in every part of the human body. Nevertheless, trying to manipulate and subsequently improve mitochondrial dynamics in MS and other diseases of the CNS is a promising target to modify disease course, especially in patients that are at an advanced stage of the disease, were there are very limited treatment options to this day.

Bibliography

Agostino, A, Invernizzi F, Tiveron C, Fagiolari G, Prelle A, Lamantea E, Giavazzi A, Battaglia G, Tatangelo L, Tiranti V, and Zeviani M (2003). "Constitutive knockout of Surf1 is associated with high embryonic lethality and mitochondrial disease and cytochrome c oxidase deficiency in mice". In: *Hum Mol Genet* 12(4), pp. 399–413.

Ahmad, T, Mukherjee S, Pattnaik B, Kumar M, Singh S, Kumar M, Rehman R, Tiwari BK, Jha KA, Barhanpurkar AP, Wani MR, Roy SS, Mabalirajan U, Ghosh B, and Agrawal A. (2014). "Miro1 regulates intercellular mitochondrial transport and enhances mesenchymal stem cell rescue efficacy". In: *EMBO J* 33(9), pp. 994–1010.

Akesson, E., A. Oturai, J. Berg, S. Fredrikson, O. Andersen, H. F. Harbo, M. Laaksonen, K. M. Myhr, H. I. Nyland, L. P. Ryder, M. Sandberg-Wollheim, P. S. Sorensen, A. Spurkland, A. Svejgaard, P. Holmans, A. Compston, J. Hillert, and S. Sawcer (2002). "A genome-wide screen for linkage in Nordic sib-pairs with multiple sclerosis". In: *Genes Immun* 3(5), pp. 279–285.

Alam, Tanfis Istiaq, Tomotake Kanki, Tsuyoshi Muta, Koutarou Ukaji, Yoshito Abe, Hiroshi Nakayama, Koji Takio, Naotaka Hamasaki, and Dongchon Kanga (2003). "Human mitochondrial DNA is packaged with TFAM". In: *Nucleic Acids Res* 31(6), 1640–1645.

Albers, R Wayne and George J Siegel (1998). "The ATP-Dependent Na+,K+ Pump". In: *Basic Neurochemistry: Molecular and Cellular and Medical Aspects* 6.

Allen, M., M. Sandberg-Wollheim, K. Sjogren, H. A. Erlich, U. Petterson, and U. Gyllensten (1994). "Association of susceptibility to multiple sclerosis in Sweden with HLA class II DRB1 and DQB1 alleles". In: *Hum Immunol* 39(1), pp. 41–48.

Amiri, Mandana and Peter J. Hollenbeck (2008). "Mitochondrial Biogenesis in the Axons of Vertebrate Peripheral Neurons". In: *Dev Neurobiol* 68(11), 1348–1361.

Andrews, H, White K, Thomson C, Edgar J, Bates D, Griffiths I, Turnbull D, and Nichols P (2006). "Increased axonal mitochondrial activity as an adaptation to myelin deficiency in the Shiverer mouse". In: *J Neurosci Res* 83(8), pp. 1533–9.

Barbarese, E, ML Nielson, and JH Carson (1983). "The effect of the shiverer mutation on myelin basic protein expression in homozygous and heterozygous mouse brain". In: *Neurochem* 40(6), pp. 1680–6.

Barnett, MH and JW Prineas (2004). "Relapsing and remitting multiple sclerosis: pathology of the newly forming lesion". In: *Ann Neurol* 55(4), pp. 458–68.

Barnett, MH, Parratt JD, Pollard JD, and Prineas JW (2009). "MS: is it one disease?" In: *Int MS J* 16(2), pp. 57–65.

Bhabha, Gira, Graham T. Johnson, Courtney M. Schroeder, and Ronald D. Vale (2016). "How dynein moves along microtubules". In: *Trends Biochem Sci* 41(1), 94–105.

Bingo, B and M Sheng (2016). "Mechanisms of mitophagy: PINK1 and Parkin and USP30 and beyond". In: *Free Radic Biol Med* 100, pp. 210–222.

Birgbauer, E, TS Rao, and M Webb (2004). "Lysolecithin induces demyelination in vitro in a cerebellar slice culture system". In: *J Neurosci Res* 78(2), pp. 157–66.

Bitsch, A., J. Schuchardt, S. Bunkowski, T. Kuhlmann, and W. Bruck (2000a). "Acute axonal injury in multiple sclerosis. Correlation with demyelination and inflammation". In: *Brain* 123 (Pt 6), pp. 1174–1183.

Bitsch, A, Schuchardt J, Bunkowski S, Kuhlmann T, and Brück W (2000b). "Acute axonal injury in multiple sclerosis. Correlation with demyelination and inflammation". In: *Brain* 123 (Pt 6), pp. 1174–83.

Bo, L., C. A. Vedeler, H. I. Nyland, B. D. Trapp, and S. J. Mork (2003). "Subpial demyelination in the cerebral cortex of multiple sclerosis patients". In: *J Neuropathol Exp Neurol* 62(7), pp. 723–732.

Bogacka, I, Xie H, Bray GA, and Smith SR (2005). "Pioglitazone induces mitochondrial biogenesis in human subcutaneous adipose tissue in vivo". In: *Diabetes* 54(5), pp. 1392–9.

Bonda, David J., Mark A. Smith, George Perry, Hyoung gon Lee, Xinglong Wang, and Xiongwei Zhu (2011). "The Mitochondrial Dynamics of Alzheimer's Disease and Parkinson's Disease Offer Important Opportunities for Therapeutic Intervention". In: *Curr Pharm Des* 17(31), 3374–3380.

Booker, SA, Campbell GR, Mysiak KS, Brophy PJ, Kind PC, Mahad DJ, and Wyllie DJ (2017). "Loss of protohaem IX farnesyltransferase in mature dentate granule cells impairs short-term facilitation at mossy fibre to CA3 pyramidal cell synapses". In: *J Physiol* 595(6), pp. 2147–2160.

Bordt, EA, Clerc P, Roelofs BA, Saladino AJ, Tretter L, Adam-Vizi V, Cherok E, Khalil A, Yadava N, Ge SX, Francis TC, Kennedy NW, Picton LK, Kumar T, Uppuluri S, Miller AM, Itoh K, Karbowski M, Sesaki H, Hill RB, and Polster BM (2017). "The Putative Drp1 Inhibitor mdivi-1 Is a Reversible Mitochondrial Complex I Inhibitor that Modulates Reactive Oxygen Species". In: *Dev Cell* 40(6), pp. 583–594.

Brand, Martin D. and David G. Nicholls (2011). "Assessing mitochondrial dysfunction in cells". In: *Biochem J* 435(Pt 2), 297–312.

Brück W, Porada P, Poser S, Rieckmann P, Hanefeld F, Kretzschmar HA, and Lassmann H (1995). "Monocyte/macrophage differentiation in early multiple sclerosis lesions". In: *Ann Neurol* 38(5), pp. 788–96.

Brickley, Kieran and F. Anne Stephenson (2011). "Trafficking Kinesin Protein (TRAK)-mediated Transport of Mitochondria in Axons of Hippocampal Neurons". In: *J Biol Chem* 286(20), 18079–18092.

Britt, Dylan J., Ginny G. Farías, Carlos M. Guardia, and Juan S. Bonifacino (2016). "Mechanisms of Polarized Organelle Distribution in Neurons". In: *Front Cell Neurosci* 10, p. 88.

Broadwater, L, Pandit A, Clements R, Azzam S, Vadnal J, Sulak M, Yong VW, Freeman EJ, Gregory RB, and McDonough J (2011). "Analysis of the mitochondrial proteome in multiple sclerosis cortex". In: *Biochim Biophys Acta* 1812(5), pp. 630–41.

Cai, Q and ZH Sheng (2009). "Mitochondrial transport and docking in axons". In: *Exp Neurol* 218(2), pp. 257–67.

Cai, Qian, Claudia Gerwin, and Zu-Hang Sheng (2005). "Syntabulin-mediated anterograde transport of mitochondria along neuronal processes". In: *J Cell Biol* 170(6), 959–969.

Campbell, CT, JE Kolesar, and BA Kaufman (2012). "Mitochondrial transcription factor A regulates mitochondrial transcription initiation and DNA packaging and and genome copy number". In: *Biochim Biophys Acta* 1819(9-10), pp. 921–9.

Campbell, G. R. and D. J. Mahad (2012). "Clonal expansion of mitochondrial DNA deletions and the progression of multiple sclerosis". In: *CNS Neurol Disord Drug Targets* 11(5), pp. 589–597.

Campbell, G. R., I. Ziabreva, A. K. Reeve, K. J. Krishnan, R. Reynolds, O. How-ell, H. Lassmann, D. M. Turnbull, and D. J. Mahad (2011). "Mitochondrial DNA deletions and neurodegeneration in multiple sclerosis". In: *Ann Neurol* 69(3), pp. 481–492.

Cassidy-Stone, A, Chipuk JE, Ingerman E, Song C, Yoo C, Kuwana T, Kurth MJ, Shaw JT, Hinshaw JE, Green DR, and Nunnari J (2008). "Chemical inhibition of the mitochondrial division dynamin reveals its role in Bax/Bak-dependent mitochondrial outer membrane permeabilization". In: *Dev Cell* 14(2), pp. 193–204.

Cavalier-Smith, Thomas (2006). "Origin of mitochondria by intracellular enslavement of a photosynthetic purple bacterium". In: *Proc Biol Sci* 273(1596), 1943–1952.

Chacinska, Agnieszka, Carla M. Koehler, Dusanka Milenkovic, Trevor Lithgow, and Nikolaus Pfanner (2009). "Importing Mitochondrial Proteins: Machineries and Mechanisms". In: *Cell* 138(4), 628–644.

Chan, DC (2006a). "Mitochondria: dynamic organelles in disease and aging and development". In: *Cell* 125(7), pp. 1241–52.

— (2006b). "Mitochondria: dynamic organelles in disease and aging and development". In: *Cell* 125(7), pp. 1241–52.

— (2012a). "Fusion and fission: interlinked processes critical for mitochondrial health". In: *Annu Rev Genet* 46, pp. 265–87.

— (2012b). "Fusion and fission: interlinked processes critical for mitochondrial health". In: *Annu Rev Genet* 46, pp. 265–87.

Chang, DT and IJ Reynolds (2006). "Mitochondrial trafficking and morphology in healthy and injured neurons". In: *Prog Neurobiol* 80(5), pp. 241–268.

Chazotte, B (2011). "Labeling mitochondria with MitoTracker dyes". In: *Cold Spring Harb Protoc* 8, pp. 990–2.

Chen, H and DC Chan (2009a). "Mitochondrial dynamics–fusion and fission and movement and and mitophagy–in neurodegenerative diseases". In: *Hum Mol Genet* 18(R2), pp. 169–76.

Chen, H, A Chomyn, and DC Chan (2005). "Disruption of fusion results in mitochondrial heterogeneity and dysfunction". In: *J Biol Chem* 280(28), pp. 26185–92.

Chen, H, JM McCaffery, and DC Chan (2007). "Mitochondrial fusion protects against neurodegeneration in the cerebellum". In: *Cell* 130(3), pp. 548–62.

Chen, Hsiuchen and David C. Chan (2009b). "Mitochondrial dynamics–fusion and fission and movement and and mitophagy–in neurodegenerative diseases". In: *Hum Mol Genet* 18, 169–176.

Chen, Hsiuchen, Scott A. Detmer, Andrew J. Ewald, Erik E. Griffin, Scott E. Fraser, and David C. Chan (2003). "Mitofusins Mfn1 and Mfn2 coordinately regulate mitochondrial fusion and are essential for embryonic development". In: *J Cell Biol* 160(2), 189–200.

Chen, Hsiuchen, Marc Vermulst, Yun E. Wang, Anne Chomyn, Tomas A. Prolla, J. Michael McCaffery, and David C. Chan (2010). "Mitochondrial fusion is required for mtDNA stability in skeletal muscle and tolerance of mtDNA mutations". In: *Cell* 141(2), 280–289.

Chen, Y, Y Liu, and GW Dorn (2011). "Mitochondrial fusion is essential for organelle function and cardiac homeostasis". In: *Circ Res* 109(12), pp. 1327–31.

Chen, Y and ZH Sheng (2013). "Kinesin-1-syntaphilin coupling mediates activity-dependent regulation of axonal mitochondrial transport". In: *J Cell Biol* 202(2), pp. 351–64.

Chernoff, GF (1981). "Shiverer: an autosomal recessive mutant mouse with myelin deficiency". In: *Hered* 72(2), p. 128.

Chiang, Hao, Nobuhiko Ohno, Yu-Lin Hsieh, Don J. Mahad, Shin Kikuchi, Hitoshi Komuro, Sung-Tsang Hsieh, and Bruce D. Trapp (2015). "Mitochondrial fission augments capsaicin-induced axonal degeneration". In: *Acta Neuropathol* 129, 81–96.

Chiu, SY (2011). "Matching mitochondria to metabolic needs at nodes of Ranvier". In: *Neuroscientist* 17(4), pp. 343–50.

Cogliati, Sara, Christian Frezza, Maria Eugenia Soriano, Tatiana Varanita, Ruben Quintana-Cabrera, Mauro Corrado, Sara Cipolat, Veronica Costa,

Alberto Casarin, Ligia C. Gomes, Ester Perales-Clemente, Leonardo Salviati, Patricio Fernandez-Silva, Jose A. Enriquez, and Luca Scorrano1 (2013). "Mitochondrial Cristae Shape Determines Respiratory Chain Supercomplexes Assembly and Respiratory Efficiency". In: *Cell* 155(1), 160–171.

Coleman, M (2005). "Axon degeneration mechanisms: commonality amid diversity". In: *Nat Rev Neurosci* 6(11), pp. 889–98.

Comi, G, Martinelli V, Rodegher M, Moiola L, Bajenaru O, Carra A, Elovaara I, Fazekas F, Hartung HP, Hillert J, King J, Komoly S, Lubetzki C, Montalban X, Myhr KM, Ravnborg M, Rieckmann P, Wynn D, Young C, and Filippi M; PreCISe study group (2009). "Effect of glatiramer acetate on conversion to clinically definite multiple sclerosis in patients with clinically isolated syndrome (PreCISe study): a randomised and double-blind and placebo-controlled trial". In: *Lancet* 374(9700).10, pp. 1503–11.

Compston, A. and A. Coles (2002). "Multiple sclerosis". In: *Lancet* 359(9313), pp. 1221–1231.

Compston, A. and S. Sawcer (2002). "Genetic analysis of multiple sclerosis". In: *Curr Neurol Neurosci Rep* 2(3), pp. 259–266.

Confavreux, C. and S. Vukusic (2006). "Natural history of multiple sclerosis: a unifying concept". In: *Brain* 129 (Pt 3), pp. 606–616.

Corona, Juan Carlos and Michael R. Duchena (2016). "PPARgamma as a therapeutic target to rescue mitochondrial function in neurological disease". In: *Free Radic Biol Med* (100), 153–163.

Craner, MJ, Hains BC, Lo AC, Black JA, and Waxman SG (2004a). "Co-localization of sodium channel Nav1.6 and the sodium-calcium exchanger at sites of axonal injury in the spinal cord in EAE". In: *Brain* 127(Pt 2), pp. 294–303.

Craner, MJ, Newcombe J, Black JA, Hartle C, Cuzner ML, and Waxman SG (2004b). "Molecular changes in neurons in multiple sclerosis: altered axonal expression of Nav1.2 and Nav1.6 sodium channels and Na+/Ca2+ exchanger". In: *Proc Natl Acad Sci U S A* 101(21), pp. 8168–73.

Cribbs, Adam P, Alan Kennedy, Bernard Gregory, and Fionula M Brennan (2013). "Simplified production and concentration of lentiviral vectors to

achieve high transduction in primary human T cells". In: *BMC Biotechnol* 13, p. 98.

Cronin, James, Xian-Yang Zhang, and Jakob Reiser (2005). "Altering the Tropism of Lentiviral Vectors through Pseudotyping". In: *Curr Gene Ther* 5(4), Curr Gene Ther. 2005 Aug; 5(4): 387–398.

Croxford, J. L., J. K. Olson, and S. D. Miller (2002). "Epitope spreading and molecular mimicry as triggers of autoimmunity in the Theiler's virus-induced demyelinating disease model of multiple sclerosis". In: *Autoimmun Rev* 1(5), pp. 251–260.

Desouza, Cyrus V and Vijay Shivaswamy (2010). "Pioglitazone in the Treatment of Type 2 Diabetes: Safety and Efficacy Review". In: *Clin Med Insights Endocrinol Diabetes* (3), 43–51.

Dimauro, S and G Davidzon (2005). "Mitochondrial DNA and disease". In: *Ann Med* 37(3), pp. 222–32.

DiMauro, S and EA Schon (2003). "Mitochondrial respiratory-chain diseases". In: *N Engl J Med* 348(26), pp. 2656–68.

Drerup, CM, Herbert AL, Monk KR, and Nechiporuk AV (2017). "Regulation of mitochondria-dynactin interaction and mitochondrial retrograde transport in axons". In: *Elife* 6, e22234.

Dull, Tom, Romain Zufferey, Michael Kelly, R. J. Mandel, Minh Nguyen, Didier Trono, and Luigi Naldini (1998). "A Third-Generation Lentivirus Vector with a Conditional Packaging System". In: *J Virol* 72(11), 8463–8471.

Durand, Stéphanie and Andrea Cimarelli (2011). "The Inside Out of Lentiviral Vectors". In: *Viruses* 3(2), 132–159.

Dutta, R., J. McDonough, X. Yin, J. Peterson, A. Chang, T. Torres, T. Gudz, W. B. Macklin, D. A. Lewis, R. J. Fox, R. Rudick, K. Mirnics, and B. D. Trapp (2006). "Mitochondrial dysfunction as a cause of axonal degeneration in multiple sclerosis patients". In: *Ann Neurol* 59(3), pp. 478–489.

Dutta, Ranjan and Bruce D. Trapp (2014). "Relapsing and progressive forms of multiple sclerosis – insights from pathology". In: *Curr Opin Neurol* 27(3), 271–278.

Elgass, K, Pakay J, Ryan MT, and Palmer CS (2013). "Recent advances into the understanding of mitochondrial fission". In: *Biochim Biophys Acta* 1833(1), pp. 150–61.

Escors, David and Karine Breckpot (2010). "Lentiviral vectors in gene therapy: their current status and future potential". In: *Arch Immunol Ther Exp (Warsz)* 58(2), 107–119.

Fawcett, J.W. and R. A. Asher (1999). "The glial scar and central nervous system repair". In: *Brain Res Bull* 49(6), pp. 377–391.

Fei, Du, Xiao-Hong Zhu, Yi Zhang, Michael Friedman, Nanyin Zhang, Kâmil Uğurbil, and Wei Chen (2008). "Tightly coupled brain activity and cerebral ATP metabolic rate". In: *Proc Natl Acad Sci U S A* 105(17), 6409–6414.

Ferguson, B., M. K. Matyszak, M. M. Esiri, and V. H. Perry (1997). "Axonal damage in acute multiple sclerosis lesions". In: *Brain* 120(Pt 3), pp. 393–399.

Filichia, Emily, Barry Hoffer, Xin Qi, and Yu Luob (2016). "Inhibition of Drp1 mitochondrial translocation provides neural protection in dopaminergic system in a Parkinson's disease model induced by MPTP". In: *Sci Rep* (6), p. 32656.

Fischer, MT, Wimmer I, Höftberger R, Gerlach S, Haider L, Zrzavy T, Hametner S, Mahad D, Binder CJ, Krumbholz M, Bauer J, Bradl M, and Lassmann H (2013). "Disease-specific molecular events in cortical multiple sclerosis lesions". In: *Brain* 136(Pt 6), pp. 1799–815.

Fünfschilling, U, Supplie LM, Mahad D, Boretius S, Saab AS, Edgar J, Brinkmann BG, Kassmann CM, Tzvetanova ID, Möbius W, Diaz F, Meijer D, Suter U, Hamprecht B, Sereda MW, Moraes CT, Frahm J, Goebbels S, and Nave KA (2012). "Glycolytic oligodendrocytes maintain myelin and long-term axonal integrity". In: *Nature* 485(7399), pp. 517–21.

Fox, RJ, Miller DH, Phillips JT, Hutchinson M, Havrdova E, Kita M, Yang M, Raghupathi K, Novas M, Sweetser MT, Viglietta V, and Dawson KT; CONFIRM Study Investigators (2012). "Placebo-controlled phase 3 study of oral BG-12 or glatiramer in multiple sclerosis". In: *N Engl J Med* 367(12), pp. 1087–97.

Frank, S, Gaume B, Bergmann-Leitner ES, Leitner WW, Robert EG, Catez F, Smith CL, and Youle RJ (2001). "The role of dynamin-related protein 1

and a mediator of mitochondrial fission and in apoptosis". In: *Dev Cell* 1(4), pp. 515–25.

Frezza, C, Cipolat S, Martins de Brito O, Micaroni M, Beznoussenko GV, Rudka T, Bartoli D, Polishuck RS, Danial NN, De Strooper B, and Scorrano L (2006). "OPA1 controls apoptotic cristae remodeling independently from mitochondrial fusion". In: *Cell* 126(1), pp. 177–89.

Friedman, Jonathan R. and Jodi Nunnari (2014). "Mitochondrial form and function". In: *Nature* 505(7483), 335–343.

Gao, Danchen, Li Zhang, Ranvir Dhillon, Ting-Ting Hong, Robin M. Shaw, and Jianhua Zhu (2013). "Dynasore Protects Mitochondria and Improves Cardiac Lusitropy in Langendorff Perfused Mouse Heart". In: *PLoS One* 8(4), e60967.

Ghasemi Nazem, Ph.D Shahnaz Razavi Ph.D Elham Nikzad B.Sc (2017). "Multiple Sclerosis: Pathogenesis and Symptoms and Diagnoses and Cell-Based Therapy". In: *Cell J* 19(1), 1–10.

Ghosh, S, Patel N, Rahn D, McAllister J, Sadeghi S, Horwitz G, Berry D, Wang KX, and Swerdlow RH (2007). "The thiazolidinedione pioglitazone alters mitochondrial function in human neuron-like cells". In: *Mol Pharmacol* 71(6), pp. 1695–702.

Gilbert, Susan P., Martin R. Webb, Martin Brune, and Kenneth A. Johnson (1995). "Pathway of processive ATP hydrolysis by kinesin". In: *Nature* 373(6516), 671–676.

Giovannoni, G, Heales SJ, Land JM, and Thompson EJ (1998). "The potential role of nitric oxide in multiple sclerosis". In: *Mult Scler* 4(3), pp. 212–6.

Glater, Elizabeth E., Laura J. Megeath, R. Steven Stowers, and Thomas L. Schwarz (2006). "Axonal transport of mitochondria requires milton to recruit kinesin heavy chain and is light chain independent". In: *J Cell Biol* 173(4), 545–557.

Goenawan, H and H Hirai (2012). "Modulation of lentiviral vector tropism in cerebellar Purkinje cells in vivo by a lysosomal cysteine protease cathepsin K". In: *J Neurovirol* 18(6), pp. 521–31.

Gold, R, Kappos L, Arnold DL, Bar-Or A, Giovannoni G, Selmaj K, Tornatore C, Sweetser MT, Yang M, Sheikh SI, and Dawson KT; DEFINE Study Investigators (2012). "Placebo-controlled phase 3 study of

oral BG-12 for relapsing multiple sclerosis". In: *N Engl J Med* 367(12), pp. 1098–107.

Gold, Stefan M and Rhonda R Voskuhl (2009). "Estrogen Treatment in Multiple Sclerosis". In: *J Neurol Sci* 286(1-2), 99–103.

Goldenberg Marvin M., PhD RPh MS (2012). "Multiple Sclerosis Review". In: *P T* 37(3), 175–184.

Guo, X, Macleod GT, Wellington A, Hu F, Panchumarthi S, Schoenfield M, Marin L, Charlton MP, Atwood HL, and Zinsmaier KE (2005). "The GTPase dMiro is required for axonal transport of mitochondria to Drosophila synapses". In: *Neuron* 47(3), pp. 379–93.

Guseo, A and K Jellinger (1975). "The significance of perivascular infiltrations in multiple sclerosis". In: *J Neurol* 211(1), pp. 51–60.

Hafler, D.A., A. Compston, S. Sawcer, E. S. Lander, M. J. Daly, P. L. De Jager, P. I. de Bakker, S. B. Gabriel, D. B. Mirel, A. J. Ivinson, M. A. Pericak-Vance, S. G. Gregory, J. D. Rioux, J. L. McCauley, J. L. Haines, L. F. Barcellos, B. Cree, J. R. Oksenberg, and S. L. Hauser (2007). "Risk alleles for multiple sclerosis identified by a genomewide study". In: *N Engl J Med* 357(9), pp. 851–862.

Haider, L., M. T. Fischer, J. M. Frischer, J. Bauer, R. Hoftberger, G. Botond, H. Esterbauer, C. J. Binder, J. L. Witztum, and H. Lassmann (2011). "Oxidative damage in multiple sclerosis lesions". In: *Brain* 134(Pt 7), pp. 1914–1924.

Haile, Y, Deng X, Ortiz-Sandoval C, Tahbaz N, Janowicz A, Lu JQ, Kerr BJ, Gutowski NJ, Holley JE, Eggleton P, Giuliani F, and Simmen T (2017a). "Rab32 connects ER stress to mitochondrial defects in multiple sclerosis". In: *J Neuroinflammation* 14(1), p. 19.

Haile, Yohannes, Xiaodan Deng, Carolina Ortiz-Sandoval, Nasser Tahbaz, Aleksandra Janowicz, Jian-Qiang Lu, Bradley J. Kerr and4 Nicholas J. Gutowski, Janet E. Holley, Paul Eggleton, Fabrizio Giuliani, and Thomas Simmen (2017b). "Rab32 connects ER stress to mitochondrial defects in multiple sclerosis J Neuroinflammation". In: 14, p. 19.

Hao, W, Chang CP, Tsao CC, and Xu J (2010). "Oligomycin-induced bioenergetic adaptation in cancer cells with heterogeneous bioenergetic organization". In: *J Biol Chem* 285(17), pp. 12647–54.

Hares, K, Kemp K, Rice C, Gray E, Scolding N, and Wilkins A (2014). "Reduced axonal motor protein expression in non-lesional grey matter in multiple sclerosis". In: *Mult Scler* 20(7), pp. 812–21.

Hasegawa, K, Yasuda T, Shiraishi C, Fujiwara K, Przedborski S, Mochizuki H, and Yoshikawa K (2016). "Promotion of mitochondrial biogenesis by necdin protects neurons against mitochondrial insults". In: *Nat Commun* (7), p. 10943.

Hayashi, J, Ohta S, Kikuchi A, Takemitsu M, Goto Y, and Nonaka I (1991). "Introduction of disease-related mitochondrial DNA deletions into HeLa cells lacking mitochondrial DNA results in mitochondrial dysfunction". In: *Proc Natl Acad Sci U S A* 88(23), pp. 10614–8.

Hayes, C. E. (2000). "Vitamin D: a natural inhibitor of multiple sclerosis". In: *Proc Nutr Soc* 59(4), pp. 531–535.

Holehonnur, Roopashri, Srihari K Lella, Anthony Ho, Jonathan A Luong, and Jonathan E Ploski (2015). "The production of viral vectors designed to express large and difficult to express transgenes within neurons". In: *Mol Brain* 8, p. 12.

Holick, M. F. (2007). "Vitamin D deficiency". In: *N Engl J Med* 357(3), pp. 266–281.

Horssen, J. van, G. Schreibelt, L. Bo, L. Montagne, B. Drukarch, F. L. van Muiswinkel, and H. E. de Vries (2006). "NAD(P)H:quinone oxidoreductase 1 expression in multiple sclerosis lesions". In: *Free Radic Biol Med* 41(2), pp. 311–317.

Horssen, J. van, M. E. Witte, G. Schreibelt, and H. E. de Vries (2011). "Radical changes in multiple sclerosis pathogenesis". In: *Biochim Biophys Acta* 1812(2), pp. 141–150.

Humpel, C (2015). "Organotypic brain slice cultures: A review". In: *Neuroscience* 305, pp. 86–98.

Iborra, FJ, H Kimura, and PR Cook (2004). "The functional organization of mitochondrial genomes in human cells". In: *BMC Biol* 2, p. 9.

Jain, IH, Zazzeron L, Goli R, Alexa K, Schatzman-Bone S, Dhillon H, Goldberger O, Peng J, Shalem O, Sanjana NE, Zhang F, Goessling W, Zapol WM, and Mootha VK (2016). "Hypoxia as a therapy for mitochondrial disease". In: *Science* 352(6281), pp. 54–61.

Jeffery, ND and WF Blakemore (1995). "Remyelination of mouse spinal cord axons demyelinated by local injection of lysolecithin". In: *J Neurocytol* 24(10), pp. 775–81.

Jonckheere, I., Jan A. M. Smeitink, and Richard J. T. Rodenburg (2012). "Mitochondrial ATP synthase: architecture and function and pathology". In: *J Inherit Metab Dis* 35(2), 211–225.

Joshi, DC, Zhang CL, Lin TM, Gusain A, Harris MG, Tree E, Yin Y, Wu C, Sheng ZH, Dempsey RJ, Fabry Z, and Chiu SY (2015). "Deletion of mitochondrial anchoring protects dysmyelinating shiverer: implications for progressive MS". In: *J Neurosci* 35(13), pp. 5293–306.

Jürgens, T, Jafari M, Kreutzfeldt M, Bahn E, Brück W, Kerschensteiner M, and Merkler D (2016). "Reconstruction of single cortical projection neurons reveals primary spine loss in multiple sclerosis". In: *Brain* 139(Pt 1), pp. 39–46.

Kang, JS, Tian JH, Pan PY, Zald P, Li C, Deng C, and Sheng ZH (2008). "Docking of axonal mitochondria by syntaphilin controls their mobility and affects short-term facilitation". In: *Cell* 132(1), pp. 137–48.

Kapfhammer, JP (2004). "Cellular and molecular control of dendritic growth and development of cerebellar Purkinje cells". In: *Prog Histochem Cytochem* 39(3), pp. 131–82.

Karcher, RL, SW Deacon, and VI Gelfand (2002). "Motor-cargo interactions: the key to transport specificity". In: *Trends Cell Biol* 12(1), pp. 21–27.

Keough, Michael B., Samuel K. Jensen, and V. Wee Yong (2015). "Experimental Demyelination and Remyelination of Murine Spinal Cord by Focal Injection of Lysolecithin". In: *J Vis Exp* 97, p. 52679.

Kholmukhamedov Andaleb, M.D., M.D. Justin M. Schwartz, and Ph.D. John J. Lemasters M.D. (2014). "MitoTracker Probes and Mitochondrial Membrane Potential". In: *Shock* 39(6), p. 543.

Kim, JY, Shen S, Dietz K, He Y, Howell O, Reynolds R, and Casaccia P (2010). "HDAC1 nuclear export induced by pathological conditions is essential for the onset of axonal damage". In: *Nat Neurosci* 13(2), pp. 180–9.

Kim, Seon Hee, Hyun Jeong Jun, Soo In Jang, and Ji Chang You (2012). "The Determination of Importance of Sequences Neighboring the Psi Sequence in Lentiviral Vector Transduction and Packaging Efficiency". In: *PLoS One* 7(11), e50148.

Kimura, T and F Murakami (2014). "Evidence that dendritic mitochondria negatively regulate dendritic branching in pyramidal neurons in the neocortex". In: *J Neurosci* 34(20), pp. 6938–51.

Kiryu-Seo, Sumiko, Ohno Nobuhiko, Kidd Grahame J., Komuro Hitoshi, and Trapp Bruce D. (2010). "Demyelination increases axonal stationary mitochondrial size and the speed of axonal mitochondrial transport". In: *J Neurosci* 30(19), 6658–6666.

Komai, H, DR Hunter, and Y Takahashi (1973). "Effect of lysolecithin treatment on the structure and functions of the mitochondrial inner membrane". In: *Biochem Biophys Res Commun* 53(1), pp. 82–9.

Kornek, B, Storch MK, Bauer J, Djamshidian A, Weissert R, Wallstroem E, Stefferl A, Zimprich F, Olsson T, Linington C, Schmidbauer M, and Lassmann H (2001). "Distribution of a calcium channel subunit in dystrophic axons in multiple sclerosis and experimental autoimmune encephalomyelitis". In: *Brain* 124(Pt 6), pp. 1114–24.

Kuhlmann, T, Lingfeld G, Bitsch A, Schuchardt J, and Brück W (2002). "Acute axonal damage in multiple sclerosis is most extensive in early disease stages and decreases over time". In: *Brain* 125(Pt 10), pp. 2202–12.

Kumar, S, Zimmermann K, Hioki H, Pfeifer A, and Baader SL (2015). "Efficient and graded gene expression in glia and neurons of primary cerebellar cultures transduced by lentiviral vectors". In: *Histochem Cell Biol* 143(1), pp. 109–21.

Kutzelnigg, A. and H. Lassmann (2014). "Pathology of multiple sclerosis and related inflammatory demyelinating diseases". In: *Handb Clin Neurol* 122, pp. 15–58.

Las, G and OS Shirihai (2014). "Miro1: new wheels for transferring mitochondria". In: *EMBO J* 33(9), pp. 939–41.

Lassmann, H. (2013). "Pathology and disease mechanisms in different stages of multiple sclerosis". In: *J Neurol Sci* 333(1-2), pp. 1–4.

Lassmann, H., W. Bruck, and C. Lucchinetti (2001). "Heterogeneity of multiple sclerosis pathogenesis: implications for diagnosis and therapy". In: *Trends Mol Med* 7(3), pp. 115–121.

Lee, YJ, Jeong SY, Karbowski M, Smith CL, and Youle RJ (2004). "Roles of the mammalian mitochondrial fission and fusion mediators Fis1, Drp1 and Opa1 in apoptosis". In: *Mol Biol Cell* 15(11), pp. 5001–11.

Legros, F, Lombès A, Frachon P, and Rojo M (2002). "Mitochondrial fusion in human cells is efficient and requires the inner membrane potential, and is mediated by mitofusins". In: *Mol Biol Cell* 13(12), pp. 4343–54.

Li, Mingjie, Nada Husic, Ying Lin, Heather Christensen, Ibrahim Malik, Sally McIver, Christine M. LaPash Daniels, David A. Harris, Paul T. Kotzbauer, Mark P. Goldberg, and B. Joy Snider (2010). "Optimal promoter usage for lentiviral vector-mediated transduction of cultured central nervous system cells". In: *J Neurosci Methods* 189(1), 56–64.

Li, Z, Okamoto K, Hayashi Y, and Sheng M (2004). "The importance of dendritic mitochondria in the morphogenesis and plasticity of spines and synapses". In: *Cell* 119(6), pp. 873–887.

Liang, H and WF Ward (2006). "PGC-1alpha: a key regulator of energy metabolism". In: *Adv Physiol Educ* 30(4), pp. 145–151.

Lin, MY and ZH Sheng (2015). "Regulation of mitochondrial transport in neurons". In: *Exp Cell Res* 334(1), pp. 35–44.

Lipton, H. L., Z. Liang, S. Hertzler, and K. N. Son (2007). "A specific viral cause of multiple sclerosis: one virus and one disease". In: *Ann Neurol* 61(6), pp. 514–523.

Liu, LiPing, Lindsey Darnall, Taofang Hu, Karen Choi, and Richard M. Ransohoff (2010). "Myelin repair is accelerated by inactivating CXCR2 on non-hematopoietic cells". In: *J Neurosci* 30(27), 9074–9083.

Liu, Raymond and David C. Chan (2015). "The mitochondrial fission receptor Mff selectively recruits oligomerized Drp1". In: *Mol Biol Cell* 26(24).

Liu, X, Weaver D, Shirihai O, and Hajnóczky G (2009). "Mitochondrial 'kiss-and-run': interplay between mitochondrial motility and fusion-fission dynamics". In: *EMBO J* 28(20), pp. 3074–89.

Lores Arnaiz, Georgina Rodríguez de and María Graciela López Ordieres (2014). "Brain Na+ and K+-ATPase Activity In Aging and Disease". In: *Int J Biomed Sci* 10(2), 85–102.

Losón, Oliver C., Zhiyin Song, Hsiuchen Chen, and David C. Chana (2013). "Fis1 and Mff and MiD49 and and MiD51 mediate Drp1 recruitment in mitochondrial fission". In: *Mol Biol Cell* 24(5), 659–667.

Love, S (2006). "Demyelinating diseases". In: *J Clin Pathol* 59(11), 1151–1159.

Lu, F., M. Selak, J. O'Connor, S. Croul, C. Lorenzana, C. Butunoi, and B. Kalman (2000). "Oxidative damage to mitochondrial DNA and activity of mitochondrial enzymes in chronic active lesions of multiple sclerosis". In: *J Neurol Sci* 177(2), pp. 95–103.

Lublin, F. D., S. C. Reingold, J. A. Cohen, G. R. Cutter, P. S. Sorensen, A. J. Thompson, J. S. Wolinsky, L. J. Balcer, B. Banwell, F. Barkhof, B. Bebo, P. A. Calabresi, M. Clanet, G. Comi, R. J. Fox, M. S. Freedman, A. D. Goodman, M. Inglese, L. Kappos, B. C. Kieseier, J. A. Lincoln, C. Lubetzki, A. E. Miller, X. Montalban, P. W. O'Connor, J. Petkau, C. Pozzilli, R. A. Rudick, M. P. Sormani, O. Stuve, E. Waubant, and C. H. Polman (2014). "Defining the clinical course of multiple sclerosis: The 2013 revisions". In: *Neurology*.

Lucchinetti Claudia F., M.D., Ph.D. Bogdan F.G. Popescu M.D., M.D. Reem F. Bunyan, Ph.D. Natalia M. Moll M.D., M.D. Shanu F. Roemer, M.D. Hans Lassmann, M.D. Wolfgang Brück, M.D. Joseph E. Parisi, M.D. Bernd W. Scheithauer, M.D. Caterina Giannini, M.S. Stephen D. Weigand, Ph.D. Jay Mandrekar, and M.D. Richard M. Ransohoff (2011). "Inflammatory Cortical Demyelination in Early Multiple Sclerosis". In: *N Engl J Med* 365(23), 2188–2197.

Magliozzi, R, Howell OW, Reeves C, Roncaroli F, Nicholas R, Serafini B, Aloisi F, and Reynolds R (2010). "A Gradient of neuronal loss and meningeal inflammation in multiple sclerosis". In: *Ann Neurol* 68(4), pp. 477–93.

Mahad, DH, BD Trapp, and H Lassmann (2015). "Pathological mechanisms in progressive multiple sclerosis". In: *Lancet Neurol* 14(2), pp. 183–93.

Mahad, DJ, Ziabreva I, Campbell G, Lax N, White K, Hanson PS, Lassmann H, and Turnbull DM (2009). "Mitochondrial changes within axons in multiple sclerosis". In: *Brain* 132(Pt 5), pp. 1161–74.

Mangeo, Pierre, Bram Prevo, and Erwin J. G. Peterman (2016). "KymographClear and KymographDirect: two tools for the automated quantitative analysis of molecular and cellular dynamics using kymographs". In: *Mol Biol Cell* 27(12), 1948–1957.

Mao, Kai and Daniel J Klionsky (2013). "Participation of mitochondrial fission during mitophagy". In: *Cell Cycle* 12(19), 3131–3132.

Marchi, S, S Patergnani, and P Pinton (2014). "The endoplasmic reticulum-mitochondria connection: one touch and multiple functions". In: *Biochim Biophys Acta* 1837(4), pp. 461–9.

Marx, Alexander, Andreas Hoenger, and Eckhard Mandelkow (2009). "Structures of Kinesin Motor Proteins". In: *Cell Motil Cytoskeleton* 66(11), 958–966.

McDonald, W. I., A. Compston, G. Edan, D. Goodkin, H. P. Hartung, F. D. Lublin, H. F. McFarland, D. W. Paty, C. H. Polman, S. C. Reingold, M. Sandberg-Wollheim, W. Sibley, A. Thompson, S. van den Noort, B. Y. Weinshenker, and J. S. Wolinsky (2001). In: *Ann Neurol* 50(1), pp. 121–127.

McKinney, Sean A, Murphy Christopher S., Hazelwood Kristin L., Davidson Michael W., and Looger Loren L. (2009). "A bright and photostable photoconvertible fluorescent protein for fusion tags". In: *Nat Methods* 6(2), 131–133.

McWilliams, TG and MM Muqit (2017). "PINK1 and Parkin: emerging themes in mitochondrial homeostasis". In: *Curr Opin Cell Biol* 45, pp. 83–91.

Merten, Otto-Wilhelm, Matthias Hebben, and Chiara Bovolenta (2016). "Production of lentiviral vectors". In: *Mol Ther Methods Clin Dev* 3, p. 16017.

Metz, I., S. D. Weigand, B. F. Popescu, J. M. Frischer, J. E. Parisi, Y. Guo, H. Lassmann, W. Bruck, and C. F. Lucchinetti (2014). "Pathologic heterogeneity persists in early active multiple sclerosis lesions". In: *Ann Neurol*.

Miglio, G, Rosa AC, Rattazzi L, Collino M, Lombardi G, and Fantozzi R (2009). "PPARgamma stimulation promotes mitochondrial biogenesis and prevents glucose deprivation-induced neuronal cell loss". In: *Neurochem Int* 55(7), pp. 496–504.

Miki, T, H Hirai, and T Takahashi (2013). "Activity-dependent neurotrophin signaling underlies developmental switch of Ca2+ channel subtypes mediating neurotransmitter release". In: *J Neurosci* 33(48), pp. 18755–63.

Miller, D. H. (1995). "Magnetic resonance imaging and spectroscopy in multiple sclerosis". In: *Curr Opin Neurol* 8(3), pp. 210–215.

Miller, D. H., R. I. Grossman, S. C. Reingold, and H. F. McFarland (1998). "The role of magnetic resonance techniques in understanding and managing multiple sclerosis". In: *Brain* 121 (Pt 1), pp. 3–24.

Minagar, A. and J. S. Alexander (2003). "Blood-brain barrier disruption in multiple sclerosis". In: *Mult Scler* 9(6), pp. 540–549.

Miron, VE, Ludwin SK, Darlington PJ, Jarjour AA, Soliven B, Kennedy TE, and Antel JP (2010). "Fingolimod (FTY720) enhances remyelination following demyelination of organotypic cerebellar slices". In: *Am J Pathol* 176(6), pp. 2682–94.

Misgeld, T, I Nikic, and M Kerschensteiner (2007). "In vivo imaging of single axons in the mouse spinal cord". In: *Nat Protoc* 2(2), pp. 263–8.

Misgeld, T, Kerschensteiner M, Bareyre FM, Burgess RW, and Lichtman JW (2007). "Imaging axonal transport of mitochondria in vivo". In: *Nat Methods* 4(7), pp. 559–61.

Mitra, Kasturi and Jennifer Lippincott-Schwartz (2011). "Analysis of mitochondrial dynamics and functions using imaging approaches". In: *Curr Protoc Cell Biol* CHAPTER: Unit–4.2521.

Mohd, Suhaila (2010). "andb Na+ and K+-ATPase: Ubiquitous Multifunctional Transmembrane Protein and its Relevance to Various Pathophysiological Conditions". In: *J Clin Med Res* 2(1), 1–17.

Moll, C, Mourre C, Lazdunski M, and Ulrich J (1991). "Increase of sodium channels in demyelinated lesions of multiple sclerosis". In: *Brain Res* 556(2), pp. 311–6.

Montalban, X, Hauser SL, Kappos L, Arnold DL, Bar-Or A, Comi G, de Seze J, Giovannoni G1, Hartung HP1, Hemmer B, Lublin F, Rammohan KW, Selmaj K, Traboulsee A, Sauter A, Masterman D, Fontoura P, Belachew S, Garren H, Mairon N, Chin P1, and Wolinsky JS; ORATORIO Clinical Investigators (2017). "Ocrelizumab versus Placebo in Primary Progressive Multiple Sclerosis". In: *N Engl J Med* 376(3), pp. 209–220.

Mordel, Jérôme, Diana Karnas, Paul Pévet, Philippe Isope, Etienne Challet, and Hilmar Meissl (2013). "The Output Signal of Purkinje Cells of the Cerebellum and Circadian Rhythmicity". In: *PLoS One* 8(3), e58457.

Morris, RL and PJ Hollenbeck (1995). "Axonal transport of mitochondria along microtubules and F-actin in living vertebrate neurons". In: *J Cell Biol* 131(5), pp. 1315–26.

Morrison, Brett M., Youngjin Lee, and Jeffrey D. Rothstein (2013). "Oligodendroglia metabolically support axons and maintain structural integrity". In: *Trends Cell Biol* 23(12).

Muster, Britta, Wladislaw Kohl, Ilka Wittig, Valentina Strecker, Friederike Joos, Winfried Haase, Jürgen Bereiter-Hahn, and Karin Busch (2010). "Respiratory Chain Complexes in Dynamic Mitochondria Display a Patchy Distribution in Life Cells". In: *PLoS One* 5(7), e11910.

Nakada, K, K Inoue, and J Hayashi (2001). "Interaction theory of mammalian mitochondria". In: *Biochem Biophys Res Commun* 288(4), pp. 743–6.

Nakada, K, Inoue K, Ono T, Isobe K, Ogura A, Goto YI, Nonaka I, and Hayashi JI (2001). "Inter-mitochondrial complementation: Mitochondria-specific system preventing mice from expression of disease phenotypes by mutant mtDNA". In: *Nat Med* 7(8), pp. 934–940.

Narendra, D, Tanaka A, Suen DF, and Youle RJ (2008). "Parkin is recruited selectively to impaired mitochondria and promotes their autophagy". In: *J Cell Biol* 183(5), pp. 795–803.

Nave, KA (2010). "Myelination and the trophic support of long axons". In: *Nat Rev Neurosci* 11(4), pp. 275–83.

Neishabouri, Ali M and Aldo A Faisal (2011). "The metabolic efficiency of myelinated vs unmyelinated axons". In: *BMC Neurosci* 12(Suppl 1), p. 100.

Neupert, W (1997). "Protein import into mitochondria". In: *Annu Rev Biochem* 66, pp. 863–917.

Nikić, I, Merkler D, Sorbara C, Brinkoetter M, Kreutzfeldt M, Bareyre FM, Brück W, Bishop D, Misgeld T, and Kerschensteiner M (2011). "A reversible form of axon damage in experimental autoimmune encephalomyelitis and multiple sclerosis". In: *Nat Med* 17(4), pp. 495–9.

Noseworthy, J. H., C. Lucchinetti, M. Rodriguez, and B. G. Weinshenker (2000). "Multiple sclerosis". In: *N Engl J Med* 343(13), pp. 938–952.

O'Hanlon, GM, Humphreys PD, Goldman RS, Halstead SK, Bullens RW, Plomp JJ, Ushkaryov Y, and Willison HJ (2003). "Calpain inhibitors protect against axonal degeneration in a model of anti-ganglioside

antibody-mediated motor nerve terminal injury". In: *Brain* 126(Pt 11), pp. 2497–509.

Ohno, N, Kidd GJ, Mahad D, Kiryu-Seo S, Avishai A, Komuro H, and Trapp BD (2011). "Myelination and axonal electrical activity modulate the distribution and motility of mitochondria at CNS nodes of Ranvier". In: *J Neurosci* 31(20), pp. 7249–58.

Ohno, N, Chiang H, Mahad DJ, Kidd GJ, Liu L, Ransohoff RM, Sheng ZH, Komuro H, and Trapp BD (2014). "Mitochondrial immobilization mediated by syntaphilin facilitates survival of demyelinated axons". In: *Proc Natl Acad Sci U S A* 111(27), pp. 9953–8.

Olson, J. K., J. L. Croxford, M. A. Calenoff, M. C. Dal Canto, and S. D. Miller (2001). "A virus-induced molecular mimicry model of multiple sclerosis". In: *J Clin Invest* 108(2), pp. 311–318.

Orrenius, S (2007). "Reactive oxygen species in mitochondria-mediated cell death". In: *Drug Metab Rev* 39(2-3), pp. 443–55.

Otera, H, Wang C, Cleland MM, Setoguchi K, Yokota S, Youle RJ, and Mihara K (2010). "Mff is an essential factor for mitochondrial recruitment of Drp1 during mitochondrial fission in mammalian cells". In: *J Cell Biol* 191(6), pp. 1141–58.

Owens, GC and DB Edelman (2015). "Photoconvertible fluorescent protein-based live imaging of mitochondrial fusion". In: *Methods Mol Biol* 1313, pp. 237–46.

Owens, GC and EC Walcott (2012). "Extensive fusion of mitochondria in spinal cord motor neurons". In: *PLoS One* 7(6), e38435.

Papadopoulos, D, D Pham-Dinh, and R Reynolds (2006). "Axon loss is responsible for chronic neurological deficit following inflammatory demyelination in the rat". In: *Exp Neurol* 197(2), pp. 373–85.

Peterson, JW, Bö L, Mörk S, Chang A, and Trapp BD (2001). "Transected neurites, apoptotic neurons, and reduced inflammation in cortical multiple sclerosis lesions". In: *Ann Neurol* 50(3), pp. 389–400.

Pham, AH and DC Chan (2014). "Analyzing mitochondrial dynamics in mouse organotypic slice cultures". In: *Methods Enzymol* 547, pp. 111–29.

Pham, Anh H., J. Michael McCaffery, and David C. Chan (2013). "Mouse lines with photo-activatable mitochondria (PhAM) to study mitochondrial dynamics". In: *Genesis* 50(11), 833–843.

Pilling, Aaron D., Dai Horiuchi, Curtis M. Lively, and William M. Saxton (2006). "Kinesin-1 and Dynein Are the Primary Motors for Fast Transport of Mitochondria in Drosophila Motor Axons". In: *Mol Biol Cell* 17(4), 2057–2068.

Pinton, P, C Giorgi, R Siviero, E Zecchini, and R Rizzuto (2008). "Calcium and apoptosis: ER-mitochondria Ca2+ transfer in the control of apoptosis". In: *Oncogene* 27(50), 6407–6418.

Polman, C. H., S. C. Reingold, B. Banwell, M. Clanet, J. A. Cohen, M. Filippi, K. Fujihara, E. Havrdova, M. Hutchinson, L. Kappos, F. D. Lublin, X. Montalban, P. O'Connor, M. Sandberg-Wollheim, A. J. Thompson, E. Waubant, B. Weinshenker, and J. S. Wolinsky (2011). "Diagnostic criteria for multiple sclerosis: 2010 revisions to the McDonald criteria". In: *Ann Neurol* 69(2), pp. 292–302.

Polman, CH, O'Connor PW, Havrdova E, Hutchinson M, Kappos L, Miller DH, Phillips JT, Lublin FD, Giovannoni G, Wajgt A, Toal M, Lynn F, Panzara MA, and Sandrock AW; AFFIRM Investigators (2006). "A randomized and placebo-controlled trial of natalizumab for relapsing multiple sclerosis". In: *N Engl J Med* 354(9), pp. 899–910.

Popescu, B. F., I. Pirko, and C. F. Lucchinetti (2013). "Pathology of multiple sclerosis: where do we stand?" In: *Continuum (Minneap Minn)* 19(4 Multiple Sclerosis), pp. 901–921.

Popescu, BF and CF Lucchinetti (2012a). "Meningeal and cortical grey matter pathology in multiple sclerosis". In: *BMC Neurol* 7, pp. 11–12.

— (2012b). "Pathology of demyelinating diseases". In: *Annu Rev Pathol* 7, pp. 185–217.

Prineas, JW and JD Parratt (2012). "Oligodendrocytes and the early multiple sclerosis lesion". In: *Ann Neurol* 72(1), pp. 18–31.

Qi, X, Qvit N, Su YC, and Mochly-Rosen D (2013). "A novel Drp1 inhibitor diminishes aberrant mitochondrial fission and neurotoxicity". In: *J Cell Sci* 126(Pt 3), pp. 789–802.

Raichle, ME and DA Gusnard (2002). "Appraising the brain's energy budget". In: *Proc Natl Acad Sci U S A* 99(16), pp. 10237–9.

Reddy P. Hemachandra, Ph.D. (2014). "Inhibitors of Mitochondrial Fission as a Therapeutic Strategy for Diseases with Oxidative Stress and Mitochondrial Dysfunction". In: *J Alzheimers Dis* 40(2), 245–256.

Redpath, CJ, Bou Khalil M, Drozdzal G, Radisic M, and McBride HM (2013). "Mitochondrial hyperfusion during oxidative stress is coupled to a dysregulation in calcium handling within a C2C12 cell model". In: *PLoS One* 8(7), e69165.

Rich, PR and A Maréchal (2010). "The mitochondrial respiratory chain". In: *Essays Biochem* 47, pp. 1–23.

Roberts, Anthony J., Takahide Kon, Peter J. Knight, Kazuo Sutoh, and Stan A. Burgess (2013). "Functions and mechanics of dynein motor proteins". In: *Nat Rev Mol Cell Biol* 14(11), 713–726.

Rumah, K. R., J. Linden, V. A. Fischetti, and T. Vartanian (2013). "Isolation of Clostrid-ium perfringens type B in an individual at first clinical presentation of multiple sclerosis provides clues for environmental triggers of the disease". In: *PLoS ONE* 8(10), e76359.

Russell, OM, RN Lightowlers, and DM Turnbull (2016). "Applying the Airbrakes: Treating Mitochondrial Disease with Hypoxia". In: *Mol Cell* 62(1), pp. 5–6.

Saab, AS, ID Tzvetanova, and KA Nave (2013). "The role of myelin and oligodendrocytes in axonal energy metabolism". In: *Curr Opin Neurobiol* 23(6), pp. 1065–72.

Sakuma, T, MA Barry, and Y Ikeda (2012). "Lentiviral vectors: basic to translational". In: *Biochem J* 443(3), pp. 603–18.

Sawcer, S., M. Maranian, E. Setakis, V. Curwen, E. Akesson, A. Hensiek, F. Coraddu, R. Roxburgh, D. Sawcer, J. Gray, J. Deans, P. N. Goodfellow, N. Walker, D. Clayton, and A. Compston (2002). "A whole genome screen for linkage disequilibrium in multiple sclerosis confirms disease associations with regions previously linked to susceptibility". In: *Brain* 125(Pt 6), pp. 1337–1347.

Saxton, William M. and Peter J. Hollenbeck (2012). "The axonal transport of mitochondria". In: *J Cell Sci* 125(9), 2095–2104.

Schain, Aaron J., Robert A. Hill, and Jaime Grutzendler (2014). "Label-free in vivo imaging of myelinated axons in health and disease with spectral confocal reflectance microscopy". In: *Nat Med* 20(4), 443–449.

Scholpa, NE, Lynn MK, Corum D, Boger H2, and Schnellmann RG (2018a). "5-HT1F receptor-mediated mitochondrial biogenesis for the treatment of Parkinson's disease". In: *Br J Pharmacol* 175(2), pp. 348–358.

Scholpa, NE, Lynn MK, Corum D, Boger HA, and Schnellmann RG (2018b). "5-HT1F receptor-mediated mitochondrial biogenesis for the treatment of Parkinson's disease". In: *Br J Pharmacol* 175(2), pp. 348–358.

Schon, EA and S Przedborski (2011). "Mitochondria: the next (neurode)generation". In: *Neuron* 70(6), pp. 1033–53.

Schuh, C., I. Wimmer, S. Hametner, L. Haider, A. M. Van Dam, R. S. Liblau, K. J. Smith, L. Probert, C. J. Binder, J. Bauer, M. Bradl, D. Mahad, and H. Lassmann (2014). "Oxidative tissue injury in multiple sclerosis is only partly reflected in experimental disease models". In: *Acta Neuropathol*.

Schwarz, Thomas L. (2013). "Mitochondrial Trafficking in Neurons". In: *Cold Spring Harb Perspect Biol* 5(6), a011304.

Scott, Iain and Richard J. Youle (2010). "Mitochondrial fission and fusion". In: *Essays Biochem* 47, 85–98.

Shchepina, LA, Pletjushkina OY, Avetisyan AV, Bakeeva LE, Fetisova EK, Izyumov DS, Saprunova VB, Vyssokikh MY, Chernyak BV, and Skulachev VP (2012). "Oligomycin and inhibitor of the F0 part of H+-ATP-synthase and suppresses the TNF-induced apoptosis". In: *Oncogene* 21(53), pp. 8149–57.

Sheng, ZH (2014). "Mitochondrial trafficking and anchoring in neurons: New insight and implications". In: *J Cell Biol* 204(7), pp. 1087–98.

Sheng, ZH and Q Cai (2012). "Mitochondrial transport in neurons: impact on synaptic homeostasis and neurodegeneration". In: *Nat Rev Neurosci* 13(2), pp. 77–93.

Sillitoe, RV and AL Joyner (2007). "Morphology and molecular codes and and circuitry produce the three-dimensional complexity of the cerebellum". In: *Annu Rev Cell Dev Biol* 23, pp. 549–77.

Skov, Vibe, Dorte Glintborg, Steen Knudsen, Qihua Tan, Thomas Jensen, Torben A. Kruse, Henning Beck-Nielsen, and Kurt Højlund (2008). "Pioglitazone Enhances Mitochondrial Biogenesis and Ribosomal Protein Biosynthesis in Skeletal Muscle in Polycystic Ovary Syndrome". In: *PLoS ONE* 3(6), e2466.

Smirnova, E, Griparic L, Shurland DL, and van der Bliek AM (2001). "Dynamin-related protein Drp1 is required for mitochondrial division in mammalian cells". In: *Mol Biol Cell* 12(8), pp. 2245–56.

Smith, KJ (2007). "Sodium channels and multiple sclerosis: roles in symptom production and damage and therapy". In: *Brain Pathol* 17(2), pp. 230–42.

Smith, KJ and H Lassmann (2002). "The role of nitric oxide in multiple sclerosis". In: *Lancet Neurol* 1(4), pp. 232–41.

Song, Z, Chen H, Fiket M, Alexander C, and Chan DC (2007). "OPA1 processing controls mitochondrial fusion and is regulated by mRNA splicing, membrane potential, and Yme1L". In: *J Cell Biol* 178(5), pp. 749–55.

Song, Zhiyin, Mariam Ghochani, J. Michael McCaffery, Terrence G. Frey, and David C. Chan (2009). "Mitofusins and OPA1 Mediate Sequential Steps in Mitochondrial Membrane Fusion". In: *Mol Biol Cell* 20(15), 3525–3532.

Sorbara, CD, Wagner NE, Ladwig A, Nikić I, Merkler D, Kleele T, Marinković P, Naumann R, Godinho L, Bareyre FM, Bishop D, Misgeld T, and Kerschensteiner M (2014). "Pervasive axonal transport deficits in multiple sclerosis models". In: *Neuron* 84(6), pp. 1183–90.

Spronsen, M van, Mikhaylova M, Lipka J, Schlager MA, van den Heuvel DJ, Kuijpers M, Wulf PS, Keijzer N, Demmers J, Kapitein LC, Jaarsma D, Gerritsen HC, Akhmanova A, and Hoogenraad CC (2013). "TRAK/Milton motor-adaptor proteins steer mitochondrial trafficking to axons and dendrites". In: *Neuron* 77(3), pp. 485–502.

Starkov, Anatoly A. (2008). "The Role of Mitochondria in Reactive Oxygen Species Metabolism and Signaling". In: *Ann N Y Acad Sci* 1147, 37–52.

Stephen, Terri-Leigh, Nathalie F. Higgs, David F. Sheehan, Sana Al Awabdh, Guillermo López-Doménech, I. Lorena Arancibia-Carcamo, and Josef T. Kittler (2015a). "Miro1 Regulates Activity-Driven Positioning of Mitochondria within Astrocytic Processes Apposed to Synapses to Regulate Intracellular Calcium Signaling". In: *J Neurosci* 35(48), 15996–16011.

Stephen, TL, Higgs NF, Sheehan DF, Al Awabdh S, López-Doménech G, Arancibia-Carcamo IL, and Kittler JT (2015b). "Miro1 Regulates Activity-Driven Positioning of Mitochondria within Astrocytic Processes Apposed to Synapses to Regulate Intracellular Calcium Signaling". In: *J Neurosci* 35(48), pp. 15996–6011.

Stetler, RA, Leak RK, Yin W, Zhang L, Wang S, Gao Y, and Chen J (2012). "Mitochondrial biogenesis contributes to ischemic neuroprotection

afforded by LPS pre-conditioning". In: *J Neurochem* 123 Suppl 2, pp. 125–137.

Stichel, C. C. and H. W. Muller (1998). "The CNS lesion scar: new vistas on an old regeneration barrier". In: *Cell Tissue Res* 294(1), pp. 1–9.

Stys, PK and Q Jiang (2002). "Calpain-dependent neurofilament breakdown in anoxic and ischemic rat central axons". In: *Neurosci Lett* 328(2), pp. 150–4.

Stys, PK, SG Waxman, and BR Ransom (1992). "Ionic mechanisms of anoxic injury in mammalian CNS white matter: role of Na+ channels and Na(+)-Ca2+ exchanger". In: *J Neurosci* 12(2), pp. 430–9.

Stys, PK, H Sontheimer, BR Ransom, and SG Waxman (1993). "Noninactivating and tetrodotoxin-sensitive Na+ conductance in rat optic nerve axons". In: *tetrodotoxin-sensitive Na+ conductance in rat optic nerve axons. Proc Natl Acad Sci U S A* 90(15), pp. 6976–80.

Su, B, Wang X, Zheng L, Perry G, Smith MA, and Zhu X (2010). "Abnormal mitochondrial dynamics and neurodegenerative diseases". In: *Biochim Biophys Acta* 1802(1), pp. 135–42.

Sun, Tao, Haifa Qiao, Ping-Yue Pan, Yanmin Chen, and Zu-Hang Sheng (2013). "Motile Axonal Mitochondria Contribute to the Variability of Presynaptic Strength". In: *Cell Rep* 4(3), 413–419.

Suter, KJ, BN Smith, and FE Dudek (1999). "Electrophysiological recording from brain slices". In: *Methods* 18(2), pp. 86–90.

Taguchi, N, Ishihara N, Jofuku A, Oka T, and Mihara K (2007). "Mitotic phosphorylation of dynamin-related GTPase Drp1 participates in mitochondrial fission". In: *J Biol Chem* 282(15), pp. 11521–9.

Tanaka, A and RJ Youle (2008). "A chemical inhibitor of DRP1 uncouples mitochondrial fission and apoptosis". In: *Mol Cell* 29(4), pp. 409–410.

Taylor, Anne M, Mathew Blurton-Jones, Seog Woo Rhee, David H Cribbs, Carl W Cotman, and Noo Li Jeon (2005). "A microfluidic culture platform for CNS axonal injury and regeneration and transport". In: *Nat Methods* 2(8), 599–605.

Tondera, D, Grandemange S, Jourdain A, Karbowski M, Mattenberger Y, Herzig S, Da Cruz S, Clerc P, Raschke I, Merkwirth C, Ehses S, Krause F, Chan DC, Alexander C, Bauer C, Youle R, Langer T, and Martinou JC

(2009). "SLP-2 is required for stress-induced mitochondrial hyperfusion". In: *EMBO J* 28(11), pp. 1589–600.

Torashima, T, Yamada N, Itoh M, Yamamoto A, and Hirai H (2006). "Exposure of lentiviral vectors to subneutral pH shifts the tropism from Purkinje cell to Bergmann glia". In: *Eur J Neurosci* 24(2), pp. 371–80.

Tornes, L, B Conway, and W Sheremata (2014). "Multiple sclerosis and the cerebellum". In: *Neurol Clin* 32(4), pp. 957–77.

Tourbah, A, Lebrun-Frenay C, Edan G, Clanet M, Papeix C, Vukusic S, De Sèze J, Debouverie M, Gout O, Clavelou P, Defer G, Laplaud DA, Moreau T, Labauge P, Brochet B, Sedel F, and Pelletier J; MS-SPI study group. (2016). "MD1003 (high-dose biotin) for the treatment of progressive multiple sclerosis: A randomised and double-blind and placebo-controlled study". In: *Mult Scler* 22(13), pp. 1719–1731.

Trapp, B. D. and P. K. Stys (2009). "Virtual hypoxia and chronic necrosis of demyelinated axons in multiple sclerosis". In: *Lancet Neurol* 8(3), pp. 280–291.

Trapp, BD, Peterson J, Ransohoff RM, Rudick R, Mörk S, and Bö L (1998). "Axonal transection in the lesions of multiple sclerosis". In: *N Engl J Med* 338(5), pp. 278–85.

Tsunoda, I and RS Fujinami (2002). "Inside-Out versus Outside-In models for virus induced demyelination: axonal damage triggering demyelination". In: *Springer Semin Immunopathol* 24(2), pp. 105–25.

Twig, G, Elorza A, Molina AJ, Mohamed H, Wikstrom JD, Walzer G, Stiles L, Haigh SE, Katz S, Las G, Alroy J, Wu M, Py BF, Yuan J, Deeney JT, Corkey BE, and Shirihai OS (2008). "Fission and selective fusion govern mitochondrial segregation and elimination by autophagy". In: *EMBO J* 27(2), pp. 433–46.

Varadi, A, Johnson-Cadwell LI, Cirulli V, Yoon Y, Allan VJ, and Rutter GA (2004). "Cytoplasmic dynein regulates the subcellular distribution of mitochondria by controlling the recruitment of the fission factor dynamin-related protein-1". In: *J Cell Sci* 117(Pt 19), pp. 4389–4400.

Varanita, Tatiana, Maria Eugenia Soriano, Vanina Romanello, Tania Zaglia, Rubén Quintana-Cabrera, Martina Semenzato, Roberta Menabò, Veronica Costa, Gabriele Civiletto, Paola Pesce, Carlo Viscomi,

Massimo Zeviani, Fabio Di Lisa, Marco Mongillo, Marco Sandri, and Luca Scorrano (2015). "The Opa1-Dependent Mitochondrial Cristae Remodeling Pathway Controls Atrophic and Apoptotic and and Ischemic Tissue Damage". In: *Cell Metab* 21(6), 834–844.

Verstreken, P, Ly CV, Venken KJ, Koh TW, Zhou Y, and Bellen HJ (2005). "Synaptic mitochondria are critical for mobilization of reserve pool vesicles at Drosophila neuromuscular junctions". In: *Neuron* 47(3), pp. 365–78.

Wakabayashi, Junko, Zhongyan Zhang, Nobunao Wakabayashi, Yasushi Tamura, Masahiro Fukaya, Thomas W. Kensler, Miho Iijima, and Hiromi Sesaki (2009). "The dynamin-related GTPase Drp1 is required for embryonic and brain development in mice". In: *J Cell Biol* 186(6), 805–816.

Wallace, D.C (2005). "A mitochondrial paradigm of metabolic and degenerative diseases and aging and and cancer: A dawn for evolutionary medicine". In: *Annu Rev Genet* 39, 359–407.

Wallace, VC, Cottrell DF, Brophy PJ, and Fleetwood-Walker SM (2003). "Focal lysolecithin-induced demyelination of peripheral afferents results in neuropathic pain behavior that is attenuated by cannabinoids". In: *J Neurosci* 23(8), pp. 3221–33.

Wanders, Ronald J. A., Jos P. N. Ruiter, Lodewijk IJlst, Hans R. Waterham, and Sander M. Houten (2010). "The enzymology of mitochondrial fatty acid beta-oxidation and its application to follow-up analysis of positive neonatal screening results". In: *J Inherit Metab Dis* 33(5), 479–494.

Wang, CH, Wu SB, Wu YT, and Wei YH (2013). "Oxidative stress response elicited by mitochondrial dysfunction: implication in the pathophysiology of aging". In: *Exp Biol Med (Maywood).* 238(5), pp. 450–460.

Wang, X (2001). "The expanding role of mitochondria in apoptosis". In: *Genes Dev* 15(22), pp. 2922–33.

Wang, Xiaoyin and Michael McManus (2009). "Lentivirus Production". In: *J Vis Exp* (32), p. 1499.

Warner, H. B. and R. I. Carp (1988). "Multiple sclerosis etiology-an Epstein-Barr virus hypothesis". In: *Med Hypotheses* 25(2), pp. 93–97.

Waxman, SG (1992). "Demyelination in spinal cord injury and multiple sclerosis: what can we do to enhance functional recovery?" In: *J Neurotrauma* 9 Suppl 1, pp. 105–17.

— (2006). "Axonal conduction and injury in multiple sclerosis: the role of sodium channels". In: *Nat Rev Neurosci* 7(12), pp. 932–41.

Weier, K, Banwell B, Cerasa A, Collins DL, Dogonowski AM, Lassmann H, Quattrone A, Sahraian MA, Siebner HR, and Sprenger T (2015). "The role of the cerebellum in multiple sclerosis". In: *Cerebellum* 14(3), pp. 364–74.

Westermann, B (2012). "Bioenergetic role of mitochondrial fusion and fission". In: *Biochim Biophys Acta* 1817(10), pp. 1833–8.

Wheeler, DG and E Cooper (2001). "Depolarization strongly induces human cytomegalovirus major immediate-early promoter/enhancer activity in neurons". In: *J Biol Chem* 276(34), pp. 31978–85.

Whitworth, AJ and LJ Pallanck (2017). "PINK1/Parkin mitophagy and neurodegeneration-what do we really know in vivo?" In: *Curr Opin Genet Dev* 44, pp. 47–53.

Wingerchuk, DM and JL Carter (2014). "Multiple sclerosis: current and emerging disease-modifying therapies and treatment strategies". In: *Mayo Clin Proc* 89(2), pp. 225–40.

Winklhofer, KF and C Haass (2010). "Mitochondrial dysfunction in Parkinson's disease". In: *Biochim Biophys Acta* 1802(1), pp. 29–44.

Witte, ME, Bø L, Rodenburg RJ, Belien JA, Musters R, Hazes T, Wintjes LT, Smeitink JA, Geurts JJ, De Vries HE, van der Valk P, and van Horssen J (2009). "Enhanced number and activity of mitochondria in multiple sclerosis lesions". In: *J Pathol* 219(2), pp. 193–204.

Witte, ME, Nijland PG, Drexhage JA, Gerritsen W, Geerts D, van Het Hof B, Reijerkerk A, de Vries HE, van der Valk P, and van Horssen J (2013). "Reduced expression of PGC-1alpha partly underlies mitochondrial changes and correlates with neuronal loss in multiple sclerosis cortex". In: *Acta Neuropathol* 125(2), pp. 231–43.

Witte, ME, Mahad DJ, Lassmann H, and van Horssen J (2014). "Mitochondrial dysfunction contributes to neurodegeneration in multiple sclerosis". In: *Trends Mol Med* 20(3), pp. 179–87.

Wollebo, Hassen S., Baheru Woldemichaele, and Martyn K. White (2014). "Lentiviral transduction of neuronal cells". In: *Methods Mol Biol* 1078, 141–146.

Xie, N, Wang C, Lian Y, Zhang H, Wu C, and Zhang Q (2013). "A selective inhibitor of Drp1, mdivi-1, protects against cell death of hippocampal neurons in pilocarpine-induced seizures in rats". In: *Neurosci Lett* 545, pp. 64–8.

Xie, XY and JN Barrett (1991). "Membrane resealing in cultured rat septal neurons after neurite transection: evidence for enhancement by Ca(2+)-triggered protease activity and cytoskeletal disassembly". In: *J Neurosci* 11(10), pp. 3257–67.

Yamaoka, Shohei and Christopher J. Leaver (2008). "EMB2473/MIRO1 and an Arabidopsis Miro GTPase and Is Required for Embryogenesis and Influences Mitochondrial Morphology in Pollen". In: *Plant Cell* 20(3), 589–601.

Yi, Muqing, David Weaver, and György Hajnóczky (2004). "Control of mitochondrial motility and distribution by the calcium signal". In: *J Cell Biol* 167(4), 661–672.

Youle, Richard J. and Alexander M. van der Bliek (2012). "Mitochondrial Fission and Fusion and Stress". In: *Science* 337(6098), 1062–1065.

Young, EA, Fowler CD, Kidd GJ, Chang A, Rudick R, Fisher E, and Trapp BD (2008). "Imaging correlates of decreased axonal Na+/K+ ATPase in chronic multiple sclerosis lesions". In: *Ann Neurol* 63(4), pp. 428–35.

Yu, M, Shi Y, Wei X, Yang Y, Zhou Y, Hao X, Zhang N, and Niu R (2007). "Depletion of mitochondrial DNA by ethidium bromide treatment inhibits the proliferation and tumorigenesis of T47D human breast cancer cells". In: *Toxicol Lett* 170(1), pp. 83–93.

Zala, D, Hinckelmann MV, Yu H, Lyra da Cunha MM, Liot G, Cordelières FP, Marco S, and Saudou F (2013). "Vesicular glycolysis provides on-board energy for fast axonal transport". In: *Cell* 152(3), pp. 479–91.

Zambonin, JL, Zhao C, Ohno N, Campbell GR, Engeham S, Ziabreva I, Schwarz N, Lee SE, Frischer JM, Turnbull DM, Trapp BD, Lassmann H, Franklin RJ, and Mahad DJ (2011). "Increased mitochondrial content in remyelinated axons: implications for multiple sclerosis". In: *Brain* 134(Pt 7), pp. 1901–13.

Zhang, Hui, Andrew A. Jarjour, Amanda Boyd, and Anna Williams (2011). "Central nervous system remyelination in culture — A tool for multiple sclerosis research". In: *Exp Neurol* 230(1-2), 138–148.

Zhou, B, Yu P, Lin MY, Sun T, Chen Y, and Sheng ZH (2016). "Facilitation of axon regeneration by enhancing mitochondrial transport and rescuing energy deficits". In: *J Cell Biol* 214(1), pp. 103–19.

Zonta, B, Desmazieres A, Rinaldi A, Tait S, Sherman DL, Nolan MF, and Brophy PJ (2011). "A critical role for Neurofascin in regulating action potential initiation through maintenance of the axon initial segment". In: *Neuron* 69(5), pp. 945–56.